

INFORMATION TO USERS

This manuscript has been reproduced from the microfilm master. UMI films the text directly from the original or copy submitted. Thus, some thesis and dissertation copies are in typewriter face, while others may be from any type of computer printer.

The quality of this reproduction is dependent upon the quality of the copy submitted. Broken or indistinct print, colored or poor quality illustrations and photographs, print bleedthrough, substandard margins, and improper alignment can adversely affect reproduction.

In the unlikely event that the author did not send UMI a complete manuscript and there are missing pages, these will be noted. Also, if unauthorized copyright material had to be removed, a note will indicate the deletion.

Oversize materials (e.g., maps, drawings, charts) are reproduced by sectioning the original, beginning at the upper left-hand corner and continuing from left to right in equal sections with small overlaps. Each original is also photographed in one exposure and is included in reduced form at the back of the book.

Photographs included in the original manuscript have been reproduced xerographically in this copy. Higher quality 6" x 9" black and white photographic prints are available for any photographs or illustrations appearing in this copy for an additional charge. Contact UMI directly to order.

UMI

A Bell & Howell Information Company
300 North Zeeb Road, Ann Arbor MI 48106-1346 USA
313/761-4700 800/521-0600

NOTE TO USERS

The original manuscript received by UMI contains pages with indistinct print. Pages were microfilmed as received.

This reproduction is the best copy available

UMI

UNIVERSITY OF ALBERTA

**NONFACTORIZATION AND TWO-BODY
HADRONIC DECAYS OF B MESONS**

By

Farook M. Al-Shamali



A thesis submitted to the Faculty of Graduate Studies and Research
in partial fulfilment of the requirements for the degree of
Doctor of Philosophy

Department of Physics

Edmonton, Alberta

Fall 1998



National Library
of Canada

Acquisitions and
Bibliographic Services

395 Wellington Street
Ottawa ON K1A 0N4
Canada

Bibliothèque nationale
du Canada

Acquisitions et
services bibliographiques

395, rue Wellington
Ottawa ON K1A 0N4
Canada

Your file Votre référence

Our file Notre référence

The author has granted a non-exclusive licence allowing the National Library of Canada to reproduce, loan, distribute or sell copies of this thesis in microform, paper or electronic formats.

The author retains ownership of the copyright in this thesis. Neither the thesis nor substantial extracts from it may be printed or otherwise reproduced without the author's permission.

L'auteur a accordé une licence non exclusive permettant à la Bibliothèque nationale du Canada de reproduire, prêter, distribuer ou vendre des copies de cette thèse sous la forme de microfiche/film, de reproduction sur papier ou sur format électronique.

L'auteur conserve la propriété du droit d'auteur qui protège cette thèse. Ni la thèse ni des extraits substantiels de celle-ci ne doivent être imprimés ou autrement reproduits sans son autorisation.

0-612-34721-4

UNIVERSITY OF ALBERTA

LIBRARY RELEASE FORM

NAME OF AUTHOR: Farook M. Al-Shamali
TITLE OF THESIS: Nonfactorization and Two-Body
Hadronic Decays of B Mesons
DEGREE: Doctor of Philosophy
YEAR THE DEGREE GRANTED: 1998

Permission is hereby granted to the University of Alberta Library to reproduce single copies of this thesis and to lend or sell such copies for private, scholarly or scientific research purposes only.

The author reserves all other publication and other rights in association with the copyright in the thesis, and except as hereinbefore provided, neither the thesis nor any substantial portion thereof may be printed or otherwise reproduced in any material form whatever without the author's prior written permission.

Farook Shamali

Farook M. Al-Shamali

Department of Physics

University of Alberta

Edmonton, Alberta T6G 2J1

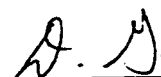
Date: Oct. 2, 1998

UNIVERSITY OF ALBERTA
FACULTY OF GRADUATE STUDIES AND RESEARCH

The undersigned certify that they have read, and recommend to the Faculty of Graduate Studies and Research for acceptance, a thesis entitled "Nonfactorization and Two-Body Hadronic Decays of B Mesons" submitted by Farook M. Al-Shamali in partial fulfilment of the requirements for the degree of Doctor of Philosophy.



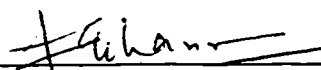
Professor A. N. Kamal (*Supervisor*)



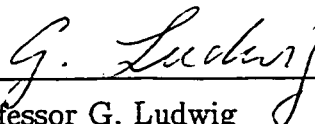
Professor A. Ali (*External Reader*)
DESY, Hamburg, Germany



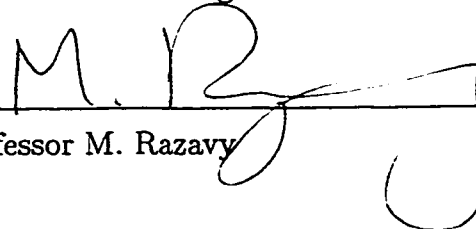
Professor D. Gingrich (*Committee Chairman*)



Professor F. C. Khanna



Professor G. Ludwig



Professor M. Razavy

Date: Sept. 29, 1998.

ABSTRACT

This work is concerned with studying the validity of the factorization assumption in two-body hadronic B -decays and investigating the importance of the nonfactorization contribution.

The study was done first on the two processes $B \rightarrow K^* J/\psi$ and $B_s \rightarrow \phi J/\psi$, in five different theoretical models for the formfactors, using the experimental branching ratios and the available world averages of longitudinal polarization. Then the study was performed using the full set of decay amplitudes for the process $B \rightarrow K^* J/\psi$ measured by the CLEO II collaboration. The knowledge on nonfactorization so gained, was used to study the processes $B_s \rightarrow J/\psi(\eta, \eta')$, $B_s \rightarrow J/\psi \phi$ and $B \rightarrow \psi(2S)K^*$. The results showed the need for the nonfactorization contribution in order to explain experimental data. They also suggest that the nonfactorization parameters do not depend strongly on the light degree of freedom in such processes.

In the third part of this work, universal values were assumed for the color-singlet (ε_1) and color octet (ε_8) nonfactorization parameters in B -decays. Two sets of color-favored processes and one set of color-suppressed processes were used to estimate these parameters quantitatively. It was found (by calculating the branching ratios for a large number of Cabibbo-favored B -decays) that the values $\varepsilon_1(\mu_0) = -0.07 \pm 0.03$ and $\varepsilon_8(\mu_0) = 0.13 \pm 0.05$ improve significantly the predictions of the factorization model.

Finally, the NLL and penguin effects on the predictions of the factorization assumption and the nonfactorization parameters ε_1 and ε_8 were calculated. It was found that the estimated values of these two parameters in LL and in NLL are very close.

To my Father and my Mother

To my wife Bahja ♡

To my children Omar and Huda

ACKNOWLEDGEMENT

I wish to express my deep appreciation to my supervisor Professor **Kamal** for his great support and guidance. I also wish to thank the other members of my thesis committee for their cooperation and constructive comments.

Thanks to the physics department and all its members (specially Lynn Chandler) for their assistance and support. Finally, I wish to thank my colleague El aaoud El hassan for the numerous and helpful discussions we had together.

Contents

1	Introduction	1
2	The Standard Model and Effective Hamiltonian	4
2.1	Electroweak Gauge Theory	5
2.2	Quantum Chromodynamics	6
2.2.1	Renormalized Strong Coupling Constant	7
2.3	\mathcal{H}_{eff} Without QCD Effects	9
2.4	\mathcal{H}_{eff} in LL	10
2.4.1	Renormalization Group Equations	12
2.4.2	Penguin Contribution	16
2.4.3	Numerical Results	19
2.5	\mathcal{H}_{eff} in NLL	20
3	Amplitudes and Formfactors	26
3.1	Current Matrix Elements	26
3.2	Decay Amplitudes	29
3.2.1	Type $b \rightarrow c\bar{u}d$ processes: Class I	29
3.2.2	Type $b \rightarrow c\bar{u}d$ processes: Class II	33
3.2.3	Type $b \rightarrow c\bar{u}d$ processes: Class III	38
3.2.4	Type $b \rightarrow c\bar{c}s$ processes: Class I	41
3.2.5	Type $b \rightarrow c\bar{c}s$ processes: Class II	43

3.3	CKM Matrix Elements	45
3.4	Decay Constants	46
3.4.1	f_{π^-}	46
3.4.2	f_ρ and f_{a_1}	47
3.4.3	$f_{J/\psi}$ and $f_{\psi(2S)}$	48
3.4.4	f_D and f_{D^*}	50
3.4.5	f_{D_s} and $f_{D_s^*}$	50
3.5	Formfactors	50
4	Nonfactorization in $B \rightarrow K^* J/\psi$ and $B_s \rightarrow \phi J/\psi$ Decays	58
4.1	Introduction	58
4.2	Formalism	59
4.3	$B \rightarrow K^* J/\psi$ Decay	61
4.3.1	Nonfactorization in One Formfactor	62
4.3.2	Nonfactorization in All Formfactors	67
4.3.3	Polarization Contours	68
4.4	$\overline{B}_s^0 \rightarrow \phi J/\psi$ Decays	74
4.4.1	Nonfactorization in One Formfactor	74
4.4.2	Nonfactorization in All Formfactors	78
4.4.3	Polarization Contours	81
4.5	Discussion	88
5	Nonfactorization and Final State Interactions in $(B, B_s) \rightarrow \psi P$ and ψV Decays	91
5.1	Introduction	91
5.2	$(B, B_s) \rightarrow \psi(\psi(2S))P$ Decays	92
5.2.1	$B \rightarrow \psi(\psi(2S))K$ decays	94
5.2.2	$B_s \rightarrow \psi(\psi(2S))\eta, \eta'$ Decays	98
5.3	$(B, B_s) \rightarrow \psi(\psi(2S))V$ Decays	99

5.3.1	$B \rightarrow \psi K^*$ Decays	102
5.3.2	$B_s \rightarrow \psi \phi$ Decays	107
5.3.3	$B \rightarrow \psi(2S)K^*$ Decays	109
5.4	Results in Factorization Approximation	109
5.5	Discussion	111
6	Nonfactorization in Cabibbo-Favored B-Decays	116
6.1	Introduction	116
6.2	Formalism	118
6.2.1	Effective Hamiltonian	118
6.2.2	Factorization and Nonfactorization	119
6.2.3	Current Matrix Elements	122
6.3	Evaluation of Nonfactorization Contribution	124
6.4	Predictions of Branching Ratios and Polarization	126
6.5	Discussion and Conclusion	132
7	NLL and Penguin Effects on Nonfactorization in B-Decays	141
7.1	Introduction	141
7.2	Wilson Coefficients in NLL	141
7.3	Effect on the Results of Factorization Approximation	145
7.3.1	Type $b \rightarrow c\bar{u}d$ Decays ($B \rightarrow D\pi, D\rho \dots etc.$)	145
7.3.2	Type $b \rightarrow c\bar{c}s$ Decays ($B \rightarrow DD_s, KJ/\psi \dots etc.$)	147
7.3.3	Type $b \rightarrow c\bar{c}d$ Decays	150
7.4	Effect on the Estimates of the Nonfactorization Parameters	151
7.5	Nonfactorization Effects on Branching Ratios	153
7.6	Discussion and Conclusion	155
8	Conclusion	159

A	Polarization Vectors	162
A.1	Free Massive Vector Field	162
A.2	Solutions of Equations of Motion	163
A.3	Polarization Vectors	164
A.3.1	Helicity Eigenstates	164
A.4	$P \rightarrow VV$ Decays	166
A.4.1	Useful Calculations	167
B	Fierz Transformation	169
B.1	The Complete Set of 4×4 Matrices	169
B.1.1	Properties	170
B.1.2	Useful Relations	172
B.2	Fierz Transformation	173
B.3	Fierz transformation and Color Algebra	174
C	Two-Body Decay Rate	176
C.1	Normalization of Wave Functions	176
C.1.1	Klein-Gordon Field	176
C.1.2	Dirac Field	177
C.2	Decay Rate	178
D	η and η' Systems	181
E	Particle Properties	183

List of Tables

2.1	Wilson Coefficients in LL at $\mu = 4.4, 4.6$ and 4.8 GeV, and for $\Lambda_{\overline{\text{MS}}}^5 = 225 \pm 85$ MeV. The last four rows are some useful combinations of $C_1(\mu)$ and $C_2(\mu)$	20
2.2	NLL Wilson Coefficients in NDR at $\mu = 4.4, 4.6$ and 4.8 GeV, and for $\Lambda_{\overline{\text{MS}}}^5 = 225$. The last four rows are some useful combinations of $C_1(\mu)$ and $C_2(\mu)$	24
3.1	BSW I model predictions of $F_0(q^2)$ and $F_1(q^2)$ formfactors for transitions of the type $B \rightarrow P$, where P is a pseudoscalar meson.	52
3.2	BSW I model predictions of $A_0(q^2)$, $A_1(q^2)$, $A_2(q^2)$, $A_3(q^2)$ and $V(q^2)$ formfactors for processes of the type $B \rightarrow V$, where V is a pseudoscalar meson.	53
3.3	BSW I model predictions of $F_0(q^2)$ and $F_1(q^2)$ formfactors for transitions of the type $B_s \rightarrow P$, where P is a pseudoscalar meson.	54
3.4	BSW I model predictions of $A_0(q^2)$, $A_1(q^2)$, $A_2(q^2)$, $A_3(q^2)$ and $V(q^2)$ formfactors for processes of the type $B_s \rightarrow V$, where V is a pseudopseudoscalar meson.	55
4.1	The different experimental measurements of the longitudinal polarization (P_0) for the process $B \rightarrow K^* J/\psi$. The first error is statistical and the second is systematic.	61

4.2	Values of the nonfactorization parameter χ_{A_1} , calculated in each theoretical model, that explain the available experimental branching ratio and longitudinal polarization for the process $B \rightarrow K^* J/\psi$. The other two nonfactorization parameters (χ_{A_2} and χ_V) were assumed to vanish.	62
4.3	Values of the nonfactorization parameter χ_{A_2} , calculated in each theoretical model, that explain the available experimental branching ratio and longitudinal polarization for the process $B \rightarrow K^* J/\psi$. The other two nonfactorization parameters (χ_{A_1} and χ_V) were assumed to vanish.	63
4.4	Values of the nonfactorization parameter χ_V , calculated in each theoretical model, that explain the available experimental branching ratio for the process $B \rightarrow K^* J/\psi$. The other two nonfactorization parameters (χ_{A_1} and χ_{A_2}) were assumed to vanish.	63
4.5	Values of the nonfactorization parameter χ_{A_1} , calculated in each theoretical model, that explain the available experimental branching ratio and longitudinal polarization for the process $\overline{B}_s^0 \rightarrow \phi J/\psi$. The other two nonfactorization parameters (χ_{A_2} and χ_V) were assumed to vanish.	76
4.6	Values of the nonfactorization parameter χ_{A_2} , calculated in each theoretical model, that explain the available experimental branching ratio and longitudinal polarization for the process $\overline{B}_s^0 \rightarrow \phi J/\psi$. The other two nonfactorization parameters (χ_{A_1} and χ_V) were assumed to vanish.	77
4.7	Values of the nonfactorization parameter χ_V , calculated in each theoretical model, that explain the available experimental branching ratio for the process $\overline{B}_s^0 \rightarrow \phi J/\psi$. The other two nonfactorization parameters (χ_{A_1} and χ_{A_2}) were assumed to vanish.	77
5.1	Model predictions of formfactor $F_1(q^2)$ at $q^2 = m_\psi^2$ or $m_{\psi(2S)}^2$. In CDDFGN model, η stands for η_8 , the octet member. This scheme cannot handle η_1 , the flavor singlet.	95

5.2	Model predictions of $A_1(m_\psi^2)$, $A_2(m_\psi^2)$, and $V(m_\psi^2)$ formfactors for the processes $B \rightarrow \psi K^*$, $B \rightarrow \psi(2S)K^*$ and $B_s \rightarrow \psi\phi$	96
5.3	Average branching ratios predicted by the theoretical models for three choices of ξ_{F_1}	99
5.4	Solutions of ξ_1 , ξ_{21} and ξ_{V1} using the latest CLEO II measurements of branching ratio, polarization and $ \hat{H}_+ ^2$ for the process $B \rightarrow \psi K^*$. In the table only positive solutions for ξ_1 are shown since for every solution of ξ_1 there is another which is its negative.	106
5.5	The branching ratios, $ \hat{H}_0 ^2$ and $ \hat{H}_- ^2$ for the process $B_s \rightarrow \psi\phi$ using for ξ_1 , ξ_{21} and ξ_{V1} the values in Table 5.4 calculated for $B \rightarrow \psi K^*$. . .	108
5.6	The branching ratios, $ \hat{H}_0 ^2$ and $ \hat{H}_- ^2$ for the process $B \rightarrow \psi(2S)K^*$ using for ξ_1 , ξ_{21} and ξ_{V1} the values in Table 5.4 calculated for $B \rightarrow \psi K^*$. .	110
5.7	Predictions of branching ratios, $ \hat{H}_0 ^2$ and $ \hat{H}_- ^2$ for the processes $B \rightarrow \psi K^*$, $B_s \rightarrow \psi\phi$ and $B \rightarrow \psi(2S)K^*$ using the factorization approximation $\xi_1 = \xi_{21} = \xi_{V1} = 1$. The errors in branching ratios are due to the errors in Wilson coefficients, decay constants and B meson life times.	112
6.1	The values of the nonfactorization parameter ξ_1^2 calculated for six color-favored processes of the type $b \rightarrow c\bar{u}d$. Column 3 represents the factorization model estimate of the branching ratios.	127
6.2	The values of the nonfactorization parameter ξ_1^2 calculated for four color-favored processes of the type $b \rightarrow c\bar{c}s$. Column 3 represents the factorization model estimate of the branching ratios.	127
6.3	The values of the nonfactorization parameter ξ_2^2 calculated for four color-suppressed processes of the type $b \rightarrow c\bar{c}s$. Column 3 represents the factorization model estimate of the branching ratios.	128

- 6.4 The predicted branching ratios for the color-favored processes of the type $b \rightarrow c\bar{u}d$ calculated, in column 2, by taking $\varepsilon_1(\mu_0) = \varepsilon_8(\mu_0) = 0$ and, in column 3, by taking $\varepsilon_1(\mu_0) = -0.07 \pm 0.03$, $\varepsilon_8(\mu_0) = 0.13 \pm 0.05$. The last column represents the available experimental measurements 132
- 6.5 The predicted branching ratios for the color-suppressed processes of the type $b \rightarrow c\bar{u}d$ calculated, in column 2, by taking $\varepsilon_1(\mu_0) = \varepsilon_8(\mu_0) = 0$ and, in column 3, by taking $\varepsilon_1(\mu_0) = -0.07 \pm 0.03$, $\varepsilon_8(\mu_0) = 0.13 \pm 0.05$. The last column represents the available experimental upper bounds. 133
- 6.6 The predicted branching ratios for the color-favored processes of the type $b \rightarrow c\bar{c}s$ calculated, in column 2, by taking $\varepsilon_1(\mu_0) = \varepsilon_8(\mu_0) = 0$ and, in column 3, by taking $\varepsilon_1(\mu_0) = -0.07 \pm 0.03$, $\varepsilon_8(\mu_0) = 0.13 \pm 0.05$. The last column represents the available experimental measurements. 133
- 6.7 The predicted branching ratios for the color-suppressed processes of the type $b \rightarrow c\bar{c}s$ calculated, in column 2, by taking $\varepsilon_1(\mu_0) = \varepsilon_8(\mu_0) = 0$ and, in column 3, by taking $\varepsilon_1(\mu_0) = -0.07 \pm 0.03$, $\varepsilon_8(\mu_0) = 0.13 \pm 0.05$. The last column represents the available experimental measurements. 134
- 6.8 The predicted branching ratios for the decays of B^- meson of the type $b \rightarrow c\bar{u}d$ calculated, in column 2, by taking $\varepsilon_1(\mu_0) = \varepsilon_8(\mu_0) = 0$ and, in column 3, by taking $\varepsilon_1(\mu_0) = -0.07 \pm 0.03$, $\varepsilon_8(\mu_0) = 0.13 \pm 0.05$. The last column represents the available experimental measurements. 134
- 6.9 The predicted branching ratios for the color-favored B_s decays of the type $b \rightarrow c\bar{u}d$ calculated, in column 2, by taking $\varepsilon_1(\mu_0) = \varepsilon_8(\mu_0) = 0$ and, in column 3, by taking $\varepsilon_1(\mu_0) = -0.07 \pm 0.03$, $\varepsilon_8(\mu_0) = 0.13 \pm 0.05$. The last column represents the available experimental limits. . . 135

6.10	The predicted branching ratios for the color-suppressed B_s decays of the type $b \rightarrow c\bar{u}d$ calculated, in column 2, by taking $\varepsilon_1(\mu_0) = \varepsilon_8(\mu_0) = 0$ and, in column 3, by taking $\varepsilon_1(\mu_0) = -0.07 \pm 0.03$, $\varepsilon_8(\mu_0) = 0.13 \pm 0.05$.	135
6.11	The predicted branching ratios for the color-suppressed B_s decays of the type $b \rightarrow c\bar{c}s$ calculated, in column 2, by taking $\varepsilon_1(\mu_0) = \varepsilon_8(\mu_0) = 0$ and, in column 3, by taking $\varepsilon_1(\mu_0) = -0.07 \pm 0.03$, $\varepsilon_8(\mu_0) = 0.13 \pm 0.05$. The last column represents the available experimental measurements.	136
6.12	Predictions of longitudinal (P_0) and transverse (P_-) polarizations for Cabibbo-favored decays of the form $B \rightarrow VV$ where V is a vector meson.	137
7.1	Effective Wilson Coefficients in NLL, evaluated using $\Lambda_{\overline{\text{MS}}}^5 = 225 \text{ MeV}$ and constituent quark masses. The values in brackets were evaluated using the running quark masses at the b -quark mass scale.	146
7.2	$\Delta\mathcal{B}_f$ represents the difference, assuming factorization, between the branching ratios calculated using the Wilson coefficients in LL (without penguin contribution), and the branching ratios calculated using the Wilson coefficients in NLL and NLL + Penguins. $\Delta\mathcal{B}_{nf}$ is the difference between the branching ratios calculated using the Wilson coefficients in LL (including nonfactorization as in the previous chapter), and the branching ratios calculated using the Wilson coefficients in NLL (including penguins and nonfactorization as in this chapter). Explicitly, entries in column 4 represent $\Delta\mathcal{B}_f = (\mathcal{B}_{LL} - \mathcal{B}_{NLL})_{\text{fac}}$, those in column 5 represent $\Delta\mathcal{B}_f = (\mathcal{B}_{LL} - \mathcal{B}_{NLL+\text{Penguin}})_{\text{fac}}$ and those in column 6 represent $\Delta\mathcal{B}_{nf} = (\mathcal{B}_{LL+\text{nonfac}} - \mathcal{B}_{NLL+\text{Penguin}+\text{nonfac}})$	152

7.3	The predicted branching ratios, in the NLL scheme with penguin contribution, for class II processes of the type $b \rightarrow c\bar{c}d$. Branching ratios in column 2 are calculated taking $\varepsilon_1 = \varepsilon_8 = 0$ and those in column 3 with $\varepsilon_1 = -0.053 \pm 0.030$, $\varepsilon_8 = 0.137 \pm 0.009$. The last column represents the available experimental measurements.	155
-----	--	-----

List of Figures

2.1	The tree-level Feynman diagram for the process $b \rightarrow c \bar{u} d$	10
2.2	One loop current \times current tree diagrams in the full theory.	11
2.3	One loop current \times current tree diagrams in the Effective theory. . .	12
2.4	$\ln(m_W^2/\mu^2)$ for μ in the range m_b to m_W	13
2.5	The tree-level Feynman diagram for the process $b \rightarrow c \bar{c} s$	16
2.6	The Penguin Feynman diagrams for the process $b \rightarrow c \bar{c} s$, a : in the full theory, b : in the effective theory.	17
2.7	The coefficients C_1 , C_2 , a_1 , a_2 , C_2/a_1 and C_1/a_2 , in LL, as a function of μ for $\Lambda_{\overline{\text{MS}}}^5 = 225 + 85 \text{ MeV}$ and $\Lambda_{\overline{\text{MS}}}^5 = 225 - 85 \text{ MeV}$	21
3.1	The flavor flow diagrams for class I processes of the type $b \rightarrow c \bar{u} d$. . .	30
3.2	The flavor flow diagrams for class II processes of the type $b \rightarrow c \bar{u} d$. .	34
3.3	The flavor flow diagrams for Class III processes of the type $b \rightarrow c \bar{u} d$. .	38
3.4	The flavor flow diagram for class I processes of the type $b \rightarrow c \bar{c} s$. . .	41
3.5	The flavor flow diagram for class II processes of the type $b \rightarrow c \bar{c} s$. . .	44
3.6	The tree-level Feynman diagram for the process $\pi \rightarrow \mu \bar{\nu}_\mu$	46
3.7	The tree-level Feynman diagram for the process $\tau^- \rightarrow \rho^- \nu_\tau$	47
3.8	The tree-level Feynman diagram for the process $J/\psi \rightarrow e^+ e^-$	49
4.1	Polarization for the process $B \rightarrow K^* J/\psi$ with $(\chi_{A_1} = \chi_{A_2} = 0)$, plotted as a function of χ_V for each model. Horizontal lines define the measured value to one standard deviation.	64

4.2	Values of the nonfactorization parameter χ_{A_1} , calculated in Table 4.2, that explain the available experimental branching ratio and longitudinal polarization of the process $B \rightarrow K^* J/\psi$. The larger dots are the solutions calculated from the branching ratio measurement, whereas the smaller ones are the solutions calculated from the polarization measurement.	65
4.3	Values of the nonfactorization parameter χ_{A_2} , calculated in Table 4.3, that explain the available experimental branching ratio and longitudinal polarization of the process $B \rightarrow K^* J/\psi$. The larger dots are the solutions calculated from the branching ratio measurement, whereas the smaller ones are the solutions calculated from the polarization measurement.	66
4.4	Values of the nonfactorization parameter χ_V , calculated in Tables 4.4, that explain the available experimental branching ratio of the process $B \rightarrow K^* J/\psi$	66
4.5	Regions in $\chi_{A_1} - \chi_{A_2}$ space bounded by experimental data on branching ratio (ellipses) and polarization (open pairs of curves) for the process $B \rightarrow K^* J/\psi$ assuming BSW I model. Each of the six graphs represent a different value for χ_V	69
4.6	Regions in $\chi_{A_1} - \chi_{A_2}$ space bounded by experimental data on branching ratio (ellipses) and polarization (open pairs of curves) for the process $B^0 \rightarrow K^{*0} J/\psi$ assuming BSW II model. Each of the six graphs represent a different value for χ_V	70
4.7	Regions in $\chi_{A_1} - \chi_{A_2}$ space bounded by experimental data on branching ratio (ellipses) and polarization (open pairs of curves) for the process $B^0 \rightarrow K^{*0} J/\psi$ assuming CDDFGN model. Each of the six graphs represent a different value for χ_V	71

4.8	Regions in $\chi_{A_1} - \chi_{A_2}$ space bounded by experimental data on branching ratio (ellipses) and polarization (open pairs of curves) for the process $B^0 \rightarrow K^{*0} J/\psi$ assuming AW model. Each of the six graphs represent a different value for χ_V	72
4.9	Regions in $\chi_{A_1} - \chi_{A_2}$ space bounded by experimental data on branching ratio (ellipses) and polarization (open pairs of curves) for the process $B^0 \rightarrow K^{*0} J/\psi$ assuming ISGW model. Each of the six graphs represent a different value for χ_V	73
4.10	Regions in $x - y$ plane allowed by experimental data on polarization for the process $B \rightarrow K^{*} J/\psi$. The shaded region between the two solid curves in each graph correspond to the factorization approximation $\chi_{A_1} = \chi_{A_2} = \chi_V = 0$. The regions between the dashed curves in each graph corresponds to (a) $\chi_{A_1} = 0.10, \chi_{A_2} = \chi_V = 0$, (b) $\chi_{A_2} = -0.08, \chi_{A_1} = \chi_V = 0$, (c) $\chi_V = -0.08, \chi_{A_1} = \chi_{A_2} = 0$, (d) $\chi_{A_1} = 0.03, \chi_{A_2} = \chi_V = -0.03$. The dots represent predictions of the theoretical models.	75
4.11	Polarization for the process $\overline{B}_s^0 \rightarrow \phi J/\psi$ with ($\chi_{A_1} = \chi_{A_2} = 0$). plotted as a function of χ_V for each model. Horizontal lines define the measured value to one standard deviation. See Fig. 4.1 for legend.	78
4.12	Values of the nonfactorization parameter χ_{A_1} , presented in Table 4.5, that explain the available experimental branching ratio and longitudinal polarization of the process $\overline{B}_s^0 \rightarrow \phi J/\psi$	79
4.13	Values of the nonfactorization parameter χ_{A_2} , calculated in Table 4.6, that explain the available experimental branching ratio and longitudinal polarization of the process $\overline{B}_s^0 \rightarrow \phi J/\psi$	79
4.14	Values of the nonfactorization parameter χ_V , calculated in Table 4.7, that explain the available experimental branching ratio of the process $\overline{B}_s^0 \rightarrow \phi J/\psi$	80

4.15	Regions in $\chi_{A_1} - \chi_{A_2}$ space bounded by experimental data on branching ratio (ellipses) and polarization (open pairs of curves) for the process $\overline{B}_s^0 \rightarrow \phi J/\psi$ assuming BSW I model. Each of the six graphs represent a different value for χ_V	82
4.16	Regions in $\chi_{A_1} - \chi_{A_2}$ space bounded by experimental data on branching ratio (ellipses) and polarization (open pairs of curves) for the process $\overline{B}_s^0 \rightarrow \phi J/\psi$ assuming BSW II model. Each of the six graphs represent a different value for χ_V	83
4.17	Regions in $\chi_{A_1} - \chi_{A_2}$ space bounded by experimental data on branching ratio (ellipses) and polarization (open pairs of curves) for the process $\overline{B}_s^0 \rightarrow \phi J/\psi$ assuming CDDFGN model. Each of the six graphs represent a different value for χ_V	84
4.18	Regions in $\chi_{A_1} - \chi_{A_2}$ space bounded by experimental data on branching ratio (ellipses) and polarization (open pairs of curves) for the process $\overline{B}_s^0 \rightarrow \phi J/\psi$ assuming AW model. Each of the six graphs represent a different value for χ_V	85
4.19	Regions in $\chi_{A_1} - \chi_{A_2}$ space bounded by experimental data on branching ratio (ellipses) and polarization (open pairs of curves) for the process $\overline{B}_s^0 \rightarrow \phi J/\psi$ assuming ISGW model. Each of the six graphs represent a different value for χ_V	86
4.20	Regions in $x - y$ plane allowed by experimental data on polarization for the process $\overline{B}_s^0 \rightarrow \phi J/\psi$. The shaded region between the two solid curves in each graph correspond to the factorization approximation $\chi_{A_1} = \chi_{A_2} = \chi_V = 0$. The region between the dashed curves in each graph corresponds to (a) $\chi_{A_1} = 0.02, \chi_{A_2} = \chi_V = 0$, (b) $\chi_{A_2} = -0.03, \chi_{A_1} = \chi_V = 0$, (c) $\chi_V = -0.08, \chi_{A_1} = \chi_{A_2} = 0$, (d) $\chi_{A_1} = 0.01, \chi_{A_2} = \chi_V = -0.01$. The dots represent predictions of the theoretical models.	87

5.1	Allowed region (bounded by the two curves) of ξ_{F_1} as a function of $F_1^{BP}(m_\psi^2)$ defined by $B^+ \rightarrow K^{*+}\psi$. The dots show the model predictions of the formfactors; from left to right: AW, ISGW, BSW I, CDDFGN, BSW II.	97
5.2	Branching ratios as functions of ξ_{F_1} in each model. Horizontal lines define the branching ratio bounds to one standard deviation. Data from [10] for $B \rightarrow \psi K$ and [16] for $B \rightarrow \psi(2S)K$	97
5.3	Branching ratios as a function of ξ_{F_1} in each model. In CDDFGN model, η stands for η_8 and there is no prediction for η' . See Fig. 5.2 for legend.	98
5.4	The region in ξ_{21} and ξ_{V1} plane allowed by the latest CLEO II measurements of $ \hat{H}_0 ^2$ (vertical bands) and $ \hat{H}_+ ^2$ (horizontal band) for $B \rightarrow \psi K^*$ in BSW I model.	105
6.1	The values of the nonfactorization parameter ξ_1^2 calculated for six color-favored processes of the type $b \rightarrow c\bar{u}d$. The shaded area represents the statistical average.	128
6.2	The values of the nonfactorization parameter ξ_1^2 calculated for four color-favored processes of the type $b \rightarrow c\bar{c}s$. The shaded area represents the statistical average.	129
6.3	The values of the nonfactorization parameter ξ_2^2 calculated for four color-suppressed processes of the type $b \rightarrow c\bar{c}s$. The shaded area represents the statistical average.	129

6.4	(a) The regions in ε_1 - ε_8 space that correspond to the amount of nonfactorizations estimated for ξ_1^2 and ξ_2^2 . The two parallel regions bounded by thin solid lines correspond to the value $\xi_1^2 = 0.80 \pm 0.06$ calculated from the color-favored processes of the type $b \rightarrow c\bar{u}d$. The regions bounded by the dotted lines correspond to the value $\xi_1^2 = 0.86 \pm 0.14$ calculated from the color-favored processes of the type $b \rightarrow c\bar{c}s$. The regions bounded by the dashed lines correspond to the value $\xi_2^2 = 6.6 \pm 2.4$ calculated from the color-suppressed processes of the type $b \rightarrow c\bar{c}s$. The two intersecting solid lines correspond to the equation $\varepsilon_1/\varepsilon_8 = 1/N_c$. (b) A magnification of the interesting region in ε_1 - ε_8 space.	130
7.1	The flavor flow diagram for Class I processes of the type $b \rightarrow c\bar{u}s$. . .	148
7.2	(a) A contour plot of the value of χ^2 in ε_1 - ε_8 space. The bullets represent minima of χ^2 ; (b) A magnification of the region containing minima 3 of χ^2 . The inner closed curve represent $\Delta\chi^2 = 1$ while the outer closed curve represent $\Delta\chi^2 = 2$	154
A.1	$P \rightarrow V_1 V_2$ in the center-of-mass frame	166

Chapter 1

Introduction

In calculating the decay amplitudes for two-body hadronic decays we encounter matrix elements of the form $\langle f_1 f_2 | Q | i \rangle$, where i is the initial state particle, f_1 and f_2 are the final state particles and Q , a product of two Dirac currents, is a four-fermion operator. In the absence of a reliable way to evaluate these matrix elements from basic principles, the common method involves the factorization assumption. In this method, the matrix element $\langle f_1 f_2 | Q | i \rangle$ is written as a product of two current matrix elements, such that

$$\langle f_1 f_2 | Q | i \rangle = \langle f_1 | J^\mu | i \rangle \langle f_2 | J'_\mu | 0 \rangle, \quad (1.1)$$

where J^μ and J'_μ are the two Dirac currents. Individual current matrix elements on the right hand side of (1.1) are then decomposed in terms of formfactors and decay constants. Any part of the decay amplitude that can not be written in the form of (1.1) (nonfactorizable part) is omitted.

Our aim in this work is to study the validity of the factorization assumption in B -decays and to investigate the importance of the nonfactorizable parts. Earlier work [1, 2, 3] on this subject constitute the basis of our study. In particular, the parametrization of the nonfactorizable amplitudes advocated by Kamal and Santra in [2] is employed in a significant portion of this work.

The thesis is divided into 8 chapters including this introduction. In chapters 2

and 3 (which are introductory chapters) we present the notion of the effective Hamiltonian and write down the decay amplitudes in the factorization assumption for the processes of interest. Also, we present the values of the formfactors and decay constants needed to evaluate the current matrix elements.

We begin our investigation of the nonfactorization contribution by a study of the two color-suppressed processes $B \rightarrow K^* J/\psi$ and $B_s \rightarrow \phi J/\psi$. The amount of nonfactorization contributing to each of these two processes is estimated in chapter 4 using the experimental branching ratio and the available world average of longitudinal polarization in five different theoretical models for the formfactors. In chapter 5, an estimate of nonfactorization parameters is made using the full set of decay amplitudes for the process $B \rightarrow K^* J/\psi$ measured by the CLEO II collaboration.

The nonfactorization contributions to the product of color-singlet and color-octet currents are separately parametrized in chapter 6. For this parametrization, we use the conventions of Neubert and Stech presented in [4]. The values of these parameters are estimated using the experimental branching ratios of three sets of B -decays. This is done by assuming universality (process independence) and equal contribution of these parameters to the different Lorentz-scalar structures in B -decays that have two vector mesons in the final state.

The calculations up to and including chapter 6 are performed using the leading logarithmic values for the Wilson coefficients and omitting the contributions from the penguin diagrams. In chapter 7, we evaluate the effects of penguin processes and next-to-leading logarithmic contributions to Wilson coefficients, on the results of chapter 6. Chapter 8 is devoted to an overall summary and conclusion of this work.

All the calculations in the thesis were carried out by me in consultation with Dr. A. N. Kamal. The idea of calculating the two nonfactorization parameters (defined by Neubert and Stech [4]) in chapter 6 was entirely mine.

Bibliography

- [1] H. Y. Cheng, Phys. Lett. B **335**, 428 (1994); Z. Phys. C **69**, 647 (1996).
- [2] A. N. Kamal and A. B. Santra, Alberta Thy 31-94 (1994); Z. Phys. C **72**, 91 (1996).
- [3] J. Soares, Phys. Rev. D **51**, 3518 (1995).
- [4] M. Neubert and B. Stech, CERN-TH/97/99, hep-ph/9705292. To appear in the Second Edition of Heavy Flavours, Edited by A. J. Buras and M. Lindner (World Scientific, Singapore).

Chapter 2

The Standard Model and Effective Hamiltonian

A few decades ago, the only known particles were electrons, protons and neutrons. These particles were believed to be the building blocks of matter. Protons and neutrons combine to form positively-charged and heavy nuclei which act like electric potential wells that trap electrons and form atoms.

In the present picture (The Standard Model), quarks and leptons are the fundamental constituents of matter, and the interactions between them are described by gauge theories. In this model, quarks exist in six flavors: up (u), down (d), strange (s), charm (c), bottom (b) and top (t). Also, there are six leptons: electron (e), muon (μ), tau (τ) and their neutrinos (ν_e), (ν_μ) and (ν_τ) respectively. Whereas quarks participate in all interactions, leptons can not feel the strong force and only weak interaction can be used to detect neutrinos.

Since strong and electromagnetic interactions do not alter quark flavors, quark decay is carried out through a weak process. However, free quarks have never been seen in nature. This is because strong interaction binds them permanently inside hadronic bound states (hadrons). Therefore, it is important to understand the impact of strong interactions on such weak processes.

2.1 Electroweak Gauge Theory

This theory arranges the left handed fermions (leptons and quarks) in pairs

$$\begin{pmatrix} \nu_e \\ e \end{pmatrix}_L, \begin{pmatrix} \nu_\mu \\ \mu \end{pmatrix}_L, \begin{pmatrix} \nu_\tau \\ \tau \end{pmatrix}_L, \begin{pmatrix} u \\ d' \end{pmatrix}_L, \begin{pmatrix} c \\ s' \end{pmatrix}_L, \begin{pmatrix} t \\ b' \end{pmatrix}_L \quad (2.1)$$

that transform as doublets under the $SU(2)_L$ weak isospin group. The corresponding right handed fermions are kept as singlets. d' , s' and b' above are mixtures of the mass eigenstates d , s and b . The mixing is carried out through the Cabibbo-Kobayashi-Maskawa (CKM) matrix as follows:

$$\begin{pmatrix} d' \\ s' \\ b' \end{pmatrix} = \begin{pmatrix} V_{ud} & V_{us} & V_{ub} \\ V_{cd} & V_{cs} & V_{cb} \\ V_{td} & V_{ts} & V_{tb} \end{pmatrix} \begin{pmatrix} d \\ s \\ b \end{pmatrix} \quad (2.2)$$

The gauge principle requires the Lagrangian to be invariant under the local transformations of the $SU(2)_L \times U(1)$ group. Since this group has four generators, four vector fields are introduced to preserve this invariance. As a result, the electroweak interaction Lagrangian is given as,

$$\mathcal{L}_{\text{int}} = e A_\mu \mathcal{J}_{\text{em}}^\mu + \frac{e}{2 \sin \theta_w \cos \theta_w} Z_\mu \mathcal{J}_{\text{NC}}^\mu + \frac{e}{2 \sqrt{2} \sin \theta_w} (W_\mu^+ \mathcal{J}_{CC}^\mu + W_\mu^- \mathcal{J}_{CC}^{\mu\dagger}), \quad (2.3)$$

where e is the electromagnetic coupling constant and θ_w is the Weinberg angle. A_μ above is the massless electromagnetic gauge field, whereas W_μ^+ , W_μ^- and Z_μ are the massive weak gauge fields.

In (2.3), the electromagnetic current is given by

$$\mathcal{J}_{\text{em}}^\mu = \sum_{l=e,\mu,\tau} -\bar{l} \gamma^\mu l + \sum_{q=u,d,s,c,b,t} Q_q \bar{q} \gamma^\mu q, \quad (2.4)$$

where Q_q are the quark charges relative to e (i. e. $Q_u = +2/3, \dots$).

The neutral weak current is given by

$$\mathcal{J}_{\text{NC}}^\mu = \sum_f \bar{f} \gamma^\mu (T_3^f (1 - \gamma_5) - 2Q_f \sin^2 \theta_w) f$$

$$\begin{aligned}
&= (\bar{\nu}_e, \bar{\nu}_\mu, \bar{\nu}_\tau) \gamma^\mu \frac{1}{2} (1 - \gamma_5) \begin{pmatrix} \nu_e \\ \nu_\mu \\ \nu_\tau \end{pmatrix} \\
&+ (\bar{e}, \bar{\mu}, \bar{\tau}) \gamma^\mu \left(-\frac{1}{2} (1 - \gamma_5) + 2 \sin^2 \theta_w \right) \begin{pmatrix} e \\ \mu \\ \tau \end{pmatrix} \\
&+ (\bar{u}, \bar{c}, \bar{t}) \gamma^\mu \left(\frac{1}{2} (1 - \gamma_5) - \frac{4}{3} \sin^2 \theta_w \right) \begin{pmatrix} u \\ c \\ t \end{pmatrix} \\
&+ (\bar{d}, \bar{s}, \bar{b}) \gamma^\mu \left(-\frac{1}{2} (1 - \gamma_5) + \frac{2}{3} \sin^2 \theta_w \right) \begin{pmatrix} d \\ s \\ b \end{pmatrix}, \tag{2.5}
\end{aligned}$$

whereas the charged weak current is given by

$$\mathcal{J}_{CC}^\mu = (\bar{\nu}_e, \bar{\nu}_\mu, \bar{\nu}_\tau) \gamma^\mu (1 - \gamma_5) \begin{pmatrix} e \\ \mu \\ \tau \end{pmatrix} + (\bar{u}, \bar{c}, \bar{t}) \gamma^\mu (1 - \gamma_5) V \begin{pmatrix} d \\ s \\ b \end{pmatrix}. \tag{2.6}$$

where V is the CKM mixing matrix.

2.2 Quantum Chromodynamics

Quantum Chromodynamics (QCD) is the gauge theory of strong interactions. In this theory, the fundamental particles which participate in the strong interaction (quarks) exist in three different colors and transform as triplets under the $SU(3)_c$ color group. The rest of the fundamental particles (leptons) are color neutral.

In order to ensure the invariance of the theory under the local $SU(3)_c$ gauge transformation, 8 gauge fields (equal in number to the generators of the $SU(3)$ group)

are introduced. These gauge fields (or gluons) are the mediators of the strong force. They are massless vector particles forming a color octet under $SU(3)_c$.

The Lagrangian density for QCD is

$$\begin{aligned}\mathcal{L} = & -\frac{1}{4}F_{\mu\nu}^a F^{a\mu\nu} + \bar{q}_i \left(i\gamma_\mu D_{ij}^\mu - m\delta_{ij} \right) q_j \\ & -\frac{1}{2\alpha} \left(\partial^\mu A_\mu^a \right)^2 + \chi^{a*} \partial^\mu \partial_\mu \chi^a + g f^{abc} (\partial^\mu \chi^{a*}) \chi^b A_\mu^c.\end{aligned}\quad (2.7)$$

where

$$F_{\mu\nu}^a = \partial_\mu A_\nu^a - \partial_\nu A_\mu^a + g f^{abc} A_\mu^b A_\nu^c, \quad (2.8)$$

and

$$D_{ij}^\mu = \partial^\mu \delta_{ij} - ig \frac{1}{2} T_{ij}^a A^{a\mu}. \quad (2.9)$$

In the equations above, A_μ^a ($a = 1, \dots, 8$) are the eight gluon fields, χ^a are the Faddeev-Popov ghost fields and q_i is the field of the quark carrying flavor ($q = u, d, s, c, b, t$) and color ($i = 1, 2, 3$). T^a and f^{abc} are the generators and structure constants of $SU(3)$ group, respectively, while g is the QCD coupling constant. Also, we have the Gauge-fixing parameter, α , (e. g. in Feynman gauge, $\alpha = 1$).

Since QCD is a renormalizable theory, all divergent loop diagrams can be rendered finite by redefining the fields and parameters in the Lagrangian [1]:

$$\begin{aligned}A_{0\mu}^a &= Z_3^{1/2} A_{R\mu}^a, & q_0 &= Z_q^{1/2} q_R, & \chi_0^a &= \tilde{Z}_3^{1/2} \chi_R^a, \\ g_0 &= Z_g g_R, & m_0 &= Z_m m_R, & \xi_0 &= Z_\xi \xi_R.\end{aligned}\quad (2.10)$$

The subscripts, 0 and R , refer to the bare and renormalized quantities respectively, while the Z factors are called the renormalization constants.

2.2.1 Renormalized Strong Coupling Constant

The action

$$\int d^d x \mathcal{L} \quad (2.11)$$

is dimensionless. So, in d dimensions the Lagrangian density must have the dimension L^{-d} , where L is a unit of length. Since the Lagrangian contains a free field term of the form $\partial A \partial A$, then each field A has the dimension $L^{1-d/2}$ (or $\mu^{d/2-1}$ where μ is a mass scale). The three-gluon interaction term has the form $g_R A A \partial A$. This gives the coupling constant a dimension $\mu^{2-d/2}$ [2].

If we define ($2\epsilon = 4 - d$), then we can relate g_R to a dimensionless coupling constant g by

$$g_R = \mu^\epsilon g. \quad (2.12)$$

The value of this dimensionless coupling constant depends on the renormalization scale used (i. e. $g = g(\mu)$). By substituting back in (2.10) we get

$$g = \mu^{-\epsilon} Z_g^{-1} g_0. \quad (2.13)$$

Differentiation of (2.13) above leads to the renormalization group equation (RGE) that governs the dependence of the coupling constant on the renormalization scale μ .

$$\mu \frac{dg}{d\mu} = -\epsilon g + \beta(g). \quad (2.14)$$

where

$$\beta(g) = -\mu \frac{g}{Z_g} \frac{dZ_g}{d\mu}. \quad (2.15)$$

By lowest order calculations of QCD renormalization constants, it is found that

$$\beta(g) = -\beta_0 \frac{g^3}{(4\pi)^2}. \quad (2.16)$$

where (defining N_f to be the number of flavors)

$$\beta_0 = 11 - \frac{2}{3} N_f. \quad (2.17)$$

Substituting (2.16) into (2.14) we arrive at the following RGE:

$$\mu \frac{d\alpha_s}{d\mu} = -2\epsilon \alpha_s - 2\beta_0 \frac{\alpha_s^2}{4\pi}. \quad (2.18)$$

where α_s is defined in an analogue to the QED fine structure constant such that,

$$\alpha_s = \frac{g_s^2}{4\pi}. \quad (2.19)$$

The term containing ϵ in (2.18) has been kept since it will be important in calculating the anomalous dimension of the local operators, later on. The solution of the differential equation above is given as

$$\alpha_s(\mu) = \frac{4\pi}{\beta_0 \ln(\mu^2/\Lambda^2)}, \quad (2.20)$$

where, Λ (called QCD scale constant) is determined experimentally .

If the calculation of the renormalization constant is extended to next-to-leading order, the beta-function is modified to be

$$\beta(g) = -\beta_0 \frac{g^3}{(4\pi)^2} - \beta_1 \frac{g^5}{(4\pi)^4}, \quad (2.21)$$

where

$$\beta_1 = 102 - \frac{38}{3}N_f, \quad (2.22)$$

and the coupling constant becomes

$$\alpha_s(\mu) = \frac{4\pi}{\beta_0 \ln(\mu^2/\Lambda^2)} \left[1 - \frac{\beta_1 \ln \ln(\mu^2/\Lambda^2)}{\beta_0^2 \ln(\mu^2/\Lambda^2)} \right]. \quad (2.23)$$

Note that $\alpha_s(\mu)$ vanishes as $\mu/\Lambda \rightarrow \infty$. This property of QCD is called asymptotic freedom.

2.3 \mathcal{H}_{eff} Without QCD Effects

Assuming that the strong interaction is turned off, let us consider the decay of the b -quark to a charm quark and two light quarks $b \rightarrow c \bar{u} d$. The tree-level Feynman diagram for this process is shown in Fig. 2.1.

Using Feynman rules, the decay amplitude is written as

$$\begin{aligned} \mathcal{A} &= \frac{-ie^2}{8m_W^2 \sin^2 \theta_w} V_{cb} V_{ud}^* \left(\frac{g^{\mu\nu} - k^\mu k^\nu / m_W^2}{1 - k^2 / m_W^2} \right) (\bar{c} \gamma^\mu (1 - \gamma_5) b) (\bar{d} \gamma^\nu (1 - \gamma_5) u) \\ &= \frac{-iG_F}{\sqrt{2}} V_{cb} V_{ud}^* (\bar{c} \gamma^\mu (1 - \gamma_5) b) (\bar{d} \gamma^\nu (1 - \gamma_5) u) + \mathcal{O} \left(\frac{k^2}{m_W^2} \right), \end{aligned} \quad (2.24)$$

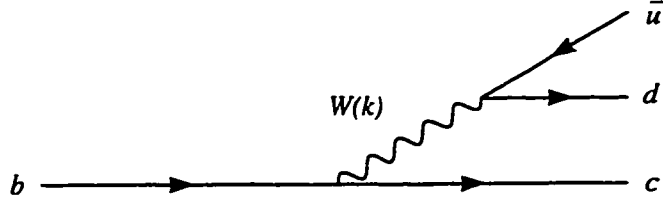


Figure 2.1: The tree-level Feynman diagram for the process $b \rightarrow c \bar{u} d$.

where the Fermi coupling constant (G_F) is defined as

$$\frac{G_F}{\sqrt{2}} = \frac{e^2}{8m_W^2 \sin^2 \theta_w}. \quad (2.25)$$

If the energies involved in the interaction are much smaller than the mass of the W boson ($k \ll m_W$), we can approximate the full amplitude by the first term only and neglect the rest of the terms in (2.24). However, this amplitude can be reached from a current \times current interaction, where, to first order, the S -matrix has the form

$$S = 1 - i \int d^4x \mathcal{H}_{\text{eff}}. \quad (2.26)$$

By comparison with (2.24), the effective Hamiltonian for the process $b \rightarrow c \bar{u} d$ is

$$\mathcal{H}_{\text{eff}} = \frac{G_F}{\sqrt{2}} V_{cb} V_{ud}^* (\bar{c}_i b_i)_L (\bar{d}_j u_j)_L. \quad (2.27)$$

where

$$(\bar{c}_i b_i)_L = \bar{c}_i \gamma^\mu (1 - \gamma_5) b_i, \quad (2.28)$$

and

$$(\bar{d}_j u_j)_L = \bar{d}_j \gamma^\mu (1 - \gamma_5) u_j. \quad (2.29)$$

The indices i and j represent color.

2.4 \mathcal{H}_{eff} in LL

When QCD effects are included, the effective Hamiltonian in (2.27) is generalized to [1, 3]

$$\mathcal{H}_{\text{eff}} = \frac{G_F}{\sqrt{2}} V_{cb} V_{ud}^* (C_1 Q_1 + C_2 Q_2), \quad (2.30)$$

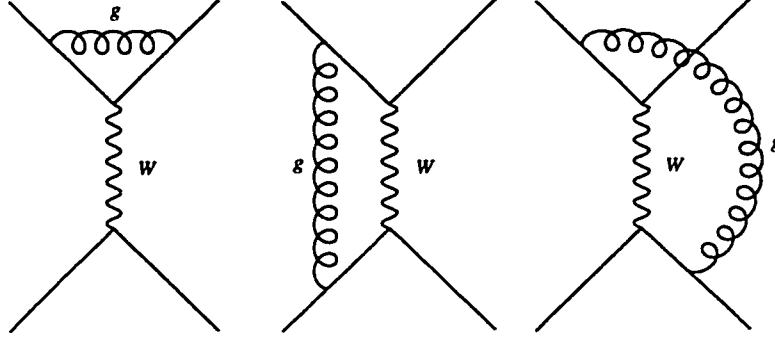


Figure 2.2: One loop current \times current tree diagrams in the full theory.

where

$$\begin{aligned} Q_1 &= (\bar{c}_i b_i)_L (\bar{d}_j u_j)_L, \\ Q_2 &= (\bar{c}_i b_j)_L (\bar{d}_j u_i)_L \end{aligned} \quad (2.31)$$

are current \times current local operators.

The Wilson Coefficients, C_1 and C_2 , are determined by requiring the effective Hamiltonian to reproduce the amplitude calculated in the full theory, i. e.

$$\mathcal{A}_{\text{full}} = \mathcal{A}_{\text{eff}} = -i \frac{G_F}{\sqrt{2}} V_{cb} V_{ud}^* (C_1 \langle Q_1 \rangle + C_2 \langle Q_2 \rangle). \quad (2.32)$$

This matching of the full theory onto the effective theory is done in three steps. First, $\mathcal{A}_{\text{full}}$ is calculated by evaluating the one loop current \times current diagrams in Fig. 2.2. In the calculation only logarithmic corrections of order $\alpha_s \ln()$ are kept while those terms containing constant contributions of order α_s are discarded. This corresponds to the leading logarithmic approximation (LL).

The second step, is to evaluate the matrix elements of the local operators O_1 and O_2 from Fig. 2.3. Unlike the full amplitude, the resulting matrix elements contain divergent terms that can not be removed by the QCD renormalization constants in (2.10). These will be called the bare matrix elements, $\langle Q_i^{(0)} \rangle$. They are related to the renormalized ones $\langle Q_i \rangle$, which have the divergent terms removed, by

$$\langle Q_i^{(0)} \rangle = Z_{ij} \langle Q_j \rangle, \quad (2.33)$$

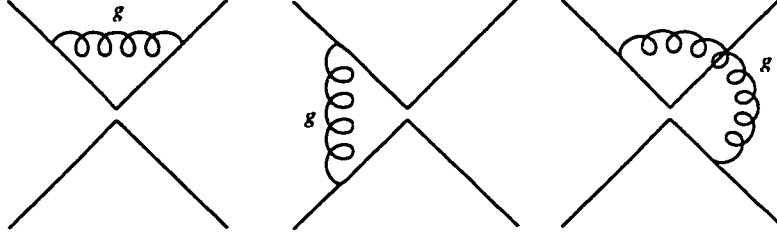


Figure 2.3: One loop current \times current tree diagrams in the Effective theory.

where Z_{ij} is a 2×2 matrix found to be [1, 3]

$$Z(\mu) = 1 + \frac{g^2}{(4\pi)^2} \frac{1}{\epsilon} \begin{pmatrix} 1 & -3 \\ -3 & 1 \end{pmatrix}. \quad (2.34)$$

Therefore, in order to be able to match the full theory and the effective theory, an additional renormalization of the local operators is needed.

So, the bare local operators should be used, instead, in evaluating \mathcal{A}_{eff} , such that

$$\begin{aligned} \frac{i\sqrt{2}}{G_F V_{cb} V_{ud}^*} \mathcal{A}_{\text{eff}} &= C_i^{(0)} \langle Q_i^{(0)} \rangle \\ &= C_i^{(0)} Z_{ij}(\mu) \langle Q_j(\mu) \rangle \\ &= (Z_{ij}^T(\mu) C_j^{(0)}) \langle Q_i(\mu) \rangle \\ &= C_i(\mu) \langle Q_i(\mu) \rangle, \end{aligned} \quad (2.35)$$

where the bare and renormalized Wilson coefficients are related by

$$C_i^{(0)} = (Z^{-1})_{ij}^T C_j. \quad (2.36)$$

2.4.1 Renormalization Group Equations

The last step, is to substitute the renormalized matrix elements, $\langle O_i \rangle$ into (2.32) and solve for the Wilson coefficients. The result is

$$\begin{aligned} C_1 &= 1 + \frac{\alpha_s}{4\pi} \ln \frac{m_W^2}{\mu^2}, \\ C_2 &= -3 \frac{\alpha_s}{4\pi} \ln \frac{m_W^2}{\mu^2}. \end{aligned} \quad (2.37)$$

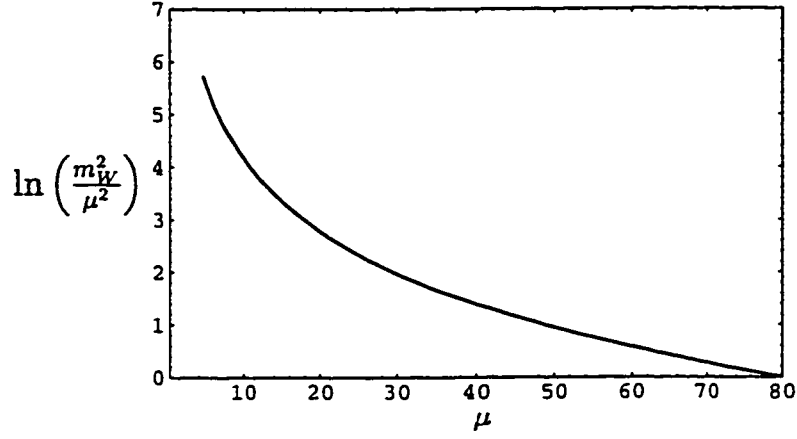


Figure 2.4: $\ln(m_W^2/\mu^2)$ for μ in the range m_b to m_W .

In this work, we are interested in the decay of B mesons. For such processes, the appropriate scale for normalizing the hadronic matrix elements is of the order of the decaying quark mass, i. e. $\mu = \mathcal{O}(m_b)$. This low scale, compared to m_W , creates large logarithms in (2.37) destroying the usefulness of ordinary perturbation theory. see Fig. 2.4.

The way out of this problem consists of two parts. First, Wilson coefficients are calculated at a scale where perturbation theory is valid. Then, the evolution matrix, derived from renormalization group equations (RGE), is used to evolve these values to the desired scale. This is called RG-improved perturbation theory.

At $\mu \approx m_W$ the logarithm $\ln(m_W^2/\mu^2)$ is very small justifying the use of ordinary perturbation theory. So, from (2.37) the Wilson coefficients in LL is given as

$$\begin{aligned} C_1(m_W) &= 1. \\ C_2(m_W) &= 0. \end{aligned} \tag{2.38}$$

Since the unrenormalized Wilson coefficients, $C_i^{(0)}$, are independent of μ , then, it is easy to derive from (2.36) the following RGE:

$$\mu \frac{d}{d\mu} \begin{pmatrix} C_1 \\ C_2 \end{pmatrix} = \gamma^T \begin{pmatrix} C_1 \\ C_2 \end{pmatrix} \tag{2.39}$$

where γ is the anomalous dimension matrix defined as

$$\gamma = \mu Z^{-1} \frac{dZ}{d\mu}. \quad (2.40)$$

From (2.13) and (2.34) we have

$$Z(\mu) = 1 + \frac{\mu^{-2\epsilon} g_0^2}{(4\pi)^2} \frac{1}{\epsilon} \begin{pmatrix} 1 & -3 \\ -3 & 1 \end{pmatrix}. \quad (2.41)$$

So,

$$\mu \frac{dZ}{d\mu} = -2 \frac{g^2}{(4\pi)^2} \begin{pmatrix} 1 & -3 \\ -3 & 1 \end{pmatrix}. \quad (2.42)$$

The anomalous dimension γ is then, up to lowest order in α_s ,

$$\gamma = \frac{\alpha_s}{4\pi} \gamma^{(0)}, \quad (2.43)$$

where

$$\gamma^{(0)} = \begin{pmatrix} -2 & 6 \\ 6 & -2 \end{pmatrix}. \quad (2.44)$$

In order to solve the RGE (2.39) let us first introduce the matrix V that diagonalizes $\gamma^{(0)T}$ such that

$$V^{-1} \gamma^{(0)T} V = \gamma_D. \quad (2.45)$$

Actually, the elements on the diagonal of γ_D are the eigenvalues of $\gamma^{(0)T}$ while the columns of V are the corresponding eigenvectors. So, we find that

$$V = \frac{1}{\sqrt{2}} \begin{pmatrix} -1 & 1 \\ 1 & 1 \end{pmatrix} = V^{-1}, \quad (2.46)$$

and

$$\gamma_D = \frac{\alpha_s}{4\pi} \begin{pmatrix} -8 & 0 \\ 0 & 4 \end{pmatrix} = \frac{\alpha_s}{4\pi} [\tilde{\gamma}^{(0)}]_D, \quad (2.47)$$

where $\tilde{\gamma}^{(0)}$ is a column vector containing the eigenvalues of $\gamma^{(0)}$ such that

$$\tilde{\gamma}^{(0)} = \begin{pmatrix} -8 \\ 4 \end{pmatrix}, \quad (2.48)$$

and the subscript D stands for diagonal matrix.

If we define the diagonal basis for the Wilson coefficients, C_{\pm} , such that

$$V^{-1} \begin{pmatrix} C_1 \\ C_2 \end{pmatrix} = \frac{1}{\sqrt{2}} \begin{pmatrix} C_2 - C_1 \\ C_2 + C_1 \end{pmatrix} = \begin{pmatrix} C_- \\ C_+ \end{pmatrix}, \quad (2.49)$$

and

$$\gamma_-^{(0)} = -8, \quad \gamma_+^{(0)} = 4, \quad (2.50)$$

then we can rewrite (2.39) as

$$\mu \frac{dC_{\pm}}{d\mu} = \frac{\alpha_s}{4\pi} \gamma_{\pm}^{(0)} C_{\pm}. \quad (2.51)$$

Using (2.18), the above equation can be written as

$$\frac{dC_{\pm}}{C_{\pm}} = -\frac{\gamma_{\pm}^{(0)}}{2\beta_0} \frac{d\alpha_s}{\alpha_s}, \quad (2.52)$$

which is easily solved to give

$$C_{\pm}(\mu) = \left(\frac{\alpha_s(m_W)}{\alpha_s(\mu)} \right)^{\frac{\gamma_{\pm}^{(0)}}{2\beta_0}} C_{\pm}(m_W). \quad (2.53)$$

Using the relation (2.49) we then have

$$\begin{pmatrix} C_1(\mu) \\ C_2(\mu) \end{pmatrix} = V \left[\frac{\alpha_s(m_W)}{\alpha_s(\mu)} \right]_D^{\frac{\gamma^{(0)}}{2\beta_0}} V^{-1} \begin{pmatrix} C_1(m_W) \\ C_2(m_W) \end{pmatrix}. \quad (2.54)$$

The following convention has been used to display the above results in a more compact form: if

$$\vec{a} = \begin{pmatrix} a_1 \\ \vdots \\ a_n \end{pmatrix}, \quad (2.55)$$

then

$$A^{\vec{a}} = \begin{pmatrix} A^{a_1} \\ \vdots \\ A^{a_n} \end{pmatrix}, \quad (2.56)$$

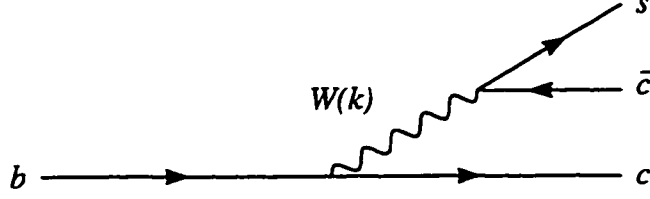


Figure 2.5: The tree-level Feynman diagram for the process $b \rightarrow c \bar{c} s$.

and

$$[A^{\bar{a}}]_D = \begin{pmatrix} A^{a_1} & & 0 \\ & \ddots & \\ 0 & & A^{a_2} \end{pmatrix}. \quad (2.57)$$

2.4.2 Penguin Contribution

Consider the process $b \rightarrow c \bar{c} s$ whose tree level Feynman diagram is shown in Fig. 2.5. Similar to (2.27), the effective Hamiltonian for this process, in the absence of QCD, is given by

$$\mathcal{H}_{\text{eff}} = \frac{G_F}{\sqrt{2}} V_{cb} V_{cs}^* (\bar{c}_i b_i)_L (\bar{s}_j c_j)_L. \quad (2.58)$$

When the effective Hamiltonian is extended to include QCD effects, the contribution of the penguin diagrams in Fig. 2.6a for the full theory and Fig. 2.6b for the effective theory should be considered beside the current \times current diagrams considered previously.

As a result, the effective Hamiltonian includes six local operators that mix and close under renormalization. Explicitly, this is given by

$$\mathcal{H}_{\text{eff}} = \frac{G_F}{\sqrt{2}} \left[V_{cb} V_{cs}^* (C_1 Q_1 + C_2 Q_2) - V_{tb} V_{ts}^* \sum_{i=3}^6 C_i Q_i \right], \quad (2.59)$$

where

$$Q_1 = (\bar{c}_i b_i)_L (\bar{s}_j c_j)_L,$$

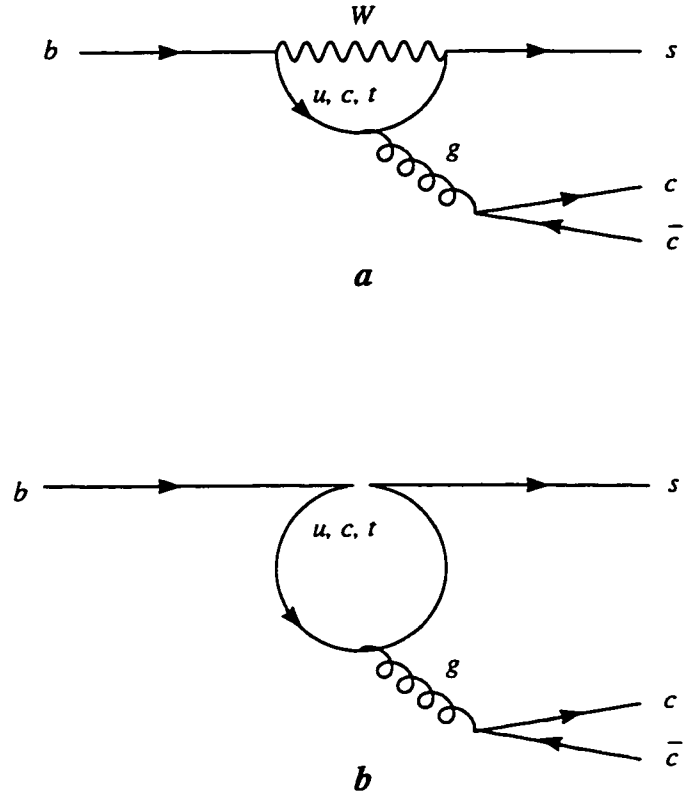


Figure 2.6: The Penguin Feynman diagrams for the process $b \rightarrow c \bar{c} s$. *a*: in the full theory, *b*: in the effective theory.

$$\begin{aligned}
Q_2 &= (\bar{c}_i b_j)_L (\bar{s}_j c_i)_L, \\
Q_3 &= (\bar{s}_i b_i)_L \sum_q (\bar{q}_j q_j)_L, \\
Q_4 &= (\bar{s}_i b_j)_L \sum_q (\bar{q}_j q_i)_L, \\
Q_5 &= (\bar{s}_i b_i)_L \sum_q (\bar{q}_j q_j)_R, \\
Q_6 &= (\bar{s}_i b_j)_L \sum_q (\bar{q}_j q_i)_R.
\end{aligned} \tag{2.60}$$

Operators O_3, \dots, O_6 are called penguin operators. In addition to the $(V - A)$ current defined in (2.28), these operators also include the $(V + A)$ current defined as

$$(\bar{q}_i q_i)_R = \bar{q}_i \gamma^\mu (1 + \gamma_5) q_i. \tag{2.61}$$

The summation in the penguin operators is carried over all the quarks in the effective theory.

The procedure of calculating the Wilson coefficients in (2.59) is similar to that performed previously except that we are dealing with six operators instead of two. Similar to (2.39), the RGE that controls the dependence of the Wilson coefficients on the renormalization scale is given by

$$\mu \frac{d}{d\mu} \begin{pmatrix} C_1 \\ \vdots \\ C_6 \end{pmatrix} = \gamma^T \begin{pmatrix} C_1 \\ \vdots \\ C_6 \end{pmatrix} \tag{2.62}$$

where, up to first order in α_s , [1, 3]

$$\begin{aligned}
\gamma &= \frac{\alpha_s}{4\pi} \gamma^{(0)} \\
&= \frac{\alpha_s}{4\pi} \begin{pmatrix} -2 & 6 & \frac{-2}{9} & \frac{2}{3} & \frac{-2}{9} & \frac{2}{3} \\ 6 & -2 & 0 & 0 & 0 & 0 \\ 0 & 0 & \frac{-22}{9} & \frac{22}{3} & \frac{-4}{9} & \frac{4}{3} \\ 0 & 0 & 6 - \frac{2}{9} N_f & -2 + \frac{2}{3} N_f & -\frac{2}{9} N_f & \frac{2}{3} N_f \\ 0 & 0 & 0 & 0 & 2 & -6 \\ 0 & 0 & -\frac{2}{9} N_f & \frac{2}{3} N_f & -\frac{2}{9} N_f & -16 + \frac{2}{3} N_f \end{pmatrix}.
\end{aligned} \tag{2.63}$$

By diagonalizing γ^T we can solve (2.62) above, as we did before, and use the convention (2.57) to write the solution as

$$\begin{pmatrix} C_1(\mu) \\ \vdots \\ C_6(\mu) \end{pmatrix} = V \left[\frac{\alpha_s(m_W)}{\alpha_s(\mu)} \right]_D^{\frac{\tilde{\gamma}^{(0)}}{2\beta_0}} V^{-1} \begin{pmatrix} C_1(m_W) \\ \vdots \\ C_6(m_W) \end{pmatrix}, \quad (2.64)$$

where V is the 6×6 matrix that diagonalizes $\gamma^{(0)T}$ such that

$$V^{-1} \gamma^{(0)T} V = [\tilde{\gamma}^{(0)}]_D. \quad (2.65)$$

2.4.3 Numerical Results

For $N_f = 5$ flavors (suitable for b -decays) the diagonalization of $\gamma^{(0)T}$ produces

$$\tilde{\gamma}^{(0)} = \begin{pmatrix} -8 \\ 4 \\ -6.49 \\ 2.23 \\ -13.8 \\ 6.27 \end{pmatrix}. \quad (2.66)$$

and the following value for V

$$V = \frac{1}{\sqrt{2}} \begin{pmatrix} -0.96 & 0.998 & 0 & 0 & 0 & 0 \\ 0.96 & 0.998 & 0 & 0 & 0 & 0 \\ -0.32 & -0.143 & -1.18 & -0.249 & 0.318 & 0.591 \\ 0.32 & -0.143 & 1.02 & -0.121 & -0.441 & 1.14 \\ 0 & 0 & 0.098 & -1.4 & 0.0696 & -0.46 \\ 0 & 0 & 0.2 & 0.514 & 1.3 & 0.388 \end{pmatrix}. \quad (2.67)$$

By extending (2.38) to include penguin operators we have

$$\begin{aligned} C_1(m_W) &= 1, \\ C_i(m_W) &= 0; \quad i = 2, \dots, 6. \end{aligned} \quad (2.68)$$

Table 2.1: Wilson Coefficients in LL at $\mu = 4.4, 4.6$ and 4.8 GeV, and for $\Lambda_{\overline{\text{MS}}}^5 = 225 \pm 85$ MeV. The last four rows are some useful combinations of $C_1(\mu)$ and $C_2(\mu)$.

	No QCD	$\mu = 4.4$ GeV	$\mu = 4.6$ GeV	$\mu = 4.8$ GeV
$C_1(\mu)$	1	1.132 ± 0.017	1.128 ± 0.016	1.125 ± 0.015
$C_2(\mu)$	0	-0.295 ± 0.030	-0.288 ± 0.029	-0.281 ± 0.028
$C_3(\mu)$	0	0.013 ± 0.002	0.013 ± 0.002	0.013 ± 0.002
$C_4(\mu)$	0	-0.030 ± 0.003	-0.029 ± 0.003	-0.029 ± 0.003
$C_5(\mu)$	0	0.009 ± 0.001	0.008 ± 0.001	0.008 ± 0.001
$C_6(\mu)$	0	-0.038 ± 0.004	-0.037 ± 0.004	-0.036 ± 0.004
a_1		1.034 ± 0.006	1.032 ± 0.006	1.031 ± 0.006
a_2		0.082 ± 0.025	0.088 ± 0.024	0.094 ± 0.023
C_2/a_1		-0.285 ± 0.027	-0.279 ± 0.027	-0.273 ± 0.026
C_1/a_2		13.72 ± 4.30	12.77 ± 3.60	11.99 ± 3.10

Using $\Lambda_{\overline{\text{MS}}}^5 = 225 \pm 85$ MeV [1] for the QCD scale constant in the effective theory of five flavors, we now calculate the Wilson coefficients from (2.64) at the scale of b -quark mass. The results are displayed in Table 2.1 for $\mu = 4.4, 4.6$ and 4.8 GeV.

It turns out that certain combinations of the Wilson Coefficients are particularly useful. The dependence of these quantities on μ is displayed in Table 2.1 and in Fig. 2.7 where a_1 and a_2 are defined as

$$a_1 = C_1 + \frac{C_2}{3}, \quad (2.69)$$

$$a_2 = C_2 + \frac{C_1}{3}. \quad (2.70)$$

2.5 \mathcal{H}_{eff} in NLL

In next-to-leading logarithmic (NLL) calculations, the terms containing constant contributions of order α_s are also kept in addition to the terms of order $\alpha_s \ln()$. This leads

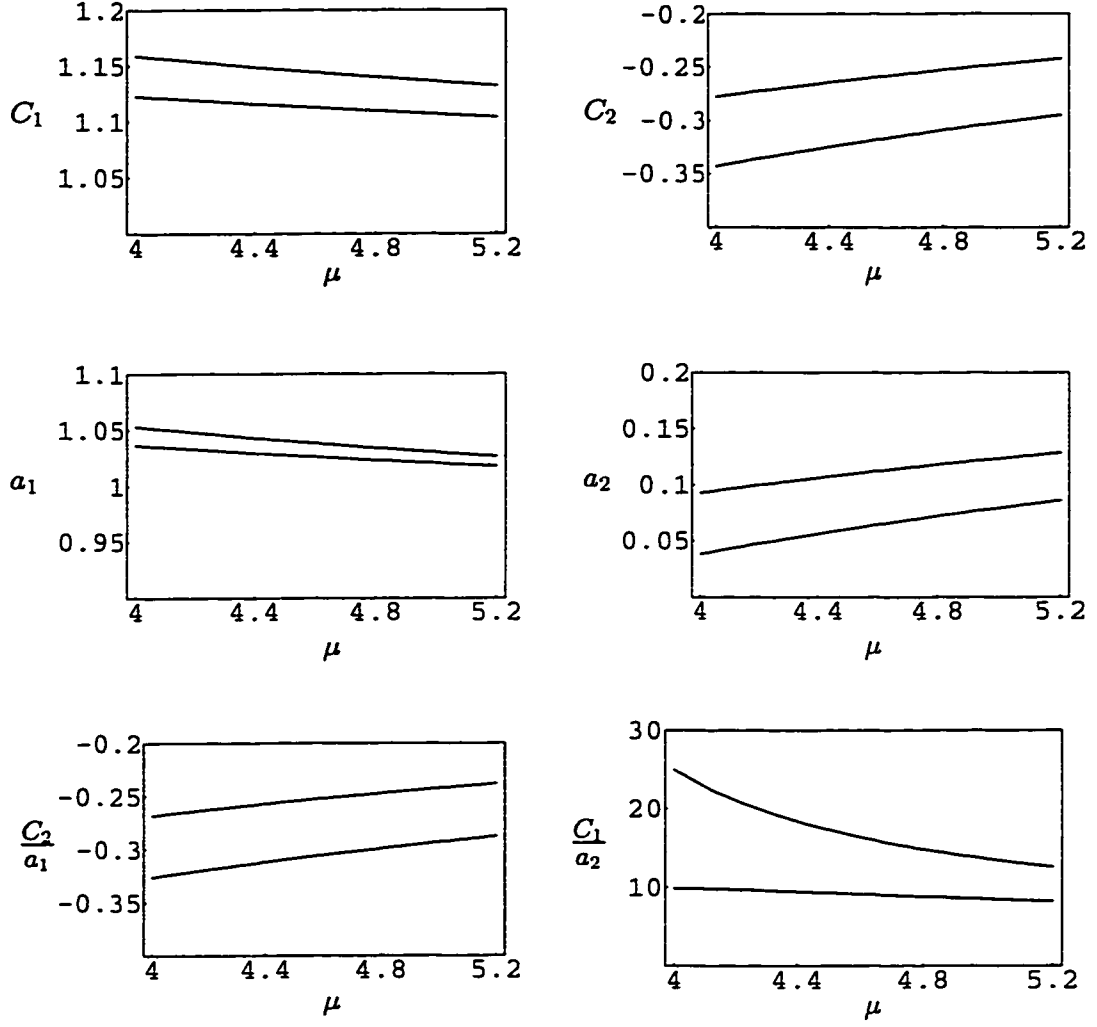


Figure 2.7: The coefficients C_1 , C_2 , a_1 , a_2 , C_2/a_1 and C_1/a_2 , in LL, as a function of μ for $\Lambda_{\overline{\text{MS}}}^5 = 225 + 85 \text{ MeV}$ and $\Lambda_{\overline{\text{MS}}}^5 = 225 - 85 \text{ MeV}$.

to modifications in the formulas derived in the previous section. Most importantly, the Wilson coefficients turn out to be regularization scheme dependent. However, if the matrix elements $\langle Q_i(\mu) \rangle$ are evaluated at the same scheme as the Wilson coefficients $C_i(\mu)$, the scheme dependence cancels out, and the effective Hamiltonian $C_i(\mu) \langle Q_i(\mu) \rangle$ becomes independent of the regularization scheme used.

In here, we choose to evaluate the Wilson coefficients using the naive dimensional regularization scheme (NDR). In this scheme, the method of dimensional regularization ($d = 4 - 2\epsilon$) is used to evaluate the divergent loop diagrams. Also, in NDR, the metric tensor in d dimensions and the commutation relations between the γ -matrices are given by [4]

$$g_{\mu\nu} = g_{\nu\mu}, \quad g_{\mu\rho}g_{\nu}^{\rho} = g_{\nu\mu}, \quad g_{\mu}^{\mu} = d, \quad (2.71)$$

and

$$\{\gamma_{\mu}, \gamma_{\nu}\} = 2g_{\mu\nu}, \quad \{\gamma_{\mu}, \gamma_5\} = 0. \quad (2.72)$$

In NLL, the anomalous dimension matrix in (2.63) extends to

$$\gamma = \frac{\alpha_s}{4\pi} \gamma^{(0)} + \left(\frac{\alpha_s}{4\pi} \right)^2 \gamma^{(1)}, \quad (2.73)$$

where [3]

$$\gamma_{\text{NDR}}^{(1)} = \begin{pmatrix} -\frac{21}{2} - \frac{2}{9}N_f & \frac{7}{2} + \frac{2}{3}N_f & -\frac{202}{243} & \frac{1354}{81} & -\frac{1192}{243} & \frac{904}{81} \\ \frac{7}{2} + \frac{2}{3}N_f & -\frac{21}{2} - \frac{2}{9}N_f & \frac{79}{9} & -\frac{7}{3} & -\frac{65}{9} & -\frac{7}{3} \\ 0 & 0 & -\frac{5911}{486} + \frac{71}{9}N_f & \frac{5983}{162} + \frac{1}{3}N_f & -\frac{2384}{243} - \frac{71}{9}N_f & \frac{1808}{81} - \frac{1}{3}N_f \\ 0 & 0 & \frac{379}{18} + \frac{56}{243}N_f & -\frac{91}{6} + \frac{808}{81}N_f & -\frac{130}{9} - \frac{502}{243}N_f & -\frac{14}{3} + \frac{646}{81}N_f \\ 0 & 0 & -\frac{61}{9}N_f & -\frac{11}{3}N_f & \frac{71}{3} + \frac{61}{9}N_f & -99 + \frac{11}{3}N_f \\ 0 & 0 & -\frac{682}{243}N_f & \frac{106}{81}N_f & -\frac{225}{2} + \frac{1676}{243}N_f & -\frac{1343}{6} + \frac{1348}{81}N_f \end{pmatrix}. \quad (2.74)$$

The Wilson coefficients in NDR are then given by [3]

$$\begin{pmatrix} C_1(\mu) \\ \vdots \\ C_6(\mu) \end{pmatrix} =$$

$$\left(1 + \frac{\alpha_s(\mu)}{4\pi} J\right) V \left[\frac{\alpha_s(m_W)}{\alpha_s(\mu)} \right]_D^{\frac{\gamma^{(0)}}{2\beta_0}} V^{-1} \left(1 - \frac{\alpha_s(m_W)}{4\pi} J\right) \begin{pmatrix} C_1(m_W) \\ \vdots \\ C_6(m_W) \end{pmatrix}. \quad (2.75)$$

In the above equation, V is the 6×6 matrix, defined in (2.65), which diagonalizes $\gamma^{(0)T}$, whereas J is defined as

$$J = V S V^{-1}, \quad (2.76)$$

where

$$S_{ij} = \delta_{ij} \gamma_i^{(0)} \frac{\beta_1}{2\beta_0^2} - \frac{G_{ij}}{2\beta_0 + \gamma_i^{(0)} - \gamma_j^{(0)}}, \quad (2.77)$$

and

$$G = V^{-1} \gamma^{(1)T} V. \quad (2.78)$$

In order to calculate the Wilson coefficients in NLL from (2.75), we need the values of $C_i(m_W)$. In NDR, these are given by [3]

$$\begin{pmatrix} C_1(m_W) \\ C_2(m_W) \\ C_3(m_W) \\ C_4(m_W) \\ C_5(m_W) \\ C_6(m_W) \end{pmatrix} = \begin{pmatrix} 1 - \frac{11}{6} \frac{\alpha_s(m_W)}{4\pi} \\ \frac{11}{2} \frac{\alpha_s(m_W)}{4\pi} \\ -\frac{\alpha_s(m_W)}{24\pi} E(x_t) \\ \frac{\alpha_s(m_W)}{8\pi} E(x_t) \\ -\frac{\alpha_s(m_W)}{24\pi} E(x_t) \\ \frac{\alpha_s(m_W)}{8\pi} E(x_t) \end{pmatrix} \quad (2.79)$$

where

$$E(x) = -\frac{2}{3} - \frac{2}{3} \ln x + \frac{x^2(15 - 16x + 4x^2)}{6(1-x)^4} \ln x + \frac{x(18 - 11x - x^2)}{12(1-x)^3}, \quad (2.80)$$

and

$$x_t = \frac{m_t^2}{m_W^2}. \quad (2.81)$$

Using the above values for $C_i(m_W)$, we calculated from (2.75) the values of the Wilson coefficients in NDR at the three scales $\mu = 4.4, 4.6$ and 4.8 GeV. The results are shown in Table 2.2

Table 2.2: NLL Wilson Coefficients in NDR at $\mu = 4.4, 4.6$ and 4.8 GeV, and for $\Lambda_{\overline{\text{MS}}}^5 = 225$. The last four rows are some useful combinations of $C_1(\mu)$ and $C_2(\mu)$.

	$\mu = 4.4$ GeV	$\mu = 4.6$ GeV	$\mu = 4.8$ GeV
$C_1(\mu)$	1.079	1.076	1.073
$C_2(\mu)$	-0.185	-0.179	-0.174
$C_3(\mu)$	0.012	0.012	0.012
$C_4(\mu)$	-0.034	-0.033	-0.033
$C_5(\mu)$	0.010	0.010	0.009
$C_6(\mu)$	-0.041	-0.040	-0.039
a_1	1.017	1.016	1.015
a_2	0.175	0.179	0.184
C_2/a_1	-0.182	-0.176	-0.171
C_1/a_2	6.172	5.998	5.843

Bibliography

- [1] G. Buchalla, A. Buras and M. Lautenbacher, Rev. M. Phys. **68**, 1125 (1996).
- [2] F. Gross, *Relativistic Quantum Mechanics and Field Theory*, (John Wiley & Sons, New York, 1993).
- [3] A. J. Buras, M. Jamin, M. Lautenbacher and P. Weisz, Nucl. Phys. B **370**, 69 (1992).
- [4] A. J. Buras and P. Weisz, Nucl. Phys. B **333**, 66 (1990).

Chapter 3

Amplitudes and Formfactors

3.1 Current Matrix Elements

Let $|I\rangle$ and $|P\rangle$ be pseudoscalar mesons and $|V\rangle$ be a vector meson. Since it is not possible, until now, to do reliable nonperturbative QCD calculations, these hadronic states are not known. However, the hadronic current matrix elements can be decomposed in terms of formfactors and decay constants using Lorentz invariance. So, we can write [1]:

$$\langle P|J_\mu|0\rangle = f_P(p_P)_\mu, \quad (3.1)$$

$$\langle V|J_\mu|0\rangle = m_V f_V \epsilon_\mu^*, \quad (3.2)$$

$$\langle P|J_\mu|I\rangle = \left(p_I + p_P - \frac{m_I^2 - m_P^2}{q^2} q\right)_\mu F_1(q^2) + \frac{m_I^2 - m_P^2}{q^2} q_\mu F_0(q^2). \quad (3.3)$$

$$\begin{aligned} \langle V|J_\mu|I\rangle = & \frac{-2i}{m_I + m_V} \epsilon_{\mu\nu\rho\sigma} \epsilon^{\nu*} p_I^\rho p_V^\sigma V(q^2) \\ & + (m_I + m_V) \epsilon_\mu^* A_1(q^2) - \frac{\epsilon^* \cdot q}{m_I + m_V} (p_I + p_V)_\mu A_2(q^2) \\ & - 2 m_V \frac{\epsilon^* \cdot q}{q^2} q_\mu (A_3(q^2) - A_0(q^2)) \end{aligned} \quad (3.4)$$

with

$$q_\mu = (p_I - p_{P(V)})_\mu, \quad (3.5)$$

$$A_3(q^2) = \frac{m_I + m_V}{2m_V} A_1(q^2) - \frac{m_I - m_V}{2m_V} A_2(q^2). \quad (3.6)$$

and

$$F_1(0) = F_0(0), \quad (3.7)$$

$$A_1(0) = A_3(0). \quad (3.8)$$

Evaluating the contractions of the above current matrix elements will be useful in studying the processes of interest in this work. This is because in the factorization scheme the matrix element of the product of two currents is equal to the product of the matrix elements of the currents. So, let us first evaluate

$$\langle P_1 | J_\mu | I \rangle \langle P_2 | J^\mu | 0 \rangle \quad (3.9)$$

where

$$p_I = p_{P_1} + p_{P_2}, \quad (3.10)$$

$$q = p_I - p_{P_1} = p_{P_2}. \quad (3.11)$$

From (3.1) and (3.3) we find that

$$\langle P_1 | J_\mu | I \rangle \langle P_2 | J^\mu | 0 \rangle = (m_I^2 - m_{P_1}^2) f_{P_2} F_0(q^2). \quad (3.12)$$

Similarly, we find that

$$\langle P | J_\mu | I \rangle \langle V | J^\mu | 0 \rangle = 2m_V f_V (\epsilon^\mu \cdot p_I) F_1(q^2). \quad (3.13)$$

$$\langle V | J_\mu | I \rangle \langle P | J^\mu | 0 \rangle = 2m_V f_P (\epsilon^\mu \cdot p_I) A_0(q^2). \quad (3.14)$$

and

$$\begin{aligned} \langle V_1 | J_\mu | I \rangle \langle V_2 | J^\mu | 0 \rangle &= -\frac{m_{V_2}}{m_I + m_{V_1}} f_{V_2} \left[2i \epsilon_{\mu\nu\rho\sigma} \epsilon_2^{\mu} \epsilon_1^{\nu} p_{V_2}^\rho p_{V_1}^\sigma V(q^2) \right. \\ &\quad \left. - (m_I + m_{V_1})^2 (\epsilon_1^\mu \cdot \epsilon_2^\mu) A_1(q^2) \right. \\ &\quad \left. + 2 (\epsilon_1^\mu \cdot p_{V_2}) (\epsilon_2^\mu \cdot p_{V_1}) A_2(q^2) \right], \end{aligned} \quad (3.15)$$

where ϵ , ϵ_1 and ϵ_2 are the polarization vectors of V , V_1 and V_2 respectively.

In decay rate calculations we often find that the absolute square of the above current matrix elements, summed over all final state polarizations, are needed. Since the absolute square of (3.12) is obvious, we consider first (3.13). This leads to

$$\sum_{r=1}^3 |\langle P|J_\mu|I\rangle \langle V|J^\mu|0\rangle|^2 = 4m_V^2 |f_V|^2 \sum_{r=1}^3 |\epsilon_r^\star \cdot p_I|^2 |F_1(q^2)|^2. \quad (3.16)$$

where r is the polarization index. However,

$$\begin{aligned} \sum_{r=1}^3 |\epsilon_r^\star \cdot p_I|^2 &= (P_I)_\mu (P_I)_\nu \sum_{r=1}^3 \epsilon_r^{\star\mu} \epsilon_r^{\nu} \\ &= (P_I)_\mu (P_I)_\nu \left[-g^{\mu\nu} + \frac{(P_V)^\mu (P_V)^\nu}{m_V^2} \right] \\ &= |\mathbf{k}|^2 \frac{m_I^2}{m_V^2}, \end{aligned} \quad (3.17)$$

where $|\mathbf{k}|$ (given explicitly in (C.29)) is the momentum of the decay products in I rest-frame. So, we end up with

$$\sum_{r=1}^3 |\langle P|J_\mu|I\rangle \langle V|J^\mu|0\rangle|^2 = 4m_I^2 |f_V|^2 |\mathbf{k}|^2 |F_1(q^2)|^2. \quad (3.18)$$

Similarly, from (3.14) we find that

$$\sum_{r=1}^3 |\langle V|J_\mu|I\rangle \langle P|J^\mu|0\rangle|^2 = 4m_I^2 |f_P|^2 |\mathbf{k}|^2 |A_0(q^2)|^2. \quad (3.19)$$

Regarding the current matrix element (3.15), let us first evaluate it for the three possible helicities of the final state using (A.34 - A.39) derived in Appendix A. The result is

$$\langle V_1|J_\mu|I\rangle \langle V_2|J^\mu|0\rangle_0 = -f_{V_2} m_{V_2} (m_I + m_{V_1}) A_1^{IV_1}(q^2) (a - b x), \quad (3.20)$$

$$\langle V_1|J_\mu|I\rangle \langle V_2|J^\mu|0\rangle_\pm = f_{V_2} m_{V_2} (m_I + m_{V_1}) A_1^{IV_1}(q^2) (1 \mp c y). \quad (3.21)$$

where [2],

$$a = \frac{m_I^2 - m_{V_2}^2 - m_{V_1}^2}{2m_{V_2} m_{V_1}},$$

$$\begin{aligned}
b &= \frac{2|\mathbf{k}|^2 m_I^2}{m_{V_2} m_{V_1} (m_I + m_{V_1})^2}, \\
c &= \frac{2|\mathbf{k}| m_I}{(m_I + m_{V_1})^2}, \\
x &= \frac{A_2^{IV_1}(q^2)}{A_1^{IV_1}(q^2)}, \\
y &= \frac{V^{IV_1}(q^2)}{A_1^{IV_1}(q^2)}.
\end{aligned} \tag{3.22}$$

The absolute square of (3.15) is given by

$$|\langle V_1 | J_\mu | I \rangle \langle V_2 | J^\mu | 0 \rangle|^2 = m_{V_2}^2 (m_I + m_{V_1})^2 |f_{V_2}|^2 |A_1^{IV_1}(q^2)|^2 \left[(a - b x)^2 + 2(1 + c^2 y^2) \right]. \tag{3.23}$$

3.2 Decay Amplitudes

Using the results of the previous section, it is now easy to write down the decay amplitudes and decay rates for the processes considered in this work, assuming factorization. This means keeping only those terms in the amplitudes that can be factorized as in (3.12 - 3.15). The nonfactorizable terms, are parameterized and studied in different ways in the chapters that follow. This will result in modifications to the formulas of this section.

3.2.1 Type $b \rightarrow c\bar{u}d$ processes: Class I

These are Cabibbo-favored processes that have $b \rightarrow c\bar{u}d$ as the basic process (see Fig. 2.1). The effective Hamiltonian, appropriate for such processes, has been derived in the previous chapter to be

$$\mathcal{H}_{\text{eff}} = \frac{G_F}{\sqrt{2}} V_{cb} V_{ud}^* \left[C_1 (\bar{c}_i b_i)_L (\bar{d}_j u_j)_L + C_2 (\bar{c}_i u_i)_L (\bar{d}_j b_j)_L \right], \tag{3.24}$$

where the values of the Wilson coefficients C_1 and C_2 are taken from Table 2.1. In what follows the color indices will be suppressed. Also, the index L indicating a left-handed current will be dropped.

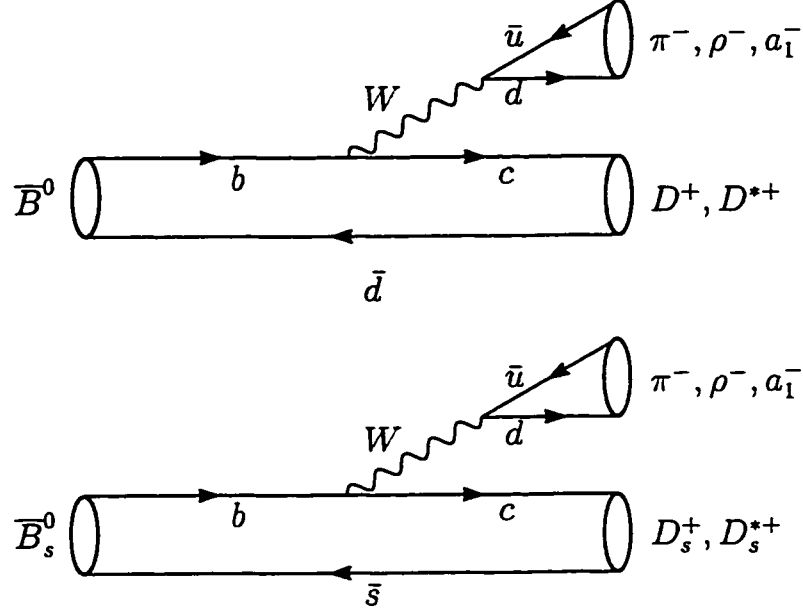


Figure 3.1: The flavor flow diagrams for class I processes of the type $b \rightarrow \bar{c}ud$.

The decays that proceed via an external W emission are called processes of class I or color favored. In Fig. 3.1. we show the flavor flow diagram for the processes of this class considered in this subsection.

In order to derive the decay amplitudes and decay rates for these processes, we need to rewrite the effective Hamiltonian in (3.24) using Fierz transformations (see Appendix B). The result is

$$\mathcal{H}_{\text{eff}} = \frac{G_F}{\sqrt{2}} V_{cb} V_{ud}^* \left[a_1 (\bar{c}b) (\bar{d}u) + C_2 \mathcal{H}^{(8)} \right], \quad (3.25)$$

where

$$a_1 = \left(C_1 + \frac{C_2}{N_c} \right), \quad (3.26)$$

and

$$\mathcal{H}^{(8)} = \frac{1}{2} \sum_a (\bar{c} \lambda^a b) (\bar{d} \lambda^a u). \quad (3.27)$$

N_c is the number of colors (taken to be 3) and λ^a are the Gell-Mann matrices.

- $\bar{B}^0 \rightarrow D^+ \pi^-$ and $\bar{B}_s^0 \rightarrow D_s^+ \pi^-$ Decays

The decay amplitude for the process $\bar{B}^0 \rightarrow D^+ \pi^-$ is given by

$$\begin{aligned} \mathcal{A}(\bar{B}^0 \rightarrow D^+ \pi^-) &= \langle D^+ \pi^- | \mathcal{H}_{\text{eff}} | \bar{B}^0 \rangle \\ &= \frac{G_F}{\sqrt{2}} V_{cb} V_{ud}^* \left[a_1 \langle D^+ \pi^- | (\bar{c}b)(\bar{d}u) | \bar{B}^0 \rangle + C_2 \langle D^+ \pi^- | \mathcal{H}^{(8)} | \bar{B}^0 \rangle \right]. \end{aligned} \quad (3.28)$$

The second term on the right hand side of (3.28) is nonfactorizable, while the first term receives both factorizable and nonfactorizable contributions. So we write

$$\begin{aligned} \mathcal{A}(\bar{B}^0 \rightarrow D^+ \pi^-) &= \frac{G_F}{\sqrt{2}} V_{cb} V_{ud}^* a_1 \left[\langle D^+ | (\bar{c}b) | \bar{B}^0 \rangle \langle \pi^- | (\bar{d}u) | 0 \rangle \right. \\ &\quad \left. + \langle D^+ \pi^- | (\bar{c}b)(\bar{d}u) | \bar{B}^0 \rangle^{nf} + \frac{C_2}{a_1} \langle D^+ \pi^- | \mathcal{H}^{(8)} | \bar{B}^0 \rangle^{nf} \right]. \end{aligned} \quad (3.29)$$

The current matrix elements in the first term above, can now be decomposed as in (3.12). Since, in this chapter, we are keeping only the factorizable terms, the decay amplitude for the process $\bar{B}^0 \rightarrow D^+ \pi^-$ is written as

$$\mathcal{A}_f(\bar{B}^0 \rightarrow D^+ \pi^-) = \frac{G_F}{\sqrt{2}} V_{cb} V_{ud}^* a_1 f_\pi (m_B^2 - m_D^2) F_0^{BD}(q^2). \quad (3.30)$$

The decay rate for this exclusive channel is then given by (see Appendix C),

$$\begin{aligned} \Gamma_f(\bar{B}^0 \rightarrow D^+ \pi^-) &= (\text{phase space factor}) \times |\mathcal{A}_f(\bar{B}^0 \rightarrow D^+ \pi^-)|^2 \\ &= \frac{G_F^2}{16\pi m_B^2} |\mathbf{k}| |V_{cb}|^2 |V_{ud}|^2 |a_1|^2 |f_\pi|^2 (m_B^2 - m_D^2)^2 |F_0^{BD}(m_\pi^2)|^2, \end{aligned} \quad (3.31)$$

where the subscript f in \mathcal{A}_f and Γ_f indicates that only the factorizable parts were considered in the evaluation of these quantities.

The decay amplitude and decay rate for the process $\bar{B}_s^0 \rightarrow D_s^+ \pi^-$ are found from above by replacing B by B_s and D by D_s .

- $\bar{B}^0 \rightarrow D^+ \rho^-(a_1^-)$ and $\bar{B}_s^0 \rightarrow D_s^+ \rho^-(a_1^-)$ Decays

In calculating the decay amplitude and decay rate for the process $\bar{B}^0 \rightarrow D^+ \rho^-$ we follow a procedure similar to that used above for the process $\bar{B}^0 \rightarrow D^+ \pi^-$. However, unlike the pion, ρ^- is a vector particle. So, from (3.13) and (3.18) we have

$$\mathcal{A}_f(\bar{B}^0 \rightarrow D^+ \rho^-) = \frac{G_F}{\sqrt{2}} V_{cb} V_{ud}^* a_1 f_\rho 2 m_\rho (\epsilon^\mu \cdot p_B) F_1^{BD}(q^2), \quad (3.32)$$

and

$$\Gamma_f(\bar{B}^0 \rightarrow D^+ \rho^-) = \frac{G_F^2}{4\pi} |\mathbf{k}|^3 |V_{cb}|^2 |V_{ud}|^2 |a_1|^2 |f_\rho|^2 |F_1^{BD}(m_\rho^2)|^2. \quad (3.33)$$

The decay amplitude and decay rate for the process $\bar{B}^0 \rightarrow D^+ a_1^-$ are found from above by replacing ρ^- by a_1^- . Regarding the processes $\bar{B}_s^0 \rightarrow D_s^+ \rho^- (a_1^-)$, the decay amplitude and decay rate are found by replacing B by B_s and D by D_s .

• $\bar{B}^0 \rightarrow D^{*+} \pi^-$ and $\bar{B}_s^0 \rightarrow D_s^{*+} \pi^-$ Decays

For the process $\bar{B}^0 \rightarrow D^{*+} \pi^-$ we use (3.14) and (3.19) to write down the decay amplitude and decay rate. The result is

$$\mathcal{A}_f(\bar{B}^0 \rightarrow D^{*+} \pi^-) = \frac{G_F}{\sqrt{2}} V_{cb} V_{ud}^* a_1 f_\pi 2 m_{D^*} (\epsilon^\mu \cdot p_B) A_0^{BD^*}(q^2), \quad (3.34)$$

$$\Gamma_f(\bar{B}^0 \rightarrow D^{*+} \pi^-) = \frac{G_F^2}{4\pi} |\mathbf{k}|^3 |V_{cb}|^2 |V_{ud}|^2 |a_1|^2 |f_\pi|^2 |A_0^{BD^*}(q^2)|^2. \quad (3.35)$$

The decay amplitude and decay rate for the process $\bar{B}_s^0 \rightarrow D_s^{*+} \pi^-$ are found from above by replacing B by B_s and D by D_s .

• $\bar{B}^0 \rightarrow D^{*+} \rho^- (a_1^-)$ and $\bar{B}_s^0 \rightarrow D_s^{*+} \rho^- (a_1^-)$ Decays

For the process $\bar{B}^0 \rightarrow D^{*+} \rho^-$, where we have two vector particles in the final state, the decay amplitude is given by

$$\begin{aligned} \mathcal{A}_f(\bar{B}^0 \rightarrow D^{*+} \rho^-) = & -\frac{G_F}{\sqrt{2}} V_{cb} V_{ud}^* a_1 f_\rho \left(\frac{m_\rho}{m_B + m_{D^*}} \right) \\ & \times \left[2i \epsilon_{\mu\nu\alpha\beta} \epsilon_\rho^\mu \epsilon_{D^*}^\nu p_\rho^\alpha p_{D^*}^\beta V^{BD^*}(q^2) \right. \\ & - (m_B + m_{D^*})^2 (\epsilon_\rho^\mu \cdot \epsilon_{D^*}^\mu) A_1^{BD^*}(q^2) \\ & \left. + 2 (\epsilon_\rho^\mu \cdot p_{D^*}) (\epsilon_{D^*}^\mu \cdot p_\rho) A_2^{BD^*}(q^2) \right]. \end{aligned} \quad (3.36)$$

Since the decaying particle is a pseudoscalar, from conservation of angular momentum the two vector mesons in the final state must have the same helicity. Using the three current matrix elements derived in (3.20) and (3.21), we can calculate the three corresponding helicity amplitudes for this decay. These are given by

$$\mathcal{A}_0 = -\frac{G_F}{\sqrt{2}} V_{cb} V_{ud}^* a_1 f_\rho m_\rho (m_B + m_{D^*}) A_1^{BD^*}(q^2) [a - b x] , \quad (3.37)$$

$$\mathcal{A}_\pm = \frac{G_F}{\sqrt{2}} V_{cb} V_{ud}^* a_1 f_\rho m_\rho (m_B + m_{D^*}) A_1^{BD^*}(q^2) [1 \mp c y] . \quad (3.38)$$

where a, b, c, x and y are defined in (3.22).

The decay rate is obtained from (3.23) to be,

$$\begin{aligned} \Gamma_f(\bar{B}^0 \rightarrow D^{*+} \rho^-) &= \frac{|\mathbf{k}|}{8\pi m_B^2} (|\mathcal{A}_0|^2 + |\mathcal{A}_+|^2 + |\mathcal{A}_-|^2) \\ &= \frac{G_F^2}{16\pi m_B^2} |\mathbf{k}| |V_{cb}|^2 |V_{ud}|^2 |a_1|^2 |f_\rho|^2 m_\rho^2 (m_B + m_{D^*})^2 |A_1^{BD^*}(m_\rho^2)|^2 \\ &\quad \times \left[(a - b x)^2 + 2(1 + c^2 y^2) \right] . \end{aligned} \quad (3.39)$$

The longitudinal (P_0) and transverse (P_\pm) polarizations of the final state are defined as

$$P_0 = \frac{|\mathcal{A}_0|^2}{|\mathcal{A}_0|^2 + |\mathcal{A}_+|^2 + |\mathcal{A}_-|^2} , \quad (3.40)$$

$$P_\pm = \frac{|\mathcal{A}_\pm|^2}{|\mathcal{A}_0|^2 + |\mathcal{A}_+|^2 + |\mathcal{A}_-|^2} . \quad (3.41)$$

The decay amplitude and decay rate for the process $\bar{B}^0 \rightarrow D^{*+} a_1^-$ are found from above by replacing ρ^- by a_1^- . Whereas for the processes $\bar{B}_s^0 \rightarrow D_s^{*+} \rho^-(a_1^-)$ they are found by replacing B by B_s and D by D_s .

3.2.2 Type $b \rightarrow c\bar{u}d$ processes: Class II

The decays that proceed via an internal W emission are called processes of class II or color suppressed. In Fig. 3.2, we show the flavor flow diagram for the processes of this class considered in this section.

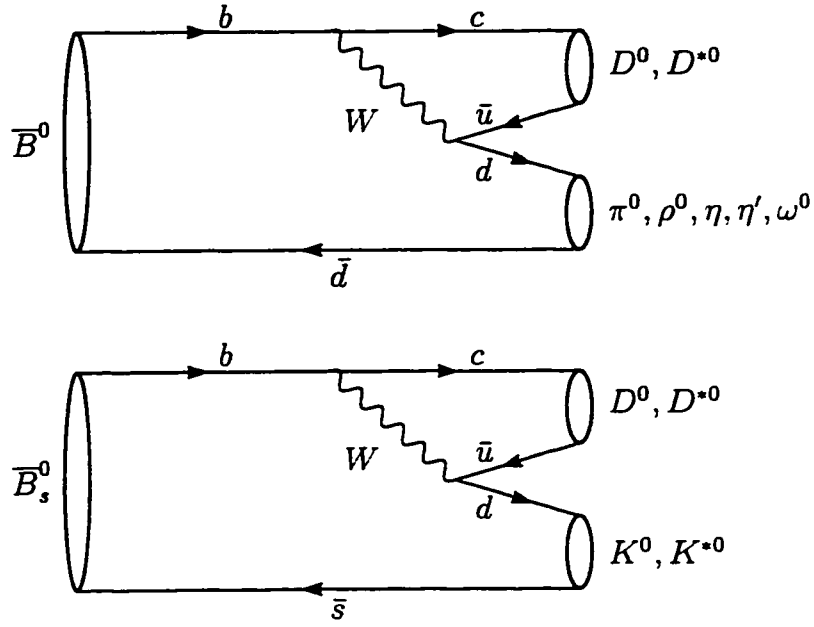


Figure 3.2: The flavor flow diagrams for class II processes of the type $b \rightarrow c\bar{u}d$.

The effective Hamiltonian, in this case, is written from (3.24) and using Fierz transformations as

$$\mathcal{H}_{\text{eff}} = \frac{G_F}{\sqrt{2}} V_{cb} V_{ud}^* \left[a_2 (\bar{c}u) (\bar{d}b) + C_2 \mathcal{H}^{(8)} \right] . \quad (3.42)$$

where

$$a_2 = \left(C_2 + \frac{C_1}{N_c} \right) , \quad (3.43)$$

and

$$\mathcal{H}^{(8)} = \frac{1}{2} \sum_a (\bar{c} \lambda^a u) (\bar{d} \lambda^a b) . \quad (3.44)$$

• $\bar{B}^0 \rightarrow D^0 \pi^0$ Decay

The decay amplitude for this process is given by

$$\begin{aligned} \mathcal{A}(\bar{B}^0 \rightarrow D^0 \pi^0) &= \langle D^0 \pi^0 | \mathcal{H}_{\text{eff}} | \bar{B}^0 \rangle \\ &= \frac{G_F}{\sqrt{2}} V_{cb} V_{ud}^* \left[a_2 \langle D^0 \pi^0 | (\bar{c}u) (\bar{d}b) | \bar{B}^0 \rangle + C_1 \langle D^0 \pi^0 | \mathcal{H}^{(8)} | \bar{B}^0 \rangle \right] . \end{aligned} \quad (3.45)$$

The second term on the right hand side of (3.45) is nonfactorizable, while the first term receives both factorizable and nonfactorizable contributions. So we write

$$\begin{aligned} \mathcal{A}(\bar{B}^0 \rightarrow D^0 \pi^0) &= \frac{G_F}{\sqrt{2}} V_{cb} V_{ud}^* a_2 \left[\langle D^0 | (\bar{c}u) | 0 \rangle \langle \pi^0 | (\bar{d}b) | \bar{B}^0 \rangle \right. \\ &\quad \left. + \langle D^0 \pi^0 | (\bar{c}u) (\bar{d}b) | \bar{B}^0 \rangle^{\text{nf}} + \frac{C_1}{a_2} \langle D^0 \pi^0 | \mathcal{H}^{(8)} | \bar{B}^0 \rangle^{\text{nf}} \right]. \end{aligned} \quad (3.46)$$

To write down the decay amplitude in terms of decay constants and formfactors, we proceed as we did previously for the decay $\bar{B}^0 \rightarrow D^+ \pi^-$. However, π^0 is mixture of $|u\bar{u}\rangle$ and $|d\bar{d}\rangle$ states. So an additional factor of $1/\sqrt{2}$ appears in the amplitude. The result is

$$\mathcal{A}_f(\bar{B}^0 \rightarrow D^0 \pi^0) = \frac{G_F}{2} V_{cb} V_{ud}^* a_2 f_D (m_B^2 - m_\pi^2) F_0^{B\pi}(q^2). \quad (3.47)$$

The decay rate is then given by,

$$\Gamma_f(\bar{B}^0 \rightarrow D^0 \pi^0) = \frac{G_F^2}{32\pi m_B^2} |\mathbf{k}| |V_{cb}|^2 |V_{ud}|^2 |a_2|^2 |f_D|^2 (m_B^2 - m_\pi^2)^2 |F_0^{B\pi}(m_D^2)|^2. \quad (3.48)$$

• $\bar{B}^0 \rightarrow D^0 \eta(\eta')$ Decays

The calculation of the decay amplitude for the process $\bar{B}^0 \rightarrow D^0 \eta$ is similar to that performed above for the process $\bar{B}^0 \rightarrow D^0 \pi^0$. However, an appropriate mixing factor should be used due to $\eta - \eta'$ mixing (see Appendix D). As a result, we have

$$\mathcal{A}_f(\bar{B}^0 \rightarrow D^0 \eta) = \frac{G_F}{\sqrt{2}} V_{cb} V_{ud}^* a_2 f_D C_\eta^d (m_B^2 - m_\eta^2) F_0^{B\eta}(q^2), \quad (3.49)$$

$$\Gamma_f(\bar{B}^0 \rightarrow D^0 \eta) = \frac{G_F^2}{16\pi m_B^2} |\mathbf{k}| |V_{cb}|^2 |V_{ud}|^2 |a_2|^2 |f_D|^2 |C_\eta^d|^2 (m_B^2 - m_\eta^2)^2 |F_0^{B\eta}(m_D^2)|^2. \quad (3.50)$$

where C_η^d is defined in (D.6).

The decay amplitude and decay rate for the process $\bar{B}^0 \rightarrow D^0 \eta'$ are found from above by replacing η with η' .

- $\overline{B}^0 \rightarrow D^{*0}\pi^0$ Decay

$$\mathcal{A}_f(\overline{B}^0 \rightarrow D^{*0}\pi^0) = \frac{G_F}{2} V_{cb} V_{ud}^* a_2 f_{D^*} 2m_{D^*} (\epsilon^* \cdot p_B) F_1^{B\pi}(q^2), \quad (3.51)$$

$$\Gamma_f(\overline{B}^0 \rightarrow D^{*0}\pi^0) = \frac{G_F^2}{8\pi} |\mathbf{k}|^3 |V_{cb}|^2 |V_{ud}|^2 |a_2|^2 |f_{D^*}|^2 \left| F_1^{B\pi}(m_{D^*}^2) \right|^2. \quad (3.52)$$

- $\overline{B}^0 \rightarrow D^{*0}\eta(\eta')$ Decays

$$\mathcal{A}_f(\overline{B}^0 \rightarrow D^{*0}\eta) = \frac{G_F}{\sqrt{2}} V_{cb} V_{ud}^* a_2 f_{D^*} C_\eta^d 2m_{D^*} (\epsilon^* \cdot p_B) F_1^{B\eta}(q^2), \quad (3.53)$$

$$\Gamma_f(\overline{B}^0 \rightarrow D^{*0}\eta) = \frac{G_F^2}{4\pi} |\mathbf{k}|^3 |V_{cb}|^2 |V_{ud}|^2 |a_2|^2 |f_{D^*}|^2 |C_\eta^d|^2 \left| F_1^{B\eta}(m_{D^*}^2) \right|^2. \quad (3.54)$$

The decay amplitude and decay rate for the process $\overline{B}^0 \rightarrow D^{*0}\eta'$ are found from above by replacing η by η' .

- $\overline{B}^0 \rightarrow D^0\rho^0(a_1^0, \omega^0)$ Decays

$$\mathcal{A}_f(\overline{B}^0 \rightarrow D^0\rho^0) = \frac{G_F}{2} V_{cb} V_{ud}^* a_2 f_D 2m_\rho (\epsilon^* \cdot p_B) A_0^{B\rho}(q^2). \quad (3.55)$$

$$\Gamma_f(\overline{B}^0 \rightarrow D^0\rho^0) = \frac{G_F^2}{8\pi} |\mathbf{k}|^3 |V_{cb}|^2 |V_{ud}|^2 |a_2|^2 |f_D|^2 |A_0^{B\rho}(m_D^2)|^2. \quad (3.56)$$

The decay amplitude and decay rate for the processes $\overline{B}^0 \rightarrow D^0 a_1^0$ and $\overline{B}^0 \rightarrow D^0 \omega^0$ are found from above by replacing ρ^0 by a_1^0 and ω^0 respectively.

- $\overline{B}^0 \rightarrow D^{*0}\rho^0(a_1^0, \omega^0)$ Decays

The decay amplitude for the process $\overline{B}^0 \rightarrow D^{*0}\rho^0$ is given by

$$\begin{aligned} \mathcal{A}(\overline{B}^0 \rightarrow D^{*0}\rho^0) = & -\frac{G_F}{2} V_{cb} V_{ud}^* a_2 f_{D^*} \left(\frac{m_{D^*}}{m_B + m_\rho} \right) \\ & \times \left[2i\varepsilon_{\mu\nu\alpha\beta} \epsilon_\rho^{\mu} \epsilon_{D^*}^{\nu} p_\rho^\alpha p_{D^*}^\beta V^{B\rho}(q^2) \right. \\ & - (m_B + m_\rho)^2 (\epsilon_\rho^* \cdot \epsilon_{D^*}^*) A_1^{B\rho}(q^2) \\ & \left. + 2(\epsilon_\rho^* \cdot p_{D^*})(\epsilon_{D^*}^* \cdot p_\rho) A_2^{B\rho}(q^2) \right], \end{aligned} \quad (3.57)$$

Which leads to the following three helicity amplitudes

$$\mathcal{A}_0 = -\frac{G_F}{2} V_{cb} V_{ud}^* a_2 f_{D^*} m_{D^*} (m_B + m_\rho) A_1^{B\rho}(q^2) (a - b x), \quad (3.58)$$

$$\mathcal{A}_\pm = \frac{G_F}{2} V_{cb} V_{ud}^* a_2 f_{D^*} m_{D^*} (m_B + m_\rho) A_1^{B\rho}(q^2) (1 \mp c y). \quad (3.59)$$

From above, we obtain the following expression for the decay rate,

$$\begin{aligned} \Gamma_f(\bar{B}^0 \rightarrow D^{*0} \rho^0) &= \frac{G_F^2}{32\pi m_B^2} |\mathbf{k}| |V_{cb}|^2 |V_{ud}|^2 |a_2|^2 |f_{D^*}|^2 m_{D^*}^2 (m_B^2 + m_\rho^2) |A_1^{B\rho}(m_{D^*}^2)|^2 \\ &\times [(a - b x)^2 + 2(1 + c^2 y^2)]. \end{aligned} \quad (3.60)$$

The decay amplitude and decay rate for the processes $\bar{B}^0 \rightarrow D^{*0} a_1^0$ and $\bar{B}^0 \rightarrow D^{*0} \omega^0$ are found from above by replacing ρ^0 by a_1^0 and ω^0 respectively.

• $\bar{B}_s^0 \rightarrow D^0 K^0$ Decay

$$\mathcal{A}_f(\bar{B}_s^0 \rightarrow D^0 K^0) = \frac{G_F}{\sqrt{2}} V_{cb} V_{ud}^* a_2 f_D (m_{B_s}^2 - m_K^2) F_0^{B,K}(q^2). \quad (3.61)$$

$$\Gamma_f(\bar{B}_s^0 \rightarrow D^0 K^0) = \frac{G_F^2}{16\pi m_{B_s}^2} |\mathbf{k}| |V_{cb}|^2 |V_{ud}|^2 |a_2|^2 |f_D|^2 (m_{B_s}^2 - m_K^2)^2 |F_0^{B,K}(m_D^2)|^2. \quad (3.62)$$

• $\bar{B}_s^0 \rightarrow D^{*0} K^0$ Decay

$$\mathcal{A}_f(\bar{B}_s^0 \rightarrow D^{*0} K^0) = \frac{G_F}{\sqrt{2}} V_{cb} V_{ud}^* a_2 f_{D^*} 2m_{D^*} (\epsilon^* \cdot p_{B_s}) F_1^{B,K}(q^2), \quad (3.63)$$

$$\Gamma_f(\bar{B}_s^0 \rightarrow D^{*0} K^0) = \frac{G_F^2}{4\pi} |\mathbf{k}|^3 |V_{cb}|^2 |V_{ud}|^2 |a_2|^2 |f_{D^*}|^2 |F_1^{B,K}(m_{D^*}^2)|^2. \quad (3.64)$$

• $\bar{B}_s^0 \rightarrow D^0 K^{*0}$ Decay

$$\mathcal{A}_f(\bar{B}_s^0 \rightarrow D^0 K^{*0}) = \frac{G_F}{\sqrt{2}} V_{cb} V_{ud}^* a_2 f_D 2m_{K^*} (\epsilon^* \cdot p_{B_s}) A_0^{B,K^*}(q^2). \quad (3.65)$$

$$\Gamma_f(\bar{B}_s^0 \rightarrow D^0 K^{*0}) = \frac{G_F^2}{4\pi} |\mathbf{k}|^3 |V_{cb}|^2 |V_{ud}|^2 |a_2|^2 |f_D|^2 |A_0^{B,K^*}(m_D^2)|^2. \quad (3.66)$$

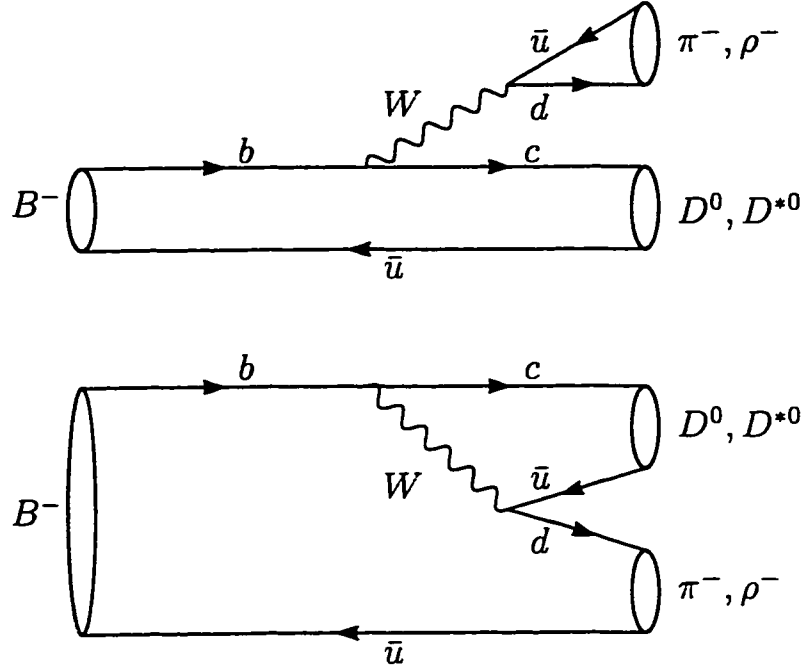


Figure 3.3: The flavor flow diagrams for Class III processes of the type $b \rightarrow c\bar{u}d$.

• $\bar{B}_s^0 \rightarrow D^{*0}K^{*0}$ Decay

$$A_0 = -\frac{G_F}{\sqrt{2}}V_{cb}V_{ud}^*a_2f_{D^*}m_{D^*}(m_{B_s} + m_{K^*})A_1^{B,K^*}(q^2)(a - bx). \quad (3.67)$$

$$A_{\pm} = \frac{G_F}{\sqrt{2}}V_{cb}V_{ud}^*a_2f_{D^*}m_{D^*}(m_{B_s} + m_{K^*})A_1^{B,K^*}(q^2)(1 \mp cy). \quad (3.68)$$

$$\begin{aligned} \Gamma_f(\bar{B}_s^0 \rightarrow D^{*0}K^{*0}) &= \frac{G_F^2}{16\pi m_{B_s}^2}|\mathbf{k}| |V_{cb}|^2|V_{ud}|^2|a_2|^2|f_{D^*}|^2m_{D^*}^2(m_{B_s}^2 + m_{K^*}^2)^2 \\ &\quad \times |A_1^{B,K^*}(m_{D^*}^2)|^2 \left[(a - bx)^2 + 2(1 + c^2y^2) \right]. \end{aligned} \quad (3.69)$$

3.2.3 Type $b \rightarrow c\bar{u}d$ processes: Class III

Processes of Class III proceed via external and internal W emissions. The flavor flow diagrams for the processes of this class considered in this subsection are shown in Fig. 3.3.

- $B^- \rightarrow D^0 \pi^-$ Decay

The factorizable decay amplitude for the process $B^- \rightarrow D^0 \pi^-$ is given by

$$\begin{aligned}
\mathcal{A}_f(B^- \rightarrow D^0 \pi^-) &= \frac{G_F}{\sqrt{2}} V_{cb} V_{ud}^* \left[a_1 \langle D^0 | (\bar{c}b) | B^- \rangle \langle \pi^- | (\bar{d}u) | 0 \rangle \right. \\
&\quad \left. + a_2 \langle \pi^- | (\bar{d}b) | B^- \rangle \langle D^0 | (\bar{u}c) | 0 \rangle \right] \\
&= \frac{G_F}{\sqrt{2}} V_{cb} V_{ud}^* \left[a_1 f_\pi (m_B^2 - m_D^2) F_0^{BD}(m_\pi^2) \right. \\
&\quad \left. + a_2 f_D (m_B^2 - m_\pi^2) F_0^{B\pi}(m_D^2) \right]. \tag{3.70}
\end{aligned}$$

The decay rate is, then, given by,

$$\begin{aligned}
\Gamma_f(B^- \rightarrow D^0 \pi^-) &= \frac{G_F^2}{16\pi m_B^2} |\mathbf{k}| |V_{cb}|^2 |V_{ud}|^2 \left| a_1 f_\pi (m_B^2 - m_D^2) F_0^{BD}(m_\pi^2) \right. \\
&\quad \left. + a_2 f_D (m_B^2 - m_\pi^2) F_0^{B\pi}(m_D^2) \right|^2. \tag{3.71}
\end{aligned}$$

- $B^- \rightarrow D^0 \rho^-$ Decay

$$\begin{aligned}
\mathcal{A}_f(B^- \rightarrow D^0 \rho^-) &= \frac{G_F}{\sqrt{2}} V_{cb} V_{ud}^* \left[a_1 \langle D^0 | (\bar{c}b) | B^- \rangle \langle \rho^- | (\bar{d}u) | 0 \rangle \right. \\
&\quad \left. + a_2 \langle \rho^- | (\bar{d}b) | B^- \rangle \langle D^0 | (\bar{u}c) | 0 \rangle \right] \\
&= \frac{G_F}{\sqrt{2}} V_{cb} V_{ud}^* 2m_\rho (\epsilon^* \cdot p_B) \\
&\quad \times \left[a_1 f_\rho F_1^{BD}(m_\rho^2) + a_2 f_D A_0^{B\rho}(m_D^2) \right], \tag{3.72}
\end{aligned}$$

$$\begin{aligned}
\Gamma_f(B^- \rightarrow D^0 \rho^-) &= \frac{G_F^2}{4\pi} |\mathbf{k}|^3 |V_{cb}|^2 |V_{ud}|^2 \\
&\quad \times \left| a_1 f_\rho F_1^{BD}(m_\rho^2) + a_2 f_D A_0^{B\rho}(m_D^2) \right|^2. \tag{3.73}
\end{aligned}$$

- $B^- \rightarrow D^{*0} \pi^-$ Decay

$$\begin{aligned}
\mathcal{A}_f(B^- \rightarrow D^{*0} \pi^-) &= \frac{G_F}{\sqrt{2}} V_{cb} V_{ud}^* \left[a_1 \langle D^{*0} | (\bar{c}b) | B^- \rangle \langle \pi^- | (\bar{d}u) | 0 \rangle \right. \\
&\quad \left. + a_2 \langle \pi^- | (\bar{d}b) | B^- \rangle \langle D^{*0} | (\bar{c}u) | 0 \rangle \right]
\end{aligned}$$

$$= \frac{G_F}{\sqrt{2}} V_{cb} V_{ud}^* 2m_D^{*0} (\epsilon^* \cdot p_B) \times [a_1 f_\pi A_0^{BD^*}(m_\pi^2) + a_2 f_{D^*} F_1^{B\pi}(m_D^2)], \quad (3.74)$$

$$\Gamma_f(B^- \rightarrow D^{*0} \pi^-) = \frac{G_F^2}{4\pi} |\mathbf{k}|^3 |V_{cb}|^2 |V_{ud}|^2 \times |a_1 f_\pi A_0^{BD^*}(m_\pi^2) + a_2 f_{D^*} F_1^{B\pi}(m_D^2)|^2. \quad (3.75)$$

• $B^- \rightarrow D^{*0} \rho^-$ Decay

The decay amplitude for the process $B^- \rightarrow D^{*0} \rho^-$ is given by

$$\mathcal{A}_f(B^- \rightarrow D^{*0} \rho^-) = \frac{G_F}{\sqrt{2}} V_{cb} V_{ud}^* [a_1 \langle D^{*0} | (\bar{c}b) | B^- \rangle \langle \rho^- | (\bar{d}u) | 0 \rangle + a_2 \langle \rho^- | (\bar{d}b) | B^- \rangle \langle D^{*0} | (\bar{c}u) | 0 \rangle], \quad (3.76)$$

which leads to the following helicity amplitudes

$$\mathcal{A}_0 = -\frac{G_F}{\sqrt{2}} V_{cb} V_{ud}^* [a_1 f_\rho m_\rho (m_B + m_{D^*}) \{a A_1^{BD^*}(m_\rho^2) - b A_2^{BD^*}(m_\rho^2)\} + a_2 f_{D^*} m_{D^*} (m_B + m_\rho) \{a' A_1^{B\rho}(m_{D^*}^2) - b' A_2^{B\rho}(m_{D^*}^2)\}], \quad (3.77)$$

$$\mathcal{A}_\pm = \frac{G_F}{\sqrt{2}} V_{cb} V_{ud}^* [a_1 f_\rho m_\rho (m_B + m_{D^*}) \{A_1^{BD^*}(m_\rho^2) \mp c V^{BD^*}(m_\rho^2)\} + a_2 f_{D^*} m_{D^*} (m_B + m_\rho) \{A_1^{B\rho}(m_{D^*}^2) \mp c' V^{B\rho}(m_{D^*}^2)\}]. \quad (3.78)$$

where a, b, c, a', b' and c' are as defined as

$$\begin{aligned} a &= \frac{m_B^2 - m_\rho^2 - m_{D^*}^2}{2m_\rho m_{D^*}} = a', \\ b &= \frac{2|\mathbf{k}|^2 m_B^2}{m_\rho m_{D^*} (m_B + m_{D^*})^2}, \\ c &= \frac{2|\mathbf{k}| m_B}{(m_B + m_{D^*})^2}, \\ b' &= \frac{2|\mathbf{k}|^2 m_B^2}{m_\rho m_{D^*} (m_B + m_\rho)^2}, \\ c' &= \frac{2|\mathbf{k}| m_B}{(m_B + m_\rho)^2}. \end{aligned} \quad (3.79)$$

The decay rate is then obtained from

$$\Gamma_f(B^- \rightarrow D^{*0} \rho^-) = \frac{|\mathbf{k}|}{8\pi m_B^2} (|\mathcal{A}_0|^2 + |\mathcal{A}_+|^2 + |\mathcal{A}_-|^2). \quad (3.80)$$

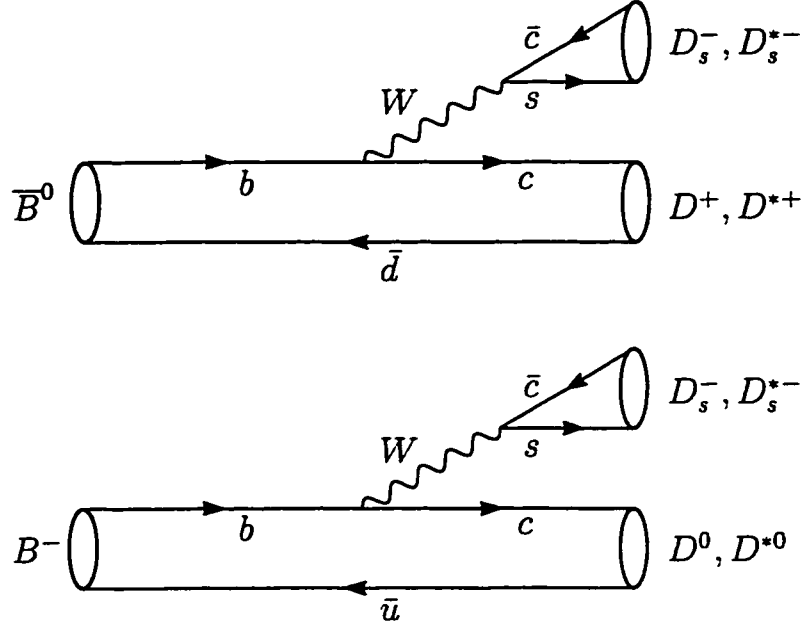


Figure 3.4: The flavor flow diagram for class I processes of the type $b \rightarrow c\bar{c}s$

3.2.4 Type $b \rightarrow c\bar{c}s$ processes: Class I

The effective Hamiltonian, appropriate for processes of the type $b \rightarrow c\bar{c}s$, is given by

$$\mathcal{H}_{\text{eff}} = \frac{G_F}{\sqrt{2}} V_{cb} V_{cs}^* [C_1 (\bar{c}_i b_i)_L (\bar{s}_j c_j)_L + C_2 (\bar{c}_i c_i)_L (\bar{s}_j b_j)_L], \quad (3.81)$$

where the values of the Wilson coefficients C_1 and C_2 are taken from Table 2.1. Using Fierz transformations, the effective Hamiltonian is written as

$$\mathcal{H}_{\text{eff}} = \frac{G_F}{\sqrt{2}} V_{cb} V_{cs}^* [a_1 (\bar{c}b) (\bar{s}c) + C_2 \mathcal{H}^{(8)}], \quad (3.82)$$

where

$$a_1 = \left(C_1 + \frac{C_2}{N_c} \right), \quad (3.83)$$

and

$$\mathcal{H}^{(8)} = \frac{1}{2} \sum_a (\bar{c} \lambda^a b) (\bar{s} \lambda^a c). \quad (3.84)$$

In Fig. 3.4, we show the flavor flow diagram for the decays of class I considered in this subsection.

• $B \rightarrow DD_s$ Decay

The forms of the decay amplitude and decay rate for this process are similar to those derived previously for $\bar{B}^0 \rightarrow D^+ \pi^-$ decay. The results are written as

$$\mathcal{A}_f(B \rightarrow DD_s) = \frac{G_F}{\sqrt{2}} V_{cb} V_{cs}^* a_1 f_{D_s} (m_B^2 - m_D^2) F_0^{BD}(q^2), \quad (3.85)$$

$$\Gamma_f(B \rightarrow DD_s) = \frac{G_F^2}{16\pi m_B^2} |\mathbf{k}| |V_{cb}|^2 |V_{cs}|^2 |a_1|^2 |f_{D_s}|^2 m_B^2 (m_B^2 - m_D^2)^2 \left| F_0^{BD}(m_{D_s}^2) \right|^2. \quad (3.86)$$

• $B \rightarrow DD_s^*$ Decay

Similar to the process $\bar{B}^0 \rightarrow D^+ \rho^-$ discussed previously, the decay amplitude and decay rate for the process $B \rightarrow DD_s^*$ are given by

$$\mathcal{A}_f(B \rightarrow DD_s^*) = \frac{G_F}{\sqrt{2}} V_{cb} V_{cs}^* a_1 f_{D_s^*} 2m_{D_s^*} (\epsilon^* \cdot p_B) F_1^{BD}(q^2), \quad (3.87)$$

$$\Gamma_f(B \rightarrow DD_s^*) = \frac{G_F^2}{4\pi} |\mathbf{k}|^3 |V_{cb}|^2 |V_{cs}|^2 |a_1|^2 |f_{D_s^*}|^2 \left| F_1^{BD}(m_{D_s^*}^2) \right|^2. \quad (3.88)$$

• $B \rightarrow D^* D_s$ Decay

$$\mathcal{A}_f(B \rightarrow D^* D_s) = \frac{G_F}{\sqrt{2}} V_{cb} V_{cs}^* a_1 f_{D_s} 2m_{D^*} (\epsilon^* \cdot p_B) A_0^{BD^*}(q^2), \quad (3.89)$$

$$\Gamma_f(B \rightarrow D^* D_s) = \frac{G_F^2}{4\pi} |\mathbf{k}|^3 |V_{cb}|^2 |V_{cs}|^2 |a_1|^2 |f_{D_s}|^2 \left| A_0^{BD^*}(q^2) \right|^2. \quad (3.90)$$

• $B \rightarrow D^* D_s^*$ Decay

$$\mathcal{A}_0 = -\frac{G_F}{\sqrt{2}} V_{cb} V_{cs}^* a_1 f_{D_s^*} m_{D_s^*} (m_B + m_{D^*}) A_1^{BD^*}(q^2) (a - b x), \quad (3.91)$$

$$\mathcal{A}_\pm = \frac{G_F}{\sqrt{2}} V_{cb} V_{cs}^* a_1 f_{D_s^*} m_{D_s^*} (m_B + m_{D^*}) A_1^{BD^*}(q^2) (1 \mp c y), \quad (3.92)$$

where a , b , c , x and y are defined in (3.22).

From above, we obtain the following expression for the decay rate,

$$\begin{aligned}
\Gamma_f(B \rightarrow D^+ D_s^+) &= \frac{|\mathbf{k}|}{8\pi m_B^2} (|\mathcal{A}_0|^2 + |\mathcal{A}_+|^2 + |\mathcal{A}_-|^2) \\
&= \frac{G_F^2}{16\pi m_B^2} |\mathbf{k}| |V_{cb}|^2 |V_{cs}|^2 |a_1|^2 |f_{D_s^+}|^2 m_{D_s^+}^2 (m_B + m_{D^+})^2 |A_1^{BD^+}(m_{D_s^+}^2)|^2 \\
&\quad \times \left[(a - bx)^2 + 2(1 + c^2 y^2) \right].
\end{aligned} \tag{3.93}$$

The polarization of the final state is defined in terms of P_0 and P_\pm as in (3.40) and (3.41).

3.2.5 Type $b \rightarrow c\bar{c}s$ processes: Class II

The flavor flow diagram for the decays of of class II considered in this subsection are shown in Fig. 3.5. The effective Hamiltonian for this case is written from (3.81) and using Fierz transformations as

$$\mathcal{H}_{\text{eff}} = \frac{G_F}{\sqrt{2}} V_{cb} V_{cs}^* \left[a_2 (\bar{c}c) (\bar{s}b) + C_2 \mathcal{H}^{(8)} \right], \tag{3.94}$$

where

$$a_2 = \left(C_2 + \frac{C_1}{N_c} \right), \tag{3.95}$$

and

$$\mathcal{H}^{(8)} = \frac{1}{2} \sum_a (\bar{c} \lambda^a c) (\bar{s} \lambda^a b). \tag{3.96}$$

• $B \rightarrow K \psi$ Decay

In here, $B \rightarrow K \psi$ represents $\bar{B}^0 \rightarrow K^0 \psi$ and $B^- \rightarrow K^- \psi$ decays, where ψ is either J/ψ or $\psi(2S)$ mesons. The forms of the factorizable decay amplitude for these processes are similar to those in $\bar{B}^0 \rightarrow D^{*0} \pi^0$ decay. The results are written as

$$\mathcal{A}_f(B \rightarrow K \psi) = \frac{G_F}{\sqrt{2}} V_{cb} V_{cs}^* a_2 f_\psi 2m_\psi (\epsilon^* \cdot p_B) F_1^{BK}(q^2), \tag{3.97}$$

$$\Gamma_f(B \rightarrow K \psi) = \frac{G_F^2}{4\pi} |\mathbf{k}|^3 |V_{cb}|^2 |V_{cs}|^2 |a_2|^2 |f_\psi|^2 \left| F_1^{BK}(m_\psi^2) \right|^2. \tag{3.98}$$

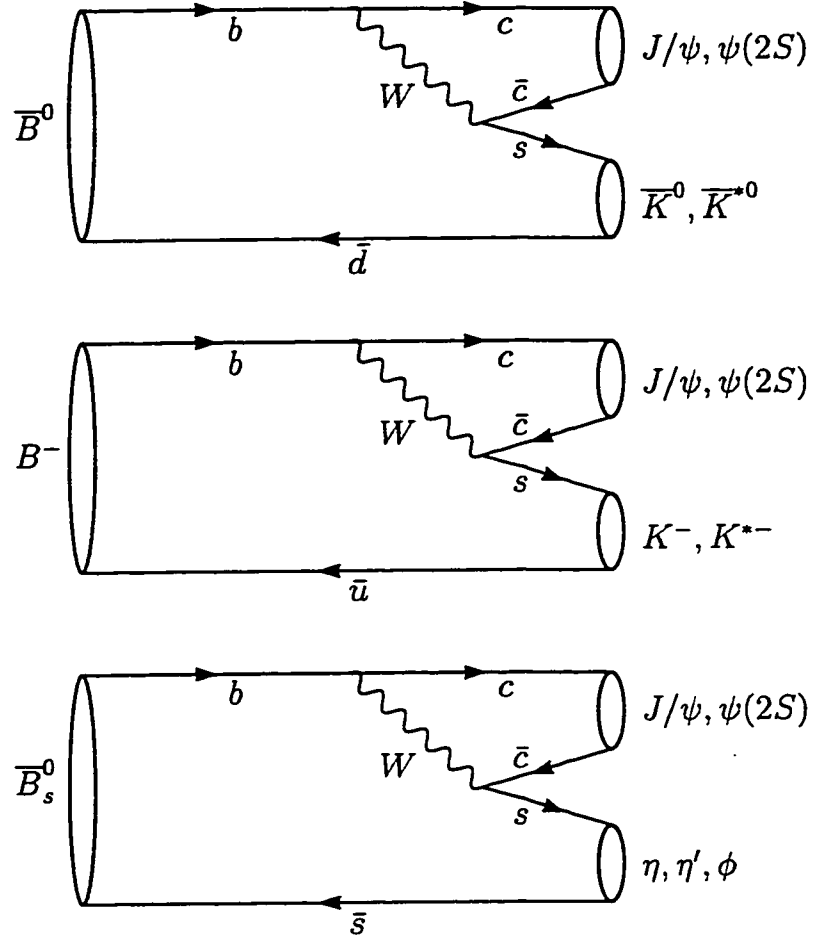


Figure 3.5: The flavor flow diagram for class II processes of the type $b \rightarrow c\bar{c}s$

- $B \rightarrow K^* \psi \bar{B}_s^0 \rightarrow \phi \psi$ Decays

$$\mathcal{A}_0 = -\frac{G_F}{\sqrt{2}} V_{cb} V_{cs}^* a_2 f_\psi m_\psi (m_B + m_{K^*}) A_1^{BK^*}(q^2) (a - b x) \quad (3.99)$$

$$\mathcal{A}_\pm = \frac{G_F}{\sqrt{2}} V_{cb} V_{cs}^* a_2 f_\psi m_\psi (m_B + m_{K^*}) A_1^{BK^*}(q^2) (1 \mp c y). \quad (3.100)$$

$$\begin{aligned} \Gamma_f(B \rightarrow K^* \psi) &= \frac{G_F^2}{16\pi m_B^2} |\mathbf{k}| |V_{cb}|^2 |V_{cs}|^2 |a_2|^2 |f_\psi|^2 m_\psi^2 (m_B + m_{K^*})^2 |A_1^{BK^*}(m_\psi^2)|^2 \\ &\times \left[(a - b x)^2 + 2(1 + c^2 y^2) \right]. \end{aligned} \quad (3.101)$$

The decay amplitude and decay rate for the process $\bar{B}_s^0 \rightarrow \phi \psi$ are found from above by replacing B by B_s and K^* by ϕ .

- $\bar{B}_s^0 \rightarrow \eta(\eta') \psi$ Decays

$$\mathcal{A}_f(\bar{B}_s^0 \rightarrow \eta \psi) = \frac{G_F}{\sqrt{2}} V_{cb} V_{cs}^* a_2 f_\psi C_\eta^s 2m_\psi (\epsilon^* \cdot p_B) F_1^{B\eta}(q^2), \quad (3.102)$$

$$\Gamma_f(\bar{B}_s^0 \rightarrow \eta \psi) = \frac{G_F^2}{4\pi} |\mathbf{k}|^3 |V_{cb}|^2 |V_{cs}|^2 |a_2|^2 |f_\psi|^2 |C_\eta^s|^2 \left| F_1^{B\eta}(m_\psi^2) \right|^2. \quad (3.103)$$

The decay amplitude and decay rate for the processes $\bar{B}_s^0 \rightarrow \eta' \psi$ is found from above by replacing η by η' .

3.3 CKM Matrix Elements

To be able to calculate the decay amplitudes of the nonleptonic processes considered in this work, we need the values of the Cabibbo-Kobayashi-Maskawa (CKM) matrix elements presented in (2.2). In Wolfenstein parametrization [3], and up to the fourth order in λ , these elements take the form

$$\begin{pmatrix} V_{ud} & V_{us} & V_{ub} \\ V_{cd} & V_{cs} & V_{cb} \\ V_{td} & V_{ts} & V_{tb} \end{pmatrix} = \begin{pmatrix} 1 - \frac{1}{2}\lambda^2 & \lambda & A\lambda^3(\rho - i\eta) \\ -\lambda(1 + iA^2\lambda^4\eta) & 1 - \frac{1}{2}\lambda^2 & A\lambda^2 \\ A\lambda^3(1 - \rho - i\eta) & -A\lambda^2 & 1 \end{pmatrix}. \quad (3.104)$$

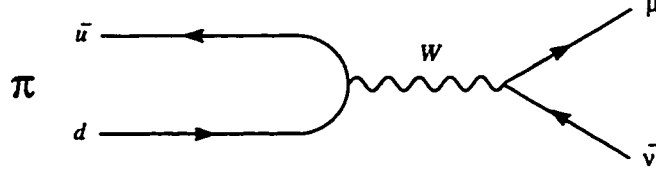


Figure 3.6: The tree-level Feynman diagram for the process $\pi \rightarrow \mu \bar{\nu}_\mu$

In a recent update of the CKM matrix [4] the following values have been presented for the four parameters in (3.104)

$$\begin{aligned}
 \lambda &= 0.2205, \\
 A &= 0.81, \\
 \rho &= 0.05, \\
 \eta &= 0.36.
 \end{aligned} \tag{3.105}$$

The CKM matrix elements calculated from these values are used throughout this work, unless it is specified otherwise.

3.4 Decay Constants

The values of the decay constants f_π , f_ρ , f_{a_1} , $f_{J/\psi}$, $f_{\psi(2S)}$, f_D , f_{D^*} , f_{D_s} and $f_{D_s^*}$ are also needed in this study. A recent calculation of most of these values was performed by Neubert and Stech in [5]. In this section we reproduce their results showing more details of the calculations.

3.4.1 f_{π^-}

This decay constant can be calculated from the pion leptonic decay $\pi^- \rightarrow \mu^- \bar{\nu}_\mu$ (see Fig. 3.6). The decay amplitude for this process up to first order is given by

$$\mathcal{A}(\pi^- \rightarrow \mu^- \bar{\nu}_\mu) = -i \frac{G_F}{\sqrt{2}} V_{ud} \left(\bar{u}_\mu \gamma_\alpha (1 - \gamma_5) v_{\bar{\nu}_\mu} \right) \langle 0 | \bar{u}_u \gamma^\alpha (1 - \gamma_5) u_d | \pi^-(p) \rangle. \tag{3.106}$$

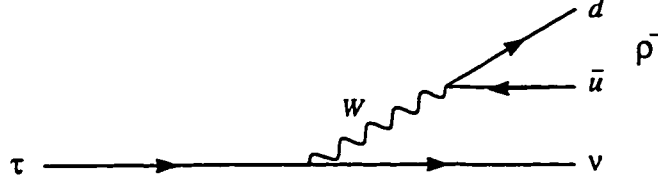


Figure 3.7: The tree-level Feynman diagram for the process $\tau^- \rightarrow \rho^- \nu_\tau$

Using the decomposition in (3.1) for the hadronic current we get

$$\mathcal{A}(\pi^- \rightarrow \mu^- \bar{\nu}_\mu) = -i \frac{G_F}{\sqrt{2}} V_{ud} f_\pi (\bar{u}_\mu \not{p} (1 - \gamma_5) v_{\bar{\nu}_\mu}). \quad (3.107)$$

By taking the absolute square of \mathcal{A} and summing over the spins in the final state we get

$$\sum |\mathcal{A}(\pi^- \rightarrow \mu^- \bar{\nu}_\mu)|^2 = 2 |G_F|^2 |V_{ud}|^2 f_\pi^2 m_\mu^2 (m_\pi^2 - m_\mu^2). \quad (3.108)$$

The decay rate is then found by multiplying the above result by the phase space factor (see C.28). So, we get

$$\Gamma(\pi^- \rightarrow \mu^- \bar{\nu}_\mu) = \frac{|G_F|^2}{8\pi} |V_{ud}|^2 f_\pi^2 m_\mu^2 m_\pi \left(1 - \frac{m_\mu^2}{m_\pi^2}\right)^2. \quad (3.109)$$

Using the experimental values for the branching ratio of $\pi^- \rightarrow \mu^- \bar{\nu}_\mu$ and the pion lifetime [6], we calculate the pion's decay constant to be around 131 MeV. However, in [6] the decay rate has been extended to include radiative corrections which produced the following result for the decay constant:

$$f_{\pi^-} = 130.7 \pm 0.37 \text{ MeV}. \quad (3.110)$$

3.4.2 f_ρ and f_{a_1}

These two decay constants can be calculated from the semileptonic τ decays, $\tau^- \rightarrow \rho^- \nu_\tau$ and $\tau^- \rightarrow a_1^- \nu_\tau$. The amplitude for the first process (see Fig. 3.7) is given by

$$\begin{aligned} \mathcal{A}(\tau^- \rightarrow \rho^- \nu_\tau) &= -i \frac{G_F}{\sqrt{2}} V_{ud} (\bar{u}_{\nu_\tau} \gamma_\alpha (1 - \gamma_5) u_\tau) \langle \rho^- | \bar{u}_d \gamma^\alpha (1 - \gamma_5) v_u | 0 \rangle, \\ &= -i \frac{G_F}{\sqrt{2}} V_{ud} m_\rho f_\rho (\bar{u}_{\nu_\tau} \not{\epsilon} (1 - \gamma_5) u_\tau), \end{aligned} \quad (3.111)$$

where we have used (3.2) for the hadronic current. After taking the absolute square of \mathcal{A} we sum over the spins in the final state and average over the spins in the initial state to get

$$\sum \left| \mathcal{A}(\tau^- \rightarrow \rho^- \nu_\tau) \right|^2 = |G_F|^2 |V_{ud}|^2 |f_\rho|^2 (m_\tau^2 - m_\rho^2)(m_\tau^2 + 2m_\rho^2). \quad (3.112)$$

Multiplying above by the phase space factor we get the following expression for the decay rate:

$$\Gamma(\tau^- \rightarrow \rho^- \nu_\tau) = \frac{|G_F|^2}{16\pi} |V_{ud}|^2 |f_\rho|^2 m_\tau^3 \left(1 - \frac{m_\rho^2}{m_\tau^2}\right)^2 \left(1 + 2\frac{m_\rho^2}{m_\tau^2}\right). \quad (3.113)$$

The decay rate for $\tau^- \rightarrow a_1^- \nu_\tau$ is found by replacing ρ by a_1 in the above equation.

The experimental values of the branching ratios are taken to be [6, 5]:

$$\begin{aligned} BR(\tau^- \rightarrow \rho^- \nu_\tau) &= 24.94 \pm 0.16\%, \\ BR(\tau^- \rightarrow a_1^- \nu_\tau) &= 17.65 \pm 0.32\%. \end{aligned} \quad (3.114)$$

This leads to the following values for the decay constants:

$$f_{\rho^-} = 207 \pm 1 \text{ MeV}, \quad (3.115)$$

$$f_{a_1^-} = 228 \pm 10 \text{ MeV}, \quad (3.116)$$

where the uncertainties are due to the experimental errors in the branching ratios, the lifetime and the mass of a_1 vector meson.

3.4.3 $f_{J/\psi}$ and $f_{\psi(2S)}$

The decay constants of these two neutral vector mesons can be found from the following electromagnetic decays: $J/\psi \rightarrow e^+ e^-$ and $\psi(2S) \rightarrow e^+ e^-$. The amplitude for these processes is given by

$$\begin{aligned} \mathcal{A}(J/\psi \rightarrow e^+ e^-) &= ie^2 Q_c \frac{1}{p^2} (\bar{u}_e \gamma_\alpha v_e) \langle 0 | \bar{c} \gamma^\alpha c | J/\psi(p) \rangle, \\ &= i \frac{e^2 Q_c}{p^2} m_{J/\psi} f_{J/\psi} (\bar{u}_e \not{\epsilon} v_e), \end{aligned} \quad (3.117)$$

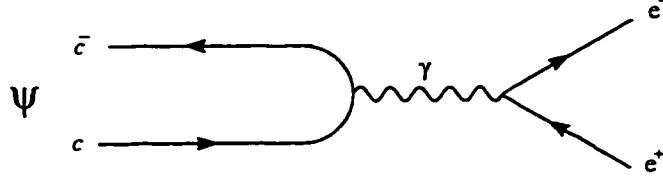


Figure 3.8: The tree-level Feynman diagram for the process $J/\psi \rightarrow e^+ e^-$

where Q_c is the charge of the c quark. In calculating the absolute square of \mathcal{A} we sum over the spins of the two electrons in the final state. Furthermore, we divide by 3 in order to average over the polarizations of the initial state to get

$$\sum |\mathcal{A}(J/\psi \rightarrow e^+ e^-)|^2 = \frac{4}{3} e^4 Q_c^2 |f_{J/\psi}|^2 \left(1 + 2 \frac{m_e^2}{m_{J/\psi}^2} \right). \quad (3.118)$$

The decay rate is then given by

$$\Gamma(J/\psi \rightarrow e^+ e^-) = \frac{4\pi}{3} \frac{\alpha^2}{m_{J/\psi}^2} |f_{J/\psi}|^2 \left(1 - 12 \frac{m_e^4}{m_{J/\psi}^4} - 16 \frac{m_e^6}{m_{J/\psi}^6} \right)^{1/2}, \quad (3.119)$$

$$\approx \frac{4\pi}{3} \frac{\alpha^2}{m_{J/\psi}^2} |f_{J/\psi}|^2. \quad (3.120)$$

By replacing J/ψ , above, by $\psi(2S)$ we get the decay rate for $\psi(2S) \rightarrow e^+ e^-$.

The experimental values of the decay rates are [6]:

$$\begin{aligned} \Gamma(J/\psi \rightarrow e^+ e^-) &= 5.26 \pm 0.37 \text{ MeV}, \\ \Gamma(\psi(2S) \rightarrow e^+ e^-) &= 2.14 \pm 0.21 \text{ MeV}. \end{aligned} \quad (3.121)$$

This leads to the following values for the decay constants:

$$f_{J/\psi} = 405 \pm 14 \text{ MeV}, \quad (3.122)$$

$$f_{\psi(2S)} = 282 \pm 14 \text{ MeV}, \quad (3.123)$$

where the uncertainties are due to the experimental errors in the decay rates.

3.4.4 f_D and f_{D^*}

Unlike the decay constants considered above, no values for f_D and f_{D^*} are available based on experimental measurements. So, we will use the values given in [5] based on theoretical models predictions:

$$f_D = 200 \text{ MeV}. \quad (3.124)$$

$$f_{D^*} = 230 \text{ MeV}. \quad (3.125)$$

3.4.5 f_{D_s} and $f_{D_s^*}$

For f_{D_s} , we use an average of the five measurements [7, 8, 9, 10, 11]. The first four of these measurements have been corrected in [11]. The result is

$$f_{D_s} = 250 \pm 27 \text{ MeV}. \quad (3.126)$$

The value of $f_{D_s^*}$ is taken to be

$$f_{D_s^*} = 275 \text{ MeV}. \quad (3.127)$$

as reported in [5] based on theoretical predictions.

The decay constants presented above are summarized in (6.41). These are the values used throughout this work unless it is specified otherwise.

3.5 Formfactors

Before proceeding to calculate the decay rates and polarization we need the values of the formfactors. In this study, several theoretical models are used to calculate the values of the needed formfactors. These are BSW [1, 12], CDDFGN [13], AW [14] and ISGW [15] models.

Out of these, BSW model is the one used the most by us. This is the original Bauer-Stech-Wirbel model [1, 12] (called BSW I here) where the formfactors are

calculated at zero momentum transfer and extrapolated to the desired momentum transfer using a monopole form for all the formfactors. The predicted formfactors in this model relevant to the processes of interest are shown in Tables 3.1 - 3.4.

We used the other models in studying a limited number of processes. The values of the formfactors needed for these studies are shown in Tables 5.1 and 5.2.

Table 3.1: BSW I model predictions of $F_0(q^2)$ and $F_1(q^2)$ formfactors for transitions of the type $B \rightarrow P$, where P is a pseudoscalar meson.

Transition	q^2	$F_0(q^2)$	$F_1(q^2)$
$B \rightarrow \pi$	0	0.335	0.335
	m_D^2	0.374	0.382
	$m_{D^*}^2$	0.381	0.391
	$m_{J/\psi}^2$	0.470	0.507
	$m_{\psi(2S)}^2$	0.565	0.644
$B \rightarrow \eta$	0	0.309	0.309
	m_D^2	0.345	0.352
	$m_{D^*}^2$	0.351	0.360
$B \rightarrow \eta'$	0	0.256	0.256
	m_D^2	0.285	0.291
	$m_{D^*}^2$	0.291	0.298
$B \rightarrow K$	0	0.381	0.381
	$m_{J/\psi}$	0.526	0.564
	$m_{\psi(2S)}^2$	0.626	0.706
$B \rightarrow D$	0	0.693	0.693
	m_π^2	0.693	0.693
	m_ρ^2	0.702	0.703
	$m_{a_1}^2$	0.717	0.720
	$m_{D^*}^2$	0.756	0.767
	$m_{D^*}^2$	0.767	0.780

Table 3.2: BSW I model predictions of $A_0(q^2)$, $A_1(q^2)$, $A_2(q^2)$, $A_3(q^2)$ and $V(q^2)$ formfactors for processes of the type $B \rightarrow V$, where V is a pseudoscalar meson.

Transition	q^2	$A_0(q^2)$	$A_1(q^2)$	$A_2(q^2)$	$A_3(q^2)$	$V(q^2)$
$B \rightarrow \rho$	0	0.283	0.284	0.285	0.283	0.330
	m_D^2	0.323	0.318	0.319	0.316	0.377
	$m_{D^*}^2$	0.331	0.324	0.325	0.322	0.385
	$m_{J/\psi}^2$	0.432	0.402	0.403	0.400	0.499
	$m_{\psi(2S)}^2$	0.553	0.487	0.488	0.484	0.635
$B \rightarrow \omega$	0	0.281	0.282	0.282	0.281	0.329
	m_D^2	0.321	0.316	0.316	0.315	0.375
	$m_{D^*}^2$	0.329	0.322	0.322	0.321	0.384
$B \rightarrow a_1$	0	0.211	0.199	0.192	0.211	0.278
	m_D^2	0.242	0.223	0.215	0.237	0.316
	$m_{D^*}^2$	0.247	0.227	0.219	0.241	0.324
	$m_{J/\psi}^2$	0.323	0.282	0.272	0.299	0.420
	$m_{\psi(2S)}^2$	0.414	0.341	0.329	0.362	0.534
$B \rightarrow K^*$	0	0.322	0.329	0.332	0.322	0.370
	$m_{J/\psi}^2$	0.481	0.459	0.463	0.449	0.548
	$m_{\psi(2S)}^2$	0.606	0.549	0.554	0.537	0.686
$B \rightarrow D^*$	0	0.628	0.656	0.691	0.628	0.708
	m_π^2	0.628	0.656	0.691	0.628	0.709
	m_ρ^2	0.637	0.665	0.700	0.636	0.719
	$m_{a_1}^2$	0.653	0.679	0.715	0.650	0.736
	$m_{D^*}^2$	0.696	0.718	0.755	0.687	0.784
	$m_{D_s^*}^2$	0.708	0.728	0.766	0.697	0.797

Table 3.3: BSW I model predictions of $F_0(q^2)$ and $F_1(q^2)$ formfactors for transitions of the type $B_s \rightarrow P$, where P is a pseudoscalar meson.

Transition	q^2	$F_0(q^2)$	$F_1(q^2)$
$B_s \rightarrow \eta$	0	0.329	0.329
	$m_{J/\psi}^2$	0.355	0.488
	$m_{\psi(2S)}^2$	0.542	0.611
$B_s \rightarrow \eta'$	0	0.276	0.276
	$m_{J/\psi}^2$	0.382	0.409
	$m_{\psi(2S)}^2$	0.454	0.512
$B_s \rightarrow K$	0	0.269	0.269
	m_D	0.300	0.307
	$m_{D^*}^2$	0.306	0.314
$B_s \rightarrow D_s$	0	0.646	0.646
	m_π^2	0.647	0.647
	m_ρ^2	0.655	0.656
	$m_{a_1}^2$	0.668	0.672

Table 3.4: BSW I model predictions of $A_0(q^2)$, $A_1(q^2)$, $A_2(q^2)$, $A_3(q^2)$ and $V(q^2)$ formfactors for processes of the type $B_s \rightarrow V$, where V is a pseudopseudoscalar meson.

Transition	q^2	$A_0(q^2)$	$A_1(q^2)$	$A_2(q^2)$	$A_3(q^2)$	$V(q^2)$
$B_s \rightarrow K^{*-}$	0	0.231	0.228	0.227	0.231	0.277
	m_D^2	0.264	0.255	0.254	0.259	0.315
	$m_{D^*}^2$	0.270	0.260	0.258	0.264	0.322
$B_s \rightarrow \phi$	0	0.267	0.267	0.268	0.267	0.314
	$m_{J/\psi}^2$	0.399	0.373	0.374	0.372	0.465
	$m_{\psi(2S)}^2$	0.502	0.447	0.447	0.445	0.582
$B_s \rightarrow D_s^{*-}$	0	0.576	0.595	0.621	0.576	0.663
	m_π^2	0.576	0.596	0.621	0.576	0.664
	m_ρ^2	0.584	0.603	0.629	0.583	0.673
	$m_{a_1}^2$	0.599	0.616	0.643	0.596	0.689

Bibliography

- [1] M. Wirbel, B. Stech and M. Bauer, Z. Phys. C **29**, 637 (1985).
- [2] M. Gourdin, A. N. Kamal and X. Y. Pham, Phys. Rev. Lett. **73**, 3355 (1994).
- [3] L. Wolfenstein, Phys. Rev. Lett. **51**, 1945 (1983).
- [4] A. Ali and D. London, Nucl. Phys. B (Proc. Suppl.) **54A**, 297 (1997).
- [5] M. Neubert and B. Stech, CERN-TH/97/99, hep-ph/9705292. To appear in the Second Edition of Heavy Flavours. Edited by A. J. Buras and M. Lindner (World Scientific, Singapore).
- [6] R. M. Barnett *et al.* (Particle Data Group), Phys. Rev. D **54**, 1 (1996).
- [7] S. Aoki *et al.* (WA75 Collaboration), Prog. Theor. Phys. **89**, 131 (1993).
- [8] D. Acosta *et al.* (CLEO Collaboration), Phys. Rev. D **49**, 5690 (1994).
- [9] J. Z. Bai *et al.* (BES Collaboration), Phys. Rev. Lett. **74**, 4599 (1995).
- [10] K. Kodama *et al.* (BES Collaboration), Phys. Lett. B **382**, 299 (1996).
- [11] M. Chadha *et al.* (CLEO Collaboration) Phys. Rev. D **58**, (1998) 32002.
- [12] M. Bauer, B. Stech and M. Wirbel, Z. Phys. C **34**, 103 (1987).

- [13] R. Casalbuoni, A. Deandrea, N. Di Bartolomeo, R. Gatto, F. Feruglio and G. Nardulli, Phys. Lett. B **299**, 139 (1993); A. Deandrea, N. Di Bartolomeo and R. Gatto, Phys. Lett. B **318**, 549 (1993).
- [14] T. Altomari and L. Wolfenstein, Phys. Rev. D **37**, 681 (1988).
- [15] N. Isgur, D. Scora, B. Grinstein and M. Wise, Phys. Rev. D **39**, 799 (1989).

Chapter 4

Nonfactorization in $B \rightarrow K^* J/\psi$ and $B_s \rightarrow \phi J/\psi$ Decays

4.1 Introduction

The $1/N_c$ expansion of hadronic matrix elements has been a very important approach in the study of weak nonleptonic decays. The leading terms of this expansion are factorizable into simpler ones, whereas the next to leading terms are not completely factorizable.

In the standard approach, Fierz transformation and color algebra are used to transform the non-leading contribution into a factorizable part, which is added to the leading terms, and a nonfactorizable part which is neglected [1]. This is called the factorization approximation which is extensively used and sometimes works well.

It was shown by Gourdin, Kamal and Pham [2] that factorization approximation in all commonly used models of formfactors could not account for the longitudinal polarization in $B \rightarrow K^* J/\psi$ and the ratio $(B \rightarrow K J/\psi)/(B \rightarrow K^* J/\psi)$. Subsequently, it was shown in [3] that inclusion of nonfactorized terms enabled one to understand both data in all the commonly used models of formfactors.

Our aim in this chapter is to investigate the nonfactorization contribution to the

processes $B \rightarrow K^* J/\psi$ and $\bar{B}_s^0 \rightarrow \phi J/\psi$ using the available world averages of decay rates and polarization. These two processes have similar flavor flow diagrams – see Fig. 3.5 – with different spectator quarks.

4.2 Formalism

Using the effective Hamiltonian (3.94), which is relevant to the processes of this chapter, we write down the decay amplitude for $B \rightarrow K^* J/\psi$ as

$$\begin{aligned} A(B \rightarrow K^* J/\psi) &= \langle K^* J/\psi | \mathcal{H}_{\text{eff}} | B \rangle \\ &= \frac{G_F}{\sqrt{2}} V_{cb} V_{cs}^* \\ &\quad \times \left[a_2 \langle K^* J/\psi | (\bar{b}s)(\bar{c}c) | B \rangle + C_1 \langle K^* J/\psi | \mathcal{H}_w^{(8)} | B \rangle \right], \end{aligned} \quad (4.1)$$

where

$$\mathcal{H}_w^{(8)} = \frac{1}{2} \sum_a (\bar{b} \lambda^a s)(\bar{c} \lambda^a c), \quad (4.2)$$

$$a_2 = \frac{C_1}{N_c} + C_2, \quad (4.3)$$

N_c is the number of colors and λ^a are the Gell-Mann matrices.

At this point, the number of colors, $N_c = 3$, will be taken seriously. Also, instead of neglecting the nonfactorizable terms (second term in (4.1) and any nonfactorized contribution to the first term), we parameterize them as in [3]. The parametrization is done in such a way that we can conveniently combine the factorizable and the nonfactorizable terms. Explicitly, this means writing the following:

$$\begin{aligned} \langle K^* J/\psi | \mathcal{H}_w^{(8)} | B \rangle &= -\frac{m_{J/\psi}}{m_B + m_{K^*}} f_{J/\psi} \left[2i \varepsilon_{\mu\nu\rho\sigma} \epsilon_{J/\psi}^{\mu} \epsilon_{K^*}^{\nu} p_{J/\psi}^{\rho} p_{K^*}^{\sigma} V^{(8)nf}(q^2) \right. \\ &\quad - (m_B + m_{K^*})^2 (\epsilon_{K^*}^{\mu} \epsilon_{J/\psi}^{\mu}) A_1^{(8)nf}(q^2) \\ &\quad \left. + 2 (\epsilon_{K^*}^{\mu} p_{J/\psi}^{\mu}) (\epsilon_{J/\psi}^{\mu} p_{K^*}^{\mu}) A_2^{(8)nf}(q^2) \right], \end{aligned} \quad (4.4)$$

where

$$q_\mu = (p_B - p_{K^*})_\mu = (p_{J/\psi})_\mu. \quad (4.5)$$

The nonfactorized contribution to the first term in (4.1) is parametrized analogously to (4.4) by writing $A_1^{(1)nf}$ in place of $A_1^{(8)nf}$, etc. .

By substituting (3.15) and (4.4) into (4.1) we arrive at the following helicity amplitudes

$$\mathcal{A}_0 = -\frac{G_F}{\sqrt{2}} V_{cb} V_{cs}^* a_2 f_\psi m_\psi (m_B + m_{K^*}) A_1^{BK^*}(q^2) [a \xi_{A_1} - b x \xi_{A_2}], \quad (4.6)$$

$$\mathcal{A}_\pm = \frac{G_F}{\sqrt{2}} V_{cb} V_{cs}^* a_2 f_\psi m_\psi (m_B + m_{K^*}) A_1^{BK^*}(q^2) [\xi_{A_1} \mp c y \xi_V], \quad (4.7)$$

where a, b, c, x and y are defined in (3.22).

Here, we introduce the parameters χ_{A_1} , χ_{A_2} and χ_V to parametrize the nonfactorization in the three formfactors A_1 , A_2 and V respectively. These are defined as

$$\chi_{A_1} = \left(A_1^{(8)nf}(m_\psi^2) + \frac{a_2}{C_1} A_1^{(1)nf}(m_\psi^2) \right) / A_1^{BK^*}(m_\psi^2), \quad (4.8)$$

$$\chi_{A_2} = \left(A_2^{(8)nf}(m_\psi^2) + \frac{a_2}{C_1} A_2^{(1)nf}(m_\psi^2) \right) / A_2^{BK^*}(m_\psi^2), \quad (4.9)$$

$$\chi_V = \left(V^{(8)nf}(m_\psi^2) + \frac{a_2}{C_1} V^{(1)nf}(m_\psi^2) \right) / V^{BK^*}(m_\psi^2). \quad (4.10)$$

These parameters are related to ξ_{A_1} , ξ_{A_2} and ξ_V , that appear in \mathcal{A}_0 and \mathcal{A}_\pm , by

$$\begin{aligned} \xi_{A_i} &= \left(1 + \frac{C_1}{a_2} \chi_{A_i} \right) \quad i = 1, 2, \\ \xi_V &= \left(1 + \frac{C_1}{a_2} \chi_V \right). \end{aligned} \quad (4.11)$$

Note that, a departure of ξ from unity, or χ from zero, signals nonfactorized contribution. This can be seen by comparing (4.6) and (4.7), above, by (3.99) and (3.100) that were derived in the previous chapter.

The decay rate and longitudinal polarization are given by

$$\Gamma(B \rightarrow K^* J/\psi) = \frac{|\mathbf{k}|}{8\pi m_B^2} (|\mathcal{A}_0|^2 + |\mathcal{A}_+|^2 + |\mathcal{A}_-|^2), \quad (4.12)$$

$$P_0(B \rightarrow K^* J/\psi) = \frac{|\mathcal{A}_0|^2}{|\mathcal{A}_0|^2 + |\mathcal{A}_+|^2 + |\mathcal{A}_-|^2}. \quad (4.13)$$

A similar formalism applies for the decay $\overline{B}_s^0 \rightarrow \phi J/\psi$.

Table 4.1: The different experimental measurements of the longitudinal polarization (P_0) for the process $B \rightarrow K^* J/\psi$. The first error is statistical and the second is systematic.

Experiment	$P_0(B \rightarrow K^* J/\psi)$
ARGUS [5]	$0.97 \pm 0.16 \pm 0.15$
CLEO II (94) [6]	$0.80 \pm 0.08 \pm 0.05$
CDF [7]	$0.65 \pm 0.10 \pm 0.04$
CLEO II (97) [8]	$0.52 \pm 0.07 \pm 0.04$

4.3 $B \rightarrow K^* J/\psi$ Decay

The decay $B \rightarrow K^* J/\psi$ proceeds through both the charged channel $B^- \rightarrow K^{*-} J/\psi$ and the neutral channel $\bar{B}^0 \rightarrow \bar{K}^{*0} J/\psi$ (see Fig. 3.5). The available experimental values for the branching ratios of these two decay modes are $(1.67 \pm 0.35) \times 10^{-3}$ and $(1.49 \pm 0.22) \times 10^{-3}$ [4], respectively. For the purposes of this chapter, we take the weighted average of these two values as the experimental value for the branching ratio of the process $B \rightarrow K^* J/\psi$. The result is

$$\mathcal{B}(B \rightarrow K^* J/\psi) = (1.54 \pm 0.19) \times 10^{-3} . \quad (4.14)$$

Regarding the longitudinal polarization, several measurements have been made with varying results, as shown in Table 4.1. From these measurements, we obtain the following average for P_0

$$P_0(B \rightarrow K^* J/\psi) = 0.66 \pm 0.05 . \quad (4.15)$$

Since nonfactorization is introduced through three parameters (χ_{A_1} , χ_{A_2} and χ_V) and only two constraints (branching ratio and longitudinal polarization) are available, we find that physics here is a little involved.

Table 4.2: Values of the nonfactorization parameter χ_{A_1} , calculated in each theoretical model, that explain the available experimental branching ratio and longitudinal polarization for the process $B \rightarrow K^* J/\psi$. The other two nonfactorization parameters (χ_{A_2} and χ_V) were assumed to vanish.

Model	fit branching ratio		fit polarization	
	Solution 1	Solution 2	Solution 1	Solution 2
BSW I	0.07 ± 0.02	-0.17 ± 0.02	0.02 ± 0.02	-0.07 ± 0.02
BSW II	0.08 ± 0.02	-0.16 ± 0.01	0.06 ± 0.03	-0.07 ± 0.02
CDDFGN	0.15 ± 0.02	-0.25 ± 0.02	0.07 ± 0.03	-0.12 ± 0.04
AW	0.10 ± 0.02	-0.16 ± 0.01	0.11 ± 0.05	-0.08 ± 0.02
ISGW	0.15 ± 0.02	-0.20 ± 0.02	0.12 ± 0.05	-0.07 ± 0.02

4.3.1 Nonfactorization in One Formfactor

The simplest approach is to assume that only one formfactor has nonfactorizable contribution. We consider this case first. In each of the five models, we find that allowing only one of χ_{A_1} , χ_{A_2} and χ_V to be nonzero, one could fit the branching ratio $\mathcal{B}(B \rightarrow K^* J/\psi)$ with appropriate amounts of nonfactorized contribution. The results of this study are shown in Tables 4.2 - 4.4. For example, in BSW I model ($\chi_{A_1} = 0.07 \pm 0.02$, $\chi_{A_2} = 0$, $\chi_V = 0$), ($\chi_{A_1} = 0$, $\chi_{A_2} = 0.42 \pm 0.04$, $\chi_V = 0$) or ($\chi_{A_1} = 0$, $\chi_{A_2} = 0$, $\chi_V = 0.45 \pm 0.07$) are the positive solutions that would fit the experimental branching ratio in (4.14).

A similar study has been done using the current world average of longitudinal polarization in (4.15). In Table 4.2, we show the values of the nonfactorization parameter χ_{A_1} , needed to reproduce the polarization value, assuming that $\chi_{A_2} = \chi_V = 0$. Table 4.3 shows the results of a similar study regarding χ_{A_2} . However, assuming that $\chi_{A_1} = \chi_{A_2} = 0$, and $\chi_V \neq 0$, we can see from Fig. 4.1 that it is difficult to find acceptable values of χ_V that produce large enough polarization to fit the experimental results.

Table 4.3: Values of the nonfactorization parameter χ_{A_2} , calculated in each theoretical model, that explain the available experimental branching ratio and longitudinal polarization for the process $B \rightarrow K^* J/\psi$. The other two nonfactorization parameters (χ_{A_1} and χ_V) were assumed to vanish.

Model	fit branching ratio		fit polarization	
	Solution 1	Solution 2	Solution 1	Solution 2
BSW I	0.42 ± 0.04	-0.20 ± 0.04	0.24 ± 0.07	-0.02 ± 0.02
BSW II	0.28 ± 0.02	-0.16 ± 0.03	0.16 ± 0.05	-0.05 ± 0.02
CDDFGN	0.63 ± 0.05	-0.41 ± 0.05	0.32 ± 0.09	-0.09 ± 0.04
AW	0.21 ± 0.02	-0.15 ± 0.02	0.13 ± 0.04	-0.08 ± 0.02
ISGW	0.25 ± 0.02	-0.21 ± 0.02	0.11 ± 0.03	-0.07 ± 0.02

Table 4.4: Values of the nonfactorization parameter χ_V , calculated in each theoretical model, that explain the available experimental branching ratio for the process $B \rightarrow K^* J/\psi$. The other two nonfactorization parameters (χ_{A_1} and χ_{A_2}) were assumed to vanish.

Model	fit branching ratio	
	Solution 1	Solution 2
BSW I	0.45 ± 0.07	-0.61 ± 0.05
BSW II	0.29 ± 0.04	-0.44 ± 0.03
CDDFGN	0.26 ± 0.04	-0.42 ± 0.03
AW	0.18 ± 0.03	-0.33 ± 0.03
ISGW	0.31 ± 0.04	-0.46 ± 0.04

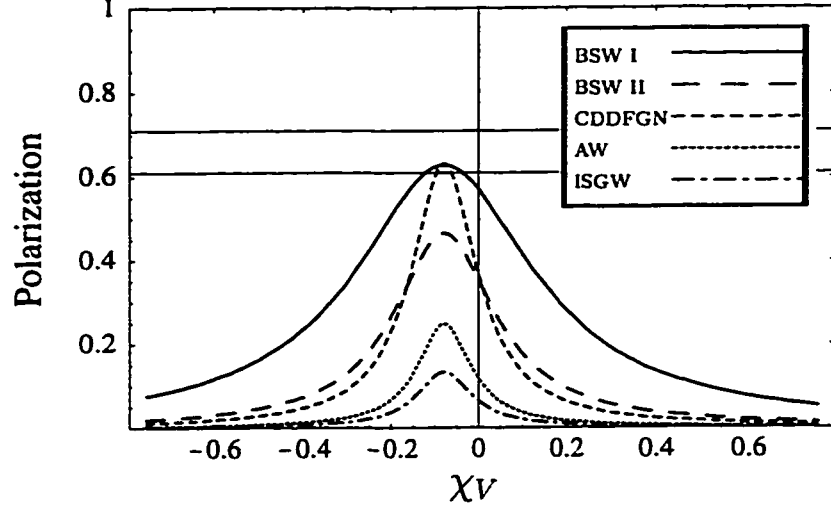


Figure 4.1: Polarization for the process $B \rightarrow K^- J/\psi$ with $(\chi_{A_1} = \chi_{A_2} = 0)$, plotted as a function of χ_V for each model. Horizontal lines define the measured value to one standard deviation.

In order to have a better picture of the results produced so far in this chapter, we combine in Fig. 4.2 the solutions of the nonfactorization parameter χ_{A_1} presented in Table 4.2. We also do a similar combination in Fig. 4.3 for the solutions of the nonfactorization parameter χ_{A_2} presented in Table 4.3.

In Fig. 4.2, the horizontal axis corresponds to the nonfactorization parameter χ_{A_1} , while the vertical axis differentiates between the various models considered. Each dot in the figure represents a solution of χ_{A_1} . The larger dots are the solutions calculated from the branching ratio measurement, whereas the smaller ones are the solutions calculated from the polarization measurement. The error bars represent one standard deviation uncertainty.

From Fig. 4.2 we see that the negative solutions of χ_{A_1} that fit the experimental branching ratio and those that fit the longitudinal polarization do not overlap for any of the five models considered. This means that the negative solutions of χ_{A_1} can not explain the available data on branching ratio and longitudinal polarization simultaneously. The positive solutions, on the other hand, can explain both branching

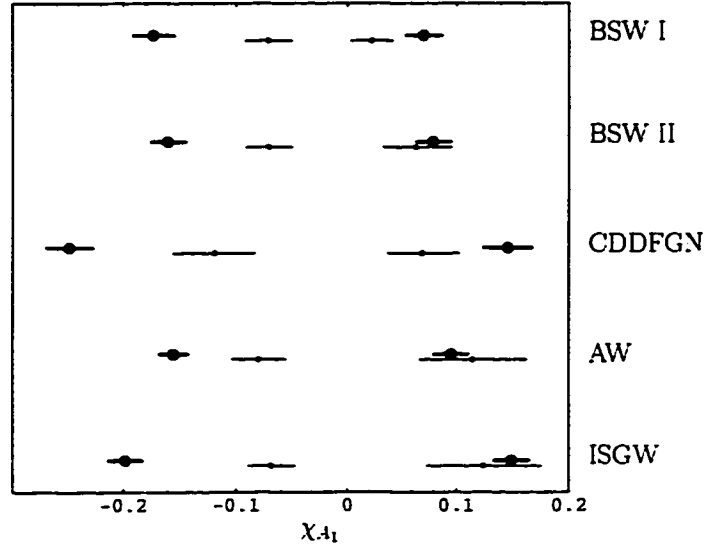


Figure 4.2: Values of the nonfactorization parameter χ_{A_1} , calculated in Table 4.2, that explain the available experimental branching ratio and longitudinal polarization of the process $B \rightarrow K^* J/\psi$. The larger dots are the solutions calculated from the branching ratio measurement, whereas the smaller ones are the solutions calculated from the polarization measurement.

ratio and polarization at the same time in three models (BSW II, AW and ISGW).

In Fig. 4.3, where the horizontal axis corresponds to the nonfactorization parameter χ_{A_2} , we notice a lack of overlap between the solutions of χ_{A_2} that fit the experimental branching ratio and those that fit the longitudinal polarization for all the models considered. So, by assuming that nonfactorization is present only in A_2 formfactor, we can not explain the available experimental data on branching ratio and polarization simultaneously.

For the sake of completeness we show in Fig. 4.4 the solutions of the nonfactorization parameter χ_V , that fit the experimental branching ratio, presented in Table 4.4.

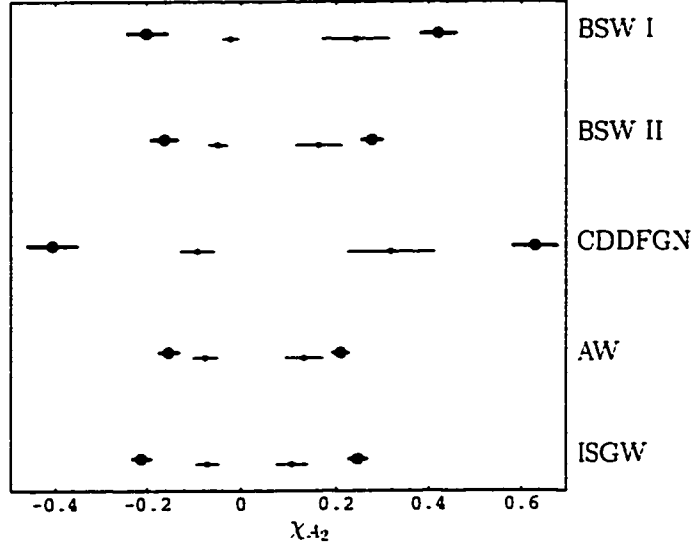


Figure 4.3: Values of the nonfactorization parameter χ_{A_2} , calculated in Table 4.3, that explain the available experimental branching ratio and longitudinal polarization of the process $B \rightarrow K^* J/\psi$. The larger dots are the solutions calculated from the branching ratio measurement, whereas the smaller ones are the solutions calculated from the polarization measurement.

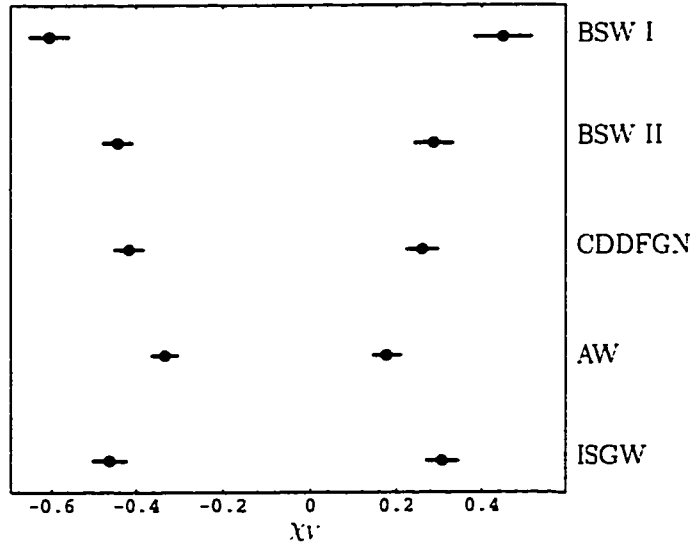


Figure 4.4: Values of the nonfactorization parameter χ_V , calculated in Tables 4.4, that explain the available experimental branching ratio of the process $B \rightarrow K^* J/\psi$.

4.3.2 Nonfactorization in All Formfactors

Next, we assume that nonfactorization is present in all formfactors (A_1 , A_2 and V). In order to do a systematic study, we draw the regions in $\chi_{A_1} - \chi_{A_2}$ space that produce the experimental value for the branching ratio. Also, in the same space, we draw the regions that produce the experimental polarization. This is done for six different values of χ_V in each model. The results are shown in Fig. 4.5 - 4.9. In these figures, the branching ratio demands that the allowed region in $\chi_{A_1} - \chi_{A_2}$ space lies between two ellipses, whereas the region allowed by the polarization measurement lies between two pairs of open curves. Thus, in general, there are four solutions where the domain allowed by the branching ratio overlaps with the domain allowed by the polarization.

Let us start by studying Fig. 4.5 which was generated using BSW I model. From this figure, we notice that nonfactorization in only one formfactor is not enough to explain both branching ratio and polarization at the same time. Nonfactorization in at least two formfactors is needed. This is consistent with the findings of the previous subsection. The graphs in Fig. 4.5 also suggest upper and lower bounds on the values of the nonfactorization parameters χ_{A_1} , χ_{A_2} and χ_V . The value of χ_{A_1} , for example, varies between -0.25 and 0.10 whereas χ_{A_2} has a larger range, from -0.80 to 0.60 . The lower and upper bounds on χ_V are -0.45 and 0.30 respectively. Even though it is not shown in Fig. 4.5, this is due to the lack of overlap between the regions that explain branching ratio and those that explain polarization for values of χ_V smaller than -0.45 or larger than 0.30 .

From Fig. 4.6, we see that in BSW II model the ranges of validity of the nonfactorization parameters χ_{A_1} , χ_{A_2} and χ_V are smaller than that in BSW I model. We also notice that, nonfactorization present in χ_{A_1} only is sufficient to explain experimental data. This can be seen from the graph corresponding to $\chi_V = 0$ where one of the four areas of overlap lies on the x -axis, i.e. $\chi_{A_2} = 0$.

From Fig. 4.7, we see that in CDDFGN model the ranges of validity of the nonfactorization parameters χ_{A_1} and χ_{A_2} are large compared to those in BSW I model.

However, χ_V has a smaller validity range. We also notice that, similar to the BSW I model, nonfactorization present in only one formfactor is not sufficient to explain experimental data.

Regarding AW model, we see from Fig. 4.8 that the range of validity of the non-factorization parameters χ_V is the smallest of all the models considered. Also, we see from the graph corresponding to $\chi_V = 0$, that the experimental values of branching ratio and polarization can be explained by assuming nonfactorization in χ_{A_1} only. This latter point is also true for the predictions of the ISGW* model as can be seen from Fig. 4.9.

4.3.3 Polarization Contours

Another way to display our results is shown in Fig. 4.10. In this figure, we plotted the regions in $x - y$ plane (x and y are defined in (3.22)) allowed by the polarization data for different choices of the nonfactorization parameters χ_{A_1} , χ_{A_2} and χ_V . The two shaded regions in each graph correspond to the factorization approximation $\chi_{A_1} = \chi_{A_2} = \chi_V = 0$. As we can see, all models lie outside the shaded areas, and the model that gives a prediction closest to the world average of longitudinal polarization is BSW I model.

If a small positive value is given to χ_{A_1} only, the allowed regions in $x - y$ plane move to the right as in Fig. 4.10 *a*. So, by choosing an appropriate value for χ_{A_1} between 0 and 10%, the prediction of any of the models considered can be fitted to the experimental value. Similarly, Fig. 4.10 *b* demonstrates how the predictions of the five models can be fitted to the experiment by choosing a value for χ_{A_2} between 0 and -8% while the other two nonfactorization parameters are taken to be zero. In Fig. 4.10 *c*, we see the allowed regions in $x - y$ plane resulting from a -8% nonfactorization in χ_V only. This region contains BSW I and CDDFGN models only. Actually, this is the best that can be done with χ_V and, as can also be seen from Fig. 4.1, no other model can be fitted to the experiment by choosing different values for χ_V . In Fig. 4.10 *d*,

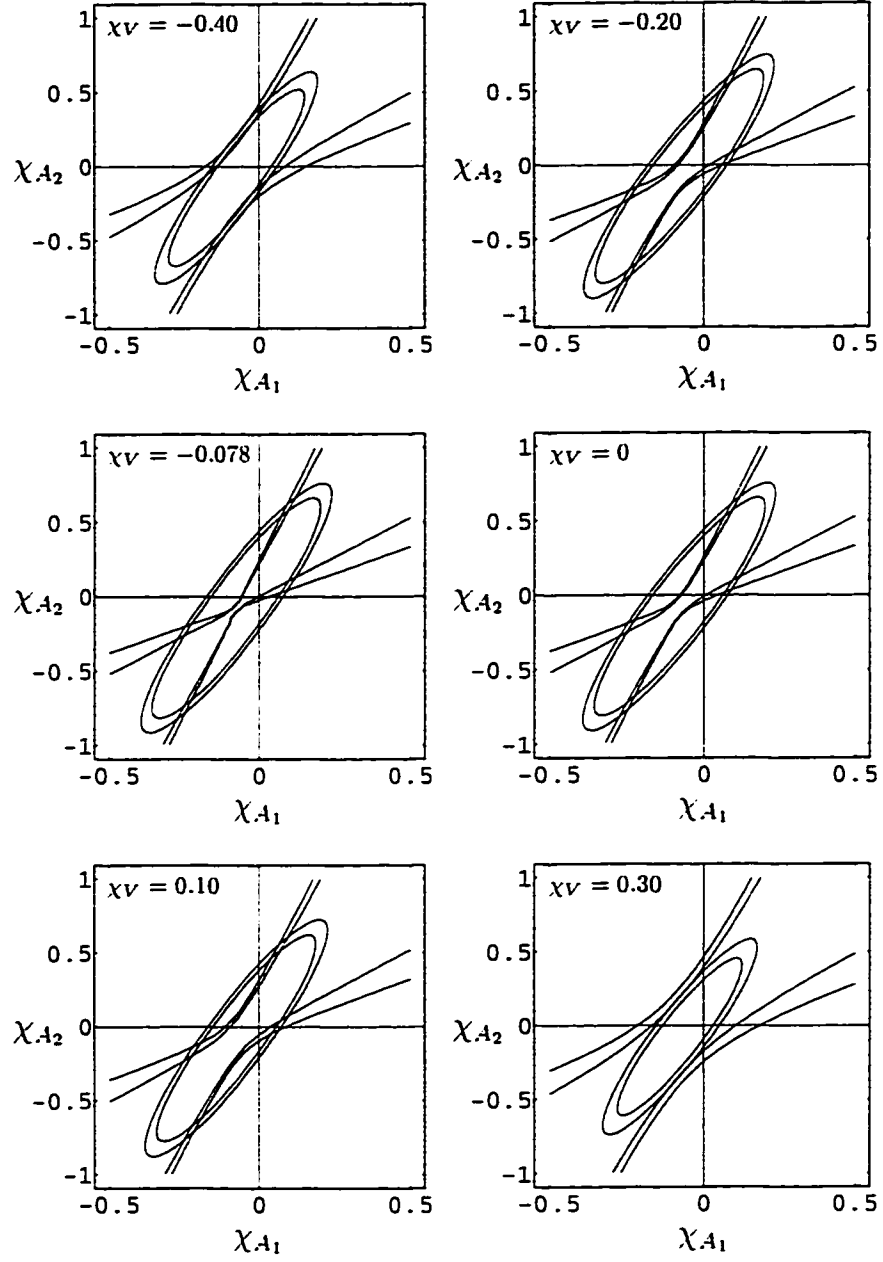


Figure 4.5: Regions in $\chi_{A_1} - \chi_{A_2}$ space bounded by experimental data on branching ratio (ellipses) and polarization (open pairs of curves) for the process $B \rightarrow K^* J/\psi$ assuming BSW I model. Each of the six graphs represent a different value for χ_V .

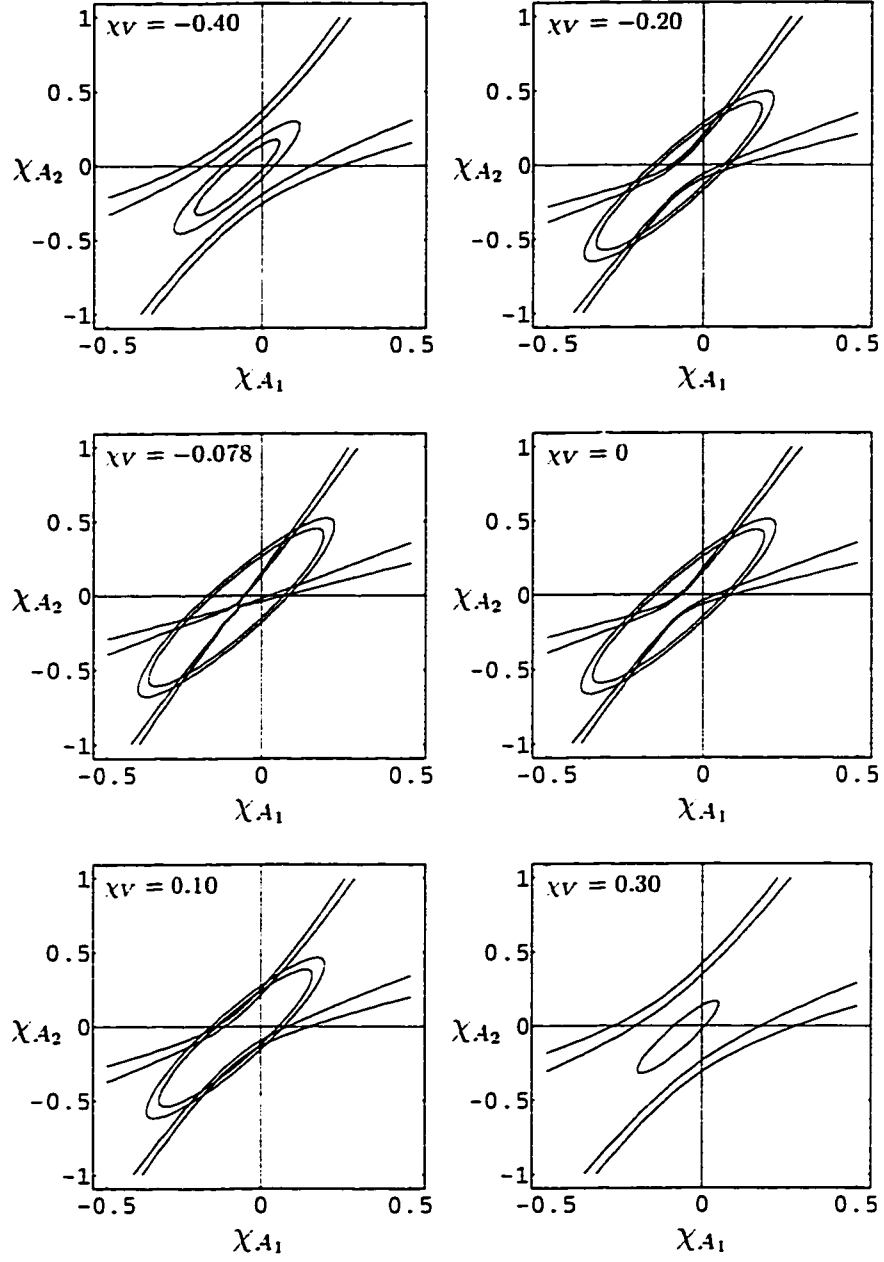


Figure 4.6: Regions in $\chi_{A_1} - \chi_{A_2}$ space bounded by experimental data on branching ratio (ellipses) and polarization (open pairs of curves) for the process $B^0 \rightarrow K^{*0} J/\psi$ assuming BSW II model. Each of the six graphs represent a different value for χ_V .

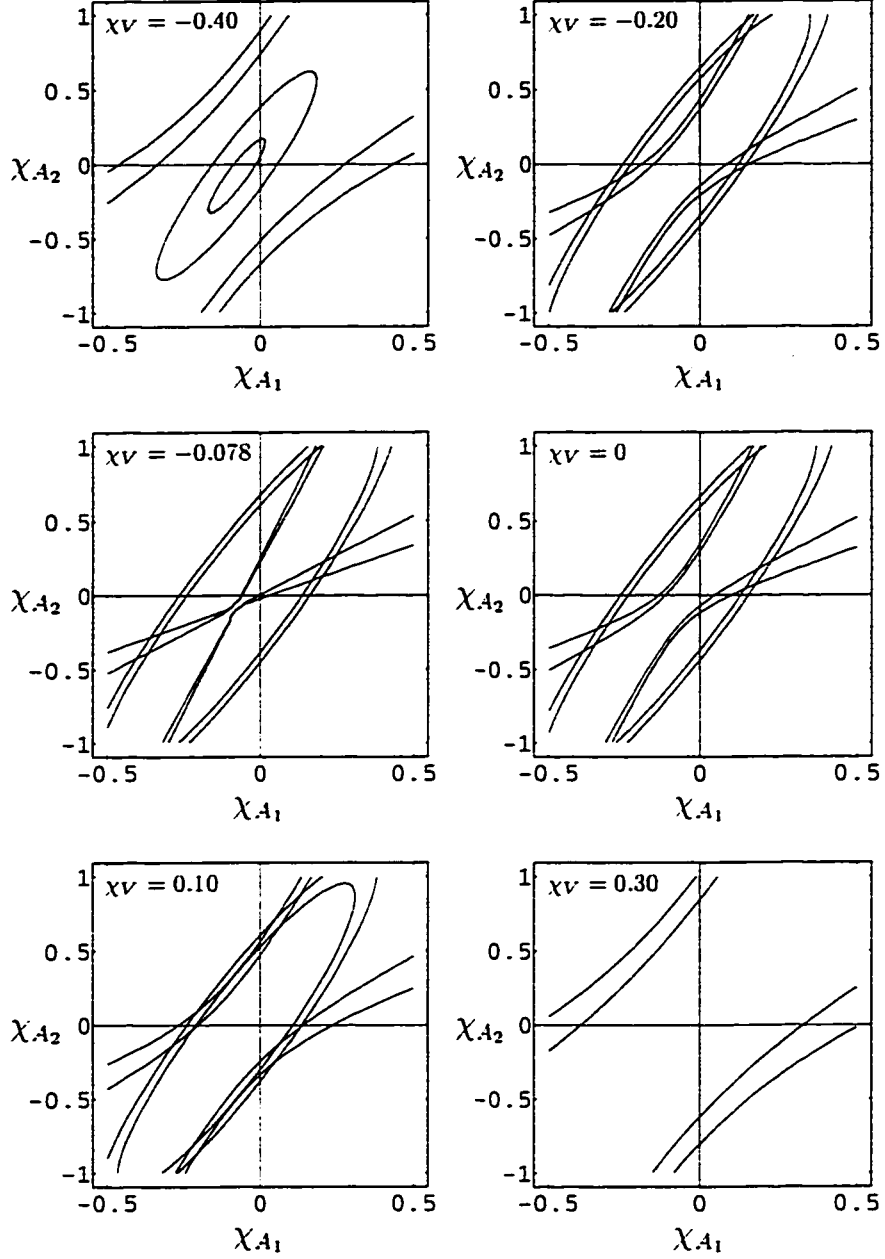


Figure 4.7: Regions in $\chi_{A_1} - \chi_{A_2}$ space bounded by experimental data on branching ratio (ellipses) and polarization (open pairs of curves) for the process $B^0 \rightarrow K^{*0} J/\psi$ assuming CDDFGN model. Each of the six graphs represent a different value for χ_V .

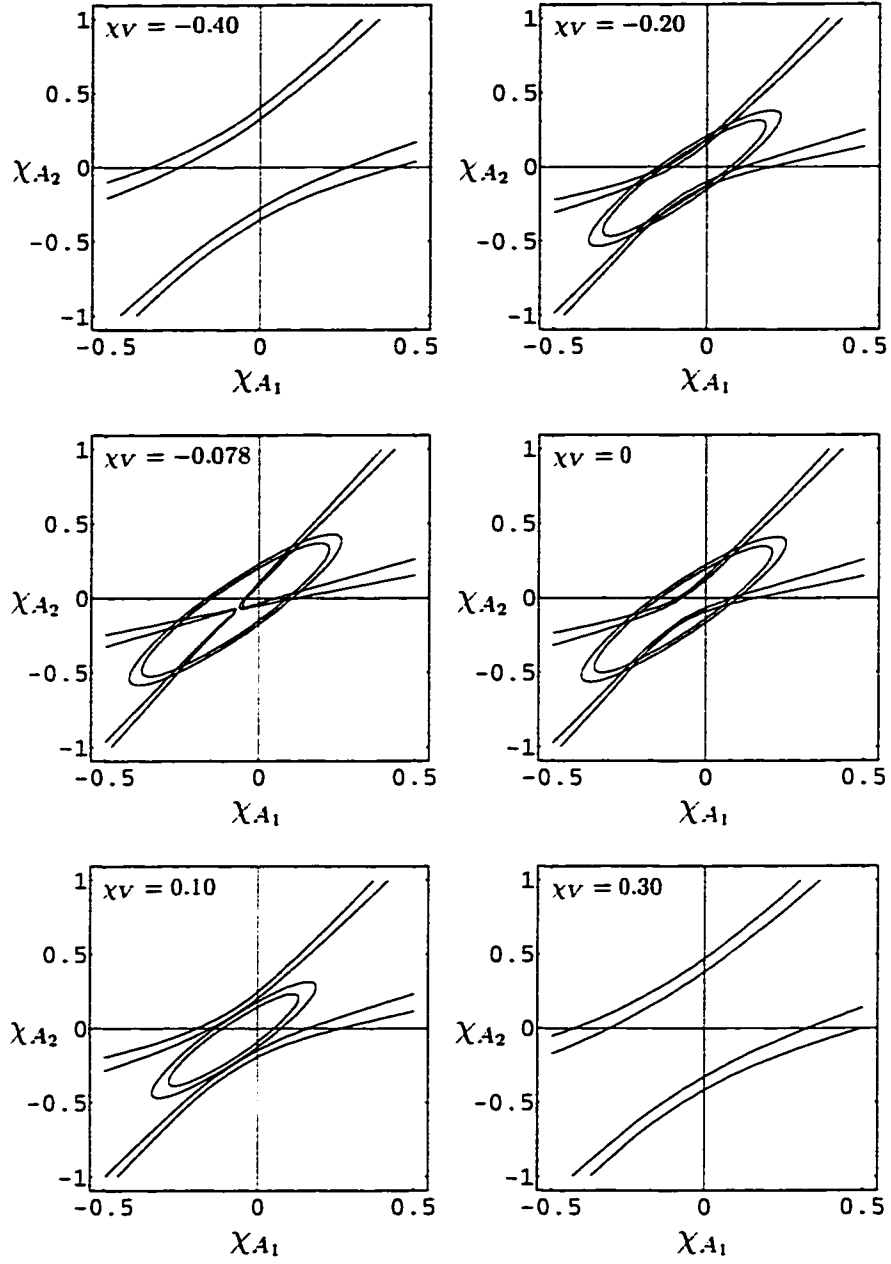


Figure 4.8: Regions in $\chi_{A_1} - \chi_{A_2}$ space bounded by experimental data on branching ratio (ellipses) and polarization (open pairs of curves) for the process $B^0 \rightarrow K^{*0} J/\psi$ assuming AW model. Each of the six graphs represent a different value for χ_V .

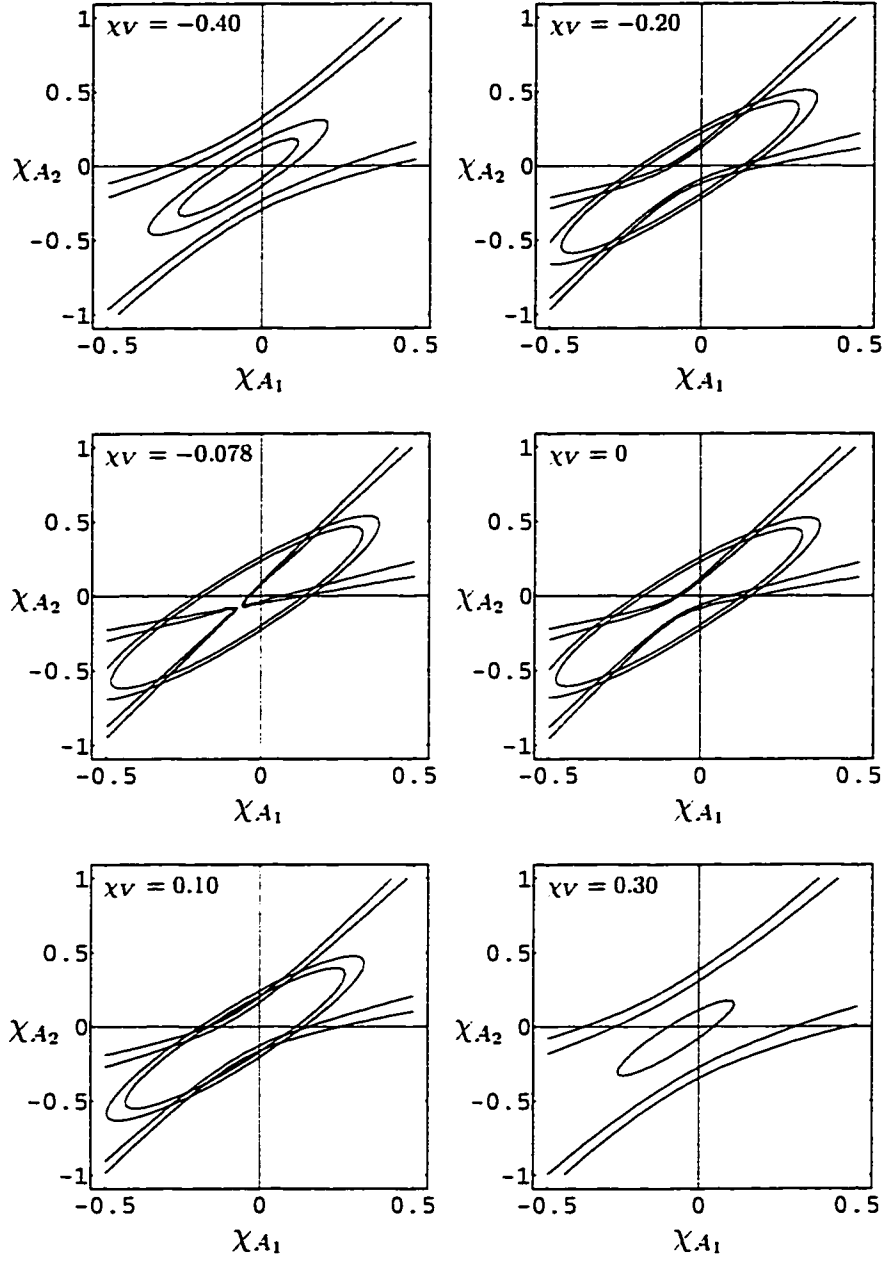


Figure 4.9: Regions in $\chi_{A_1} - \chi_{A_2}$ space bounded by experimental data on branching ratio (ellipses) and polarization (open pairs of curves) for the process $B^0 \rightarrow K^{*0} J/\psi$ assuming ISGW model. Each of the six graphs represent a different value for χ_V .

we show the allowed regions $x - y$ plane that correspond to $\chi_{A_1} = 3\%$, $\chi_{A_2} = -3\%$ and $\chi_V = -3\%$.

The values of χ_{A_1} , χ_{A_2} , and χ_V chosen above are only to illustrate the effect of nonfactorization on longitudinal polarization.

4.4 $\overline{B}_s^0 \rightarrow \phi J/\psi$ Decays

Not much is known about the decays of the B_s meson. To the best of our knowledge, the available values for the branching ratio and longitudinal polarization of the decay $\overline{B}_s^0 \rightarrow \phi J/\psi$ are [9, 7]

$$\mathcal{B}(B_s \rightarrow \phi J/\psi) = (0.93 \pm 0.33) \times 10^{-3} \quad (4.16)$$

and

$$P_0(B_s \rightarrow \phi J/\psi) = 0.56 \pm 0.21, \quad (4.17)$$

respectively. Even though these experimental results have relatively large errors, they are still useful for the purposes of our study and they can be used to investigate the importance of the nonfactorization contribution in the decay $\overline{B}_s^0 \rightarrow \phi J/\psi$. The analysis done in this section is similar to that performed in the previous one for the process $B \rightarrow K^* J/\psi$.

4.4.1 Nonfactorization in One Formfactor

In the first part of this analysis, we assume that only one formfactor contains nonfactorization contribution. By solving for the corresponding nonfactorization parameter using the experimental value for the branching ratio and longitudinal polarization, we arrive at the results in Tables 4.5 - 4.7. The first two columns of data in Table 4.5, for example, correspond to the values of the nonfactorization parameter χ_{A_1} , calculated in each theoretical model considered, that can explain the experimental branching ratio (of course χ_{A_2} and χ_V are taken to be zero). Fig. 4.11 shows the longitudinal

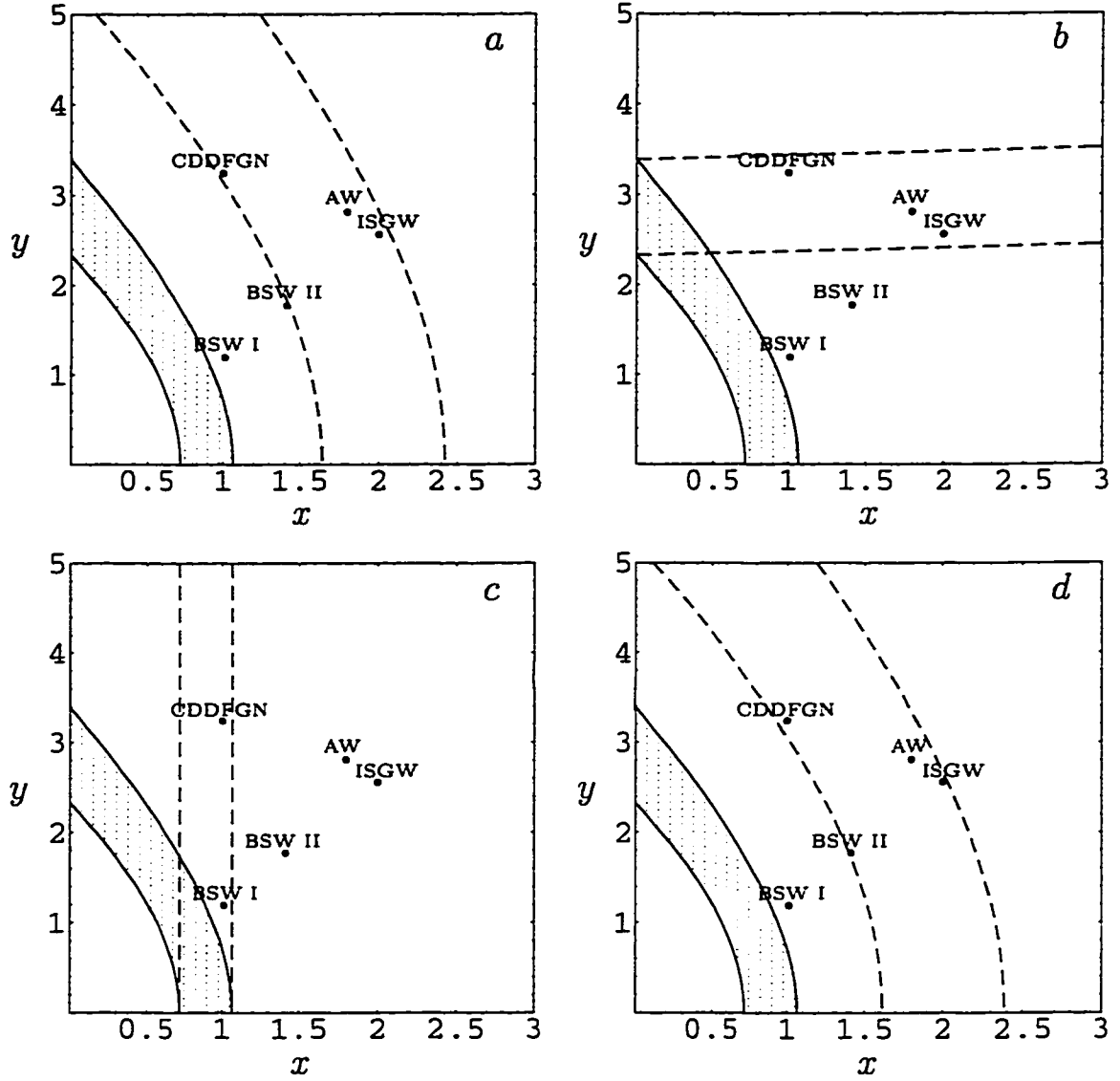


Figure 4.10: Regions in $x - y$ plane allowed by experimental data on polarization for the process $B \rightarrow K^* J/\psi$. The shaded region between the two solid curves in each graph correspond to the factorization approximation $\chi_{A_1} = \chi_{A_2} = \chi_V = 0$. The regions between the dashed curves in each graph corresponds to (a) $\chi_{A_1} = 0.10, \chi_{A_2} = \chi_V = 0$, (b) $\chi_{A_2} = -0.08, \chi_{A_1} = \chi_V = 0$, (c) $\chi_V = -0.08, \chi_{A_1} = \chi_{A_2} = 0$, (d) $\chi_{A_1} = 0.03, \chi_{A_2} = \chi_V = -0.03$. The dots represent predictions of the theoretical models.

Table 4.5: Values of the nonfactorization parameter χ_{A_1} , calculated in each theoretical model, that explain the available experimental branching ratio and longitudinal polarization for the process $\overline{B}_s^0 \rightarrow \phi J/\psi$. The other two nonfactorization parameters (χ_{A_2} and χ_V) were assumed to vanish.

Model	fit branching ratio		fit polarization	
	Solution 1	Solution 2	Solution 1	Solution 2
BSW I	0.07 ± 0.03	-0.17 ± 0.03	0.002 ± 0.042	-0.07 ± 0.02
BSW II	0.07 ± 0.03	-0.16 ± 0.03	0.04 ± 0.06	-0.07 ± 0.02
CDDFGN	0.11 ± 0.04	-0.22 ± 0.04	0.05 ± 0.07	-0.11 ± 0.05
AW	0.05 ± 0.03	-0.13 ± 0.02	0.07 ± 0.08	-0.08 ± 0.03
ISGW	0.15 ± 0.04	-0.23 ± 0.04	0.06 ± 0.08	-0.07 ± 0.03

polarization, in each model, as function of χ_V when both χ_{A_1} and χ_{A_2} are assumed not to contribute.

As we did in the previous section, the results presented in Table 4.5 regarding the amount of nonfactorization in A_1 , are combined in Fig. 4.12. Similarly, in Fig. 4.13 we combine the solutions of the nonfactorization parameter χ_{A_2} presented in Table 4.6.

From Fig. 4.12 we see that the negative solutions of χ_{A_1} that fit the experimental branching ratio do not overlap with those that fit the longitudinal polarization except in the case of AW model. This means that, similar to the case of $B \rightarrow K^* J/\psi$ decay, the negative solutions of χ_{A_1} do not seem to explain the available data on branching ratio and longitudinal polarization simultaneously. The positive solutions, on the other hand, can explain both branching ratio and polarization at the same time in all the models considered.

In Fig. 4.13, which corresponds to assuming nonfactorization in A_2 only, we notice that there are no overlaps between the solutions of χ_{A_2} that fit the experimental branching ratio and those that fit the longitudinal polarization in four of the five considered models. In the case of AW model, a 20% or -10% nonfactorization in χ_{A_2}

Table 4.6: Values of the nonfactorization parameter χ_{A_2} , calculated in each theoretical model, that explain the available experimental branching ratio and longitudinal polarization for the process $\bar{B}_s^0 \rightarrow \phi J/\psi$. The other two nonfactorization parameters (χ_{A_1} and χ_V) were assumed to vanish.

Model	fit branching ratio		fit polarization	
	Solution 1	Solution 2	Solution 1	Solution 2
BSW I	0.45 ± 0.07	-0.21 ± 0.08	0.25 ± 0.09	-0.003 ± 0.053
BSW II	0.30 ± 0.05	-0.17 ± 0.05	0.16 ± 0.06	-0.04 ± 0.04
CDDFGN	0.55 ± 0.09	-0.33 ± 0.10	0.30 ± 0.12	-0.07 ± 0.08
AW	0.21 ± 0.04	-0.11 ± 0.05	0.16 ± 0.07	-0.06 ± 0.05
ISGW	0.36 ± 0.06	-0.28 ± 0.06	0.13 ± 0.06	-0.05 ± 0.04

Table 4.7: Values of the nonfactorization parameter χ_V , calculated in each theoretical model, that explain the available experimental branching ratio for the process $\bar{B}_s^0 \rightarrow \phi J/\psi$. The other two nonfactorization parameters (χ_{A_1} and χ_{A_2}) were assumed to vanish.

Model	fit branching ratio	
	Solution 1	Solution 2
BSW I	0.40 ± 0.12	-0.56 ± 0.11
BSW II	0.25 ± 0.08	-0.41 ± 0.07
CDDFGN	0.18 ± 0.06	-0.34 ± 0.06
AW	0.09 ± 0.05	-0.25 ± 0.04
ISGW	0.36 ± 0.09	-0.51 ± 0.09

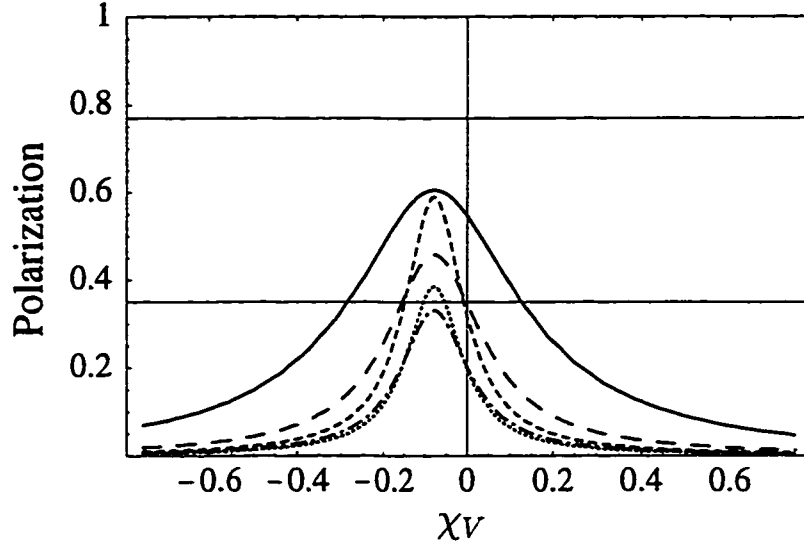


Figure 4.11: Polarization for the process $\bar{B}_s^0 \rightarrow \phi J/\psi$ with $(\chi_{A_1} = \chi_{A_2} = 0)$, plotted as a function of χ_V for each model. Horizontal lines define the measured value to one standard deviation. See Fig. 4.1 for legend.

can predict both experimental branching ratio and polarization simultaneously.

The solutions of the nonfactorization parameter χ_V , that fit the experimental branching ratio are presented in Table 4.7. They are also displayed in Fig. 4.14. However, unlike the decay considered in the previous section, most of the models considered can predict the experimental polarization within error by assuming appropriate nonfactorization present only in χ_V . Only ISGW model failed to predict the experimental polarization for any value of χ_V . This can be seen clearly from Fig 4.11.

4.4.2 Nonfactorization in All Formfactors

In the second part of this analysis, we assume that nonfactorization is present in A_1 , A_2 and V formfactors. The regions in $\chi_{A_1} - \chi_{A_2}$ space that produce the experimental value for the branching ratio, and those that produce the experimental value for longitudinal polarization are generated for six different values of χ_V . The results for each of the five models considered are shown in Fig. 4.15 - 4.19. As we saw before

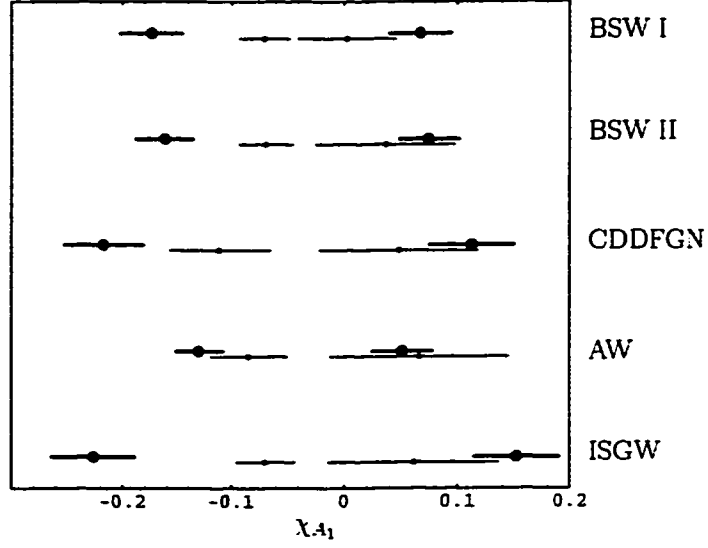


Figure 4.12: Values of the nonfactorization parameter χ_{A_1} , presented in Table 4.5, that explain the available experimental branching ratio and longitudinal polarization of the process $\overline{B}_s^0 \rightarrow \phi J/\psi$.

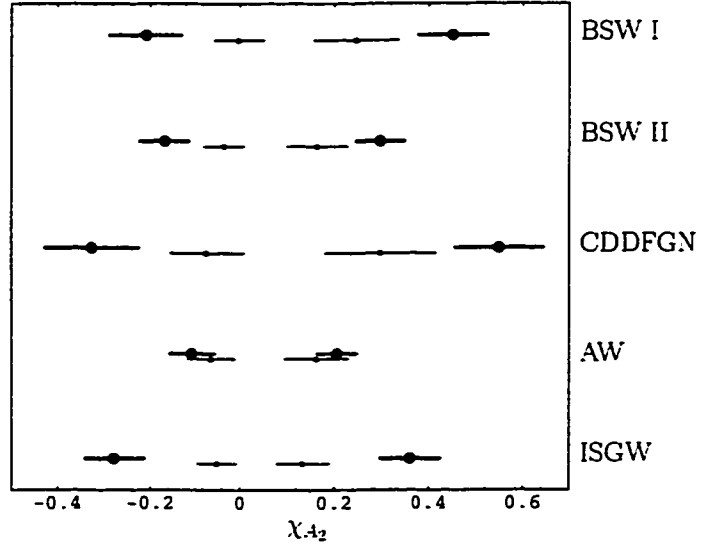


Figure 4.13: Values of the nonfactorization parameter χ_{A_2} , calculated in Table 4.6, that explain the available experimental branching ratio and longitudinal polarization of the process $\overline{B}_s^0 \rightarrow \phi J/\psi$.

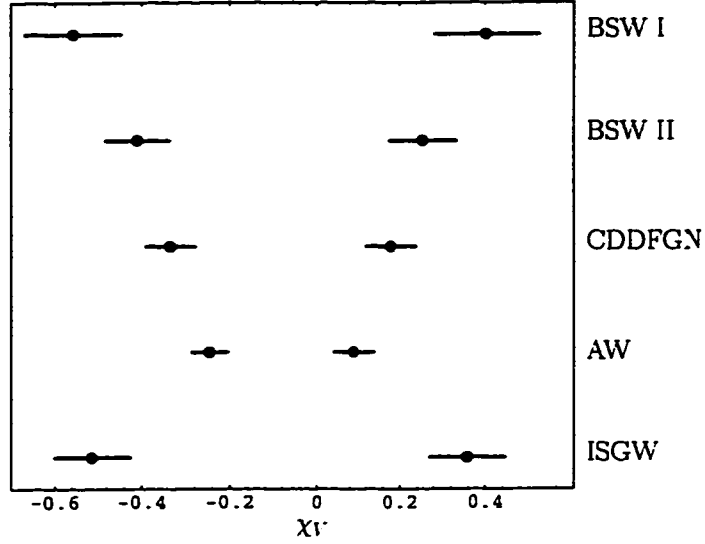


Figure 4.14: Values of the nonfactorization parameter χ_V , calculated in Table 4.7, that explain the available experimental branching ratio of the process $\bar{B}_s^0 \rightarrow \phi J/\psi$.

for the case of $B \rightarrow K^* J/\psi$ decay, the branching ratio demands that the allowed region in $\chi_{A_1} - \chi_{A_2}$ space lies between two ellipses, whereas the region allowed by the polarization measurement lies between two pairs of open curves. Thus, in general, by fixing χ_V there are four solutions for χ_{A_1} and χ_{A_2} .

If we begin by Fig. 4.15, which was generated using BSW I model, we notice that, unlike the decay $B \rightarrow K^* J/\psi$, nonfactorization in A_1 only is enough to explain both branching ratio and polarization at the same time. This can be seen from the graph corresponding to $\chi_V = 0$ in Fig. 4.15 where one of the four solutions lies on the χ_{A_1} -axis. On the other hand, we see that nonfactorization in A_2 or V only can not fit the experimental data, which is also consistent with previous subsection's results. As also suggested by Fig. 4.15, the upper and lower bounds on the value of χ_{A_1} are -0.30 and 0.10 , respectively, χ_{A_2} has a larger range, from -0.80 to 0.70 , and χ_V varies between -0.50 and 0.40 .

From Fig. 4.16, we see that in BSW II model the ranges of validity of the nonfactorization parameters χ_{A_1} , χ_{A_2} and χ_V are smaller than that in BSW I model.

This was also the case for the decay $B \rightarrow K^* J/\psi$ considered in the previous section. We also notice that, nonfactorization present in A_1 only is sufficient to explain experimental data.

From Fig. 4.17, we see that in CDDFGN model the ranges of validity of the nonfactorization parameters χ_{A_1} and χ_{A_2} are large compared to those in BSW I model. However, χ_V has a smaller validity range. We also notice that, similar to the BSW I model, nonfactorization present in A_1 only is sufficient to explain experimental data.

As for the AW model, Fig. 4.18 suggests that χ_V has the the smallest range of validity amongst the models considered in this work. Also the graph corresponding to $\chi_V = 0$ shows that the experimental values of branching ratio and polarization can be explained by assuming nonfactorization in A_1 only or A_2 only.

In ISGW model, we seen from Fig. 4.19 that χ_{A_1} has a relatively large range. Also, notice that nonfactorization in A_1 only is sufficient to explain experimental data.

4.4.3 Polarization Contours

The third part of this analysis is displayed in Fig. 4.20. In this figure, we plotted the regions in $x - y$ plane allowed by the polarization data for different choices of the nonfactorization parameters χ_{A_1} , χ_{A_2} and χ_V . The two shaded regions in each graph correspond to the factorization assumption ($\chi_{A_1} = \chi_{A_2} = \chi_V = 0$). As we can see, both BSW I and BSW II models lie inside the shaded areas suggesting that, in these two models, nonfactorization is not needed to explain the polarization data. However, as can be seen from Fig. 4.20, by assuming a small positive nonfactorization in A_1 and/or small negative nonfactorizations in χ_{A_2} and χ_V all models will be able to fit to the experimental results of polarization

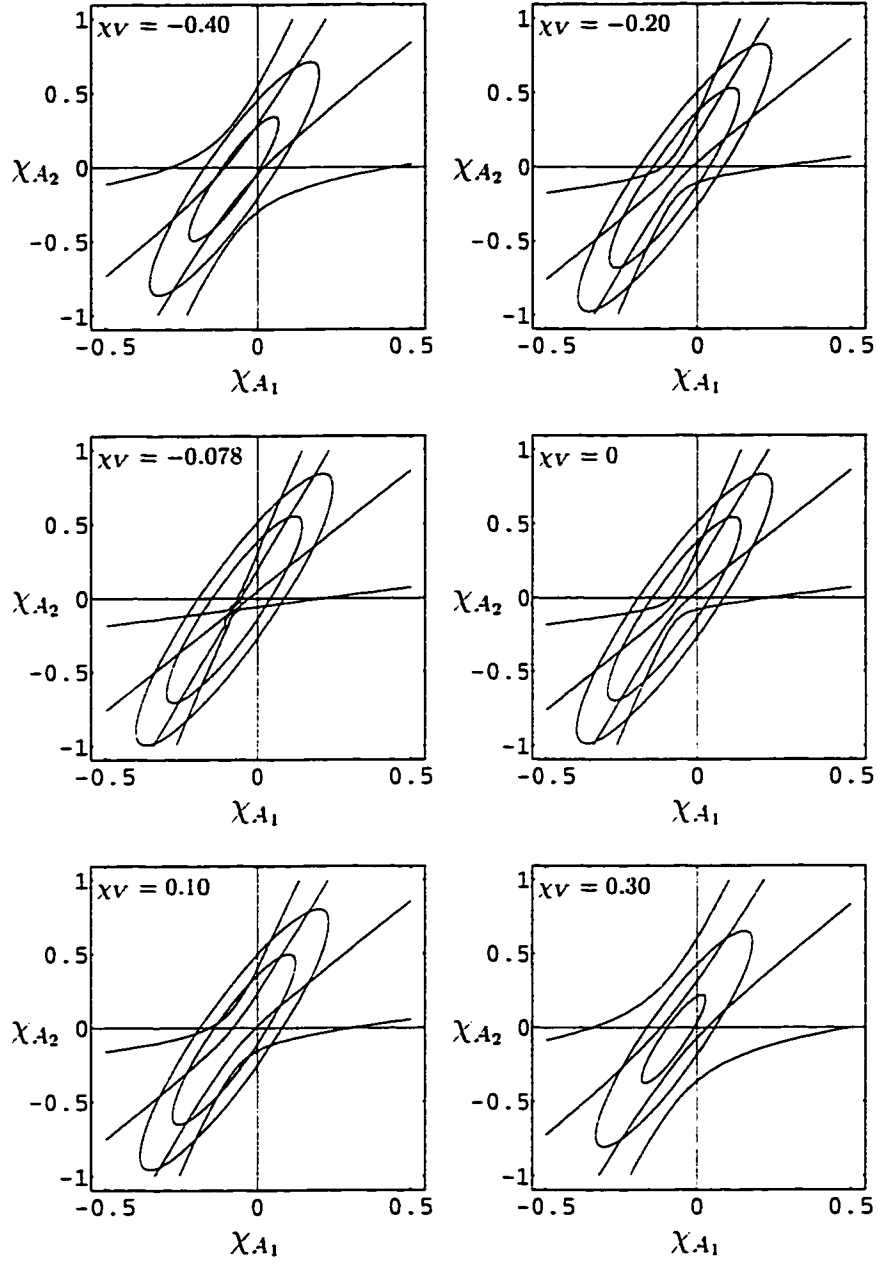


Figure 4.15: Regions in $\chi_{A_1} - \chi_{A_2}$ space bounded by experimental data on branching ratio (ellipses) and polarization (open pairs of curves) for the process $\overline{B}_s^0 \rightarrow \phi J/\psi$ assuming BSW I model. Each of the six graphs represent a different value for χ_V .

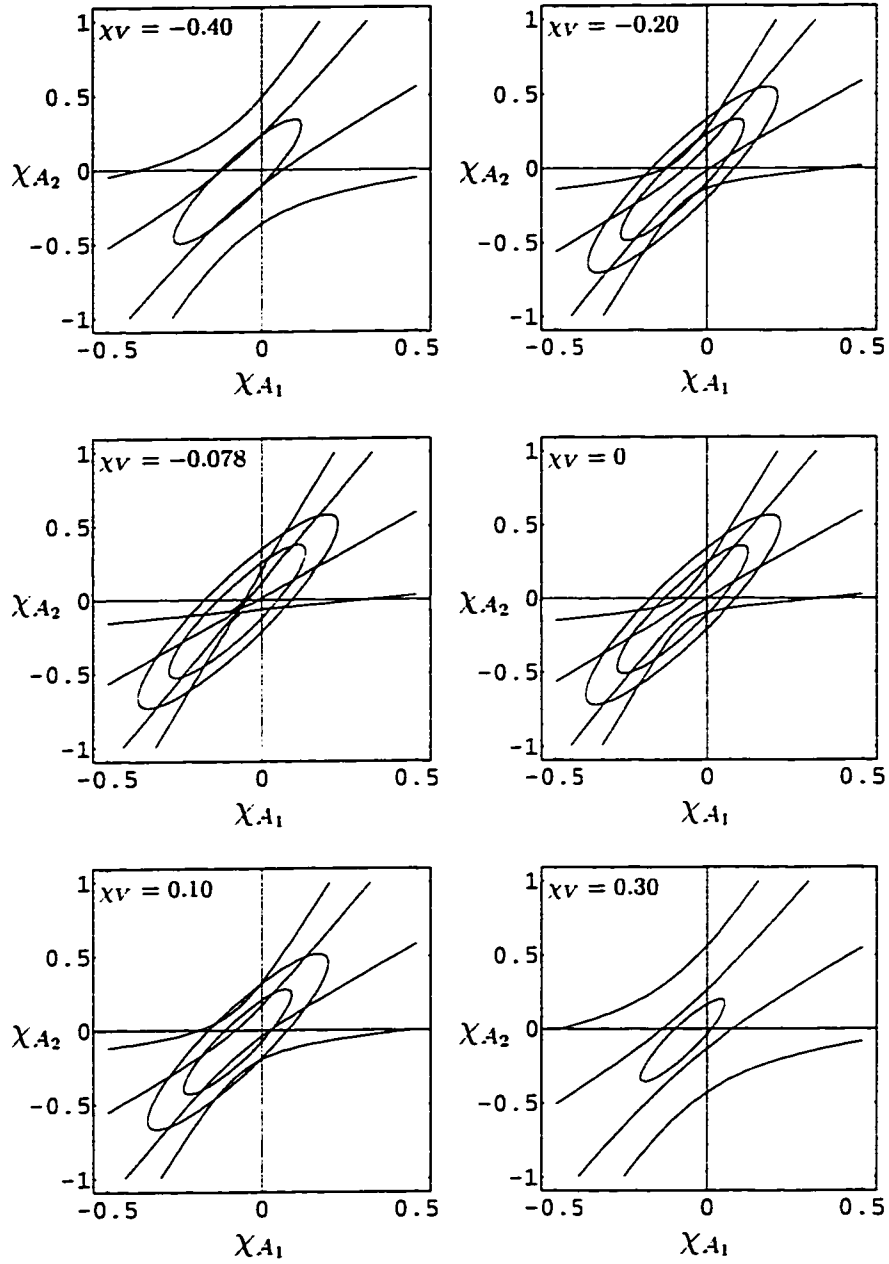


Figure 4.16: Regions in $\chi_{A_1} - \chi_{A_2}$ space bounded by experimental data on branching ratio (ellipses) and polarization (open pairs of curves) for the process $\overline{B}_s^0 \rightarrow \phi J/\psi$ assuming BSW II model. Each of the six graphs represent a different value for χ_V .

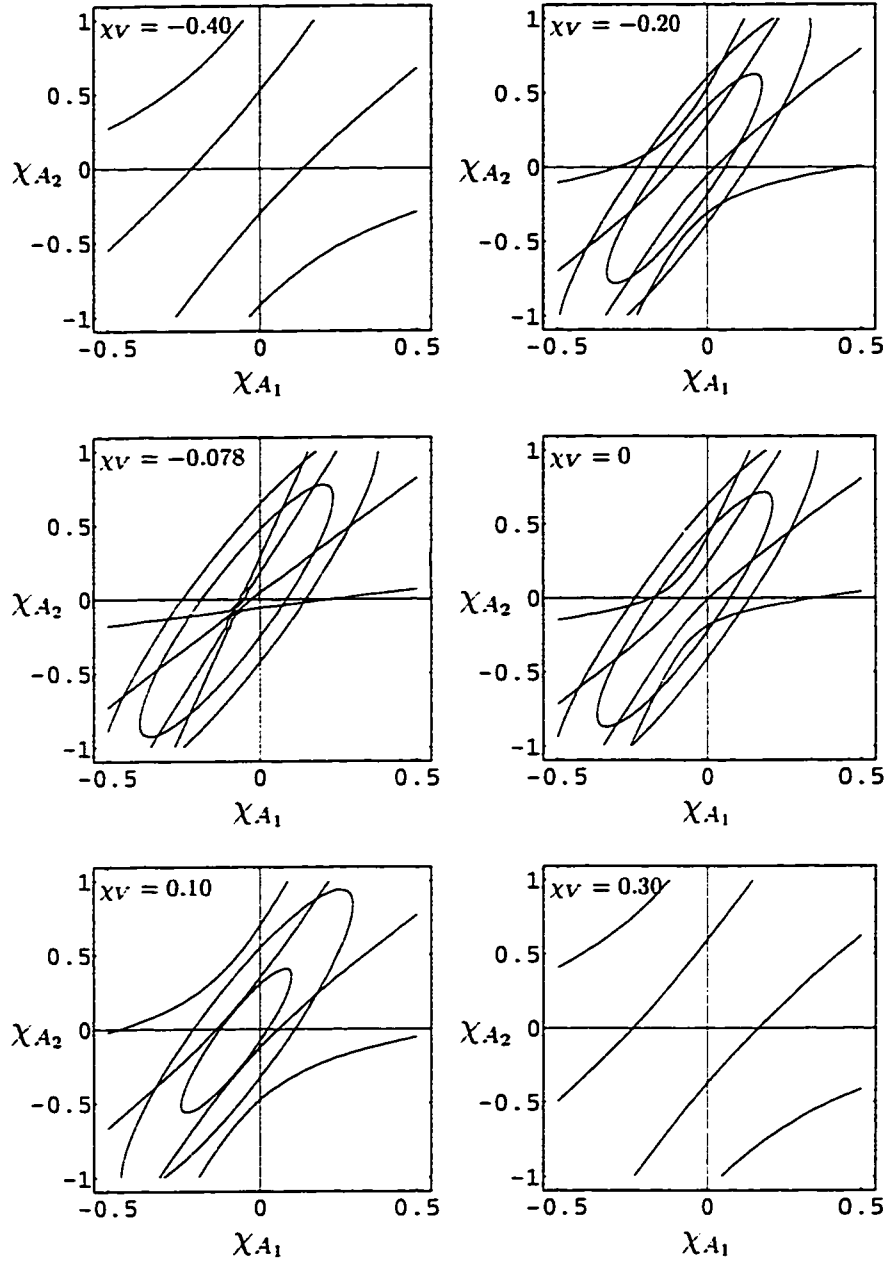


Figure 4.17: Regions in $\chi_{A_1} - \chi_{A_2}$ space bounded by experimental data on branching ratio (ellipses) and polarization (open pairs of curves) for the process $\overline{B}_s^0 \rightarrow \phi J/\psi$ assuming CDDFGN model. Each of the six graphs represent a different value for χ_V .

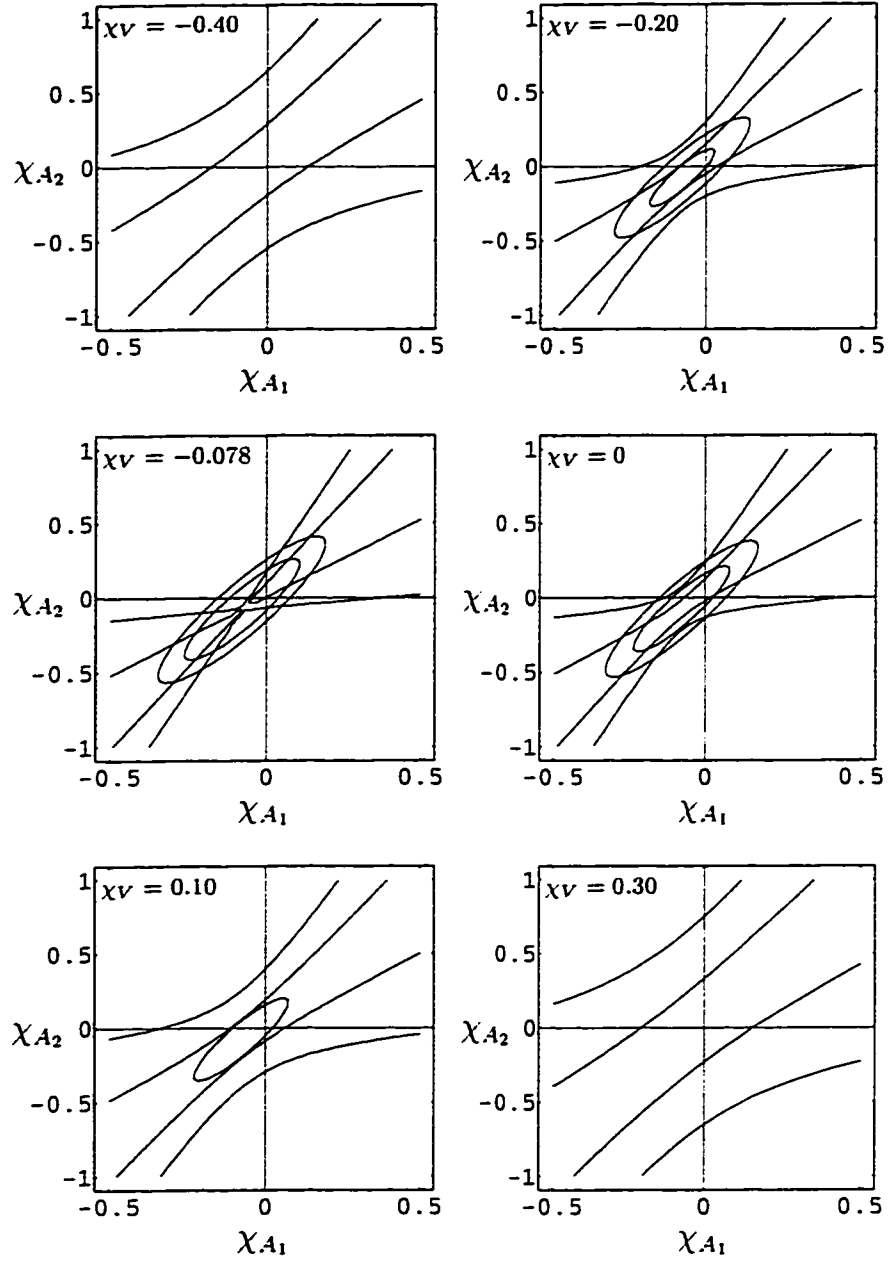


Figure 4.18: Regions in $\chi_{A_1} - \chi_{A_2}$ space bounded by experimental data on branching ratio (ellipses) and polarization (open pairs of curves) for the process $\overline{B}_s^0 \rightarrow \phi J/\psi$ assuming AW model. Each of the six graphs represent a different value for χ_V .

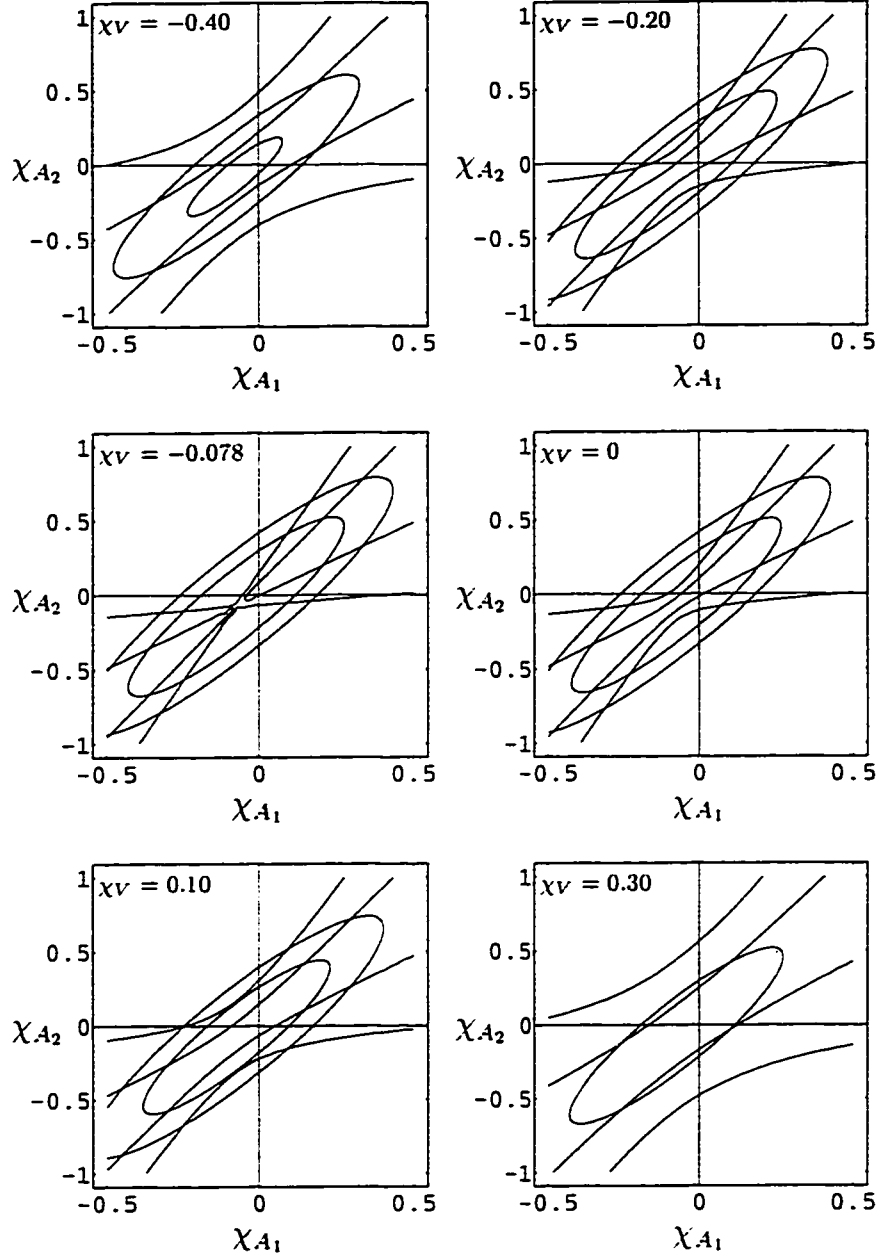


Figure 4.19: Regions in $\chi_{A_1} - \chi_{A_2}$ space bounded by experimental data on branching ratio (ellipses) and polarization (open pairs of curves) for the process $\bar{B}_s^0 \rightarrow \phi J/\psi$ assuming ISGW model. Each of the six graphs represent a different value for χ_V .

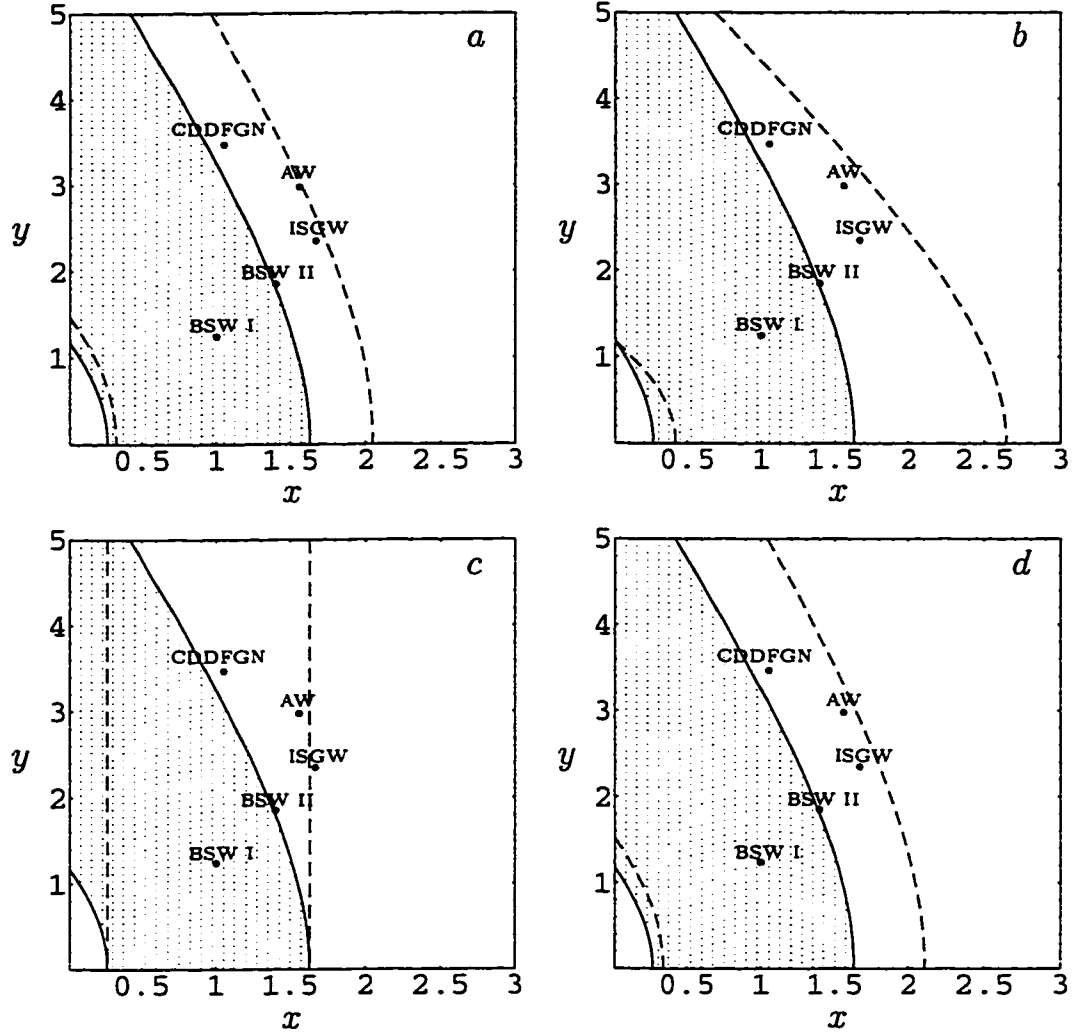


Figure 4.20: Regions in $x - y$ plane allowed by experimental data on polarization for the process $\bar{B}_s^0 \rightarrow \phi J/\psi$. The shaded region between the two solid curves in each graph correspond to the factorization approximation $\chi_{A_1} = \chi_{A_2} = \chi_V = 0$. The region between the dashed curves in each graph corresponds to (a) $\chi_{A_1} = 0.02, \chi_{A_2} = \chi_V = 0$, (b) $\chi_{A_2} = -0.03, \chi_{A_1} = \chi_V = 0$, (c) $\chi_V = -0.08, \chi_{A_1} = \chi_{A_2} = 0$, (d) $\chi_{A_1} = 0.01, \chi_{A_2} = \chi_V = -0.01$. The dots represent predictions of the theoretical models.

4.5 Discussion

Since only the world averages of branching ratio and longitudinal polarization of the decay $B \rightarrow K^* J/\psi$ are considered, one can at best derive a constraint between any two of the three nonfactorization parameters χ_{A_1} , χ_{A_2} , and χ_V . The values of these parameters depend on the theoretical values of the formfactors A_1 , A_2 and V . Due to the fact that of the three parameters, a , b and c (see (3.22)), a is the largest, it is most economical (largest effect for the least amount) to put nonfactorization in χ_{A_1} . We saw that (7 - 15)% nonfactorization in χ_{A_1} only allows most of the formfactor models to be consistent with the branching ratio and longitudinal polarization data.

We analyzed the decay $B \rightarrow K^* J/\psi$ in three ways. In the first way, we assumed that only one formfactor has nonfactorization contribution. Then, we solved for the corresponding nonfactorization parameter using the available world average on the branching ratio and then using the available world average on the longitudinal polarization. What we found is that by assuming nonfactorization in A_2 alone or V alone we can not explain branching ratio and polarization simultaneously. Appropriate positive nonfactorization in A_1 , however, can fit the experimental data in the BSW II, AW and ISGW models.

In the second way, we plotted the regions in χ_{A_1} - χ_{A_2} space that explain the experimental branching ratio and those that explain the experimental polarization for different choices of χ_V (-0.40, -0.20, -0.078, 0, 0.10 and 0.30). This was repeated for each of the formfactor models considered. From the graphs generated in this analysis we were able to set limits for the three nonfactorization parameters χ_{A_1} , χ_{A_2} , and χ_V . The limits depend on the model used.

In the third way, we made use of the fact that longitudinal polarization depends only on the following ratios of the formfactors: $x = A_2(m_\psi^2)/A_1(m_\psi^2)$ and $y = V(m_\psi^2)/A_1(m_\psi^2)$. The regions in x - y space that explain the experimental polarization by assuming factorization and nonfactorization were drawn. The results showed the need for nonfactorization in order to explain the data.

Regarding the decay $B_s \rightarrow \phi J/\psi$, a similar analysis as above was performed. The errors in the experimental values for this process are relatively large which resulted in less precise conclusions specially those obtained from the polarization contours.

However, the two processes $B \rightarrow K^* J/\psi$ and $B_s \rightarrow \phi J/\psi$ turned out to be similar in the amount of nonfactorization needed to explain the experimental data. This suggests that the nonfactorization parameters do not depend strongly on the light degree of freedom in such processes.

Bibliography

- [1] M. Wirbel, Progress in Particle and Nuclear Physics V21, (1988).
- [2] M. Gourdin, A. N. Kamal and X. Y. Pham, Phys. Rev. Lett. **73**, 3355 (1994).
- [3] A. N. Kamal and A. B. Santra, Alberta Thy 31-94 (1994); Z. Phys. C **72**, 91 (1996).
- [4] R. M. Barnett et al., *Particle Data Group, Review of Particle Porperties*, Phys. Rev. D **54**, 1 (1996) and 1997 off-year partial update for the 1998 edition.
- [5] H. Albrecht *et al.* (ARGUS Collaboration), Phys. Lett. B **340**, 217 (1994).
- [6] M. S. Alam *et al.* (CLEO Collaboration), Phys. Rev. D **50**, 43 (1994).
- [7] F. Abe *et al.* (CDF Collaboration), Phys. Rev. Lett. **75**, 3068 (1995).
- [8] C. P. Jessop *et al.* (CLEO Collaboration), Phys. Rev. Lett. **79**, 4533 (1997).
- [9] F. Abe *et al.* (CDF Collaboration), Phys. Rev. D **54**, 6596 (1996).

Chapter 5

Nonfactorization and Final State Interactions in $(B, B_s) \rightarrow \psi P$ and ψV Decays

5.1 Introduction

It was shown in [1, 2] that factorization approximation used in conjunction with formfactors derived in most commonly used models failed to account for the ratio $(B \rightarrow \psi K)/(B \rightarrow \psi K^*)$ and the longitudinal polarization Γ_L/Γ in $B \rightarrow \psi K^*$ decays. Subsequently, it was realized [3] that nonfactorized contributions could play an important role in these color-suppressed decays, and it was demonstrated [4, 5, 6] how such contributions could lead to an understanding of $B \rightarrow \psi K^*$ and ψK data.

Our aim in this work is to investigate the role of nonfactorization and, where relevant, final state interactions (*fsi*). The most recent CLEO data [7] enable us a complete amplitude analysis of $B \rightarrow \psi K^*$ decay. We use this to determine the three partial wave amplitudes, S, P and D, and the two relative phases. We exploit this knowledge in our work (see [6] for a more restricted analysis).

With the knowledge gained from the study of $B \rightarrow \psi K$ and ψK^* decays, we have

also investigated the processes $B_s \rightarrow \psi\eta, \psi\eta', \psi\phi$ with special emphasis on the role of nonfactorization. Furthermore, we have extended our analysis to channels with $\psi(2S)$, instead of ψ , in the final state.

5.2 $(B, B_s) \rightarrow \psi(\psi(2S))P$ Decays

We begin with the formulation for B decays involving ψ (or $\psi(2S)$) and a pseudoscalar particle in the final state. The decay amplitude, in the notation of [5], is written as

$$\begin{aligned} A(B \rightarrow \psi P) &= \langle \psi P | \mathcal{H}_{\text{eff}} | B \rangle \\ &= \frac{G_F}{\sqrt{2}} V_{cb}^* V_{cs} \left[a_2 \langle \psi P | (\bar{b}s)(\bar{c}c) | B \rangle + C_1 \langle \psi P | \mathcal{H}_w^{(8)} | B \rangle \right], \end{aligned} \quad (5.1)$$

where the brackets $(\bar{b}s)$ etc. represent $(V - A)$ quark currents and

$$\mathcal{H}_w^{(8)} = \frac{1}{2} \sum_a (\bar{b}\lambda^a s)(\bar{c}\lambda^a c), \quad (5.2)$$

$$a_2 = \frac{C_1}{N_c} + C_2. \quad (5.3)$$

N_c is the number of colors (taken to be 3) and λ^a are the Gell-Mann matrices. C_1 and C_2 are the standard Wilson coefficients for which we take the values [5],

$$C_1 = 1.12 \pm 0.01, \quad C_2 = -0.27 \pm 0.03, \quad (5.4)$$

which are consistent with the choice in [8].

While the second term in (5.1), the matrix element of $\mathcal{H}_w^{(8)}$, is nonfactorized, the first term receives both factorized and nonfactorized contributions [9]. We introduce the following definitions to proceed further,

$$\langle \psi | (\bar{c}c) | 0 \rangle = \epsilon^\mu m_\psi f_\psi, \quad (5.5)$$

$$\langle P | (\bar{b}s) | B \rangle = \left(p_B + p_P - \frac{m_B^2 - m_P^2}{q^2} q \right)_\mu F_1^{BP}(q^2) + \frac{m_B^2 - m_P^2}{q^2} q_\mu F_0^{BP}(q^2). \quad (5.6)$$

The first matrix element in (5.1) is then written as

$$\langle \psi P | (\bar{b}s)(\bar{c}c) | B \rangle = \langle P | (\bar{b}s) | B \rangle \langle \psi | (\bar{c}c) | 0 \rangle + \langle \psi P | (\bar{b}s)(\bar{c}c) | B \rangle^{nf} \quad (5.7)$$

$$\equiv 2m_\psi f_\psi C_P(\epsilon \cdot p_B) \left[F_1^{BP}(q^2) + F_1^{(1)nf}(q^2) \right], \quad (5.8)$$

where we have defined

$$\langle \psi P | (\bar{b}s)(\bar{c}c) | B \rangle^{nf} = 2m_\psi f_\psi C_P(\epsilon, p_B) F_1^{(1)nf}(q^2). \quad (5.9)$$

In (5.8) and (5.9), C_P has the following values,

$$C_P = \begin{cases} \sqrt{\frac{2}{3}} \left(\cos \theta_P + \frac{1}{\sqrt{2}} \sin \theta_P \right) & P \equiv \eta \\ \sqrt{\frac{2}{3}} \left(\frac{1}{\sqrt{2}} \cos \theta_P - \sin \theta_P \right) & P \equiv \eta' \\ 1 & P \equiv K^0, K^+ \end{cases} \quad (5.10)$$

with the $\eta - \eta'$ mixing angle $\theta_P = -20^\circ$. The superscript (1) in $F_1^{(1)nf}(q^2)$ denotes 'color-singlet'. The nonfactorized matrix element of $\mathcal{H}_w^{(8)}$ is parametrized as

$$\langle \psi P | \mathcal{H}_w^{(8)} | B \rangle^{nf} = 2m_\psi f_\psi C_P(\epsilon, p_B) F_1^{(8)nf}(q^2). \quad (5.11)$$

In terms of the definitions in (4) - (8), the decay amplitude for $B \rightarrow \psi P$ is written as

$$A(B \rightarrow \psi P) = \frac{G_F}{\sqrt{2}} V_{cb}^* V_{cs} a_2^{eff} 2m_\psi f_\psi C_P(\epsilon, p_B) F_1^{BP}(q^2), \quad (5.12)$$

where

$$a_2^{eff} = a_2 \left[1 + \frac{F_1^{(1)nf}(q^2)}{F_1^{BP}(q^2)} + \frac{C_1}{a_2} \frac{F_1^{(8)nf}(q^2)}{F_1^{BP}(q^2)} \right]. \quad (5.13)$$

As a short-hand notation, we introduce two parameters χ_{F_1} and ξ_{F_1} as measures of nonfactorized contributions, as follows:

$$a_2^{eff} \equiv a_2 \left(1 + \frac{C_1}{a_2} \chi_{F_1} \right) \equiv a_2 \xi_{F_1}, \quad (5.14)$$

where,

$$\chi_{F_1} \equiv \frac{a_2}{C_1} \frac{F_1^{(1)nf}(q^2)}{F_1^{BP}(q^2)} + \frac{F_1^{(8)nf}(q^2)}{F_1^{BP}(q^2)}. \quad (5.15)$$

Note that as C_1/a_2 is of the order of 10, the nonfactorized contribution from color-octet current is greatly enhanced. A departure of ξ_{F_1} from unity, or χ_{F_1} from zero, signals nonfactorized contribution.

In terms of the quantities defined in (5.8) - (5.13), the decay rate for the exclusive channel $B \rightarrow \psi P$ is given by,

$$\Gamma(B \rightarrow \psi P) = \frac{G_F^2}{4\pi} |V_{cb}|^2 |V_{cs}|^2 |a_2^{eff}|^2 f_\psi^2 |C_P|^2 |\mathbf{k}|^3 |F_1^{BP}(m_\psi^2)|^2, \quad (5.16)$$

where $|\mathbf{k}|$ is the momentum of the decay products in B rest-frame.

Other parameters we used were, $V_{cs} = 0.974$, $V_{cb} = 0.04$ [10], $f_\psi = 0.384 \pm 0.014$ GeV and $f_{\psi(2S)} = 0.282 \pm 0.014$ GeV [11].

5.2.1 $B \rightarrow \psi(\psi(2S))K$ decays

We first consider the decay $B^+ \rightarrow \psi K^+$ whose branching ratio is more precisely measured than that of the neutral mode [10]. The decay rate formula for this process, (5.16), can be rearranged and written as

$$\xi_{F_1} = \frac{\sqrt{\Gamma(B^+ \rightarrow \psi K^+)}}{(78.422 \times 10^{12} \text{ GeV}^{-2} \text{ sec}^{-1})^{1/2} |V_{cs}| |V_{cb}| a_2 f_\psi F_1^{BK}(m_\psi^2)}. \quad (5.17)$$

A departure of ξ_{F_1} from unity signals the failure of the factorization assumption for a particular model-value of the formfactor. We employed five different models for $F_1^{BK}(m_\psi^2)$. They were: (i) BSW I [12], where the formfactors are calculated at $q^2 = 0$ and extrapolated using a monopole form with the pole masses given in [12], (ii) BSW II, where a dipole extrapolation is used for $F_1(q^2)$, $A_2(q^2)$ and $V(q^2)$, with the same pole masses as in [12], (iii) CDDEGN [13], where the normalization of the formfactors are extrapolated using a monopole form, (iv) AW [14], where the formfactors are evaluated at the zero-recoil point corresponding to the maximum momentum transfer and then extrapolated down to the required q^2 using a monopole form, and (v) ISGW [15], where the formfactors are calculated at the maximum q^2 and extrapolated down to the needed value of q^2 with an exponential form. The predicted formfactors in these five models relevant to the processes of interest are shown in Tables 5.1 and 5.2.

We allowed $F_1^{BK}(m_\psi^2)$ to vary continuously and determined the allowed values of ξ_{F_1} from data. The results are shown in Fig. 5.1, where the dots represent the

Table 5.1: Model predictions of formfactor $F_1(q^2)$ at $q^2 = m_\psi^2$ or $m_{\psi(2S)}^2$. In CDDFGN model, η stands for η_8 , the octet member. This scheme cannot handle η_1 , the flavor singlet.

	BSW I	BSW II	CDDFGN	AW	ISGW
$B^+ \rightarrow \psi K^+$	0.565	0.837	0.726	0.542	0.548
$B^+ \rightarrow \psi(2S)K^+$	0.707	1.31	0.909	0.678	0.760
$B_s^0 \rightarrow \psi \eta$	0.49	0.726	0.771	0.534	0.293
$B_s^0 \rightarrow \psi(2S)\eta$	0.613	1.14	0.964	0.668	0.475
$B_s^0 \rightarrow \psi \eta'$	0.411	0.609	—	1.06	0.463
$B_s^0 \rightarrow \psi(2S)\eta'$	0.514	0.954	—	1.33	0.752

values of $F_1^{BK}(m_\psi^2)$ in various models which read from the left, AW, ISGW, BSW I, CDDFGN, and BSW II, in that order. ξ_{F_1} different from unity (or χ_{F_1} different from zero), signals presence of nonfactorization contributions.

We repeated the above analysis for $B^0 \rightarrow \psi \bar{K}^0$ and $B^+ \rightarrow \psi(2S)K^+$. The results are displayed in the plots of Fig. 5.2. For $B^+ \rightarrow \psi K^+$, this is simply another way to display the results shown in Fig. 5.1. In Fig. 5.2 we have plotted the branching ratios predicted in the five different models we have considered against the parameter ξ_{F_1} . One can read-off the amount of nonfactorization needed to understand the measured branching ratios in each model. Clearly, nonfactorized contributions are needed to explain data. For example, $B^+ \rightarrow \psi K^+$ branching ratio requires that the nonfactorization parameter ξ_{F_1} is in the range (2 - 3.5), while $B^0 \rightarrow \psi \bar{K}^0$ data require ξ_{F_1} to be in the range (1.5 - 3). BSW II model requires the least amount of nonfactorization due to the fact that a dipole extrapolation of the formfactors allows the factorized term to be larger thereby reducing the necessity for the nonfactorized contribution.

Table 5.2: Model predictions of $A_1(m_\psi^2)$, $A_2(m_\psi^2)$, and $V(m_\psi^2)$ formfactors for the processes $B \rightarrow \psi K^*$, $B \rightarrow \psi(2S)K^*$ and $B_s \rightarrow \psi\phi$

		A_1	A_2	V	x	y
$B \rightarrow \psi K^*$	BSW I	0.458	0.462	0.548	1.01	1.19
	BSW II	0.458	0.645	0.812	1.41	1.77
	CDDFGN	0.279	0.279	0.904	1.00	3.24
	AW	0.425	0.766	1.19	1.80	2.81
	ISGW	0.316	0.631	0.807	2.00	2.56
$B \rightarrow \psi(2S)K^*$	BSW I	0.549	0.554	0.685	1.01	1.25
	BSW II	0.549	0.924	1.27	1.68	2.32
	CDDFGN	0.334	0.334	1.13	1.00	3.39
	AW	0.509	0.916	1.49	1.80	2.94
	ISGW	0.438	0.875	1.12	2.00	2.56
$B_s \rightarrow \psi\phi$	BSW I	0.374	0.375	0.466	1.00	1.24
	BSW II	0.374	0.523	0.691	1.40	1.85
	CDDFGN	0.265	0.279	0.919	1.05	3.47
	AW	0.449	0.703	1.34	1.56	2.98
	ISGW	0.237	0.396	0.558	1.67	2.35

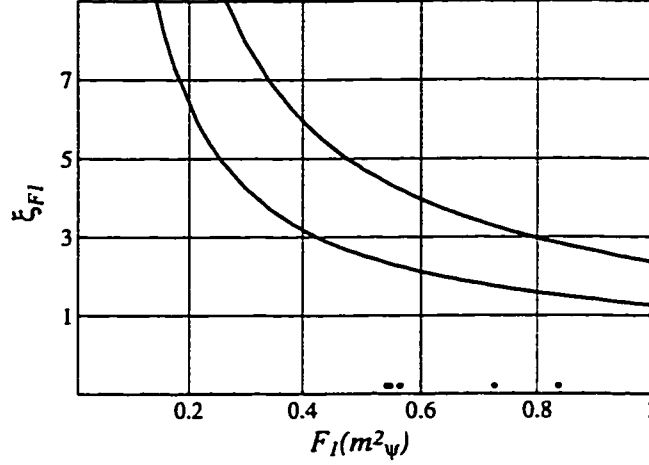


Figure 5.1: Allowed region (bounded by the two curves) of ξ_{F1} as a function of $F_1^{BP}(m_\psi^2)$ defined by $B^+ \rightarrow K^+\psi$. The dots show the model predictions of the formfactors; from left to right: AW, ISGW, BSW I, CDDFGN, BSW II.

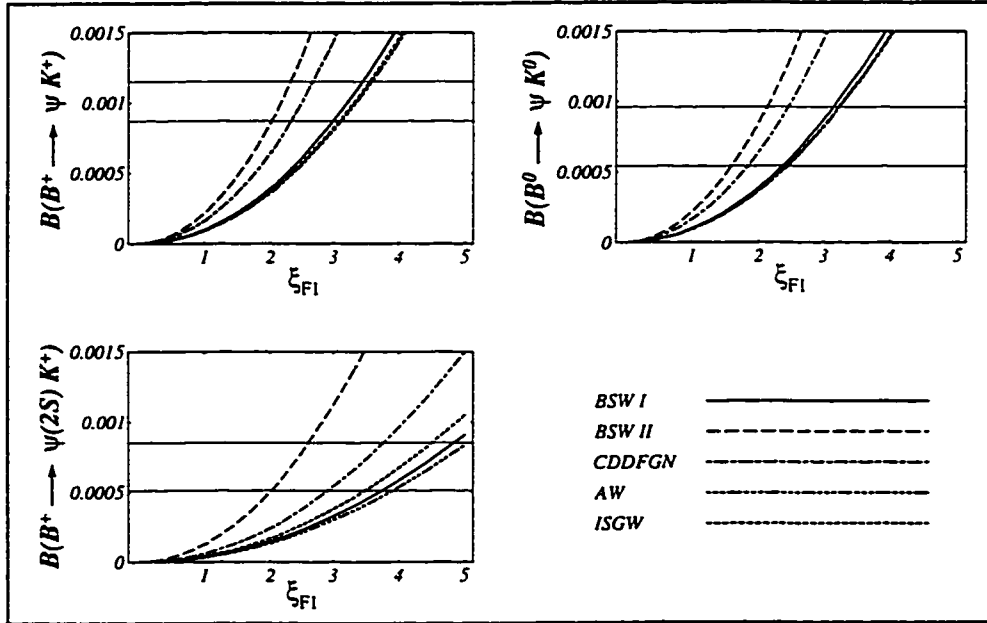


Figure 5.2: Branching ratios as functions of ξ_{F1} in each model. Horizontal lines define the branching ratio bounds to one standard deviation. Data from [10] for $B \rightarrow \psi K$ and [16] for $B \rightarrow \psi(2S)K$

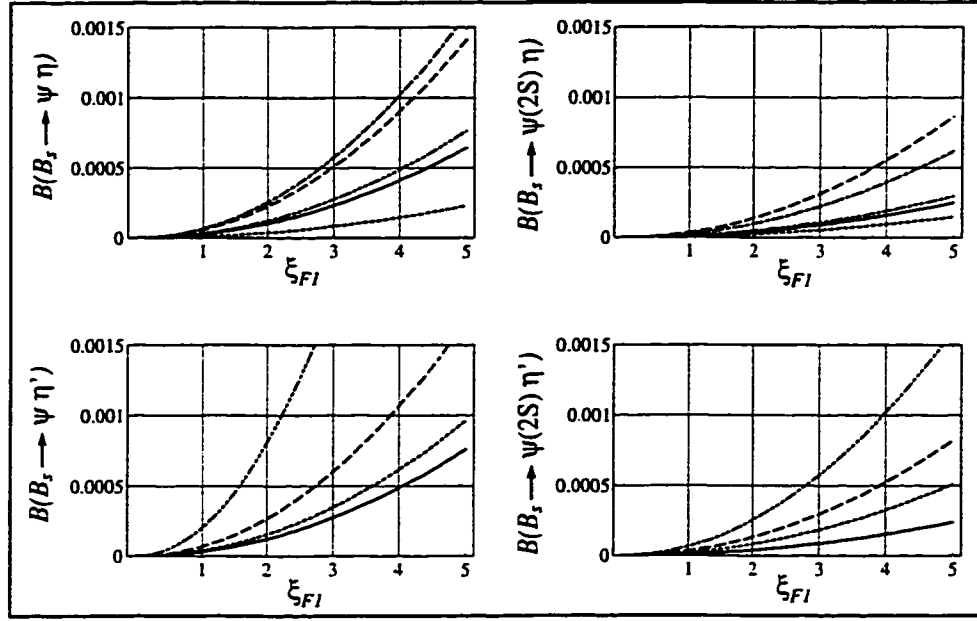


Figure 5.3: Branching ratios as a function of ξ_{F1} in each model. In CDDFGN model, η stands for η_8 and there is no prediction for η' . See Fig. 5.2 for legend.

5.2.2 $B_s \rightarrow \psi(\psi(2S))\eta, \eta'$ Decays

The analysis of the branching ratio data for $B \rightarrow \psi(\psi(2S))K$ decays can be used to predict the branching ratios for B_s decays into ψ or $\psi(2S)$ and η or η' if we assume that the amount of nonfactorized contribution is approximately independent of the light flavor. The calculation proceeds in a straight forward manner. We show the results in Fig. 5.3 where the branching ratios for $B_s \rightarrow (\psi\eta), (\psi(2S)\eta), (\psi\eta')$ or $(\psi(2S)\eta')$ are plotted as functions of ξ_{F1} for the five models we have considered.

For a given ξ_{F1} , BSW II model produces the largest branching ratios for $B_s \rightarrow \psi(\psi(2S))\eta$. For $B_s \rightarrow \psi(\psi(2S))\eta'$ decays, the largest branching ratios for a given ξ_{F1} are generated in the AW model followed by those in BSW II scheme. In order to get some feel for the predicted branching ratios, we have presented the model-averaged branching ratios in Table 5.3 for $\xi_{F1} = 1$ (factorization), $\xi_{F1} = 2$ and $\xi_{F1} = 3$.

Table 5.3: Average branching ratios predicted by the theoretical models for three choices of ξ_{F_1} .

	(Factorization)	($\xi_{F_1} = 2$)	($\xi_{F_1} = 3$)
	$\times 10^{-3}$	$\times 10^{-3}$	$\times 10^{-3}$
$\mathcal{B}(B_s \rightarrow \psi\eta)$	0.037	0.15	0.33
$\mathcal{B}(B_s \rightarrow \psi(2S)\eta)$	0.017	0.07	0.16
$\mathcal{B}(B_s \rightarrow \psi\eta')$	0.084	0.34	0.76
$\mathcal{B}(B_s \rightarrow \psi(2S)\eta')$	0.032	0.13	0.28

5.3 $(B, B_s) \rightarrow \psi(\psi(2S)V$ Decays

The decay amplitude for $B \rightarrow \psi V$ in the notation of [5] is

$$\begin{aligned}
A(B \rightarrow \psi V) = & \frac{G_F}{\sqrt{2}} V_{cb} V_{cs}^* a_2 m_\psi f_\psi \\
& \times \left\{ (m_B + m_V)(\epsilon_1^\mu \cdot \epsilon_2^\mu) \left(A_1^{BV}(m_\psi^2) + A_1^{(1)nf} + \frac{C_1}{a_2} A_1^{(8)nf} \right) \right. \\
& - \frac{(\epsilon_2^\mu \cdot (p_B - p_V))(\epsilon_1^\mu \cdot (p_B + p_V))}{(m_B + m_V)} \left(A_2^{BV}(m_\psi^2) + A_2^{(1)nf} + \frac{C_1}{a_2} A_2^{(8)nf} \right) \\
& \left. + \frac{2i}{(m_B + m_V)} \epsilon_{\mu\nu\alpha\beta} \epsilon_1^\mu \epsilon_2^\nu p_V^\alpha p_B^\beta \left(V^{BV}(m_\psi^2) + V^{(1)nf} + \frac{C_1}{a_2} V^{(8)nf} \right) \right\}.
\end{aligned} \tag{5.18}$$

In (5.18), ϵ_1 and ϵ_2 are the ψ and V polarization vectors respectively. A_1^{BV} , A_2^{BV} and V^{BV} are the formfactors defined in [12] which contribute to the factorized part of the decay amplitude. $A_1^{(8)nf}$, $A_2^{(8)nf}$ and $V^{(8)nf}$ are the nonfactorized contributions arising from the color-octet current products $(\bar{c}c)(\bar{s}b)$, the analogues of $F_1^{(8)nf}$ in (5.11). And $A_1^{(1)nf}$, $A_2^{(1)nf}$ and $V^{(1)nf}$ are the analogues of $F_1^{(1)nf}$ in (5.8).

The following definitions [5], in analogy with Eq. (5.14), facilitate shorter forms for the equations that follow.

$$\begin{aligned}
\xi_i &= 1 + \frac{A_i^{(1)nf}}{A_i^{BV}(m_\psi^2)} + \frac{C_1}{a_2} \frac{A_i^{(8)nf}}{A_i^{BV}(m_\psi^2)} \equiv 1 + \frac{C_1}{a_2} \chi_i, \quad (i = 1, 2) \\
\xi_V &= 1 + \frac{V^{(1)nf}}{V^{BV}(m_\psi^2)} + \frac{C_1}{a_2} \frac{V^{(8)nf}}{V^{BV}(m_\psi^2)} \equiv 1 + \frac{C_1}{a_2} \chi_V.
\end{aligned} \tag{5.19}$$

$B \rightarrow \psi V$ decays can be discussed in three equivalent basis-amplitudes: Helicity basis (H_0, H_+, H_-), Trasversity basis ($A_0, A_{\parallel}, A_{\perp}$), and Partial-wave basis (S, P, D). They are related through the following definitions [17, 18],

$$\begin{aligned} H_0 &= -\frac{1}{\sqrt{3}}S + \sqrt{\frac{2}{3}}D \\ H_+ &= \frac{1}{\sqrt{3}}S + \frac{1}{\sqrt{2}}P + \frac{1}{\sqrt{6}}D \\ H_- &= \frac{1}{\sqrt{3}}S - \frac{1}{\sqrt{2}}P + \frac{1}{\sqrt{6}}D, \end{aligned} \quad (5.20)$$

$$\begin{aligned} A_0 &= H_0 = -\frac{1}{\sqrt{3}}S + \sqrt{\frac{2}{3}}D \\ A_{\parallel} &= \frac{1}{\sqrt{2}}(H_+ + H_-) = \sqrt{\frac{2}{3}}S + \frac{1}{\sqrt{3}}D \\ A_{\perp} &= \frac{1}{\sqrt{2}}(H_+ - H_-) = P. \end{aligned} \quad (5.21)$$

All amplitudes in (5.20) and (5.21) are, in principle, complex, their phases defined by the following (total angular momentum $J = 0$, uniquely determines the spin angular momentum once the orbital angular momentum is specified):

$$\begin{aligned} S &= |S|e^{i\delta_S} \\ P &= |P|e^{i\delta_P} \\ D &= |D|e^{i\delta_D}. \end{aligned} \quad (5.22)$$

The process of generating complex amplitudes in terms of δ_S , δ_P and δ_D is as follows: Helicity amplitudes are evaluated directly from (5.18) *before final-state interaction (fsi) phases are put in*. This allows us to determine the *real* partial wave amplitudes, *before fsi*, through

$$\begin{aligned} S &= \frac{1}{\sqrt{3}}(H_+ + H_- - H_0) = \sqrt{\frac{2}{3}}A_{\parallel} - \frac{1}{\sqrt{3}}A_0 \\ P &= \frac{1}{\sqrt{2}}(H_+ - H_-) = A_{\perp} \\ D &= \frac{1}{\sqrt{6}}(H_+ + H_- + 2H_0) = \frac{1}{\sqrt{3}}A_{\parallel} + \sqrt{\frac{2}{3}}A_0. \end{aligned} \quad (5.23)$$

Once the real S , P and D amplitudes are determined, *their phase are put in by hand* as in (5.22), and with these complex S , P and D wave amplitudes one can write down complex (H_0, H_+, H_-) from (5.20) or complex $(A_0, A_{||}, A_{\perp})$ from (5.21).

With these definitions, the following expressions for the decay rate are obtained

$$\begin{aligned}\Gamma(B \rightarrow \psi V) &= \frac{|\mathbf{k}|}{8\pi m_B^2} (|H_0|^2 + |H_+|^2 + |H_-|^2) \\ &= \frac{|\mathbf{k}|}{8\pi m_B^2} (|A_0|^2 + |A_{||}|^2 + |A_{\perp}|^2) \\ &= \frac{|\mathbf{k}|}{8\pi m_B^2} (|S|^2 + |P|^2 + |D|^2),\end{aligned}\tag{5.24}$$

where \mathbf{k} is the momentum in B rest-frame.

The longitudinal and transverse polarizations are defined as.

$$P_L = \frac{\Gamma_L}{\Gamma} = \frac{|H_0|^2}{|H_0|^2 + |H_+|^2 + |H_-|^2}\tag{5.25}$$

$$P_T = 1 - P_L.\tag{5.26}$$

We note from (5.20) that both P_L and P_T depend on the relative phase between the S and D waves, ($\delta_{SD} = \delta_S - \delta_D$), through $\cos \delta_{SD}$ in a compensatory manner such that $P_L + P_T = 1$. Alternatively, one can define in term of transversity amplitudes [17, 7].

$$P_{||} = \frac{\Gamma_{||}}{\Gamma} = \frac{|A_{||}|^2}{|A_0|^2 + |A_{||}|^2 + |A_{\perp}|^2}\tag{5.27}$$

$$P_{\perp} = \frac{\Gamma_{\perp}}{\Gamma} = \frac{|A_{\perp}|^2}{|A_0|^2 + |A_{||}|^2 + |A_{\perp}|^2}\tag{5.28}$$

$$P_0 = 1 - P_{||} - P_{\perp}.\tag{5.29}$$

From (5.21), one notes that while $P_{||}$ depends on δ_{SD} , P_{\perp} is independent of the strong phases, δ_S , δ_P and δ_D . Eq. (5.20) also shows that the only way information on P wave phase can be obtained is via $\Gamma_+ \propto |H_+|^2$ or $\Gamma_- \propto |H_-|^2$. $\Gamma_T = \Gamma_+ + \Gamma_-$ is independent of the P-wave phase. With these definitions, we now consider the specific case of $B \rightarrow \psi K^*$.

5.3.1 $B \rightarrow \psi K^*$ Decays

With the definitions introduced in the preceding section, the helicity amplitudes for $B \rightarrow \psi K^*$ decays are (before *f**s**i* phases are introduced),

$$H_0 = -\frac{G_F}{\sqrt{2}} V_{cb} V_{cs}^* f_\psi m_\psi (m_B + m_{K^*}) a_2 A_1^{BK^*}(m_\psi^2) (a\xi_1 - b\xi_2 x) \quad (5.30)$$

$$H_\pm = -\frac{G_F}{\sqrt{2}} V_{cb} V_{cs}^* f_\psi m_\psi (m_B + m_{K^*}) a_2 A_1^{BK^*}(m_\psi^2) (\xi_1 \mp c\xi_V y) \quad (5.31)$$

where [1],

$$\begin{aligned} a &= \frac{m_B^2 - m_\psi^2 - m_{K^*}^2}{2m_\psi m_{K^*}}, \\ b &= \frac{2|\mathbf{k}|^2 m_B^2}{m_\psi m_{K^*} (m_B + m_{K^*})^2}, \\ c &= \frac{2|\mathbf{k}| m_B}{(m_B + m_{K^*})^2}, \\ x &= \frac{A_2^{BK^*}(m_\psi^2)}{A_1^{BK^*}(m_\psi^2)}, \\ y &= \frac{V^{BK^*}(m_\psi^2)}{A_1^{BK^*}(m_\psi^2)}. \end{aligned} \quad (5.32)$$

With these helicity amplitudes, we can write the transversity amplitudes or the partial wave amplitudes via (5.21) and (5.23).

We start with an amplitude analysis using the latest CLEO data [7]. Working in the transversity basis, they [7] determined the following branching ratio, dimensionless amplitudes (denoted by \hat{A}_0 , \hat{A}_\perp and \hat{A}_\parallel) and their phases.

$$\begin{aligned} \mathcal{B}(B \rightarrow \psi K^*) &= (1.35 \pm 0.18) \times 10^{-3} \\ |\hat{A}_0|^2 &= \frac{|A_0|^2}{\Gamma} = 0.52 \pm 0.08 \\ |\hat{A}_\perp|^2 &= \frac{|A_\perp|^2}{\Gamma} = 0.16 \pm 0.09 \\ |\hat{A}_\parallel|^2 &= \frac{|A_\parallel|^2}{\Gamma} = 1 - |\hat{A}_\perp|^2 - |\hat{A}_0|^2 = 0.32 \pm 0.12 \\ \phi_\parallel &= 3.00 \pm 0.37 \text{ radians} \\ \phi_\perp &= -0.11 \pm 0.46 \text{ radians,} \end{aligned} \quad (5.33)$$

where ϕ_{\parallel} and ϕ_{\perp} are the phases of the amplitudes A_{\parallel} and A_{\perp} , respectively, with the choice $\phi_0 = 0$ [7]. The important feature is that the amplitudes are relatively real.

Using the relation between the helicity, transversity and partial wave phases, the CLEO analysis (5.33) can then be restated in the following equivalent forms,

Helicity basis:

$$\begin{aligned}
|\hat{H}_0|^2 &= \frac{|H_0|^2}{\Gamma} = 0.52 \pm 0.08 \\
|\hat{H}_+|^2 &= \frac{|H_+|^2}{\Gamma} = 0.014 \pm 0.034 \\
|\hat{H}_-|^2 &= \frac{|H_-|^2}{\Gamma} = 1 - |\hat{H}_0|^2 - |\hat{H}_+|^2 = 0.47 \pm 0.08 \\
\phi_+ &= 2.92 \pm 1.70 \text{ radians} \\
\phi_- &= 3.01 \pm 0.29 \text{ radians.}
\end{aligned} \tag{5.34}$$

Partial-wave basis:

$$\begin{aligned}
|\hat{S}|^2 &= \frac{|S|^2}{\Gamma} = 0.77 \pm 0.12 \\
|\hat{P}|^2 &= \frac{|P|^2}{\Gamma} = 0.16 \pm 0.09 \\
|\hat{D}|^2 &= \frac{|D|^2}{\Gamma} = 1 - |\hat{S}|^2 - |\hat{P}|^2 = 0.073 \pm 0.044 \\
\phi_S &= 3.07 \pm 0.19 \text{ radians} \\
\phi_P &= -0.11 \pm 0.46 \text{ radians} \\
\phi_D &= 0.17 \pm 0.44 \text{ radians,}
\end{aligned} \tag{5.35}$$

The phases in (5.34) and (5.35) are evaluated relative to ϕ_0 as in the CLEO analysis [7]. From (5.35) we note that $|S| > |P| > |D|$ as one might intuitively anticipate.

Next, having determined the helicity amplitudes, we are in a position to extract information on the parameters ξ_1 , ξ_2 and ξ_V in a given model for the formfactors. We summarize our method below.

The helicity amplitudes in terms of ξ_1 , ξ_2 and ξ_V are given in Eqs. (5.30) and (5.31). The parameters ξ_1 , ξ_2 and ξ_V , representing nonfactorization, are then obtained from

the constraints,

$$|\hat{H}_0|^2 = \frac{(a - bx\xi_{21})^2}{2(1 + c^2y^2\xi_{V1}^2) + (a - bx\xi_{21})^2} = 0.52 \pm 0.08, \quad (5.36)$$

$$|\hat{H}_+|^2 = \frac{(1 - cy\xi_{V1})^2}{2(1 + c^2y^2\xi_{V1}^2) + (a - bx\xi_{21})^2} = 0.014 \pm 0.034, \quad (5.37)$$

and

$$\begin{aligned} \mathcal{B}(B \rightarrow \psi K^*) &= \frac{G_F^2 |\mathbf{k}|}{16\pi m_B^2} |V_{cb}|^2 |V_{cs}|^2 f_\psi^2 m_\psi^2 (m_B + m_{K^*})^2 a_2^2 |A_1(m_\psi^2)|^2 \xi_1^2 \\ &\quad \times \left\{ (a - bx\xi_{21})^2 + 2(1 + c^2y^2\xi_{V1}^2) \right\} \\ &= (1.35 \pm 0.18) \times 10^{-3} \end{aligned} \quad (5.38)$$

where we have defined the ratios,

$$\xi_{21} = \frac{\xi_2}{\xi_1} \quad \text{and} \quad \xi_{V1} = \frac{\xi_V}{\xi_1}. \quad (5.39)$$

The regions in ξ_{21} and ξ_{V1} space that explain the experimental value of polarization ($|\hat{H}_0|^2$) are shown by the two vertical bands in Fig. 5.4, while the region between the two horizontal curves corresponds to non-negative values for $|\hat{H}_+|^2$ within the error. The boxes in Fig. 5.4 show the four solutions we get by solving (5.36) and (5.37) for ξ_{21} and ξ_{V1} . The errors in ξ_{21} and ξ_{V1} are correlated as parts of the boxes lie outside the overlap of the horizontal and vertical bands.

Clearly, in BSW I model, within errors, there are solutions with $\xi_{21} = 1$ and $\xi_{V1} = 1$ i.e. $\xi_1 = \xi_2 = \xi_V$. This is the class of solutions discussed in [6]. The value of ξ_1 is then obtained from (5.38) and does not allow $\xi_1 = 1$ solution. We repeated this procedure for other models of the formfactors. the results are tabulated in Table 5.4.

From Table 5.4 it is evident that only BSW I model permits solutions with $\xi_1 = \xi_2 = \xi_V$ (but $\xi_1 \neq 1$); other models do not allow solutions with $\xi_1 = \xi_2 = \xi_V$. There are no solutions to the latest CLEO data [7] consistent with factorization i.e., $\xi_1 = \xi_2 = \xi_V = 1$ in any of the models we have considered.

We chose to work with CLEO data only rather than use the world average for the longitudinal polarization because it is only the CLEO data which allow a

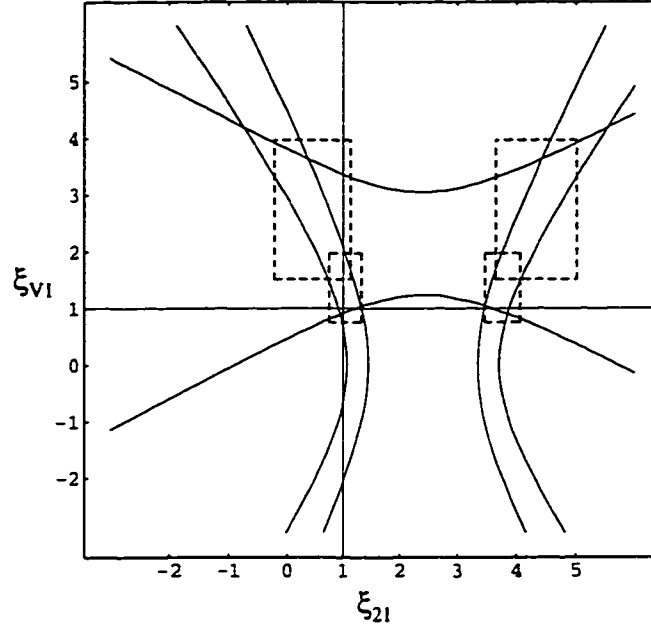


Figure 5.4: The region in ξ_{21} and ξ_{V1} plane allowed by the latest CLEO II measurements of $|\hat{H}_0|^2$ (vertical bands) and $|\hat{H}_+|^2$ (horizontal band) for $B \rightarrow \psi K^*$ in BSW I model.

Table 5.4: Solutions of ξ_1 , ξ_{21} and ξ_{V1} using the latest CLEO II measurements of branching ratio, polarization and $|\hat{H}_+|^2$ for the process $B \rightarrow \psi K^*$. In the table only positive solutions for ξ_1 are shown since for every solution of ξ_1 there is another which is its negative.

Model		Solution 1	Solution 2	Solution 3	Solution 4
BSW I	ξ_1	1.79 ± 0.62	1.79 ± 0.62	1.26 ± 0.55	1.26 ± 0.55
	ξ_{21}	1.03 ± 0.29	3.77 ± 0.29	0.46 ± 0.68	4.34 ± 0.68
	ξ_{V1}	1.36 ± 0.61	1.36 ± 0.61	2.74 ± 1.20	2.74 ± 1.20
BSW II	ξ_1	1.79 ± 0.62	1.79 ± 0.62	1.26 ± 0.55	1.26 ± 0.55
	ξ_{21}	0.74 ± 0.21	2.70 ± 0.21	0.33 ± 0.49	3.11 ± 0.49
	ξ_{V1}	0.92 ± 0.41	0.92 ± 0.41	1.84 ± 0.83	1.84 ± 0.83
CDDFGN	ξ_1	2.94 ± 1.00	2.94 ± 1.00	2.07 ± 0.91	2.07 ± 0.91
	ξ_{21}	1.04 ± 0.29	3.80 ± 0.29	0.46 ± 0.68	4.38 ± 0.68
	ξ_{V1}	0.50 ± 0.22	0.50 ± 0.22	1.01 ± 0.45	1.01 ± 0.45
AW	ξ_1	1.93 ± 0.67	1.93 ± 0.67	1.36 ± 0.60	1.36 ± 0.60
	ξ_{21}	0.58 ± 0.16	2.11 ± 0.16	0.26 ± 0.38	2.43 ± 0.38
	ξ_{V1}	0.58 ± 0.26	0.58 ± 0.26	1.16 ± 0.52	1.16 ± 0.52
ISGW	ξ_1	2.60 ± 0.90	2.60 ± 0.90	1.83 ± 0.80	1.83 ± 0.80
	ξ_{21}	0.52 ± 0.15	1.90 ± 0.15	0.23 ± 0.34	2.19 ± 0.34
	ξ_{V1}	0.63 ± 0.28	0.63 ± 0.28	1.27 ± 0.57	1.27 ± 0.57

complete determination of the decay amplitude. For the record, the world average (our estimate) of all measurements [19, 20, 21, 7] of the longitudinal polarization in $B \rightarrow \psi K^*$ is

$$P_L = 0.66 \pm 0.05. \quad (5.40)$$

To one standard deviation there is no overlap of the world average and the CLEO data. However, within errors there are values of ξ_{21} and ξ_{V1} , shown in Table 5.4 that fit the world-averaged P_L .

5.3.2 $B_s \rightarrow \psi\phi$ Decays

If it is assumed that nonfactorization contributions are independent of the flavor of the light degree of freedom we can use the values of ξ_1 , $\xi_{2,1}$ and $\xi_{V,1}$ in Table 5.4 to predict the branching ratio, polarization and transversity for $B_s \rightarrow \psi\phi$. Indeed, the branching ratio, longitudinal polarization and trasverse polarization ($|\hat{H}_-|^2$) for $B_s \rightarrow \psi\phi$ can be related directly to the those for $B \rightarrow \psi K^*$ by eliminating ξ_1 , ξ_{21} and ξ_{V1} . The result is shown in Table 5.5. The following experimental data for $B_s \rightarrow \psi\phi$ are now available [21, 22]

$$\begin{aligned} \mathcal{B}(B_s \rightarrow \psi\phi) &= (0.93 \pm 0.33) \times 10^{-3} \\ P_L = |\hat{H}_0|^2 &= 0.56 \pm 0.21. \end{aligned} \quad (5.41)$$

By studying the results presented in Table 5.5, we note the following: (i) Most of the predictions (those given by BSW I model, BSW II model, CDDFGN model and both first and third solutions of the ISGW model) are consistent with available experimental results. (ii) The predictions of the BSW I, BSW II and CDDFGN models show very little sensitivity to the solution-type. (iii) $|\hat{H}_+|^2$ (which is equal to $1 - |\hat{H}_0|^2 - |\hat{H}_-|^2$) has a very small value in all the formfactor models considered.

Table 5.5: The branching ratios, $|\hat{H}_0|^2$ and $|\hat{H}_-|^2$ for the process $B_s \rightarrow \psi\phi$ using for ξ_1 , ξ_{21} and ξ_{V1} the values in Table 5.4 calculated for $B \rightarrow \psi K^*$.

Model		Solution 1	Solution 2	Solution 3	Solution 4
BSW I	BR $\times 10^{-3}$	0.91 ± 0.14	0.75 ± 0.12	0.88 ± 0.14	0.77 ± 0.12
	$ \hat{H}_0 ^2$	0.50 ± 0.07	0.39 ± 0.08	0.48 ± 0.07	0.40 ± 0.08
	$ \hat{H}_- ^2$	0.49 ± 0.08	0.60 ± 0.09	0.50 ± 0.08	0.58 ± 0.10
BSW II	BR $\times 10^{-3}$	0.91 ± 0.14	0.75 ± 0.12	0.89 ± 0.14	0.78 ± 0.12
	$ \hat{H}_0 ^2$	0.49 ± 0.07	0.39 ± 0.08	0.48 ± 0.08	0.41 ± 0.08
	$ \hat{H}_- ^2$	0.49 ± 0.08	0.59 ± 0.09	0.51 ± 0.08	0.58 ± 0.10
CDDFGN	BR $\times 10^{-3}$	1.20 ± 0.19	1.20 ± 0.19	1.20 ± 0.19	1.20 ± 0.19
	$ \hat{H}_0 ^2$	0.47 ± 0.08	0.47 ± 0.08	0.46 ± 0.08	0.46 ± 0.08
	$ \hat{H}_- ^2$	0.52 ± 0.09	0.52 ± 0.09	0.52 ± 0.09	0.52 ± 0.09
AW	BR $\times 10^{-3}$	1.70 ± 0.28	0.96 ± 0.17	1.50 ± 0.27	1.00 ± 0.18
	$ \hat{H}_0 ^2$	0.53 ± 0.06	0.19 ± 0.08	0.49 ± 0.07	0.24 ± 0.09
	$ \hat{H}_- ^2$	0.45 ± 0.08	0.79 ± 0.08	0.50 ± 0.06	0.73 ± 0.13
ISGW	BR $\times 10^{-3}$	0.82 ± 0.15	0.42 ± 0.07	0.71 ± 0.14	0.43 ± 0.07
	$ \hat{H}_0 ^2$	0.57 ± 0.06	0.15 ± 0.08	0.54 ± 0.06	0.23 ± 0.11
	$ \hat{H}_- ^2$	0.41 ± 0.07	0.80 ± 0.08	0.46 ± 0.06	0.76 ± 0.13
Experiment [21, 22]		$\mathcal{B}(B_s \rightarrow \psi\phi) = (0.93 \pm 0.33) \times 10^{-3}$			
		$P_L = \hat{H}_0 ^2 = 0.56 \pm 0.21$			

5.3.3 $B \rightarrow \psi(2S)K^*$ Decays

The branching ratio, longitudinal polarization and transverse polarization ($|\hat{H}_-|^2$) for $B \rightarrow \psi(2S)K^*$ can also be related directly to those for $B \rightarrow \psi K^*$ by eliminating ξ_1 , ξ_{21} and ξ_{V1} . The result is shown in Table 5.6. To the best of our knowledge, only the branching ratio for this process is available [16],

$$\mathcal{B}(B \rightarrow \psi(2S)K^*) = (0.9 \pm 0.29) \times 10^{-3}. \quad (5.42)$$

From Table 5.6 we notice that the predictions of the branching ratio, $|\hat{H}_0|^2$ and $|\hat{H}_-|^2$ are almost model independent. The predictions of solutions 1 and 3 are the closest to available experimental data. The other two solutions yield low branching ratios and close to zero longitudinal polarization.

5.4 Results in Factorization Approximation

For the sake of completeness, we present in this section the factorization approximation ($\xi_1 = \xi_{21} = \xi_{V1} = 1$) prediction for branching ratio, $|\hat{H}_0|^2$ and $|\hat{H}_-|^2$ using the five theoretical models considered for the formfactors. These predictions are presented in Table 5.7.

From Table 5.7, we see that the factorization approximation predicts low values for the branching ratios compared to experiment. For the processes $B \rightarrow \psi K^*$ and $B_s \rightarrow \psi \phi$, with the exception of BSW I model, the factorization approximation also underestimates the longitudinal polarization.

If we scale the branching ratio by a factor of 3.5, we find that the BSW I model predictions agree, within error, with the available experimental data. This could be achieved by giving the nonfactorization parameters the values,

$$\xi_1 = \sqrt{3.5}, \quad \xi_{21} = \xi_{V1} = 1 \quad (5.43)$$

Table 5.6: The branching ratios, $|\hat{H}_0|^2$ and $|\hat{H}_-|^2$ for the process $B \rightarrow \psi(2S)K^*$ using for ξ_1 , ξ_{21} and ξ_{V1} the values in Table 5.4 calculated for $B \rightarrow \psi K^*$.

Model		Solution 1	Solution 2	Solution 3	Solution 4
BSW I	$\text{BR} \times 10^{-3}$	0.80 ± 0.19	0.43 ± 0.11	0.62 ± 0.17	0.37 ± 0.09
	$ \hat{H}_0 ^2$	0.46 ± 0.04	0.001 ± 0.006	0.43 ± 0.05	0.03 ± 0.05
	$ \hat{H}_- ^2$	0.49 ± 0.08	0.91 ± 0.10	0.57 ± 0.05	0.97 ± 0.06
BSW II	$\text{BR} \times 10^{-3}$	0.80 ± 0.17	0.52 ± 0.12	0.71 ± 0.16	0.52 ± 0.11
	$ \hat{H}_0 ^2$	0.39 ± 0.06	0.07 ± 0.04	0.36 ± 0.06	0.11 ± 0.06
	$ \hat{H}_- ^2$	0.58 ± 0.08	0.89 ± 0.07	0.63 ± 0.06	0.87 ± 0.10
CDDFGN	$\text{BR} \times 10^{-3}$	0.79 ± 0.19	0.43 ± 0.11	0.62 ± 0.17	0.36 ± 0.09
	$ \hat{H}_0 ^2$	0.46 ± 0.04	0.001 ± 0.006	0.43 ± 0.05	0.031 ± 0.05
	$ \hat{H}_- ^2$	0.49 ± 0.08	0.91 ± 0.10	0.57 ± 0.05	0.97 ± 0.06
AW	$\text{BR} \times 10^{-3}$	0.79 ± 0.19	0.43 ± 0.11	0.62 ± 0.17	0.36 ± 0.09
	$ \hat{H}_0 ^2$	0.46 ± 0.04	0.001 ± 0.006	0.43 ± 0.05	0.031 ± 0.05
	$ \hat{H}_- ^2$	0.49 ± 0.08	0.91 ± 0.10	0.57 ± 0.05	0.97 ± 0.06
ISGW	$\text{BR} \times 10^{-3}$	1.10 ± 0.25	0.56 ± 0.15	0.81 ± 0.23	0.47 ± 0.12
	$ \hat{H}_0 ^2$	0.46 ± 0.04	0.001 ± 0.006	0.44 ± 0.05	0.03 ± 0.05
	$ \hat{H}_- ^2$	0.48 ± 0.08	0.90 ± 0.10	0.56 ± 0.05	0.97 ± 0.05
Experiment [16]		$\mathcal{B}(B \rightarrow \psi(2S)K^*) = (0.9 \pm 0.29) \times 10^{-3}$			

or

$$\xi_1 = \xi_2 = \xi_V = \sqrt{3.5} . \quad (5.44)$$

This is what has been referred to as new factorization in [6].

5.5 Discussion

We have shown that $B \rightarrow \psi K$ and $\psi(2S)K$ data require nonfactorized contributions in all of the five formfactor models we have considered. The smallest amount of nonfactorized contribution is needed for the BSW II model while the AW model requires the largest. We have calculated the branching ratios for $B_s \rightarrow \psi\eta$, $\psi\eta'$, $\psi(2S)\eta$, and $\psi(2S)\eta'$ in each model as functions of ξ_{F_1} and displayed the result in Fig. 5.3. These branching ratios averaged over the five models are tabulated in Table 5.3 for a few values of the parameter ξ_{F_1} .

We have used the latest CLEO data on $\mathcal{B}(B \rightarrow \psi K^{*-})$ and the transversity amplitudes to determine the three nonfactorization parameters ξ_1 , ξ_2 and ξ_V defined in (5.19). There are four solutions which are expressed in terms of ξ_1 and the ratios $\xi_{21} = \xi_2/\xi_1$, and $\xi_{V1} = \xi_V/\xi_1$. These solutions are displayed in Fig. 5.4 for BSW I model and in Table 5.4 for all the five models. We find that solutions exist for $\xi_{2,1} = 1$ and $\xi_{V,1} = 1$ only in BSW I model but then $\xi_1 \neq 1$, i.e. there are no solutions where $\xi_1 = \xi_2 = \xi_V = 1$ which would signal factorization.

Assuming that the parameters ξ_{21} and ξ_{V1} determined from $B \rightarrow \psi K^{*-}$ are the same in $B_s \rightarrow \psi\phi$ decay, we calculated the branching ratio, longitudinal and transverse polarizations of $B_s \rightarrow \psi\phi$ decay in all five models. Present data are consistent with model predictions but for a few exceptions as is seen from Table 5.5.

The branching ratio, longitudinal and transverse polarizations of $B \rightarrow \psi(2S)K^{*-}$ decay were also calculated assuming that the parameters ξ_{21} and ξ_{V1} determined from $B \rightarrow \psi K^{*-}$ are the same in $B \rightarrow \psi(2S)K^{*-}$ decay. The results are shown in Table 5.6.

Finally, we find that in the factorization approximation none of the formfactor

Table 5.7: Predictions of branching ratios, $|\hat{H}_0|^2$ and $|\hat{H}_-|^2$ for the processes $B \rightarrow \psi K^*$, $B_s \rightarrow \psi \phi$ and $B \rightarrow \psi(2S)K^*$ using the factorization approximation $\xi_1 = \xi_{21} = \xi_{V1} = 1$. The errors in branching ratios are due to the errors in Wilson coefficients, decay constants and B meson life times.

		$BR \times 10^{-3}$	$ \hat{H}_0 ^2$	$ \hat{H}_- ^2$
$B \rightarrow \psi K^*$	BSW I	0.40 ± 0.24	0.57	0.39
	BSW II	0.33 ± 0.20	0.35	0.64
	CDDFGN	0.24 ± 0.14	0.37	0.62
	AW	0.33 ± 0.19	0.12	0.87
	ISGW	0.15 ± 0.09	0.06	0.93
	Experiment [7]	1.35 ± 0.18	0.52 ± 0.08	0.47 ± 0.08
$B_s \rightarrow \psi \phi$	BSW I	0.27 ± 0.16	0.55	0.41
	BSW II	0.23 ± 0.14	0.35	0.64
	CDDFGN	0.22 ± 0.13	0.32	0.66
	AW	0.44 ± 0.26	0.20	0.79
	ISGW	0.09 ± 0.06	0.20	0.80
	Experiment [21, 22]	0.93 ± 0.33	0.56 ± 0.21	-
$B \rightarrow \psi(2S)K^*$	BSW I	0.24 ± 0.14	0.49	0.43
	BSW II	0.23 ± 0.13	0.29	0.69
	CDDFGN	0.13 ± 0.07	0.35	0.65
	AW	0.22 ± 0.13	0.23	0.76
	ISGW	0.14 ± 0.08	0.22	0.77
	Experiment [16]	0.90 ± 0.29	-	-

models predict correctly the branching ratios for $B \rightarrow \psi K^*$, $B_s \rightarrow \psi \phi$ and $B \rightarrow \psi(2S)K^*$. As for the longitudinal polarizations, $|\hat{H}_0|^2$, in $B \rightarrow \psi K^*$ and $B_s \rightarrow \psi \phi$, only the BSW I model predicts them correctly. BSW I also predicts $|\hat{H}_-|^2$ correctly for $B \rightarrow \psi K^*$.

Bibliography

- [1] M. Gourdin, A. N. Kamal and X. Y. Pham, Phys. Rev. Lett. **73**, 3355 (1994).
- [2] R. Aleksan, A. Le Yaouanc, L. Oliver, O. Pene and J. C. Raynal, Phys. Rev. D**51**, 6235 (1995).
- [3] H. Y. Cheng, Phys. Lett. B**335**, 428 (1994); J. M. Soares, Phys. Rev. D**51**, 3518 (1995).
- [4] H. Y. Cheng, Z. Phys. C**69**, 647 (1996).
- [5] A. N. Kamal and A. B. Santra, Z. Phys. C**72**, 91 (1996).
- [6] H. Y. Cheng, Phys. Lett. B**395**, 345 (1997).
- [7] C. P. Jessop *et al.* (CLEO Collaboration), CLNS 96/1455, CLEO 96-24 (1997); Phys. Rev. Lett. **79**, 4533 (1997).
- [8] R. Rückl, Habilitationsschrift, University of Munich (1983).
- [9] A. N. Kamal, A. B. Santra, T. Uppal and R.C. Verma, Phys. Rev. D**53**, 2506 (1996).
- [10] *Particle Data Group, Review of Particle Properties*, Phys. Rev. D **54**, 1 (1996).
- [11] M. Neubert, V. Rieckert, B. Stech and Q. P. Xu, in *Heavy Flavors*, ed. A. J. Buras and M. Lindner, World Scientific (Singapore) 1992.

- [12] M. Bauer, B. Stech and M. Wirbel, Z. Phys. C **34**,103 (1987); M. Wirbel, B. Stech and M. Bauer, Z. Phys. C **29**, 637 (1985).
- [13] R. Casalbuoni, A Deandrea, N. Di Bartolomeo, R. Gatto, F. Feruglio and G. Nardulli, Phys. Lett. B **299**, 139 (1993); A. Deandrea, N. Di Bartolomeo and R. Gatto, Phys. Lett. B **318**, 549 (1993).
- [14] T. Altomari and L. Wolfenstein, Phys. Rev. D **37**, 681 (1988).
- [15] N. Isgur, D. Scora, B. Grinstein and M. Wise, Phys. Rev. D **39**, 799 (1989).
- [16] The CDF Collaboration, FERMILAB-CONF-96/160-E, (1996);
- [17] A. S. Dighe, I. Dunietz, H. Lipkin and J. L. Rosner, Phys. Lett. **B369**, 144 (1996).
- [18] We follow the convention $A_0 = H_0$ of ref. [17] rather than $A_0 = -H_0$ of ref. [7].
- [19] H. Albrecht *et al.* (ARGUS Collaboration), Phys. Lett. **B340**, 217 (1994).
- [20] M. S. Alam *et al.* (CLEO Collaboration), Phys. Rev. D **50**, 43 (1994).
- [21] F. Abe *et al.* (CDF Collaboration), Phys. Rev. Lett. **75**, 3068 (1995).
- [22] F. Abe *et al.* (CDF Collaboration), Phys. Rev. D **54**, 6596 (1996).

Chapter 6

Nonfactorization in Cabibbo-Favored B -Decays

6.1 Introduction

The idea of nonfactorization in D and B decays was introduced in the last few years by several authors [1, 2, 3]. There are two equivalent ways of introducing nonfactorized contributions in a calculation: Either, use the number of colors, N_c equal to 3 and explicitly add a nonfactorized contribution to each Lorentz scalar in the decay amplitude as in [2, 3]. Or, introduce an effective number of colors, N_c^{eff} . The later approach has been adopted in several papers [4, 5, 6] dealing with B decays into light mesons.

Though the nonfactorized amplitude remains incalculable, a few statements about it can be made. First, what is estimated to be the nonfactorized contribution depends on the model of formfactors used to calculate the factorized contribution. Second, within a chosen model for the formfactors, the nonfactorized contributions are process dependent. Third, if nonfactorization is characterized through an effective number of colors, N_c^{eff} , is it the same (as assumed in [4] and [5]) for the tree and the penguin generated processes or different (as in [6])? Ref. [6] goes so far as to suggest that

N_c^{eff} , is different for the $(V - A)(V - A)$ and $(V - A)(V + A)$ type of penguin terms. In the language of [2], where $N_c = 3$ is assumed, different N_c^{eff} , for the tree and penguin driven processes imply that the nonfactorized contributions for the tree and penguin driven processes are different. This is not unlikely as the calculation of the penguin driven amplitudes in the factorization assumption involves additional assumptions, an effective value of q^2 for example.

Unlike the papers listed in [4, 5, 6], in this chapter we study B decays into a heavy and a light meson. As such they are all Cabibbo-favored $b \rightarrow c$ transitions. Following, [7] we use $N_c = 3$ and introduce nonfactorized contributions explicitly. To calculate the factorized contributions we use Bauer, Stech and Wirbel (BSW) model [8]. Our work is related to that in [3] whose methods are made use of here.

To achieve simplicity of description, we assume that the nonfactorized effects associated with the three Lorentz-scalar structures in $B \rightarrow VV$ decays are the same. Using experimental data, we then calculate the average nonfactorization factors for color-favored $b \rightarrow c\bar{u}d$ and $b \rightarrow c\bar{c}s$ processes. We repeat this for color-suppressed $b \rightarrow c\bar{c}s$ processes. We relate these nonfactorization factors to the scale dependent parameters $\varepsilon_1(\mu)$ and $\varepsilon_8(\mu)$ of [9] and determine them at $\mu_0 = 4.6$ GeV. The details are explained in the text of this paper. Finally, having isolated the parameters $\varepsilon_1(\mu_0)$ and $\varepsilon_8(\mu_0)$, we make predictions for the decay rates of Cabibbo-favored modes measured and as yet unmeasured. The measured rates are shown to agree well with the predictions with few exceptions.

6.2 Formalism

6.2.1 Effective Hamiltonian

In the absence of strong interactions, the effective Hamiltonian for the process $b \rightarrow c \bar{u} d$ is given by

$$\mathcal{H}_{\text{eff}} = \frac{G_F}{\sqrt{2}} V_{cb} V_{ud}^* (\bar{c}b)_L (\bar{d}u)_L. \quad (6.1)$$

where

$$(\bar{c}b)_L = \bar{c}_i \gamma^\mu (1 - \gamma_5) b_i, \quad (6.2)$$

and i is the color index.

When QCD effects are included, the effective Hamiltonian is generalized to [10, 11]

$$\mathcal{H}_{\text{eff}} = \frac{G_F}{\sqrt{2}} V_{cb} V_{ud}^* \left[C_1 (\bar{c}b)_L (\bar{d}u)_L + C_2 (\bar{c}u)_L (\bar{d}b)_L \right], \quad (6.3)$$

where $(\bar{c}b)_L (\bar{d}u)_L$ and $(\bar{c}u)_L (\bar{d}b)_L$ are current \times current local operators.

The Wilson coefficients, C_1 and C_2 , include the short-distance QCD corrections. Their values depend on the renormalization scale μ through the following RGE

$$\mu \frac{dC_\pm}{d\mu} = \frac{\alpha_s}{4\pi} \gamma_\pm C_\pm. \quad (6.4)$$

where

$$C_\pm = \frac{1}{\sqrt{2}} (C_2 \pm C_1), \quad (6.5)$$

and

$$\alpha_s(\mu) = \frac{4\pi}{\beta_0 \ln(\mu^2/\Lambda^2)}. \quad (6.6)$$

In the leading order the coefficient β_0 is given by

$$\beta_0 = \frac{1}{3} (11 N_c - 2 N_f), \quad (6.7)$$

where N_c is the number of colors and N_f the number of flavors. The eigenvalues of the anomalous dimension matrix are

$$\gamma_- = -8, \quad \gamma_+ = 4. \quad (6.8)$$

When (6.4) is solved it gives

$$C_{\pm}(\mu) = \left(\frac{\alpha_s(m_W)}{\alpha_s(\mu)} \right)^{\gamma_{\pm}/2\beta_0} C_{\pm}(m_W). \quad (6.9)$$

At a particular scale ($\mu_0 = 4.6 \text{ GeV} \sim m_b$) and taking ($\Lambda = \Lambda_{\overline{\text{MS}}}^5 = 225 \pm 85 \text{ MeV}$ [11]) for the QCD scale, we have

$$\begin{aligned} C_1 &= 1.128 \pm 0.016 \\ C_2 &= -0.288 \pm 0.029. \end{aligned} \quad (6.10)$$

The errors in C_1 and C_2 are due to the errors in $\Lambda_{\overline{\text{MS}}}^5$.

Similarly, the other Cabibbo-favored process ($b \rightarrow c \bar{c} s$) occurs through the Hamiltonian

$$\mathcal{H}_{\text{eff}} = \frac{G_F}{\sqrt{2}} V_{cb} V_{cs}^* [C_1 (\bar{c}b)_L (\bar{s}c)_L + C_2 (\bar{c}c)_L (\bar{s}b)_L] , \quad (6.11)$$

with the same values for the Wilson coefficients as in (6.10).

6.2.2 Factorization and Nonfactorization

Consider the color-favored decay $\bar{B}^0 \rightarrow D^+ \pi^-$. The decay amplitude for this process is given by

$$\begin{aligned} \mathcal{A}(\bar{B}^0 \rightarrow D^+ \pi^-) &= \langle D^+ \pi^- | \mathcal{H}_{\text{eff}} | \bar{B}^0 \rangle = \frac{G_F}{\sqrt{2}} V_{cb} V_{ud}^* \\ &\times \left[a_1 \langle D^+ \pi^- | (\bar{c}b) (\bar{d}u) | \bar{B}^0 \rangle + C_2 \langle D^+ \pi^- | \frac{1}{2} \sum_a (\bar{c} \lambda^a b) (\bar{d} \lambda^a u) | \bar{B}^0 \rangle \right] \end{aligned} \quad (6.12)$$

where Fierz transformation and color-algebra have been used to rearrange the quark flavors. In (6.12)

$$a_1(\mu) = \left(C_1(\mu) + \frac{C_2(\mu)}{N_c} \right), \quad (6.13)$$

where λ^a are the Gell-Mann matrices.

The second term on the right hand side of (6.12) is nonfactorizable, while the first term receives both factorizable and nonfactorizable contributions. So we write

[1, 3, 9]

$$\begin{aligned} \mathcal{A}(\bar{B}^0 \rightarrow D^+ \pi^-) &= \frac{G_F}{\sqrt{2}} V_{cb} V_{ud}^* a_1 \left[\langle D^+ | (\bar{c}b) | \bar{B}^0 \rangle \langle \pi^- | (\bar{d}u) | 0 \rangle \right. \\ &\quad \left. + \langle D^+ \pi^- | (\bar{c}b) (\bar{d}u) | \bar{B}^0 \rangle^{nf} + \frac{C_2}{a_1} \langle D^+ \pi^- | \frac{1}{2} \sum_a (\bar{c} \lambda^a b) (\bar{d} \lambda^a u) | \bar{B}^0 \rangle^{nf} \right]. \end{aligned} \quad (6.14)$$

Following the conventions in [9], we define the following color-singlet and color-octet nonfactorization parameters:

$$\varepsilon_1^{(BD,\pi)} = \frac{\langle D^+ \pi^- | (\bar{c}b) (\bar{d}u) | \bar{B}^0 \rangle^{nf}}{\langle D^+ | (\bar{c}b) | \bar{B}^0 \rangle \langle \pi^- | (\bar{d}u) | 0 \rangle}, \quad (6.15)$$

$$\varepsilon_8^{(BD,\pi)} = \frac{\langle D^+ \pi^- | \frac{1}{2} \sum_a (\bar{c} \lambda^a b) (\bar{d} \lambda^a u) | \bar{B}^0 \rangle^{nf}}{\langle D^+ | (\bar{c}b) | \bar{B}^0 \rangle \langle \pi^- | (\bar{d}u) | 0 \rangle}. \quad (6.16)$$

These are named Y and X, respectively, in [3]. The decay amplitude then takes the form

$$\mathcal{A}(\bar{B}^0 \rightarrow D^+ \pi^-) = \frac{G_F}{\sqrt{2}} V_{cb} V_{ud}^* a_1 \xi_1^{(BD,\pi)} \langle D^+ | (\bar{c}b) | \bar{B}^0 \rangle \langle \pi^- | (\bar{d}u) | 0 \rangle, \quad (6.17)$$

where

$$\xi_1^{(BD,\pi)}(\mu) = \left(1 + \varepsilon_1^{(BD,\pi)}(\mu) + \frac{C_2}{a_1} \varepsilon_8^{(BD,\pi)}(\mu) \right). \quad (6.18)$$

If we consider the color-suppressed decay $\bar{B}^0 \rightarrow D^0 \pi^0$, the effective Hamiltonian (6.3) is rewritten, using Fierz transformations, as

$$\mathcal{H}_{\text{eff}} = \frac{G_F}{\sqrt{2}} V_{cb} V_{ud}^* \left[a_2 (\bar{c}u) (\bar{d}b) + C_1 \frac{1}{2} \sum_a (\bar{c} \lambda^a u) (\bar{d} \lambda^a b) \right], \quad (6.19)$$

where

$$a_2(\mu) = \left(C_2(\mu) + \frac{C_1(\mu)}{N_c} \right). \quad (6.20)$$

The decay amplitude, then, takes the form

$$\mathcal{A}(\bar{B}^0 \rightarrow D^0 \pi^0) = \frac{G_F}{\sqrt{2}} V_{cb} V_{ud}^* a_2 \xi_2^{(B\pi,D)} \langle \pi^0 | (\bar{c}u) | \bar{B}^0 \rangle \langle D^0 | (\bar{d}b) | 0 \rangle, \quad (6.21)$$

where

$$\xi_2^{(B\pi,D)}(\mu) = \left(1 + \varepsilon_1^{(B\pi,D)}(\mu) + \frac{C_1}{a_2} \varepsilon_8^{(B\pi,D)}(\mu) \right). \quad (6.22)$$

In this work, we will assume that ε_1 and ε_8 are universal constants for all Cabibbo-favored B decays. For this reason, their superscripts will be dropped from now on.

The decay amplitudes for the other processes of class I (color-favored) and processes of class II (color-suppressed) considered in this work, are derived from (6.17) and (6.21), respectively, by making appropriate replacements. However, for processes of class III, which receive contributions from both a_1 and a_2 , we use a suitable combination of the above mentioned equations to derive their amplitude. For example, the decay amplitude for the process $B^- \rightarrow D^0 \pi^-$ is given by

$$\mathcal{A}(B^- \rightarrow D^0 \pi^-) = \frac{G_F}{\sqrt{2}} V_{cb} V_{ud}^* \left[a_1 \xi_1 \langle D^0 | (\bar{c}b) | B^- \rangle \langle \pi^- | (\bar{d}u) | 0 \rangle + a_2 \xi_2 \langle \pi^- | (\bar{d}b) | B^- \rangle \langle D^0 | (\bar{c}u) | 0 \rangle \right]. \quad (6.23)$$

Equations (6.17) and (6.21) suggest the following definitions for the effective a_1 and a_2

$$a_1^{eff} = a_1 \xi_1 = a_1 [1 + \varepsilon_1] + C_2 \varepsilon_8 \quad (6.24)$$

$$a_2^{eff} = a_2 \xi_2 = a_2 [1 + \varepsilon_1] + C_1 \varepsilon_8. \quad (6.25)$$

The coefficients a_1^{eff} and a_2^{eff} are independent of the renormalization scale since the μ dependence of the Wilson coefficients is compensated by the μ dependence of nonfactorization parameters. So, the RGE in (6.4) leads to [9]

$$\begin{aligned} \varepsilon_1(\mu) &= \frac{1}{2} \left[\left(1 + \frac{1}{N_c} \right) [1 + \varepsilon_1(\mu_0)] + \varepsilon_8(\mu_0) \right] \left[\frac{\alpha_s(\mu)}{\alpha_s(\mu_0)} \right]^{\gamma_+/2\beta_0} \\ &+ \frac{1}{2} \left[\left(1 - \frac{1}{N_c} \right) [1 + \varepsilon_1(\mu_0)] - \varepsilon_8(\mu_0) \right] \left[\frac{\alpha_s(\mu)}{\alpha_s(\mu_0)} \right]^{\gamma_-/2\beta_0} - 1 \end{aligned} \quad (6.26)$$

and

$$\begin{aligned} \varepsilon_8(\mu) &= \frac{1}{2} \left[\left(1 - \frac{1}{N_c^2} \right) [1 + \varepsilon_1(\mu_0)] + \left(1 - \frac{1}{N_c} \right) \varepsilon_8(\mu_0) \right] \left[\frac{\alpha_s(\mu)}{\alpha_s(\mu_0)} \right]^{\gamma_+/2\beta_0} \\ &- \frac{1}{2} \left[\left(1 - \frac{1}{N_c^2} \right) [1 + \varepsilon_1(\mu_0)] - \left(1 + \frac{1}{N_c} \right) \varepsilon_8(\mu_0) \right] \left[\frac{\alpha_s(\mu)}{\alpha_s(\mu_0)} \right]^{\gamma_-/2\beta_0}, \end{aligned} \quad (6.27)$$

where μ_0 is arbitrary.

From $1/N_c$ expansion [9, 12, 13] it is found that

$$\begin{aligned}\varepsilon_1(\mu) &= \mathcal{O}(1/N_c^2), \\ \varepsilon_8(\mu) &= \mathcal{O}(1/N_c).\end{aligned}\tag{6.28}$$

A simple way to see this is to realize that whereas only one gluon exchange is needed to cause color-octet current to couple to color-singlet hadrons, two gluons are needed in the case of color-singlet currents.

6.2.3 Current Matrix Elements

Let $|I\rangle$ and $|P\rangle$ be pseudoscalar mesons and $|V\rangle$ be a vector meson. The hadronic current matrix elements can be decomposed in terms of formfactors and decay constants using Lorentz invariance. We define [8]:

$$\langle P|J_\mu|0\rangle = f_P(p_P)_\mu,\tag{6.29}$$

$$\langle V|J_\mu|0\rangle = m_V f_V \epsilon_\mu^*.\tag{6.30}$$

$$\begin{aligned}\langle P|J_\mu|I\rangle &= \left(p_I + p_P - \frac{m_I^2 - m_P^2}{q^2}q\right)_\mu F_1(q^2) \\ &\quad + \frac{m_I^2 - m_P^2}{q^2}q_\mu F_0(q^2),\end{aligned}\tag{6.31}$$

$$\begin{aligned}\langle V|J_\mu|I\rangle &= \frac{-2i}{m_I + m_V} \varepsilon_{\mu\nu\rho\sigma} \epsilon^{\nu*} p_I^\rho p_V^\sigma V(q^2) \\ &\quad + (m_I + m_V) \epsilon_\mu^* A_1(q^2) - \frac{\epsilon^* \cdot q}{m_I + m_V} (p_I + p_V)_\mu A_2(q^2) \\ &\quad - 2m_V \frac{\epsilon^* \cdot q}{q^2} q_\mu (A_3(q^2) - A_0(q^2))\end{aligned}\tag{6.32}$$

with

$$q_\mu = (p_I - p_{P(V)})_\mu,\tag{6.33}$$

$$A_3(q^2) = \frac{m_I + m_V}{2m_V} A_1(q^2) - \frac{m_I - m_V}{2m_V} A_2(q^2),\tag{6.34}$$

and

$$F_1(0) = F_0(0),\tag{6.35}$$

$$A_1(0) = A_3(0).\tag{6.36}$$

The factorized current \times current matrix elements, needed to calculate the decay amplitudes, are evaluated using the above decomposition to be

$$\langle P_1 | J_\mu | I \rangle \langle P_2 | J^\mu | 0 \rangle = (m_I^2 - m_{P_1}^2) f_{P_2} F_0(q^2), \quad (6.37)$$

$$\langle P | J_\mu | I \rangle \langle V | J^\mu | 0 \rangle = 2m_V f_V (\epsilon^\mu \cdot p_I) F_1(q^2), \quad (6.38)$$

$$\langle V | J_\mu | I \rangle \langle P | J^\mu | 0 \rangle = 2m_V f_P (\epsilon^\mu \cdot p_I) A_0(q^2), \quad (6.39)$$

and

$$\begin{aligned} \langle V_1 | J_\mu | I \rangle \langle V_2 | J^\mu | 0 \rangle = & -\frac{m_{V_2}}{m_I + m_{V_1}} f_{V_2} \left[2i \epsilon_{\mu\nu\rho\sigma} \epsilon_2^{\mu} \epsilon_1^{\nu} p_{V_2}^\rho p_{V_1}^\sigma V(q^2) \right. \\ & - (m_I + m_{V_1})^2 (\epsilon_1^\mu \cdot \epsilon_2^\mu) A_1(q^2) \\ & \left. + 2(\epsilon_1^\mu \cdot p_{V_2})(\epsilon_2^\mu \cdot p_{V_1}) A_2(q^2) \right]. \end{aligned} \quad (6.40)$$

where ϵ_1 and ϵ_2 are the polarization vectors of V_1 and V_2 respectively.

For the formfactors, we use the original BSW model [8] where the formfactors are calculated at zero momentum transfer and extrapolated to the desired momentum transfer using a monopole form for all the formfactors.

Regarding the decay constants we adopt the following values: [9, 14, 15, 16]

$$\begin{aligned} f_\pi &= 130.7 \pm 0.37 \text{ MeV} \\ f_\rho &= 207 \pm 1 \text{ MeV} \\ f_{a_1} &= 228 \pm 10 \text{ MeV} \\ f_{J/\psi} &= 405 \pm 14 \text{ MeV} \\ f_{\psi(2S)} &= 282 \pm 14 \text{ MeV} \\ f_D &= 200 \pm 10\% \text{ MeV} \\ f_{D^*} &= 230 \pm 10\% \text{ MeV} \\ f_{D_s} &= 250 \pm 27 \text{ MeV} \\ f_{D_s^*} &= 275 \pm 10\% \text{ MeV} \end{aligned} \quad (6.41)$$

Now, from (6.17), (6.21), (6.23) and (6.37 - 6.40) we can calculate the two-body decay amplitudes $\mathcal{A}(B \rightarrow M_1 M_2)$ where M_1 and M_2 are the two mesons (pseudoscalar

or vector) in the final state. As a result, the branching ratios are given by

$$\mathcal{B}(B \rightarrow M_1 M_2) = \frac{|\mathbf{k}|}{8\pi m_B^2} |\mathcal{A}(B \rightarrow M_1 M_2)|^2 \tau_B, \quad (6.42)$$

where

$$|\mathbf{k}| = \frac{[(m_B^2 - m_1^2 - m_2^2)^2 - 4m_1^2 m_2^2]^{1/2}}{2m_B} \quad (6.43)$$

is the momentum of the decay products in the B rest-frame.

For the case when both M_1 and M_2 are vector mesons, the decay amplitude can be written in terms of the three helicity amplitudes (\mathcal{A}_0 , \mathcal{A}_+ and \mathcal{A}_-). The longitudinal (P_0) and transverse (P_+ and P_-) polarizations are then defined as

$$P_0 = \frac{|\mathcal{A}_0|^2}{|\mathcal{A}_0|^2 + |\mathcal{A}_+|^2 + |\mathcal{A}_-|^2} \quad (6.44)$$

$$P_{\pm} = \frac{|\mathcal{A}_{\pm}|^2}{|\mathcal{A}_0|^2 + |\mathcal{A}_+|^2 + |\mathcal{A}_-|^2}. \quad (6.45)$$

6.3 Evaluation of Nonfactorization Contribution

Equations (6.26) and (6.27) give the explicit dependence of ε_1 and ε_8 on the renormalization scale if the values of these parameters are known at a particular point (e.g. μ_0). However, the μ dependence is cancelled by the μ dependence of the Wilson coefficients such that the decay amplitude is μ independent. Our goal in this section is to deduce the values of $\varepsilon_1(\mu_0)$ and $\varepsilon_8(\mu_0)$ using available experimental data on color-favored and color-suppressed channels.

Let us first consider the color-favored processes of the type $b \rightarrow c\bar{u}d$. By calculating the branching ratios of these decays using the factorization assumption ($\varepsilon_1 = \varepsilon_8 = 0$) and then by comparing it with experimental measurements we calculate ξ_1^2 in each decay channel using the simple relation:

$$\xi^2 = \frac{\mathcal{B}(\text{Experiment})}{\mathcal{B}(\text{Factorization})}. \quad (6.46)$$

The results are shown in Table 6.1 and displayed in Fig. 6.1.

We can see from these results that ξ_1^2 is almost channel independent except when the a_1 meson is present in the final state. By averaging the amount of nonfactorization in these channels we get the value, $\xi_1^2(\mu_0) = 0.80 \pm 0.06$. This corresponds to a 20% deviation from the factorization assumption.

The second set of processes considered, are the color-favored decays of the type $b \rightarrow c\bar{c}s$. The experimental value used for each decay mode were taken to be a weighted average over the charged and neutral decay channels. The resulting amount of nonfactorization in these decays are shown in Table 6.2 and displayed in Fig. 6.2. The weighted average of the amount of nonfactorization in these processes, $\xi_1^2(\mu_0) = 0.86 \pm 0.15$, is in good agreement with that found in the decay processes of kind $b \rightarrow c\bar{u}d$.

Finally, we considered the color-suppressed processes of the type $b \rightarrow c\bar{c}s$. These processes give predictions regarding the nonfactorization parameter $\xi_2^2(\mu_0)$ using (6.46). In Table 6.3 and in Fig. 6.3 we show the results of these calculations. On the average, a value of $\xi_2^2(\mu_0) = 6.6 \pm 2.4$ is calculated.

Figure 6.4, shows the regions in ε_1 - ε_8 space that correspond to the average values of ξ_1^2 and ξ_2^2 as predicted in Tables 6.1, 6.2 and 6.3. In this figure, the two parallel regions bounded by thin solid lines correspond to the value, $\xi_1^2 = 0.80 \pm 0.06$, calculated from the color-favored processes of the type $b \rightarrow c\bar{u}d$. The regions bounded by the dotted lines correspond to the value, $\xi_1^2 = 0.86 \pm 0.14$, calculated from the color-favored processes of the type $b \rightarrow c\bar{c}s$. The value, $\xi_2^2 = 6.6 \pm 2.4$, calculated from the color-suppressed processes of the type $b \rightarrow c\bar{c}s$ corresponds to the two horizontal bands bounded by dashed lines.

In Fig. 6.4, we also show two intersecting solid lines. These have been drawn in light of (6.28) and correspond to the equation

$$\frac{\varepsilon_1}{\varepsilon_8} = \frac{1}{N_c}. \quad (6.47)$$

We realize that this relation need not be exact, nevertheless we use it to restrict our solutions.

As seen in Fig. 6.4, these regions intersect in four areas labelled 1, 2, 3 and 4. Areas 1 and 2 are excluded due to the severe violation of (6.47). Area 4 is also excluded because it produces negative a_2^{eff} which is not supported by the mainstream data on B -decays. So, we are left with area 3. From the size and location of this area in the ε_1 - ε_8 space, we get the following predictions for the color-singlet and color-octet nonfactorization parameters at μ_0 ,

$$\begin{aligned}\varepsilon_1(\mu_0) &= -0.07 \pm 0.03, \\ \varepsilon_8(\mu_0) &= 0.13 \pm 0.05 .\end{aligned}\tag{6.48}$$

These values correspond to

$$\begin{aligned}\xi_1(\mu_0) = 0.89 \pm 0.03 &\longrightarrow a_1^{eff} = 0.92 \pm 0.03 , \\ \xi_2(\mu_0) = 2.59 \pm 0.79 &\longrightarrow a_2^{eff} = 0.23 \pm 0.06 ,\end{aligned}\tag{6.49}$$

and in the language of [3], they correspond to

$$\begin{aligned}\tilde{a}_1(\mu_0) &= a_1^{eff} - a_1(\mu_0) = -0.11 \pm 0.03 , \\ \tilde{a}_2(\mu_0) &= a_2^{eff} - a_2(\mu_0) = 0.14 \pm 0.06 .\end{aligned}\tag{6.50}$$

The predicted value of ε_8 is in agreement with that predicted in [9] using a more limited set of processes.

6.4 Predictions of Branching Ratios and Polarization

Assuming universality of the nonfactorization parameters, ε_1 and ε_8 , we calculated the branching ratios for a large number of Cabibbo-favored decay channels which are shown in Tables 6.4 - 6.11. The errors that appear in the theoretical calculations are due to the uncertainties in the Wilson coefficients, the decay constants, the B -meson lifetime and (where applicable) the mass of a_1 meson.

Table 6.1: The values of the nonfactorization parameter ξ_1^2 calculated for six color-favored processes of the type $b \rightarrow c\bar{u}d$. Column 3 represents the factorization model estimate of the branching ratios.

Process	Branching Ratio $\times 10^{-3}$		ξ_1^2
	Experiment [14]	Factorization	
$\bar{B}^0 \rightarrow D^+\pi^-$	3.0 ± 0.4	4.0 ± 0.1	0.74 ± 0.10
$\bar{B}^0 \rightarrow D^+\rho^-$	7.9 ± 1.4	9.5 ± 0.3	0.83 ± 0.15
$\bar{B}^0 \rightarrow D^+a_1^-$	6.0 ± 3.3	10.3 ± 1.0	0.58 ± 0.32
$\bar{B}^0 \rightarrow D^{*+}\pi^-$	2.6 ± 0.4	3.1 ± 0.1	0.84 ± 0.13
$\bar{B}^0 \rightarrow D^{*+}\rho^-$	7.3 ± 1.5	9.0 ± 0.3	0.81 ± 0.17
$\bar{B}^0 \rightarrow D^{*+}a_1^-$	13.0 ± 2.7	13.1 ± 1.2	0.99 ± 0.23
Weighted Average			0.80 ± 0.06

Table 6.2: The values of the nonfactorization parameter ξ_1^2 calculated for four color-favored processes of the type $b \rightarrow c\bar{c}s$. Column 3 represents the factorization model estimate of the branching ratios.

Process	Branching Ratio $\times 10^{-3}$		ξ_1^2
	Experiment [14]	Factorization	
$B \rightarrow DD_s$	9.8 ± 2.4	13.8 ± 3.0	0.70 ± 0.23
$B \rightarrow DD_s^*$	9.4 ± 3.1	9.6 ± 1.9	0.98 ± 0.38
$B \rightarrow D^*D_s$	10.4 ± 2.8	6.3 ± 1.4	1.64 ± 0.57
$B \rightarrow D^*D_s^*$	22.3 ± 5.7	26.5 ± 5.4	0.84 ± 0.28
Weighted Average			0.86 ± 0.15

Table 6.3: The values of the nonfactorization parameter ξ_2^2 calculated for four color-suppressed processes of the type $b \rightarrow c\bar{c}s$. Column 3 represents the factorization model estimate of the branching ratios.

Process	Branching Ratio $\times 10^{-4}$		ξ_2^2
	Experiment [14]	Factorization	
$B \rightarrow K J/\psi$	9.6 ± 1.1	0.73 ± 0.40	13.1 ± 7.3
$B \rightarrow K \psi(2S)$	6.9 ± 3.1	0.25 ± 0.14	28.1 ± 20
$B \rightarrow K^* J/\psi$	15.4 ± 1.9	3.10 ± 1.70	5.0 ± 2.8
$B \rightarrow K^* \psi(2S)$	14.0 ± 9.0	1.64 ± 0.90	8.5 ± 7.2
Weighted Average			6.6 ± 2.4

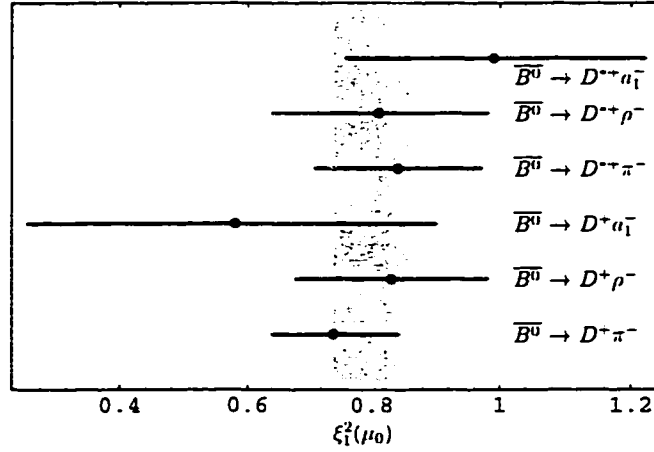


Figure 6.1: The values of the nonfactorization parameter ξ_1^2 calculated for six color-favored processes of the type $b \rightarrow c\bar{u}d$. The shaded area represents the statistical average.

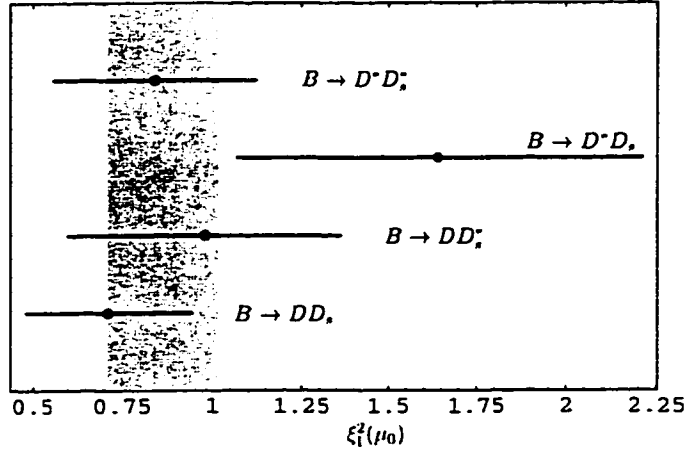


Figure 6.2: The values of the nonfactorization parameter ξ_1^2 calculated for four color-favored processes of the type $b \rightarrow c\bar{c}s$. The shaded area represents the statistical average.

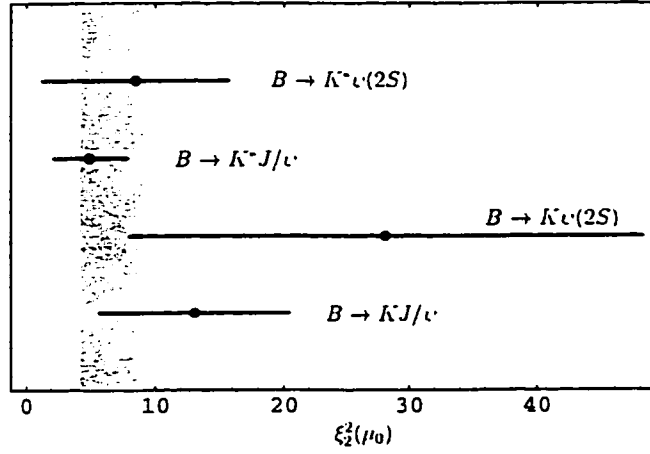


Figure 6.3: The values of the nonfactorization parameter ξ_2^2 calculated for four color-suppressed processes of the type $b \rightarrow c\bar{c}s$. The shaded area represents the statistical average.

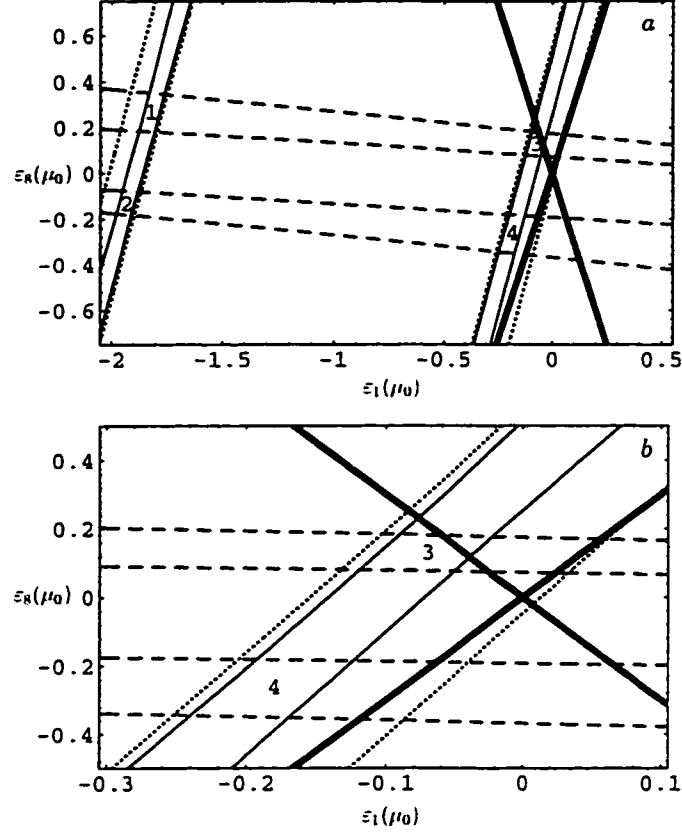


Figure 6.4: (a) The regions in ε_1 - ε_8 space that correspond to the amount of nonfactorizations estimated for ξ_1^2 and ξ_2^2 . The two parallel regions bounded by thin solid lines correspond to the value $\xi_1^2 = 0.80 \pm 0.06$ calculated from the color-favored processes of the type $b \rightarrow c\bar{u}d$. The regions bounded by the dotted lines correspond to the value $\xi_1^2 = 0.86 \pm 0.14$ calculated from the color-favored processes of the type $b \rightarrow c\bar{c}s$. The regions bounded by the dashed lines correspond to the value $\xi_2^2 = 6.6 \pm 2.4$ calculated from the color-suppressed processes of the type $b \rightarrow c\bar{c}s$. The two intersecting solid lines correspond to the equation $\varepsilon_1/\varepsilon_8 = 1/N_c$. (b) A magnification of the interesting region in ε_1 - ε_8 space.

We start by studying six color-favored processes of the type $b \rightarrow c\bar{u}d$ shown in Table 6.4. From this table, it can be seen that the inclusion of nonfactorization improves the predictions of the factorization assumption and produces a much better fit to experimental measurements. In Table 6.5, we show the predicted branching ratios for ten color-suppressed processes of the type $b \rightarrow c\bar{u}d$. As the results show, the inclusion of nonfactorization in these decays enhances their decay rates, pushing them closer to the present upper bounds.

Tables 6.6 and 6.7 show the predictions of the branching ratios for the color-favored and color-suppressed decays of the type $b \rightarrow c\bar{c}s$. By comparing these results with experimental data we find a significant improvement in the theoretical predictions, specially for the color-suppressed modes. The experimental value shown for each decay mode is a weighted average over the charged and neutral decay channels which differ in the flavor of their spectator quark.

The four decay channels of B^- meson shown in Table 6.8 receive contributions from two diagrams. As a result the decay amplitudes contain interference between $a_1^{\epsilon ff}$ and $a_2^{\epsilon ff}$. Using the values of the nonfactorization parameters in (6.48) results in a constructive interference between the two diagrams and small modifications to the predictions of the factorization assumption. The predictions are in good agreement with experiments. However, if we used for the nonfactorization parameters the values $\varepsilon_1(\mu_0) = -0.18$ and $\varepsilon_8(\mu_0) = -0.26$, which are taken from area 4 in Fig. 6.4, the interference between the two diagrams becomes destructive. This results in lower values for the branching ratios and poor agreement with experiment supporting our choice of the solution in area 3 as discussed in the previous section.

Finally, we calculated the effect of nonfactorization contribution on the branching ratios of three sets of B_s -decays. The results of these calculations are shown in Tables 6.9 - 6.11. Even though, experimental data on B_s -decays are very limited, the measured branching ratio of $\overline{B}_s \rightarrow \phi J/\psi$ [17] shows encouraging agreement with our predictions.

Table 6.4: The predicted branching ratios for the color-favored processes of the type $b \rightarrow c\bar{u}d$ calculated, in column 2, by taking $\varepsilon_1(\mu_0) = \varepsilon_8(\mu_0) = 0$ and, in column 3, by taking $\varepsilon_1(\mu_0) = -0.07 \pm 0.03$, $\varepsilon_8(\mu_0) = 0.13 \pm 0.05$. The last column represents the available experimental measurements

Process	Branching Ratio $\times 10^{-3}$		
	Fac.	Nonfac.	Exp. [14]
$\bar{B}^0 \rightarrow D^+\pi^-$	4.0 ± 0.1	3.2 ± 0.3	3.0 ± 0.4
$\bar{B}^0 \rightarrow D^+\rho^-$	9.5 ± 0.3	7.6 ± 0.6	7.9 ± 1.4
$\bar{B}^0 \rightarrow D^+a_1^-$	10.3 ± 1.0	8.2 ± 1.0	6.0 ± 3.3
$\bar{B}^0 \rightarrow D^{*+}\pi^-$	3.1 ± 0.1	2.5 ± 0.2	2.6 ± 0.4
$\bar{B}^0 \rightarrow D^{*+}\rho^-$	9.0 ± 0.3	7.2 ± 0.6	7.3 ± 1.5
$\bar{B}^0 \rightarrow D^{*+}a_1^-$	13.1 ± 1.2	10.5 ± 1.3	13.0 ± 2.7

The predictions of longitudinal (P_0) and transverse (P_-) polarizations of processes of the form $B \rightarrow VV$ are shown in Table 6.12. The available experimental measurements show good agreement with the predicted values. Notice that in doing polarization calculations of color-favored and color-suppressed decays, the nonfactorization parameters cancel out. This is due to the assumed universality of ε_1 and ε_8 . As a result, the polarization predictions are the same as in the factorization model though the branching ratios are scaled by an overall factor.

6.5 Discussion and Conclusion

Strictly speaking, we know that the factorization assumption can not be correct. This is because it produces a scale dependent transition amplitude. However, quoting authors of ref. [9],

” what one may hope for is that it provides a useful approximation if the Wilson coefficients (or equivalently the QCD coefficients a_1 and a_2) are

Table 6.5: The predicted branching ratios for the color-suppressed processes of the type $b \rightarrow c\bar{u}d$ calculated, in column 2, by taking $\varepsilon_1(\mu_0) = \varepsilon_8(\mu_0) = 0$ and, in column 3, by taking $\varepsilon_1(\mu_0) = -0.07 \pm 0.03$, $\varepsilon_8(\mu_0) = 0.13 \pm 0.05$. The last column represents the available experimental upper bounds.

Process	Branching Ratio $\times 10^{-4}$		
	Fac.	Nonfac.	Exp. [14]
$\bar{B}^0 \rightarrow D^0 \pi^0$	0.13 ± 0.08	0.88 ± 0.50	< 4.8
$\bar{B}^0 \rightarrow D^{*0} \pi^0$	0.14 ± 0.08	0.92 ± 0.51	< 9.7
$\bar{B}^0 \rightarrow D^0 \eta$	0.07 ± 0.04	0.49 ± 0.28	< 6.8
$\bar{B}^0 \rightarrow D^{*0} \eta$	0.07 ± 0.04	0.50 ± 0.28	< 6.9
$\bar{B}^0 \rightarrow D^0 \eta'$	0.02 ± 0.01	0.15 ± 0.08	< 8.6
$\bar{B}^0 \rightarrow D^{*0} \eta'$	0.02 ± 0.01	0.15 ± 0.08	< 27
$\bar{B}^0 \rightarrow D^0 \rho^0$	0.07 ± 0.04	0.44 ± 0.25	< 5.5
$\bar{B}^0 \rightarrow D^{*0} \rho^0$	0.26 ± 0.15	1.74 ± 0.98	< 11.7
$\bar{B}^0 \rightarrow D^0 \omega$	0.06 ± 0.04	0.43 ± 0.24	< 6.3
$\bar{B}^0 \rightarrow D^{*0} \omega$	0.26 ± 0.15	1.72 ± 0.97	< 21

Table 6.6: The predicted branching ratios for the color-favored processes of the type $b \rightarrow c\bar{c}s$ calculated, in column 2, by taking $\varepsilon_1(\mu_0) = \varepsilon_8(\mu_0) = 0$ and, in column 3, by taking $\varepsilon_1(\mu_0) = -0.07 \pm 0.03$, $\varepsilon_8(\mu_0) = 0.13 \pm 0.05$. The last column represents the available experimental measurements.

Process	Branching Ratio $\times 10^{-3}$		
	Fac.	Nonfac.	Exp. [14]
$B \rightarrow DD_s$	13.8 ± 3.0	11.1 ± 2.5	9.8 ± 2.4
$B \rightarrow DD_s^*$	9.6 ± 1.9	7.6 ± 1.7	9.4 ± 3.1
$B \rightarrow D^* D_s$	6.3 ± 1.4	5.0 ± 1.2	10.4 ± 2.8
$B \rightarrow D^* D_s^*$	26.5 ± 5.4	21.2 ± 4.6	22.3 ± 5.7

Table 6.7: The predicted branching ratios for the color-suppressed processes of the type $b \rightarrow c\bar{c}s$ calculated, in column 2, by taking $\varepsilon_1(\mu_0) = \varepsilon_8(\mu_0) = 0$ and, in column 3, by taking $\varepsilon_1(\mu_0) = -0.07 \pm 0.03$, $\varepsilon_8(\mu_0) = 0.13 \pm 0.05$. The last column represents the available experimental measurements.

Process	Branching Ratio $\times 10^{-4}$		
	Fac.	Nonfac.	Exp. [14]
$B \rightarrow KJ/\psi$	0.73 ± 0.40	4.90 ± 2.6	9.6 ± 1.1
$B \rightarrow K\psi(2S)$	0.25 ± 0.14	1.65 ± 0.88	6.9 ± 3.1
$B \rightarrow K^*J/\psi$	3.10 ± 1.70	20.8 ± 11.0	15.4 ± 1.9
$B \rightarrow K^*\psi(2S)$	1.64 ± 0.90	11.0 ± 5.9	14.0 ± 9.0

Table 6.8: The predicted branching ratios for the decays of B^- meson of the type $b \rightarrow c\bar{u}d$ calculated, in column 2, by taking $\varepsilon_1(\mu_0) = \varepsilon_8(\mu_0) = 0$ and, in column 3, by taking $\varepsilon_1(\mu_0) = -0.07 \pm 0.03$, $\varepsilon_8(\mu_0) = 0.13 \pm 0.05$. The last column represents the available experimental measurements.

Process	Branching Ratio $\times 10^{-3}$		
	Fac.	Nonfac.	Exp. [14]
$B^- \rightarrow D^0\pi^-$	5.1 ± 0.2	5.3 ± 0.6	5.3 ± 0.5
$B^- \rightarrow D^0\rho^-$	10.5 ± 0.4	9.6 ± 0.7	13.4 ± 1.8
$B^- \rightarrow D^{*0}\pi^-$	4.2 ± 0.2	4.5 ± 0.5	5.2 ± 0.8
$B^- \rightarrow D^{*0}\rho^-$	11.0 ± 0.5	11.3 ± 1.2	15.5 ± 3.1

Table 6.9: The predicted branching ratios for the color-favored B_s decays of the type $b \rightarrow c\bar{u}d$ calculated, in column 2, by taking $\varepsilon_1(\mu_0) = \varepsilon_8(\mu_0) = 0$ and, in column 3, by taking $\varepsilon_1(\mu_0) = -0.07 \pm 0.03$, $\varepsilon_8(\mu_0) = 0.13 \pm 0.05$. The last column represents the available experimental limits.

Process	Branching Ratio $\times 10^{-3}$		
	Fac.	Nonfac.	Exp. [14]
$\overline{B}_s \rightarrow D_s^+ \pi^-$	3.6 ± 0.2	2.9 ± 0.3	< 120
$\overline{B}_s \rightarrow D_s^+ \rho^-$	8.6 ± 0.4	6.8 ± 0.6	—
$\overline{B}_s \rightarrow D_s^+ a_1^-$	9.3 ± 1.0	7.4 ± 0.9	—
$\overline{B}_s \rightarrow D_s^{*+} \pi^-$	2.7 ± 0.1	2.1 ± 0.2	—
$\overline{B}_s \rightarrow D_s^{*+} \rho^-$	7.8 ± 0.4	6.2 ± 0.6	—
$\overline{B}_s \rightarrow D_s^{*+} a_1^-$	11.3 ± 1.2	9.0 ± 1.1	—

Table 6.10: The predicted branching ratios for the color-suppressed B_s decays of the type $b \rightarrow c\bar{u}d$ calculated, in column 2, by taking $\varepsilon_1(\mu_0) = \varepsilon_8(\mu_0) = 0$ and, in column 3, by taking $\varepsilon_1(\mu_0) = -0.07 \pm 0.03$, $\varepsilon_8(\mu_0) = 0.13 \pm 0.05$.

Process	Branching Ratio $\times 10^{-4}$		
	Fac.	Nonfac.	Exp. [14]
$\overline{B}_s \rightarrow D^0 K^0$	0.18 ± 0.10	1.2 ± 0.7	—
$\overline{B}_s \rightarrow D^{*0} K^0$	0.18 ± 0.10	1.2 ± 0.7	—
$\overline{B}_s \rightarrow D^0 K^{*0}$	0.10 ± 0.06	0.6 ± 0.4	—
$\overline{B}_s \rightarrow D^{*0} K^{*0}$	0.34 ± 0.20	2.3 ± 1.3	—

Table 6.11: The predicted branching ratios for the color-suppressed B_s decays of the type $b \rightarrow c\bar{c}s$ calculated, in column 2, by taking $\varepsilon_1(\mu_0) = \varepsilon_8(\mu_0) = 0$ and, in column 3, by taking $\varepsilon_1(\mu_0) = -0.07 \pm 0.03$, $\varepsilon_8(\mu_0) = 0.13 \pm 0.05$. The last column represents the available experimental measurements.

Process	Branching Ratio $\times 10^{-4}$		
	Fac.	Nonfac.	Exp.
$\bar{B}_s \rightarrow \eta J/\psi$	0.20 ± 0.11	1.3 ± 0.7	—
$\bar{B}_s \rightarrow \eta\psi(2S)$	0.07 ± 0.04	0.5 ± 0.2	—
$\bar{B}_s \rightarrow \eta' J/\psi$	0.23 ± 0.13	1.6 ± 0.8	—
$\bar{B}_s \rightarrow \eta'\psi(2S)$	0.07 ± 0.04	0.4 ± 0.2	—
$\bar{B}_s \rightarrow \phi J/\psi$	2.05 ± 1.10	13.8 ± 7.3	9.3 ± 3.3 [17]
$\bar{B}_s \rightarrow \phi\psi(2S)$	1.26 ± 0.70	8.5 ± 4.5	—

evaluated at a suitable scale μ_f , the factorization point . "

In B decays, the Wilson coefficients are usually evaluated at $(\mu \sim m_b)$. If this is the factorization scale, then we should expect the nonfactorization parameters ($\varepsilon_1(m_b)$ and $\varepsilon_8(m_b)$) to vanish. However, since the predictions of the factorization assumption are generally not in agreement with data, specially for color-suppressed decays, this could indicate that the nonfactorizable parts of the decay amplitude are not negligible at the B -mass scale.

In this chapter, we tried to answer the following question: Is it possible via the introduction of a minimum number of new parameters to improve the predictions of the factorization assumption and explain the bulk of available experimental data on Cabibbo-favored B -decays?

In answering this question, we assumed universality of the color-singlet (ε_1) and the color-octet (ε_8) nonfactorization parameters. Two sets of color-favored processes (Tables 6.1 and 6.2) and one set of color-suppressed processes (Tables 6.3) were used to give quantitative estimates of these parameters. It has been found (by calculating

Table 6.12: Predictions of longitudinal (P_0) and transverse (P_-) polarizations for Cabibbo-favored decays of the form $B \rightarrow VV$ where V is a vector meson.

Process	P_0		P_-	
	Fac.	Exp.	Fac.	Exp.
$\bar{B}^0 \rightarrow D^{*+} \rho^-$	0.87	0.90 ± 0.08 [18]	0.11	—
$\bar{B}^0 \rightarrow D^{*+} a_1^-$	0.74	—	0.23	—
$\bar{B}^0 \rightarrow D^{*0} \rho^0$	0.72	—	0.28	—
$\bar{B}^0 \rightarrow D^{*0} \omega$	0.72	—	0.28	—
$B \rightarrow D^* D_s^*$	0.52	—	0.39	—
$B \rightarrow K^{*-} J/\psi$	0.57	0.52 ± 0.08 [19]	0.39	0.47 ± 0.08 [19, 7]
$B \rightarrow K^{*-} \psi(2S)$	0.49	—	0.42	—
$B^- \rightarrow D^{*0} \rho^-$	0.86	—	0.12	—
$\bar{B}_s \rightarrow D^{*+} \rho^-$	0.88	—	0.11	—
$\bar{B}_s \rightarrow D^{*+} a_1^-$	0.74	—	0.22	—
$\bar{B}_s \rightarrow D^{*0} K^{*0}$	0.70	—	0.29	—
$\bar{B}_s \rightarrow \phi J/\psi$	0.55	0.56 ± 0.21 [20]	0.41	—
$\bar{B}_s \rightarrow \phi \psi(2S)$	0.48	—	0.42	—

the branching ratios for a large number of Cabibbo-favored B -decays) that the values $\varepsilon_1(\mu_0) = -0.07 \pm 0.03$ and $\varepsilon_8(\mu_0) = 0.13 \pm 0.05$ improve significantly the predictions of the factorization assumption even though the Wilson coefficients were evaluated at LL and only the tree diagrams were considered. These results support the argument that nonfactorization is an important contributor to the decay amplitude of B -decays.

Bibliography

- [1] H. Y. Cheng, Phys. Lett. B **335**, 428 (1994); Z. Phys. C **69**, 647 (1996).
- [2] A. N. Kamal and A. B. Santra, Alberta Thy 31-94 (1994); Z. Phys. C **72**, 91 (1996).
- [3] J. Soares, Phys. Rev. D **51**, 3518 (1995).
- [4] A. Ali and C. Greub, Phys. Rev. D **57**, 2996 (1998).
- [5] A. Ali, G. Kramer and C. D. Lu, DESY 98-041, hep-ph/9804363.
- [6] H. Y. Cheng and B. Tsang, IP-ASTP-01-98, hep-ph/9803457.
- [7] F. M. Al-Shamali and A. N. Kamal, Eur. Phys. J. C **4**, 669 (1998).
- [8] M. Bauer, B. Stech and M. Wirbel, Z. Phys. C **34**, 103 (1987); M. Wirbel, B. Stech and M. Bauer, Z. Phys. C **29**, 637 (1985).
- [9] M. Neubert and B. Stech, CERN-TH/97/99, hep-ph/9705292. To appear in the Second Edition of Heavy Flavours, Edited by A. J. Buras and M. Lindner (World Scientific, Singapore).
- [10] A. J. Buras, M. Jamin, M. Lautenbacher and P. Weisz, Nucl. Phys. B **370**, 69 (1992).
- [11] G. Buchalla, A. Buras and M. Lautenbacher, Rev. M. Phys. **68**, 1125 (1996).

- [12] E. Witten, Nucl. Phys. B **160**, 57 (1979).
- [13] A. J. Buras, J. M. Gérard and R. Rückl, Nucl. Phys. B **268**, 16 (1986).
- [14] R. M. Barnett et al., *Particle Data Group, Review of Particle Properties*, Phys. Rev. D **54**, 1 (1996) and 1997 off-year partial update for the 1998 edition.
- [15] J. Richman, in ICHEP'96, Proceedings of the 28th International Conference on High Energy Physics, Warsaw, Poland, edited by Z. Scora A. Wroblewski (World Scientific, Singapore, 1997), hep-ex/9701014.
- [16] CLEO Collaboration, CLNS 97/1526, CLEO 97-28, hep-ex/9712014.
- [17] F. Abe *et al.* (CDF Collaboration), Phys. Rev. D **54**, 6596 (1996).
- [18] T. E. Browder and K. Honscheid, *Progress in Nuclear and Particle Physics*, Vol. 35, ed. K. Faessler, 81 (1995).
- [19] C. P. Jessop *et al.* (CLEO Collaboration), Phys. Rev. Lett. **79**, 4533 (1997).
- [20] F. Abe *et al.* (CDF Collaboration), Phys. Rev. Lett. **75**, 3068 (1995).

Chapter 7

NLL and Penguin Effects on Nonfactorization in B -Decays

7.1 Introduction

So far in our calculations, we used the Wilson coefficients (C_1 and C_2) evaluated in leading logarithms (LL) and neglected all contributions from the penguin diagrams. In here, we extend the work of the previous chapter and investigate the effects caused by working in next-to-leading logarithms (NLL) and by including the contributions from the QCD penguin diagrams.

Also, toward the end of this chapter we investigate the effect of nonfactorization on a set of Cabibbo-suppressed processes of type $b \rightarrow c\bar{c}d$.

7.2 Wilson Coefficients in NLL

As mentioned in section 2.5, the Wilson coefficients in NLL are renormalization scale and scheme dependent. Working in the naive dimensional regularization (NDR) scheme, the Wilson coefficients at different scales ($\mu = 4.4, 4.6$ and 4.8 GeV) are listed in Table 2.2.

Consider process of the type $b \rightarrow c\bar{c}s$ which receive contributions from both tree and penguin diagrams. For the purposes of this chapter, we rewrite the effective Hamiltonian introduced in (2.59) as [5, 6]

$$\begin{aligned} \mathcal{H}_{\text{eff}} = & \frac{G_F}{\sqrt{2}} \left[V_{ub}V_{us}^* (C_1 Q_1^u + C_2 Q_2^u) + V_{cb}V_{cs}^* (C_1 Q_1^c + C_2 Q_2^c) \right. \\ & \left. + (V_{ub}V_{us}^* + V_{cb}V_{cs}^*) \sum_{i=3}^6 C_i Q_i \right], \end{aligned} \quad (7.1)$$

where

$$\begin{aligned} Q_1^u &= (\bar{u}_i b_i)_L (\bar{s}_j u_j)_L \\ Q_2^u &= (\bar{u}_i b_j)_L (\bar{s}_j u_i)_L \\ Q_1^c &= (\bar{c}_i b_i)_L (\bar{s}_j c_j)_L \\ Q_2^c &= (\bar{c}_i b_j)_L (\bar{s}_j c_i)_L \\ Q_3 &= (\bar{s}_i b_i)_L \sum_q (\bar{q}_j q_j)_L \\ Q_4 &= (\bar{s}_i b_j)_L \sum_q (\bar{q}_j q_i)_L \\ Q_5 &= (\bar{s}_i b_i)_L \sum_q (\bar{q}_j q_j)_R \\ Q_6 &= (\bar{s}_i b_j)_L \sum_q (\bar{q}_j q_i)_R. \end{aligned} \quad (7.2)$$

Even though, the local operators Q_1^u and Q_2^u don't contribute to process of the type $b \rightarrow c\bar{c}s$ through tree diagrams, they do contribute through penguin diagrams. In writing (7.1), we have made use of the following unitarity condition of the CKM matrix elements

$$V_{ub}V_{us}^* + V_{cb}V_{cs}^* + V_{tb}V_{ts}^* = 0. \quad (7.3)$$

From (2.35), we see that the decay amplitude in the effective theory is given by

$$\mathcal{A}_{\text{eff}} \propto C_i(\mu) \langle Q_i(\mu) \rangle, \quad (7.4)$$

where the matrix elements $\langle Q_i(\mu) \rangle$ are evaluated at the same scale and in the same scheme as the Wilson coefficients $C_i(\mu)$. If these matrix elements are related to the

tree matrix elements by

$$\langle Q_i(\mu) \rangle = g_{ij}(\mu) \langle Q_j \rangle^{\text{tree}}, \quad (7.5)$$

then we can write the effective amplitude as

$$\begin{aligned} \mathcal{A}_{\text{eff}} &\propto C_i(\mu) g_{ij}(\mu) \langle Q_j \rangle^{\text{tree}}, \\ &\propto C_i^{\text{eff}} \langle Q_i \rangle^{\text{tree}}. \end{aligned} \quad (7.6)$$

At the quark level, the scale and scheme dependence of $\langle Q_i(\mu) \rangle$, which is carried by $g(\mu)$, cancel the scale and scheme dependence of the Wilson coefficients [3, 4, 5, 6]. So, both C_i^{eff} and $\langle Q_i \rangle^{\text{tree}}$ are scale and scheme independent.

From above, we can write the decay amplitude as

$$\begin{aligned} \langle \mathcal{H}_{\text{eff}} \rangle &= \frac{G_F}{\sqrt{2}} \left[V_{cb} V_{cs}^* \left(C_1^{\text{eff}} \langle Q_1^c \rangle^{\text{tree}} + C_2^{\text{eff}} \langle Q_2^c \rangle^{\text{tree}} \right) \right. \\ &\quad \left. + \sum_{i=3}^6 \left(V_{ub} V_{us}^* C_i^{\text{eff}} + V_{cb} V_{cs}^* C_i^{\text{eff}} \right) \langle Q_i \rangle^{\text{tree}} \right], \end{aligned} \quad (7.7)$$

where the penguin contributions from $\langle Q_{i=1,2}^u \rangle$ and $\langle Q_{i=1,2}^c \rangle$ are included in $C_{i=3,\dots,6}^{\text{eff}}$ and $C_{i=3,\dots,6}^{\text{eff}}$, respectively. Using the conventions of [5], the explicit forms of C_i^{eff} are given by

$$\begin{aligned} C_1^{\text{eff}} &= C_1 + \frac{\alpha_s}{4\pi} \left(r_V^T + \gamma_V^T \ln \frac{m_b}{\mu} \right)_{1j} C_j \\ C_2^{\text{eff}} &= C_2 + \frac{\alpha_s}{4\pi} \left(r_V^T + \gamma_V^T \ln \frac{m_b}{\mu} \right)_{2j} C_j \\ C_3^{\text{eff}} &= C_3 - \frac{\alpha_s}{24\pi} (C_t(m_q) + C_p) + \frac{\alpha_s}{4\pi} \left(r_V^T + \gamma_V^T \ln \frac{m_b}{\mu} \right)_{3j} C_j \\ C_4^{\text{eff}} &= C_4 + \frac{\alpha_s}{8\pi} (C_t(m_q) + C_p) + \frac{\alpha_s}{4\pi} \left(r_V^T + \gamma_V^T \ln \frac{m_b}{\mu} \right)_{4j} C_j \\ C_5^{\text{eff}} &= C_3 - \frac{\alpha_s}{24\pi} (C_t(m_q) + C_p) + \frac{\alpha_s}{4\pi} \left(r_V^T + \gamma_V^T \ln \frac{m_b}{\mu} \right)_{5j} C_j \\ C_6^{\text{eff}} &= C_4 + \frac{\alpha_s}{8\pi} (C_t(m_q) + C_p) + \frac{\alpha_s}{4\pi} \left(r_V^T + \gamma_V^T \ln \frac{m_b}{\mu} \right)_{6j} C_j, \end{aligned} \quad (7.8)$$

where $q = u, c$. In (7.8), the quantities $C_t(m_q)$ and C_p arise from the penguin-like diagrams of the operators $Q_{i=1,2}^q$ and $Q_{i=3,\dots,6}$, respectively, whereas the matrix $(r_V + \gamma_V \ln \frac{m_k}{\mu})$ is due to the vertex and self-energy corrections to the operators $Q_{i=1,\dots,6}$. These quantities are given by [5]

$$r_V = \begin{pmatrix} \frac{7}{3} & -7 & 0 & 0 & 0 & 0 \\ -7 & \frac{7}{3} & 0 & 0 & 0 & 0 \\ 0 & 0 & \frac{7}{3} & -7 & 0 & 0 \\ 0 & 0 & -7 & \frac{7}{3} & 0 & 0 \\ 0 & 0 & 0 & 0 & -\frac{1}{3} & 1 \\ 0 & 0 & 0 & 0 & -3 & \frac{35}{3} \end{pmatrix}, \quad (7.9)$$

$$\gamma_V = \begin{pmatrix} -2 & 6 & 0 & 0 & 0 & 0 \\ 6 & -2 & 0 & 0 & 0 & 0 \\ 0 & 0 & -2 & 6 & 0 & 0 \\ 0 & 0 & 6 & -2 & 0 & 0 \\ 0 & 0 & 0 & 0 & 2 & -6 \\ 0 & 0 & 0 & 0 & 0 & -16 \end{pmatrix}. \quad (7.10)$$

$$C_t(m_q) = C_1(\mu) \left[\frac{2}{3} + \frac{2}{3} \ln \frac{m_q^2}{\mu^2} - \Delta F_1 \left(\frac{k^2}{m_q^2} \right) \right], \quad (7.11)$$

$$C_p = C_3(\mu) \left[\frac{4}{3} + \frac{2}{3} \ln \frac{m_s^2}{\mu^2} + \frac{2}{3} \ln \frac{m_b^2}{\mu^2} - \Delta F_1 \left(\frac{k^2}{m_s^2} \right) - \Delta F_1 \left(\frac{k^2}{m_b^2} \right) \right] \\ + (C_4(\mu) + C_6(\mu)) \sum_{i=u,d,s,c,b} \left[\frac{2}{3} \ln \frac{m_i^2}{\mu^2} - \Delta F_1 \left(\frac{k^2}{m_i^2} \right) \right], \quad (7.12)$$

and

$$\Delta F_1(z) = -4 \int_0^1 dx \, x(1-x) \ln[1 - z x(1-x)]. \quad (7.13)$$

Here, k is the momentum carried by the gluon of Fig. 2.6.

The calculation of the penguin driven amplitudes in the factorization assumption involves additional assumptions, an effective value of k^2 for example. In a complete

calculation [7] k^2 would not be a variable; it would be integrated over the wave functions of the hadrons with its own uncertainties. In the absence of a complete knowledge of the hadronic wave functions, the choice is either to select k^2 judiciously or to admit new unknowns through the hadronic wave functions. In penguin calculations, one generally opts for the first alternative and chooses k^2 in the range: $m_b^2/4 \leq k^2 \leq m_b^2/2$. In the calculations presented here we have chosen $k^2 = m_b^2/2$.

Using the definitions in (7.8) we calculate in Table 7.1 the values of the effective Wilson coefficients C_i^{eff} . For $C_3^{\text{eff}} - C_6^{\text{eff}}$, which include the contributions from the QCD penguin diagrams, we list two sets of values, depending on which quark is in the loop (see Fig. 2.6). For quark masses, we used the constituent masses [5] $m_u = m_d = 0.2$ GeV, $m_s = 0.5$ GeV, $m_c = 1.5$ GeV and $m_b = 4.88$ GeV. We also show (in brackets in Table 7.1) the values of the Wilson coefficients evaluated using the following running quark masses at the b -quark mass scale [8]: $m_u = 3.17$ MeV, $m_d = 6.37$ MeV, $m_s = 0.127$ GeV, $m_c = 0.949$ GeV and $m_b = 4.34$ GeV. For the t -quark mass, we always used $m_t = 170$ GeV.

The values of the effective Wilson coefficients calculated using the constituent quark masses and those calculated using the running quark masses are numerically close, and using either set of values does not produce major changes in the results of this chapter. So, for the purposes of this chapter, we use the set of values calculated from the constituent masses, which is also the choice adopted in [5].

7.3 Effect on the Results of Factorization Approximation

7.3.1 Type $b \rightarrow c\bar{u}d$ Decays ($B \rightarrow D\pi$, $D\rho \dots etc.$)

In processes of this type, there are no contributions from the penguin diagrams. So, the effective Hamiltonian relevant to these processes is similar to the one in (3.24),

Table 7.1: Effective Wilson Coefficients in NLL, evaluated using $\Lambda_{\overline{\text{MS}}}^5 = 225 \text{ MeV}$ and constituent quark masses. The values in brackets were evaluated using the running quark masses at the b -quark mass scale.

C_1^{eff}	1.138 (1.145)	
C_2^{eff}	-0.310 (-0.324)	
	$q = u$	$q = c$
C_3^{eff}	$0.0175 + 0.0050 i$ (0.0184 + 0.0049 i)	$0.0209 + 0.0029 i$ (0.0199 + 0.0044 i)
C_4^{eff}	$-0.0394 - 0.0149 i$ (-0.0410 - 0.0146 i)	$-0.0498 - 0.0087 i$ (-0.0457 - 0.0133 i)
C_5^{eff}	$0.0126 + 0.0050 i$ (0.0131 + 0.0049 i)	$0.0161 + 0.0029 i$ (0.0146 + 0.0044 i)
C_6^{eff}	$-0.0502 - 0.0149 i$ (-0.0527 - 0.0146 i)	$-0.0606 - 0.0087 i$ (-0.0573 - 0.0133 i)

except that for C_1 and C_2 we use the values in Table 7.1. As we saw before, processes of this type are divided into three classes, I, II and III.

In processes of class I (examples are $\overline{B}^0 \rightarrow D^+ \pi^-$, $D^+ \rho^- \dots etc.$), the factorizable part of the decay amplitude is proportional to $a_1 = C_1 + C_2/3$. (see section 3.2.1). From Tables 2.1 and 7.1, we see that the values of this parameter in LL and NLL are almost the same

$$\begin{aligned}
 a_1^{\text{LL}} &= 1.032 \\
 a_1^{\text{NLL}} &= 1.035.
 \end{aligned} \tag{7.14}$$

Since the branching ratios are proportional to $|a_1|^2$, the above values for a_1 gives a difference ($\Delta \mathcal{B}_f$) between the branching ratios calculated using the Wilson coefficients in LL and the branching ratios calculated using the Wilson coefficients in NLL of less than 1 % (see Table 7.2).

In processes of class II (examples are $\overline{B}^0 \rightarrow D^0 \pi^0$, $D^0 \rho^0 \dots etc.$), the factorizable

part of the decay amplitude is proportional to $a_2 = C_1/3 + C_2$. The values of this parameter in LL and NLL are given by

$$\begin{aligned} a_2^{\text{LL}} &= 0.088 \\ a_2^{\text{NLL}} &= 0.069. \end{aligned} \quad (7.15)$$

As a result, the predicted branching ratios (see Table 7.2 for listing) in the factorization approximation, drop by about 38 % when working in NLL.

The third class (for example, $B^- \rightarrow D^0 \pi^-$, $D^0 \rho^- \dots etc.$) of processes considered here is a little different from the other two. This is because the decay amplitudes receive contributions from two tree diagrams (see Fig. 3.3) which causes both a_1 and a_2 to contribute to the amplitudes (see (6.23) for an explicit example). As a result, $\Delta \mathcal{B}_f$ is different for each process of this class. However, as can be seen from Table 7.2 these changes are small and are less than 3 %. This is because, the part of the amplitude containing a_1 (which almost has the same value in LL and NLL) dominates over that containing a_2 .

7.3.2 Type $b \rightarrow c\bar{c}s$ Decays ($B \rightarrow DD_s, KJ/\psi \dots etc.$)

Processes of this type, receive contributions from both tree and penguin diagrams (see Fig 7.1). The relevant effective Hamiltonian is shown in (7.1).

Consider first, the four processes of class I shown in Fig 7.1. The contributions to the decay amplitude from Q_1 and Q_2 were already derived in section 3.2.4. The contributions from Q_3 and Q_4 are evaluated in a similar way. Regarding Q_5 , we first use Fierz transformation and color algebra (see Appendix B) to rewrite it as [5]

$$\begin{aligned} Q_5 &= (\bar{s}b)_L (\bar{c}c)_R \\ &= [\bar{s}_i \gamma_\mu (1 - \gamma_5) b_i] [\bar{c}_j \gamma^\mu (1 + \gamma_5) c_j] \\ &= -2 [\bar{c}_j (1 - \gamma_5) b_i] [\bar{s}_i (1 + \gamma_5) c_j] \\ &= -\frac{2}{3} [\bar{c}(1 - \gamma_5)b] [\bar{s}(1 + \gamma_5)c] - [\bar{c}\lambda^a(1 - \gamma_5)b] [\bar{s}\lambda^a(1 + \gamma_5)c]. \end{aligned} \quad (7.16)$$

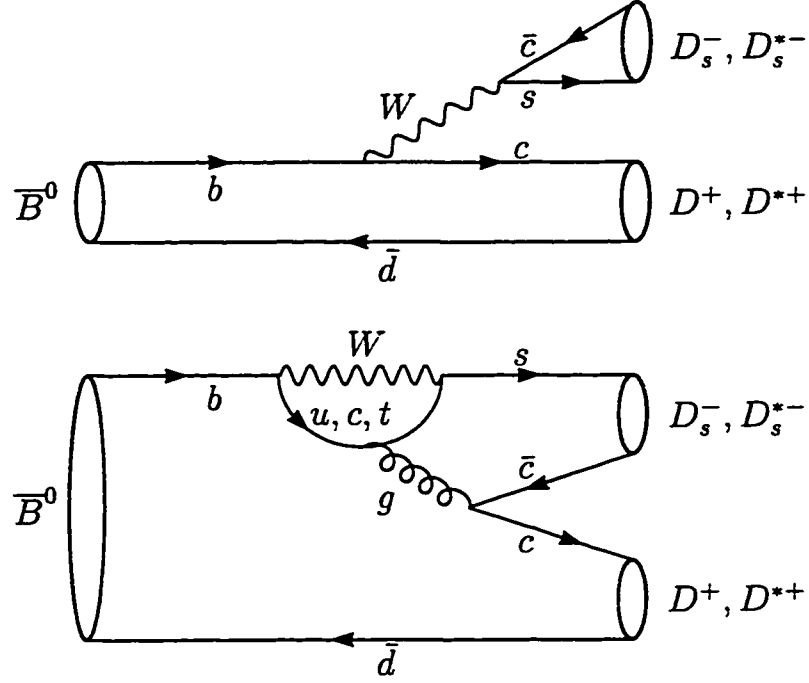


Figure 7.1: The flavor flow diagram for Class I processes of the type $b \rightarrow c\bar{u}s$.

For O_6 , we just use Fierz transformation to rewrite it as

$$\begin{aligned}
 Q_6 &= (\bar{s}_i b_j)_L (\bar{c}_j c_i)_R \\
 &= [\bar{s}_i \gamma_\mu (1 - \gamma_5) b_j] [\bar{c}_j \gamma^\mu (1 + \gamma_5) c_i] \\
 &= -2 [\bar{c}(1 - \gamma_5)b] [\bar{s}(1 + \gamma_5)c].
 \end{aligned} \tag{7.17}$$

However, from the Dirac equation we can easily derive the following relations between $(S + P)$ and $(S - P)$ Dirac bilinears, and V and A bilinears

$$[\bar{s}(1 + \gamma_5)c] = -i \left[\frac{-1}{m_c - m_s} \partial^\mu (\bar{s} \gamma_\mu c) + \frac{1}{m_c + m_s} \partial^\mu (\bar{s} \gamma_\mu \gamma_5 c) \right] \tag{7.18}$$

$$[\bar{c}(1 - \gamma_5)b] = i \left[\frac{1}{m_b - m_c} \partial^\mu (\bar{c} \gamma_\mu b) + \frac{1}{m_b + m_c} \partial^\mu (\bar{c} \gamma_\mu \gamma_5 b) \right]. \tag{7.19}$$

Using the relations developed above, we can write, assuming factorization, the decay amplitude for the processes $\bar{B}^0 \rightarrow D^+ D_s^-$, $\bar{B}^0 \rightarrow D^+ D_s^{*-}$, $\bar{B}^0 \rightarrow D^{*+} D_s^-$ and $\bar{B}^0 \rightarrow D^{*+} D_s^{*-}$ as

$$\mathcal{A}_f(\bar{B}^0 \rightarrow D^+ D_s^-)$$

$$\begin{aligned}
&= \frac{G_F}{\sqrt{2}} \left[V_{cb} V_{cs}^* a_1 + \sum_{q=u,c} V_{qb} V_{qs}^* \left(a_4^{\oplus} + 2a_6^{\oplus} \frac{m_{D_s}^2}{(m_b - m_c)(m_c + m_s)} \right) \right] \\
&\times \langle D^+ | (\bar{c}b)_L | \bar{B}^0 \rangle \langle D_s^- | (\bar{s}c)_L | 0 \rangle,
\end{aligned} \tag{7.20}$$

$$\begin{aligned}
&\mathcal{A}_f(\bar{B}^0 \rightarrow D^+ D_s^{*-}) \\
&= \frac{G_F}{\sqrt{2}} \left[V_{cb} V_{cs}^* a_1 + \sum_{q=u,c} V_{qb} V_{qs}^* \left(a_4^{\oplus} + 2a_6^{\oplus} \frac{m_{D_s^*}^2}{(m_b - m_c)(m_c - m_s)} \right) \right] \\
&\times \langle D^+ | (\bar{c}b)_L | \bar{B}^0 \rangle \langle D_s^{*-} | (\bar{s}c)_L | 0 \rangle,
\end{aligned} \tag{7.21}$$

$$\begin{aligned}
&\mathcal{A}_f(\bar{B}^0 \rightarrow D^{*+} D_s^-) \\
&= \frac{G_F}{\sqrt{2}} \left[V_{cb} V_{cs}^* a_1 + \sum_{q=u,c} V_{qb} V_{qs}^* \left(a_4^{\oplus} - 2a_6^{\oplus} \frac{m_{D_s}^2}{(m_b + m_c)(m_c + m_s)} \right) \right] \\
&\times \langle D^{*+} | (\bar{c}b)_L | \bar{B}^0 \rangle \langle D_s^- | (\bar{s}c)_L | 0 \rangle
\end{aligned} \tag{7.22}$$

and

$$\begin{aligned}
&\mathcal{A}_f(\bar{B}^0 \rightarrow D^{*+} D_s^{*-}) \\
&= \frac{G_F}{\sqrt{2}} \left[V_{cb} V_{cs}^* a_1 + \sum_{q=u,c} V_{qb} V_{qs}^* \left(a_4^{\oplus} + 2a_6^{\oplus} \frac{m_{D_s^*}^2}{(m_b - m_c)(m_c - m_s)} \right) \right] \\
&\times \langle D^{*+} | \bar{c} \gamma_\mu b | \bar{B}^0 \rangle \langle D_s^{*-} | (\bar{s}c)_L | 0 \rangle \\
&- \frac{G_F}{\sqrt{2}} \left[V_{cb} V_{cs}^* a_1 + \sum_{q=u,c} V_{qb} V_{qs}^* \left(a_4^{\oplus} - 2a_6^{\oplus} \frac{m_{D_s^*}^2}{(m_b + m_c)(m_c - m_s)} \right) \right] \\
&\times \langle D^{*+} | \bar{c} \gamma_\mu \gamma_5 b | \bar{B}^0 \rangle \langle D_s^{*-} | (\bar{s}c)_L | 0 \rangle,
\end{aligned} \tag{7.23}$$

where

$$\begin{aligned}
a_3^{\oplus} &= C_3^{\oplus} + \frac{1}{3} C_4^{\oplus}, & a_4^{\oplus} &= C_4^{\oplus} + \frac{1}{3} C_3^{\oplus}, \\
a_5^{\oplus} &= C_5^{\oplus} + \frac{1}{3} C_6^{\oplus}, & a_6^{\oplus} &= C_6^{\oplus} + \frac{1}{3} C_5^{\oplus}; & q &= u, c.
\end{aligned} \tag{7.24}$$

Note that the factorization approximation has been used to evaluate the penguin contributions.

If we do not include the penguins, the effect of working in NLL instead of LL is very small. Actually, $\Delta\mathcal{B}_f$ is less than 1 %, the same as that calculated in section 7.3.1 for the color-favored decays of type $b \rightarrow c\bar{u}d$. However, if the contributions from the

penguin diagrams are included we get relatively large effects. The branching ratios for the processes $B \rightarrow D^+ D_s^-$ and $B \rightarrow D^+ D_s^{*-}$ get reduced by 28 % and 38 %, respectively, while the branching ratios for $B \rightarrow D^* D_s$ and $B \rightarrow D^* D_s^*$ are increased by 8 % and 13 %, respectively (see Table 7.2).

To demonstrate the cause of these large changes, let us look at the decay $B \rightarrow D^+ D_s^-$. In a rough calculation, we substitute the following approximations in (7.20): $a_1 \sim 1$, $a_4^\oplus \sim -0.4$, $a_6^\oplus \sim -0.6$, $V_{ub}V_{us}^* \sim 0$ and $m_{D_s}^2/(m_b - m_c)(m_c + m_s) \sim 1$. The change in the amplitude due to penguins is, then, about $1 - (1 - 0.4 - 2 \times 0.6) = -16$ % and the change in the branching ratio is $1 - (1 - 0.4 - 2 \times 0.6)^2 \sim -29$ %.

The decay amplitude for class II processes (like $B \rightarrow K J/\psi$, $K \psi(2S) \dots etc.$) is simpler to derive than that for class I processes. For example, the factorized decay amplitude for the process $\bar{B}^0 \rightarrow \bar{K}^0 J/\psi$ is given by

$$\begin{aligned} \mathcal{A}_f(\bar{B}^0 \rightarrow \bar{K}^0 J/\psi) &= \frac{G_F}{\sqrt{2}} \left[V_{cb}V_{cs}^* a_2 + \sum_{q=u,c} V_{qb}V_{qs}^* (a_3^\oplus + a_5^\oplus) \right] \\ &\times \langle \bar{K}^0 | (\bar{s}b)_L | \bar{B}^0 \rangle \langle J/\psi | (\bar{c}c)_L | 0 \rangle. \end{aligned} \quad (7.25)$$

Other processes of this class, considered in the previous chapter, have similar decay amplitudes.

When the Wilson coefficients generated by the penguin diagrams are set to zero, the change in the branching ratio ($\Delta\mathcal{B}_f$) as a result of working in NLL is the same as that calculated for class II decays of type $b \rightarrow c\bar{u}d$ (about -38 %). The penguin effects, however, turns out to be very small (< 0.5 %). This is because the values for a_3 and a_5 are very close in magnitude and have opposite signs which results in a destructive interference between the two.

7.3.3 Type $b \rightarrow c\bar{c}d$ Decays

The effective Hamiltonian for this type of processes is similar to (7.1) except that the s flavor is replaced by the d flavor. The Wilson coefficients are calculated from (7.8),

using the following form for C_p

$$C_p = C_3(\mu) \left[\frac{4}{3} + \frac{2}{3} \ln \frac{m_d^2}{\mu^2} + \frac{2}{3} \ln \frac{m_b^2}{\mu^2} - \Delta F_1 \left(\frac{k^2}{m_d^2} \right) - \Delta F_1 \left(\frac{k^2}{m_b^2} \right) \right] \\ + (C_4(\mu) + C_6(\mu)) \sum_{i=u,d,s,c,b} \left[\frac{2}{3} \ln \frac{m_i^2}{\mu^2} - \Delta F_1 \left(\frac{k^2}{m_i^2} \right) \right]. \quad (7.26)$$

However, the numerical values for $C_{i=1,\dots,6}^{\text{eff}}$ turn out to be the same as those in Table 7.1 without noticeable changes.

In this section we are interested in class II processes of this type (for example, $B^- \rightarrow \pi^- J/\psi$, $\rho^- J/\psi \dots etc.$). The amplitudes for these decays, have the same form as the amplitudes for class II processes of type $b \rightarrow c\bar{c}s$ (see (7.25)). As a result, the effect of penguin diagrams on the branching ratios is also very small for the same reason mentioned above for class II processes of type $b \rightarrow c\bar{c}s$. The results are shown in Table 7.2.

7.4 Effect on the Estimates of the Nonfactorization Parameters

In the previous chapter, nonfactorization was introduced through the two parameters ε_1 and ε_8 defined in (6.15) and (6.16). These two parameters represent the size of the color-singlet and color-octet nonfactorizable parts in the decay amplitude. Assuming universality of ε_1 and ε_8 , their values were estimated from two sets of class I processes (Tables 6.1 and 6.2) and one set of class II processes (Tables 6.3).

In the light of new features (Wilson coefficients in NLL and penguin effects), we re-estimate the values of the nonfactorization parameters ε_1 and ε_8 using a χ^2 fit to the experimental branching ratios of the same set of processes mentioned above. We use the Wilson coefficients calculated up to NLL and include, in the color-singlet part of the amplitude, the contributions from the penguin diagrams. Regarding the color-octet part, we only include the contributions from the operators Q_1 and Q_2 .

Table 7.2: $\Delta\mathcal{B}_f$ represents the difference, assuming factorization, between the branching ratios calculated using the Wilson coefficients in LL (without penguin contribution), and the branching ratios calculated using the Wilson coefficients in NLL and NLL + Penguins. $\Delta\mathcal{B}_{nf}$ is the difference between the branching ratios calculated using the Wilson coefficients in LL (including nonfactorization as in the previous chapter), and the branching ratios calculated using the Wilson coefficients in NLL (including penguins and nonfactorization as in this chapter). Explicitly, entries in column 4 represent $\Delta\mathcal{B}_f = (\mathcal{B}_{LL} - \mathcal{B}_{NLL})_{fac}$, those in column 5 represent $\Delta\mathcal{B}_f = (\mathcal{B}_{LL} - \mathcal{B}_{NLL+Penguin})_{fac}$ and those in column 6 represent $\Delta\mathcal{B}_{nf} = (\mathcal{B}_{LL+nonfac} - \mathcal{B}_{NLL+Penguin+nonfac})$.

Type	Class	Processes	$\Delta\mathcal{B}_f$ due to		$\Delta\mathcal{B}_{nf}$
			NLL	NLL & Penguin	
$b \rightarrow c\bar{u}d$	I	$\bar{B}^0 \rightarrow D^+\pi^- \dots etc.$	1 %		3 %
$b \rightarrow c\bar{u}d$	II	$\bar{B}^0 \rightarrow D^0\pi^0 \dots etc.$	- 38 %	penguins	-10 %
$b \rightarrow c\bar{u}d$	III	$B^- \rightarrow D^0\pi^-$	-3 %	do not	2 %
		$B^- \rightarrow D^0\rho^-$	-1 %	contribute	2 %
		$B^- \rightarrow D^0a_1^-$	-1 %	to processes	3 %
		$B^- \rightarrow D^{*0}\rho^-$	-3 %	of type	2 %
		$B^- \rightarrow D^{*0}\rho^-$	-3 %	$b \rightarrow c\bar{u}d$	2 %
		$B^- \rightarrow D^{*0}a_1^-$	-1 %		2 %
$b \rightarrow c\bar{c}s$	I	$B \rightarrow DD_s$	1 %	-28 %	-27 %
		$B \rightarrow DD_s^*$	1 %	-38 %	-37 %
		$B \rightarrow D^*D_s$	1 %	8 %	12 %
		$B \rightarrow D^*D_s^*$	1 %	13 %	16 %
$b \rightarrow c\bar{c}s$	II	$B \rightarrow KJ/\psi \dots etc.$	- 37.9 %	- 37.6 %	-6%
$b \rightarrow c\bar{c}d$	II	$B^- \rightarrow \pi^- J/\psi \dots etc.$	- 37.9 %	- 37.6 %	-6%

For example, the decay amplitude for the process $\bar{B}^0 \rightarrow \bar{K}^0 J/\psi$, after including the nonfactorization parameters, is given by

$$\begin{aligned} \mathcal{A}(\bar{B}^0 \rightarrow \bar{K}^0 J/\psi) &= \frac{G_F}{\sqrt{2}} V_{cb} V_{cs}^* \left[\left(a_2 + \sum_{q=u,c} \frac{V_{qb} V_{qs}^*}{V_{cb} V_{cs}^*} (a_3^{\oplus} + a_5^{\oplus}) \right) (1 + \varepsilon_1) + C_1 \varepsilon_8 \right] \\ &\times \langle \bar{K}^0 | (\bar{s}b)_L | \bar{B}^0 \rangle \langle J/\psi | (\bar{c}c)_L | 0 \rangle. \end{aligned} \quad (7.27)$$

In Fig. 7.2 we show a contour plot of the value of χ^2 in ε_1 - ε_8 space. In this figure, we see four minima of χ^2 , labeled 1, 2, 3 and 4, which can be compared with the corresponding regions in Fig. 6.4. The value of χ^2 per degree of freedom for these minima is 2.9. By using the same arguments as in section 6.3, we exclude solutions 1, 2 and 4 and take solution 3 as the estimate of the nonfactorization parameters. The result is

$$\begin{aligned} \varepsilon_1 &= -0.053 \pm 0.030, \\ \varepsilon_8 &= 0.137 \pm 0.009. \end{aligned} \quad (7.28)$$

The uncertainties in ε_1 and ε_8 correspond to $\Delta\chi^2 = 1$.

So, we notice that the value of ε_8 , estimated from the above fit, is about 5 % higher than that estimated in the previous chapter. The value of $|\varepsilon_1|$, on the other hand, is reduced by about 24 % and gets closer to zero.

7.5 Nonfactorization Effects on Branching Ratios

Using the values in (7.28) for the nonfactorization parameters, in a scheme with NLL Wilson coefficients and penguins contributions, we can calculate the branching ratios for all the processes considered in the previous chapter. The resulting branching ratios, are then compared with those listed in column 3 of Tables 6.4-6.11 (which represent the branching ratios without the the penguin contributions, evaluated in LL and include nonfactorization as in (6.48)). The differences between the two, called $\Delta\mathcal{B}_{\text{nf}}$, are summarized in Table 7.2.

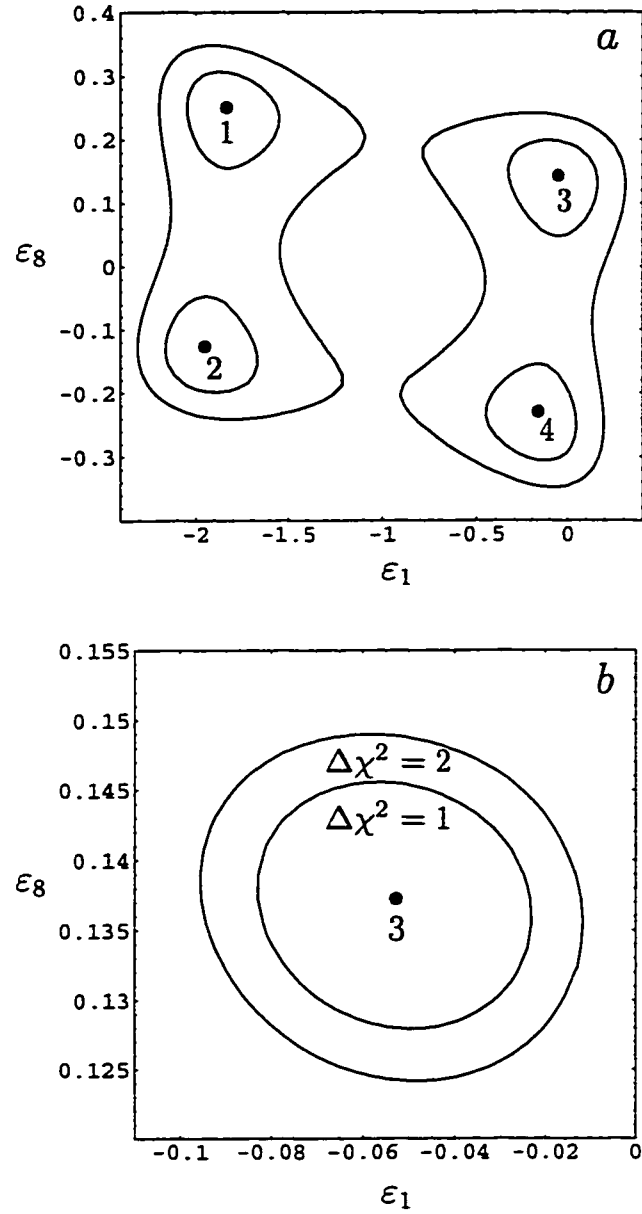


Figure 7.2: (a) A contour plot of the value of χ^2 in ϵ_1 - ϵ_8 space. The bullets represent minima of χ^2 ; (b) A magnification of the region containing minima 3 of χ^2 . The inner closed curve represent $\Delta\chi^2 = 1$ while the outer closed curve represent $\Delta\chi^2 = 2$.

Table 7.3: The predicted branching ratios, in the NLL scheme with penguin contribution, for class II processes of the type $b \rightarrow c\bar{c}d$. Branching ratios in column 2 are calculated taking $\varepsilon_1 = \varepsilon_8 = 0$ and those in column 3 with $\varepsilon_1 = -0.053 \pm 0.030$, $\varepsilon_8 = 0.137 \pm 0.009$. The last column represents the available experimental measurements.

Process	Branching Ratio $\times 10^{-5}$		
	Fac.	Nonfac.	Exp. [2]
$B^- \rightarrow \pi^- J/\psi$	0.22 ± 0.02	2.2 ± 0.3	5.0 ± 1.5
$B^- \rightarrow \rho^- J/\psi$	0.91 ± 0.07	9.3 ± 1.1	< 77
$B^- \rightarrow a_1^- J/\psi$	0.33 ± 0.03	3.3 ± 0.4	< 120
$B^- \rightarrow \pi^- \psi(2S)$	0.08 ± 0.01	0.8 ± 0.1	—
$B^- \rightarrow \rho^- \psi(2S)$	0.51 ± 0.05	5.2 ± 0.7	—
$B^- \rightarrow a_1^- \psi(2S)$	0.15 ± 0.02	1.5 ± 0.2	—

By assuming that the universality of ε_1 and ε_8 extends to include Cabibbo-suppressed processes, we evaluate the branching ratios (in the NLL scheme for Wilson coefficients with the inclusion of penguin processes) in the factorization approximation, and with the nonfactorization contribution included for six color-suppressed processes of type $b \rightarrow c\bar{c}d$. The results are shown in Table 7.3. This set of processes was not considered in the previous chapter.

The available experimental value for $\mathcal{B}(B^- \rightarrow \pi^- J/\psi)$ [2], shows that the inclusion of nonfactorization has improved significantly the predicted branching ratio.

7.6 Discussion and Conclusion

In chapter 6, it was demonstrated that the factorization approximation, in LL and with no penguins, gives reasonable predictions (as compared with experimental measurements) for the branching ratios of class I and class III processes. However, for class II processes the predicted branching ratios are very low. Also, it was demon-

strated that, including nonfactorization through the parameters ε_1 and ε_8 , improves considerably the predicted branching ratios for class II (also called color-suppressed) processes while preserving the reasonable predictions for the other two classes.

In this chapter, we saw that by working in NLL (with no penguins) the predicted branching ratios of class I and class III processes are very close to the LL predictions and to the experimental values (see Table 7.2). For class II processes, on the other hand, the predicted branching ratios are considerably lower (by about 38%) than the LL predictions making the fit with experimental values even worse than in the LL case. However, this problem is greatly remedied by including nonfactorization contribution.

From Table 7.2 we can see that, for class II processes of type $b \rightarrow c\bar{u}d$ the change ($\mathcal{B}_{LL} - \mathcal{B}_{NLL}$) in the predicted branching ratios, when nonfactorization is included, is considerably smaller than that when factorization is assumed. So, for color-suppressed processes, the inclusion of nonfactorization reduces the sensitivity of the predicted branching ratios on whether the Wilson coefficients are evaluated in LL or NLL. For class I and class III processes, the small values of ($\mathcal{B}_{LL} - \mathcal{B}_{NLL}$) in the factorization approximation is maintained after including nonfactorization contribution. So, the inclusion of nonfactorization contribution (but not the penguin processes) results in low sensitivity on whether LL or NLL Wilson coefficients are used, for all the three classes of decays.

Contributions from the penguin diagrams appear in processes of types $b \rightarrow c\bar{c}s$ and $b \rightarrow c\bar{c}d$. In both of these types, class II processes are affected only slightly by the penguin contributions. This is due to the destructive interference between the different terms, in the amplitude, generated by the penguins. On the other hand, for class I processes of type $b \rightarrow c\bar{c}s$ this cancellation does not happen and the decay amplitudes receive significant contribution from the penguin diagrams (see Table 7.2). Also, we note that nonfactorization does not have a large effect on the penguin contribution for this later class of processes.

Finally, it is interesting to note that the values of the nonfactorization parameters, ε_1 and ε_8 , estimated in chapter 6 in LL and without penguin contributions, are close to the values estimated in this chapter using NLL and penguin contributions.

Bibliography

- [1] A. J. Buras, M. Jamin, M. Lautenbacher and P. Weisz, Nucl. Phys. B **370**, 69 (1992).
- [2] R. M. Barnett et al., *Particle Data Group, Review of Particle Properties*, Phys. Rev. D **54**, 1 (1996) and 1997 off-year partial update for the 1998 edition.
- [3] R. Fleischer, Z. Phys. C **58**, 483 (1993); Z. Phys. C **62**, 81 (1994);
- [4] G. Kramer, W. F. Palmer and H. Simma, Nucl. Phys. B **428**, 77 (1994).
- [5] A. Ali and C. Greub, Phys. Rev. D **57**, 2996 (1998).
- [6] H. Cheng and B. Tseng, IP-ASTO-01-98; hep-ph/9803457.
- [7] A. N. Kamal and C. W. Luo, Phys. Lett. B **393** 151 (1997);
- [8] H. Fusaoka and Y. Koshio, Phys. Rev. D **57**, 3986 (1998).

Chapter 8

Conclusion

Since every chapter (other than the first three introductory chapters) has its own summary and discussion, this concluding chapter is not intended to be a repetition of what has already been said. Instead, it is an overall look at the collective results of the previous chapters.

Our aim at the beginning of this work, was to investigate the importance of the nonfactorizable parts of the decay amplitudes in two-body hadronic B -decays. The anticipation (which was borne to be correct) was that the effects of nonfactorization would be most important in color-suppressed processes. This is because, in this kind of processes, the part of the amplitude generated by the color-octet current has a large coefficient ($C_1/a_2 \sim 10$) as compared to the factorizable part. So, color-suppressed processes (also called class II processes) were given considerable amount of attention in this work.

In chapters 4 and 5, we concentrated our study on the color-suppressed decays $B \rightarrow K^* J/\psi$ and $B_s \rightarrow \phi J/\psi$. In both chapters, nonfactorization was introduced such that it contributed differently to the three Lorentz-scalar structures in the decay amplitudes. Explicitly, three factors $\xi_{A_1} = (1 + C_1/a_2 \chi_{A1})$, $\xi_{A_2} = (1 + C_1/a_2 \chi_{A2})$ and $\xi_V = (1 + C_1/a_2 \chi_V)$ were included in the factorized amplitudes as coefficients to the form factors A_1 , A_2 and V , respectively. In the factorization assumption, these

three factors are equal to unity.

The study of chapter 4 made use of the available world averages of decay rates and longitudinal polarization. i.e., two data points were available while the theory had three parameters ξ_{A_1} , ξ_{A_2} and ξ_V . In contrast, in chapter 5, we used the first extraction of the full set of decay amplitudes for the process $B \rightarrow K^* J/\psi$ made by the CLEO II collaboration which measured, in addition to the decay and longitudinal polarization, the transverse polarization. In both studies, it was found that the amount of nonfactorization needed to explain the experimental data is model dependent. However, it was interesting to observe that BSW I model, in factorization approximation, could predict the available measurements of the longitudinal and transverse polarizations but underestimated the branching ratios (see section 5.4). This implied that the problem was that of an overall scale factor, i.e. the three parameters ξ_{A_1} , ξ_{A_2} and ξ_V were approximately equal. Hence, these three parameters were replaced by one (ξ) which acts as a multiplicative factor for the factorized decay amplitude. The other interesting observation is that in BSW I model this factor seems to be process independent, at least for the three processes $B \rightarrow K^* J/\psi$, $B_s \rightarrow \phi J/\psi$ and $B \rightarrow K^* \psi(2S)$ (see Table 5.7).

The above observations encouraged us to do the following: First, we separated the nonfactorization contributions due to the color-singlet (ε_1) and the color-octet (ε_8) currents. Second, by assuming that nonfactorization contributes equally to the three Lorentz-scalar structures in $B \rightarrow VV$ decays, the values of ε_1 and ε_8 were estimated using available experimental measurements of branching ratios for two sets of color-favored processes and one set of color-suppressed processes in BSW I model. Finally, the estimated values of ε_1 and ε_8 were used to calculate the branching ratios for a large number of Cabibbo-favored B -decays. The results obtained showed good support to the above assumptions (see chapter 6).

In the three studies that preceded chapter 7, we used Wilson coefficients evaluated in LL and ignored penguin diagram contributions. In chapter 7, however, we

investigated the effects of (i) using the NLL values for the Wilson coefficients and (ii) including the penguin contributions to the color-singlet part of the decay amplitude. The new estimates of ε_1 and ε_8 turned out to be very close to the estimates of chapter 6. For the case of color-suppressed processes, it was found that the penguins had only a small effect ($< 10\%$) on the predicted branching ratios. Also, when nonfactorization was included, the predicted branching ratios of most processes considered had small dependence on the set of values (i.e. LL or NLL values) used for the Wilson coefficients. The exception was the set of color-favored processes $B \rightarrow D^{(*)}D_s^{(*)}$ which receives considerable penguin contributions. However, the predicted branching ratios are still reasonably close to the available experimental measurements.

Appendix A

Polarization Vectors

A.1 Free Massive Vector Field

Assume that we have a vector field $A^\mu(x)$ with a Lagrangian density given by

$$\mathcal{L}(x) = -\frac{1}{4}F_{\mu\nu}F^{\mu\nu} + \frac{1}{2}m^2 A_\mu A^\mu, \quad (\text{A.1})$$

where

$$F^{\mu\nu} = (\partial^\mu A^\nu - \partial^\nu A^\mu). \quad (\text{A.2})$$

Using the least action principle, we find that this field satisfies the following equation of motion:

$$\partial_\nu F^{\nu\mu} + m^2 A^\mu = 0. \quad (\text{A.3})$$

Since $F^{\mu\nu}$ is antisymmetric under the exchange of μ and ν , then

$$\partial_\mu \partial_\nu F^{\mu\nu} = 0. \quad (\text{A.4})$$

So, taking the four divergence of (A.3) leads to

$$m^2 \partial_\mu A^\mu = 0. \quad (\text{A.5})$$

Since ($m \neq 0$), then the vector field must satisfy the Lorentz condition ¹

$$\partial_\mu A^\mu = 0. \quad (\text{A.6})$$

The equation of motion (A.3) can be written as

$$\partial_\nu \partial^\nu A^\mu - \partial^\mu \partial_\nu A^\nu + m^2 A^\mu = 0. \quad (\text{A.7})$$

Since all solutions of the above equation satisfy the Lorentz condition (A.6), then the equations of motion for the massive vector field can be written as

$$(\partial_\nu \partial^\nu + m^2) A^\mu = 0. \quad (\text{A.8})$$

$$\partial_\mu A^\mu = 0. \quad (\text{A.9})$$

A.2 Solutions of Equations of Motion

Our aim here is to find all vector fields that satisfy (A.8) and (A.9) simultaneously. From (A.8), we see that every component of A^μ satisfies the Klein-Gordon equation. So, knowing that A^μ is a 4-vector we can write the following general solution satisfying (A.8)

$$A^\mu = N \epsilon^\mu e^{\pm i k \cdot x}, \quad (\text{A.10})$$

where

$$k^\mu = (k^0, \mathbf{k}). \quad (\text{A.11})$$

ϵ^μ is called the polarization vector and N is a normalization constant.

The next step is to choose those A^μ that satisfy the Lorentz condition. By substituting (A.10) into (A.9) we get

$$k \cdot \epsilon = 0, \quad (\text{A.12})$$

which reduces the degrees of freedom of ϵ^μ from four to three.

¹F. Gross, *Relativistic Quantum Mechanics and Field Theory*, (John Wiley & Sons, New York, 1993).

A.3 Polarization Vectors

If the coordinate system is chosen such that \mathbf{k} is along the z-axis, then we have

$$k^\mu = (k^0, 0, 0, |\mathbf{k}|). \quad (\text{A.13})$$

By substitution in (A.12) we find that ϵ^μ has the following general form

$$\epsilon^\mu = (\epsilon^0, \epsilon^1, \epsilon^2, \frac{k^0}{|\mathbf{k}|} \epsilon^0). \quad (\text{A.14})$$

Since ϵ^μ has three degrees of freedom, then the set of all polarization vectors can be spanned by three basis vectors. For example, the following three independent polarization vectors

$$\epsilon^\mu(0) = \frac{1}{m} (|\mathbf{k}|, 0, 0, k^0), \quad (\text{A.15})$$

$$\epsilon^\mu(1) = (0, 1, 0, 0), \quad (\text{A.16})$$

$$\epsilon^\mu(2) = (0, 0, 1, 0), \quad (\text{A.17})$$

can be chosen as a basis.

A.3.1 Helicity Eigenstates

For a vector particle, the wave function transforms as a 4-vector under the Lorentz group. In particular, rotations about the z-axis form a subgroup whose elements are represented by

$$\mathcal{R}(\theta) = \begin{pmatrix} 1 & 0 & 0 & 0 \\ 0 & \cos \theta & -\sin \theta & 0 \\ 0 & \sin \theta & \cos \theta & 0 \\ 0 & 0 & 0 & 1 \end{pmatrix}. \quad (\text{A.18})$$

The generator of this group is the third component of the spin operator. S_z . It is given by

$$S_z = i \left(\frac{d\mathcal{R}(\theta)}{d\theta} \right)_{\theta=0} = \begin{pmatrix} 0 & 0 & 0 & 0 \\ 0 & 0 & -i & 0 \\ 0 & i & 0 & 0 \\ 0 & 0 & 0 & 0 \end{pmatrix}. \quad (\text{A.19})$$

Helicity, measures the spin of the particle along its direction of motion ². So, for a vector particle moving in the positive direction of the z-axis the helicity operator is the third component of the spin operator,

$$\frac{\mathbf{k} \cdot \mathbf{S}}{|\mathbf{k}|} = S_z. \quad (\text{A.20})$$

So, the helicity eigenvalues (λ) and eigenvectors ($\epsilon(\lambda)$) are defined such that

$$S_z \epsilon(\lambda) = \lambda \epsilon(\lambda). \quad (\text{A.21})$$

From (A.19) we see that S_z has three distinct eigenvalues. These are shown below with the corresponding eigenvectors:

$$\begin{aligned} \lambda = 0 & \quad \epsilon(0) = (a, 0, 0, b), \\ \lambda = +1 & \quad \epsilon(+) = (0, c, ic, 0), \\ \lambda = -1 & \quad \epsilon(-) = (0, d, -id, 0), \end{aligned}$$

where a , b , c and d are arbitrary constants. However, the Lorentz condition (A.12) restricts $\epsilon(0)$ to have the form

$$\epsilon(0) = (a, 0, 0, \frac{k^0}{|\mathbf{k}|} a). \quad (\text{A.22})$$

By choosing appropriate normalization we end up with the following three independent polarization vectors representing the three possible helicity states:

$$\epsilon(0) = \frac{1}{m}(|\mathbf{k}|, 0, 0, k^0),$$

²B. De Wit and J. Smith, *Field Theory in Particle Physics*, (North Elsevier Science Publishers B. V., Amsterdam 1986).

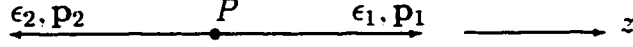


Figure A.1: $P \rightarrow V_1 V_2$ in the center-of-mass frame

$$\begin{aligned}\epsilon(+)&= \frac{-1}{\sqrt{2}}(0, 1, i, 0), \\ \epsilon(-)&= \frac{1}{\sqrt{2}}(0, 1, -i, 0).\end{aligned}\tag{A.23}$$

A.4 $P \rightarrow VV$ Decays

For the process $P \rightarrow V_1 V_2$ we define ϵ_1^μ and ϵ_2^μ to be the polarization vectors of the V_1 and V_2 particles respectively. If we work in the center-of-mass frame (P rest frame), and take the three momentum of the first vector meson (\mathbf{p}_1) to be in the positive direction of the z -axis, then, we have

$$\begin{aligned}p_1^\mu &= (E_1, 0, 0, |\mathbf{p}_1|), \\ p_2^\mu &= (E_2, 0, 0, -|\mathbf{p}_2|), \\ p_P^\mu &= (m_P, 0, 0, 0).\end{aligned}\tag{A.24}$$

From conservation of momentum, we have

$$E_1 + E_2 = m_P,\tag{A.25}$$

and

$$|\mathbf{p}_1| = |\mathbf{p}_2| = |\mathbf{p}|.\tag{A.26}$$

From the Lorentz condition (A.9), the polarization vectors for the two vector mesons satisfy the following relations:

$$p_1 \cdot \epsilon_1 = 0,\tag{A.27}$$

$$p_2 \cdot \epsilon_2 = 0.\tag{A.28}$$

Since \mathbf{p}_1 is pointing in the positive direction of the z-axis, we can write the three polarization vectors for V_1 directly from (A.23) as:

$$\begin{aligned}\epsilon_1(0) &= \frac{1}{m_1}(|\mathbf{p}_1|, 0, 0, E_1). \\ \epsilon_1(\pm) &= \frac{\mp 1}{\sqrt{2}}(0, 1, \pm i, 0).\end{aligned}\tag{A.29}$$

\mathbf{p}_2 , however, is pointing in the negative direction of the z-axis. So, we have from (A.24) and (A.28)

$$p_2 \cdot \epsilon_2 = E_2 \epsilon_2^0 + |\mathbf{p}| \epsilon_2^3 = 0,\tag{A.30}$$

which leads to

$$\epsilon_2^3 = -\frac{E_2}{|\mathbf{p}|} \epsilon_2^0.\tag{A.31}$$

So, the longitudinal polarization vector takes the form

$$\epsilon_2(0) = \frac{1}{m_2}(-|\mathbf{p}|, 0, 0, E_2).\tag{A.32}$$

Also, the eigenstates of S_z with eigenvalues ± 1 will be the eigenstates of helicity with eigenvalues ∓ 1 respectively. So, the two transverse polarization vectors become

$$\epsilon_2(\pm) = \frac{\mp 1}{\sqrt{2}}(0, -1, \pm i, 0).\tag{A.33}$$

A.4.1 Useful Calculations

By contracting the polarization vectors defined above we get the following results:

$$(\epsilon_1(0) \cdot \epsilon_2(0)) = -\frac{m_P^2 - m_1^2 - m_2^2}{2m_1 m_2},\tag{A.34}$$

$$(\epsilon_1(\pm) \cdot \epsilon_2(\pm)) = 1.\tag{A.35}$$

Also the following combinations are useful:

$$(\epsilon_1(0) \cdot p_2)(\epsilon_2(0) \cdot p_1) = -\frac{m_P^2}{m_1 m_2} |\mathbf{p}|^2,\tag{A.36}$$

$$(\epsilon_1(\pm) \cdot p_2)(\epsilon_2(\pm) \cdot p_1) = 0,\tag{A.37}$$

$$\epsilon_{\mu\nu\rho\sigma} \epsilon_1^\mu(0) \epsilon_2^\nu(0) p_1^\rho p_2^\sigma = 0,\tag{A.38}$$

$$\epsilon_{\mu\nu\rho\sigma} \epsilon_1^\mu(\pm) \epsilon_2^\nu(\pm) p_1^\rho p_2^\sigma = \pm i m_P |\mathbf{p}|,\tag{A.39}$$

where, from (A.25) and (A.26) we can derive

$$|\mathbf{p}| = \left[\frac{(m_P^2 - m_1^2 - m_2^2)^2 - 4m_1^2 m_2^2}{4m_P^2} \right]^{\frac{1}{2}}. \quad (\text{A.40})$$

Appendix B

Fierz Transformation

B.1 The Complete Set of 4×4 Matrices

Consider the following set of 4×4 matrices (to be named Γ^A ; $A = 1, \dots, 16$) ¹

$$\begin{aligned}\Gamma^A = & 1, \\ & \gamma_0, i\gamma_1, i\gamma_2, i\gamma_3, \\ & i\gamma_2\gamma_3, i\gamma_3\gamma_1, i\gamma_1\gamma_2, \gamma_1\gamma_0, \gamma_2\gamma_0, \gamma_3\gamma_0, \\ & \gamma_1\gamma_2\gamma_3, i\gamma_1\gamma_2\gamma_0, i\gamma_3\gamma_1\gamma_0, i\gamma_2\gamma_3\gamma_0, \\ & i\gamma_1\gamma_2\gamma_3\gamma_0 .\end{aligned}\tag{B.1}$$

Note that $\Gamma^{16} = \gamma^5$.

¹References used are

- A. N. Kamal, lecture notes (unpublished), University of Alberta (1995).
- W. Greiner, *Relativistic Quantum Mechanics*, (Springer-Verlag, Berlin, 1990).
- Marshak, Riazuddin and C. P. Ryan, *Theory of Weak Interactions in Particle Physics*, (Wiley-Interscience, New York, 1969).

B.1.1 Properties

For these matrices, several properties can deduced.

- All Γ^A above satisfy

$$\left(\Gamma^A\right)^2 = 1. \quad (\text{B.2})$$

- For each Γ^A (except Γ^1) there exists a Γ^B such that

$$\Gamma^B \Gamma^A \Gamma^B = -\Gamma^A. \quad (\text{B.3})$$

As can be verified easily by explicit calculations, the values of A and the corresponding values of B that satisfy the above equation are

A	2	3	4	5	6	7	8	9	10	11	12	13	14	15	16
B	9	4	3	3	4	5	3	2	2	2	2	6	6	7	2

(B.4)

- Each Γ^A (except Γ^1) is traceless. This can be proved easily using the above two properties as follows:

$$\begin{aligned} \text{tr}(\Gamma^A) &= -\text{tr}(\Gamma^B \Gamma^A \Gamma^B) \\ &= -\text{tr}(\Gamma^B \Gamma^B \Gamma^A) \\ &= -\text{tr}(\Gamma^A). \end{aligned}$$

So, we have

$$\text{tr}(\Gamma^A) = 0 \quad ; A = 2, \dots, 16 \quad (\text{B.5})$$

- It can be proved by explicit calculations that

$$\Gamma^A \Gamma^B = \begin{cases} 1 & ; A = B \\ \propto \Gamma^C \ (C \neq 1) & ; A \neq B \end{cases} \quad (\text{B.6})$$

So, from (B.5) and (B.6) we have

$$\text{tr}(\Gamma^A \Gamma^B) = \begin{cases} 4 & ; A = B \\ 0 & ; A \neq B \end{cases} \quad (\text{B.7})$$

- The Γ^A matrices are linearly independent.

Proof:

Let us assume the existence of the following linear combination of γ^A 's:

$$\sum_{A=1}^{16} a_A \Gamma^A = 0, \quad (\text{B.8})$$

which can be rewritten as

$$a_B \Gamma^B + \sum_{A \neq B} a_A \Gamma^A = 0. \quad (\text{B.9})$$

If we multiplying the above equation by Γ^B we get

$$a_B + \sum_{A \neq B} a_A \Gamma^A \Gamma^B = 0. \quad (\text{B.10})$$

By taking the trace and using (B.7) we conclude that

$$a_B = 0 \quad : B = 1, \dots, 16. \quad (\text{B.11})$$

- Each 4×4 matrix can be expanded in terms of the Γ^A 's. This is evident since the Γ^A 's are 16 linearly-independent 4×4 matrices.

So, if X is 4×4 matrix, then it can be written as

$$X = \sum_{A=1}^{16} a_A \Gamma^A. \quad (\text{B.12})$$

Multiplying both sides by Γ^A and then taking the trace we get

$$a_A = \frac{1}{4} \text{tr} (\Gamma^A X). \quad (\text{B.13})$$

By substituting (B.13) into (B.12) we get

$$X = \frac{1}{4} \sum_{A=1}^{16} \text{tr} (\Gamma^A X) \Gamma^A. \quad (\text{B.14})$$

So, the elements of X satisfy

$$X_{\alpha\beta} = \frac{1}{4} \sum_{A=1}^{16} \sum_{\gamma,\delta=1}^4 X_{\gamma\delta} (\Gamma^A)_{\delta\gamma} (\Gamma^A)_{\alpha\beta}. \quad (\text{B.15})$$

For the special case

$$X_{\alpha\beta} = \delta_{\alpha\sigma}\delta_{\rho\beta} \quad (\text{B.16})$$

we have

$$\begin{aligned} \delta_{\alpha\sigma}\delta_{\rho\beta} &= \frac{1}{4} \sum_{A=1}^{16} \sum_{\gamma,\delta=1}^4 \delta_{\gamma\sigma}\delta_{\rho\delta} (\Gamma^A)_{\delta\gamma} (\Gamma^A)_{\alpha\beta} \\ &= \frac{1}{4} \sum_{A=1}^{16} (\Gamma^A)_{\alpha\beta} (\Gamma^A)_{\rho\sigma}. \end{aligned} \quad (\text{B.17})$$

If F and G are two 4×4 matrices, then we can write

$$\begin{aligned} F_{\alpha\sigma}G_{\rho\beta} &= \sum_{\gamma,\delta=1}^4 \delta_{\gamma\sigma}\delta_{\rho\delta} F_{\alpha\gamma}G_{\delta\beta} \\ &= \frac{1}{4} \sum_{A=1}^{16} \sum_{\gamma,\delta=1}^4 (\Gamma^A)_{\gamma\delta} (\Gamma^A)_{\rho\sigma} F_{\alpha\gamma}G_{\delta\beta} \\ &= \frac{1}{4} \sum_{A=1}^{16} (F \Gamma^A G)_{\alpha\beta} (\Gamma^A)_{\rho\sigma}, \end{aligned} \quad (\text{B.18})$$

where the relation (B.17) has been used in the above calculations.

B.1.2 Useful Relations

It can be proven by direct calculations that

$$\gamma^\mu \Gamma^A \gamma_\mu = C_A \Gamma^A, \quad (\text{B.19})$$

$$\gamma^5 \Gamma^A \gamma^5 = C'_A \Gamma^A, \quad (\text{B.20})$$

where

$$C_A = \begin{cases} 4 & ; A = 1 \\ -2 & ; A = 2, 3, 4, 5 \\ 0 & ; A = 6, 7, 8, 9, 10, 11 \\ 2 & ; A = 12, 13, 14, 15 \\ -4 & ; A = 16, \end{cases} \quad (\text{B.21})$$

and

$$C'_A = \begin{cases} 1 & ; A = 1; 6, 7, 8, 9, 10, 11; 16 \\ -1 & ; A = 2, 3, 4, 5; 12, 13, 14, 15. \end{cases} \quad (\text{B.22})$$

From above we can easily derive the following relations:

$$\sigma^{\mu\nu} \Gamma^A \sigma_{\mu\nu} = (C_A^2 - 4) \Gamma^A. \quad (\text{B.23})$$

$$\gamma^\mu \gamma^5 \Gamma^A \gamma_\mu \gamma^5 = -C_A C'_A \Gamma^A. \quad (\text{B.24})$$

$$\gamma^\mu (1 - \gamma^5) \Gamma^A \gamma_\mu (1 - \gamma^5) = C_A (1 - C'_A) (1 + \gamma^5) \Gamma^A. \quad (\text{B.25})$$

$$\gamma^\mu (1 - \gamma^5) \Gamma^A \gamma_\mu (1 + \gamma^5) = C_A (1 + C'_A) (1 + \gamma^5) \Gamma^A. \quad (\text{B.26})$$

B.2 Fierz Transformation

If F and G are 4×4 matrices, and $\psi^{1,2,3,4}$ are 4 Dirac spinors then, relation (B.18) can be used to rearrange the spinors as follows:

$$\begin{aligned} (\bar{\psi}^1 F \psi^2) (\bar{\psi}^3 G \psi^4) &= \bar{\psi}_\alpha^1 \psi_\sigma^2 \bar{\psi}_\rho^3 \psi_\beta^4 F_{\alpha\sigma} G_{\rho\beta} \\ &= -\bar{\psi}_\alpha^1 \psi_\beta^4 \bar{\psi}_\rho^3 \psi_\sigma^2 F_{\alpha\sigma} G_{\rho\beta} \\ &= -\frac{1}{4} \sum_{A=1}^{16} (\bar{\psi}^1 F \Gamma^A G \psi^4) (\bar{\psi}^3 \Gamma^A \psi^2). \end{aligned} \quad (\text{B.27})$$

As a special case we have

$$\begin{aligned} &(\bar{\psi}^1 \gamma^\mu (1 - \gamma^5) \psi^2) (\bar{\psi}^3 \gamma_\mu (1 - \gamma^5) \psi^4) \\ &= -\frac{1}{4} \sum_{A=1}^{16} (\bar{\psi}^1 \gamma^\mu (1 - \gamma^5) \Gamma^A \gamma_\mu (1 - \gamma^5) \psi^4) (\bar{\psi}^3 \Gamma^A \psi^2) \\ &= -\frac{1}{4} \sum_{A=1}^{16} C_A (1 - C'_A) (\bar{\psi}^1 (1 + \gamma^5) \Gamma^A \psi^4) (\bar{\psi}^3 \Gamma^A \psi^2) \\ &= \sum_{A=2}^5 (\bar{\psi}^1 (1 + \gamma^5) \Gamma^A \psi^4) (\bar{\psi}^3 \Gamma^A \psi^2) \\ &\quad - \sum_{A=12}^{15} (\bar{\psi}^1 (1 + \gamma^5) \Gamma^A \psi^4) (\bar{\psi}^3 \Gamma^A \psi^2) \\ &= (\bar{\psi}^1 \gamma^\mu (1 - \gamma^5) \psi^4) (\bar{\psi}^3 \gamma_\mu (1 - \gamma^5) \psi^2), \end{aligned} \quad (\text{B.28})$$

where we have made use of (B.25).

Similarly, we can show that

$$\left(\bar{\psi}^1 \gamma^\mu (1 - \gamma^5) \psi^2\right) \left(\bar{\psi}^3 \gamma_\mu (1 + \gamma^5) \psi^4\right) = -2 \left(\bar{\psi}^1 (1 + \gamma^5) \psi^4\right) \left(\bar{\psi}^3 (1 - \gamma^5) \psi^2\right). \quad (\text{B.29})$$

B.3 Fierz transformation and Color Algebra

The eight generators (λ^a) of the $SU(3)$ group satisfy the following relation

$$\sum_{a=1}^8 \lambda_{ij}^a \lambda_{kl}^a = -\frac{2}{3} \delta_{ij} \delta_{kl} + 2 \delta_{il} \delta_{kj}. \quad (\text{B.30})$$

Below we will make use of this relation in order to evaluate

$$\left(\bar{\psi}^1 \lambda^a \gamma^\mu (1 - \gamma^5) \psi^2\right) \left(\bar{\psi}^3 \lambda^a \gamma_\mu (1 \pm \gamma^5) \psi^4\right). \quad (\text{B.31})$$

where the summations over a and μ are understood.

We first start by writing

$$\begin{aligned} & \left(\bar{\psi}^1 \lambda^a \gamma^\mu (1 - \gamma^5) \psi^2\right) \left(\bar{\psi}^3 \lambda^a \gamma_\mu (1 \pm \gamma^5) \psi^4\right) \\ &= \left(\bar{\psi}_i^1 \gamma^\mu (1 - \gamma^5) \psi_j^2\right) \left(\bar{\psi}_k^3 \gamma_\mu (1 \pm \gamma^5) \psi_l^4\right) \lambda_{ij}^a \lambda_{kl}^a, \end{aligned} \quad (\text{B.32})$$

where the indices above represent color. By substituting from (B.30) into (B.32) we get

$$\begin{aligned} & \left(\bar{\psi}^1 \lambda^a \gamma^\mu (1 - \gamma^5) \psi^2\right) \left(\bar{\psi}^3 \lambda^a \gamma_\mu (1 \pm \gamma^5) \psi^4\right) \\ &= -\frac{2}{3} \left(\bar{\psi}_i^1 \gamma^\mu (1 - \gamma^5) \psi_i^2\right) \left(\bar{\psi}_k^3 \gamma_\mu (1 \pm \gamma^5) \psi_k^4\right) \\ &+ 2 \left(\bar{\psi}_i^1 \gamma^\mu (1 - \gamma^5) \psi_k^2\right) \left(\bar{\psi}_k^3 \gamma_\mu (1 \pm \gamma^5) \psi_i^4\right). \end{aligned} \quad (\text{B.33})$$

Using the Fierz transformations (B.28) and (B.29) we end up with the following results

$$\begin{aligned} & \left(\bar{\psi}^1 \lambda^a \gamma^\mu (1 - \gamma^5) \psi^2\right) \left(\bar{\psi}^3 \lambda^a \gamma_\mu (1 - \gamma^5) \psi^4\right) \\ &= -\frac{2}{3} \left(\bar{\psi}_i^1 \gamma^\mu (1 - \gamma^5) \psi_i^2\right) \left(\bar{\psi}_j^3 \gamma_\mu (1 - \gamma^5) \psi_j^4\right) \\ &+ 2 \left(\bar{\psi}_i^1 \gamma^\mu (1 - \gamma^5) \psi_i^4\right) \left(\bar{\psi}_j^3 \gamma_\mu (1 - \gamma^5) \psi_j^2\right), \end{aligned} \quad (\text{B.34})$$

and

$$\begin{aligned}
& \left(\bar{\psi}^1 \lambda^a \gamma^\mu (1 - \gamma^5) \psi^2 \right) \left(\bar{\psi}^3 \lambda^a \gamma_\mu (1 + \gamma^5) \psi^4 \right) \\
&= -\frac{2}{3} \left(\bar{\psi}_i^1 \gamma^\mu (1 - \gamma^5) \psi_i^2 \right) \left(\bar{\psi}_j^3 \gamma_\mu (1 + \gamma^5) \psi_j^4 \right) \\
&\quad - 4 \left(\bar{\psi}_i^1 (1 + \gamma^5) \psi_i^4 \right) \left(\bar{\psi}_j^3 (1 - \gamma^5) \psi_j^2 \right). \tag{B.35}
\end{aligned}$$

Appendix C

Two-Body Decay Rate

C.1 Normalization of Wave Functions

C.1.1 Klein-Gordon Field

The Lagrangian for a complex scalar field is given by

$$\mathcal{L}_{KG} = \partial_\mu \phi^* \partial^\mu \phi - m^2 \phi^* \phi. \quad (\text{C.1})$$

Using the least action principle, we can derive the equation of motion for the scalar field. This is called the Klein-Gordon Equation and it is given by

$$\partial^\mu \partial_\mu \phi + m^2 \phi = 0. \quad (\text{C.2})$$

The above Lagrangian is invariant under the phase transformation $\phi \rightarrow e^{-i\alpha} \phi$. Therefore, from Noethers Theorem, the following conserved current is associated with this symmetry:

$$J_{KG}^\mu = i [\phi^* (\partial^\mu \phi) - (\partial^\mu \phi^*) \phi]. \quad (\text{C.3})$$

Assume that we are interested in the solutions of the Klein-Gordon Equation inside a box of volume $V = L^3$ centered about the origin. Since the behavior of ϕ outside the box is not important, it can be taken to be a periodic continuation of ϕ inside the box. So, $\phi(t, x, y, z) = \phi(t, x + L, y, z)$, and so on.

As a result, the solutions of the Klein-Gordon Equation are

$$\phi_{\mathbf{n}}^{(\pm)} = N e^{\mp i k_{\mathbf{n}} \cdot x}, \quad (\text{C.4})$$

where

$$\begin{aligned} \mathbf{k}_{\mathbf{n}} &= \frac{2\pi}{L} \mathbf{n}, \\ \mathbf{n} &= (n_1, n_2, n_3); \quad n_i = 0, \pm 1, \pm 2, \dots \end{aligned} \quad (\text{C.5})$$

and

$$k_{\mathbf{n}}^0 = \sqrt{|\mathbf{k}_{\mathbf{n}}|^2 + m^2}. \quad (\text{C.6})$$

The normalization constant (N) is chosen such that the integral of the temporal component of the conserved current is unity. In other words, we are normalizing to one particle in the volume V . So, the normalized complete set of solutions of the Klein-Gordon Equation are

$$\phi_{\mathbf{n}}^{(\pm)} = \frac{1}{\sqrt{2k_{\mathbf{n}}^0 V}} e^{\mp i k_{\mathbf{n}} \cdot x}. \quad (\text{C.7})$$

C.1.2 Dirac Field

The Lagrangian for a free Dirac field is given by

$$\mathcal{L}_D = \bar{\psi}(x) (i\gamma^\mu \partial_\mu - m) \psi(x). \quad (\text{C.8})$$

Using the least action principle, we can derive the equation of motion for this field. This is called the Dirac Equation and it is given by

$$(i\gamma^\mu \partial_\mu - m) \psi(x) = 0. \quad (\text{C.9})$$

Similar to scalar field, the above Lagrangian is invariant under the global phase transformation $\psi \rightarrow e^{-i\alpha} \psi$. So, from Noethers Theorem, the following conserved current is associated with this symmetry:

$$J_D^\mu = \bar{\psi} \gamma^\mu \psi. \quad (\text{C.10})$$

Also here, we will find solutions inside a box of volume $V = L^3$ centered about the origin and normalize the wave functions to one particle in this volume. As a result, we see that the following solutions of the Dirac Equation for a complete set:

$$\frac{1}{\sqrt{2k_n^0 V}} u(\mathbf{k}_n, s) e^{-ik_n \cdot x}, \quad (\text{C.11})$$

$$\frac{1}{\sqrt{2k_n^0 V}} v(\mathbf{k}_n, s) e^{ik_n \cdot x}, \quad ; s = 1, 2 \quad (\text{C.12})$$

where k_n is defined in (C.5) and (C.6). $u(\mathbf{k}_n, s)$ and $v(\mathbf{k}_n, s)$, called the Dirac spinors, are given by

$$u(\mathbf{k}_n, s) = \sqrt{k_n^0 + m} \begin{pmatrix} \chi^s \\ \frac{\boldsymbol{\sigma} \cdot \mathbf{k}}{k_n^0 + m} \chi^s \end{pmatrix}, \quad (\text{C.13})$$

$$v(\mathbf{k}_n, s) = \sqrt{k_n^0 + m} \begin{pmatrix} \frac{\boldsymbol{\sigma} \cdot \mathbf{k}}{k_n^0 + m} \chi^s \\ \chi^s \end{pmatrix}. \quad (\text{C.14})$$

C.2 Decay Rate

If P is a pseudoscalar particle and P_1 and P_2 are two particles at particular spin states then, the decay amplitude for the process $P \rightarrow P_1 P_2$ takes the following form

$$\mathcal{A}(P \rightarrow P_1 P_2) = \int_{TV} d^4x \frac{e^{-ip \cdot x}}{(2p^0 V)^{1/2}} \frac{e^{ip_1 \cdot x}}{(2p_1^0 V)^{1/2}} \frac{e^{ip_2 \cdot x}}{(2p_2^0 V)^{1/2}} \mathcal{M}(P \rightarrow P_1 P_2), \quad (\text{C.15})$$

where p , p_1 and p_2 are the 4-momenta of P , P_1 and P_2 respectively. V is the volume of the space. T is the interaction time and \mathcal{M} is the Feynman amplitude.

From (C.15) we see that the transition probability to one definite final state is given by

$$|\mathcal{A}(P \rightarrow P_1 P_2)|^2 = |\delta_{TV}|^2 \frac{1}{(2p^0 V)} \frac{1}{(2p_1^0 V)} \frac{1}{(2p_2^0 V)} |\mathcal{M}(P \rightarrow P_1 P_2)|^2, \quad (\text{C.16})$$

where

$$\delta_{TV} = \int_{TV} d^4x e^{-i(p - p_1 - p_2) \cdot x}. \quad (\text{C.17})$$

Since the momenta of the initial and final state particles are discrete (see (C.5)), we can write

$$\delta_{TV} = \begin{cases} 0 & p \neq p_1 + p_2 \\ TV & p = p_1 + p_2 \end{cases}, \quad (\text{C.18})$$

which leads to

$$\begin{aligned} |\delta_{TV}|^2 &= \delta_{TV} \delta_{TV} \\ &= TV \delta_{TV}. \end{aligned} \quad (\text{C.19})$$

In the limit $T \rightarrow \infty$ and $V \rightarrow \infty$ we end up with a continuum of momenta. So, it is more convenient to introduce the transition probability to a group of final states with momenta in the intervals $\mathbf{p}_1 \pm d\mathbf{p}_1$ and $\mathbf{p}_2 \pm d\mathbf{p}_2$. To do this, we multiply (C.16) by the number of states in these intervals. So, the decay probability is written as

$$\begin{aligned} |\mathcal{A}(P \rightarrow P_1 P_2)|^2 &= \lim_{T,V \rightarrow \infty} TV \delta_{TV} \frac{1}{(2p^0 V)} \frac{1}{(2p_1^0 V)} \frac{1}{(2p_2^0 V)} \frac{V d^3 \mathbf{p}_1}{(2\pi)^3} \frac{V d^3 \mathbf{p}_2}{(2\pi)^3} \\ &\times |\mathcal{M}(P \rightarrow P_1 P_2)|^2. \end{aligned} \quad (\text{C.20})$$

However, from (C.17)

$$\lim_{T,V \rightarrow \infty} \delta_{TV} = (2\pi)^4 \delta^4(p - p_1 - p_2). \quad (\text{C.21})$$

So, the transition probability per unit time (or decay rate) is given by

$$d\Gamma = (2\pi)^4 \delta^4(p - p_1 - p_2) \frac{1}{2p^0} \frac{d^3 \mathbf{p}_1}{2p_1^0 (2\pi)^3} \frac{d^3 \mathbf{p}_2}{2p_2^0 (2\pi)^3} |\mathcal{M}(P \rightarrow P_1 P_2)|^2. \quad (\text{C.22})$$

In order to complete the calculation of the decay rate we need to integrate $d\Gamma$ over the final state momenta. To do this let us first rewrite (C.22) as

$$d\Gamma = \frac{1}{32\pi^2} \delta^3(\mathbf{p} - \mathbf{p}_1 - \mathbf{p}_2) \frac{\delta(p^0 - p_1^0 - p_2^0)}{p^0 p_1^0 p_2^0} d^3 \mathbf{p}_1 d^3 \mathbf{p}_2 |\mathcal{M}(P \rightarrow P_1 P_2)|^2. \quad (\text{C.23})$$

The energies of the particles involved are

$$\begin{aligned} p^0 &= (|\mathbf{p}|^2 + m^2)^{1/2} = m, \\ p_1^0 &= (|\mathbf{p}_1|^2 + m_1^2)^{1/2}, \\ p_2^0 &= (|\mathbf{p}_2|^2 + m_2^2)^{1/2}, \end{aligned} \quad (\text{C.24})$$

where $\mathbf{p} = 0$ since we are working in the centre-of-mass frame. So,

$$d\Gamma = \frac{1}{32\pi^2} \delta^3(\mathbf{p}_1 + \mathbf{p}_2) \frac{\delta(m - (|\mathbf{p}_1|^2 + m_1^2)^{1/2} - (|\mathbf{p}_2|^2 + m_2^2)^{1/2})}{m (|\mathbf{p}_1|^2 + m_1^2)^{1/2} (|\mathbf{p}_2|^2 + m_2^2)^{1/2}} d^3\mathbf{p}_1 d^3\mathbf{p}_2 \times |\mathcal{M}(P \rightarrow P_1 P_2)|^2. \quad (\text{C.25})$$

By performing the integration over \mathbf{p}_1 and \mathbf{p}_2 we get

$$\Gamma = \frac{1}{8\pi m} \int_0^\infty \frac{\delta(m - (|\mathbf{p}_1|^2 + m_1^2)^{1/2} - (|\mathbf{p}_1|^2 + m_2^2)^{1/2})}{(|\mathbf{p}_1|^2 + m_1^2)^{1/2} (|\mathbf{p}_1|^2 + m_2^2)^{1/2}} |\mathbf{p}_1|^2 d|\mathbf{p}_1| \times |\mathcal{M}(P \rightarrow P_1 P_2)|^2. \quad (\text{C.26})$$

To simplify this integral let us define

$$q = (|\mathbf{p}_1|^2 + m_1^2)^{1/2} + (|\mathbf{p}_1|^2 + m_2^2)^{1/2}, \quad (\text{C.27})$$

and substitute back into (C.26). The result is

$$\begin{aligned} \Gamma &= \frac{1}{8\pi m} \int_{m_1+m_2}^\infty \delta(m - q) \frac{[(q^2 - m_1^2 - m_2^2)^2 - 4m_1^2 m_2^2]^{1/2}}{2q^2} dq \\ &\quad \times |\mathcal{M}(P \rightarrow P_1 P_2)|^2, \\ &= \frac{1}{8\pi m^2} \frac{[(m^2 - m_1^2 - m_2^2)^2 - 4m_1^2 m_2^2]^{1/2}}{2m} |\mathcal{M}(P \rightarrow P_1 P_2)|^2 \\ &= \frac{|\mathbf{p}_1|}{8\pi m^2} |\mathcal{M}(P \rightarrow P_1 P_2)|^2, \end{aligned} \quad (\text{C.28})$$

where

$$|\mathbf{p}_1| = \frac{[(m^2 - m_1^2 - m_2^2)^2 - 4m_1^2 m_2^2]^{1/2}}{2m} = |\mathbf{p}_2| \quad (\text{C.29})$$

is the momentum of the decay products in the P rest-frame (see A.40).

Appendix D

η and η' Systems

In describing the physical states η and η' , we use the conventions ¹

$$\begin{aligned} |\eta\rangle &= |\eta_8\rangle \cos \theta_P - |\eta_1\rangle \sin \theta_P, \\ |\eta'\rangle &= |\eta_8\rangle \sin \theta_P + |\eta_1\rangle \cos \theta_P. \end{aligned} \quad (\text{D.1})$$

where the flavor-singlet and flavor-octet states are defined as

$$\begin{aligned} |\eta_1\rangle &= \frac{1}{\sqrt{3}} |u\bar{u} + d\bar{d} + s\bar{s}\rangle \\ |\eta_8\rangle &= \frac{1}{\sqrt{6}} |u\bar{u} + d\bar{d} - 2s\bar{s}\rangle. \end{aligned} \quad (\text{D.2})$$

θ_P is the mixing angle taken to be

$$\theta_P \approx -20^\circ. \quad (\text{D.3})$$

From (D.1) and (D.2) we get ²

$$|\eta\rangle = C_\eta^u |u\bar{u}\rangle + C_\eta^d |d\bar{d}\rangle + C_\eta^s |s\bar{s}\rangle, \quad (\text{D.4})$$

$$|\eta'\rangle = C_{\eta'}^u |u\bar{u}\rangle + C_{\eta'}^d |d\bar{d}\rangle + C_{\eta'}^s |s\bar{s}\rangle, \quad (\text{D.5})$$

¹R. M. Barnett *et al.* (Particle Data Group), Phys. Rev. D **54**, 1 (1996).

²A. N. Kamal, Q. P. Xu and A. Czarnecki, Phys. Rev. D **49**, 1330 (1994).

where

$$C_{\eta}^u = C_{\eta}^d = \frac{1}{\sqrt{3}} \left(\frac{1}{\sqrt{2}} \cos \theta_P - \sin \theta_P \right), \quad (\text{D.6})$$

$$C_{\eta}^s = -\sqrt{\frac{2}{3}} \left(\cos \theta_P + \frac{1}{\sqrt{2}} \sin \theta_P \right), \quad (\text{D.7})$$

$$C_{\eta'}^u = C_{\eta'}^d = \frac{1}{\sqrt{3}} \left(\cos \theta_P + \frac{1}{\sqrt{2}} \sin \theta_P \right), \quad (\text{D.8})$$

$$C_{\eta'}^s = \sqrt{\frac{2}{3}} \left(\frac{1}{\sqrt{2}} \cos \theta_P - \sin \theta_P \right). \quad (\text{D.9})$$

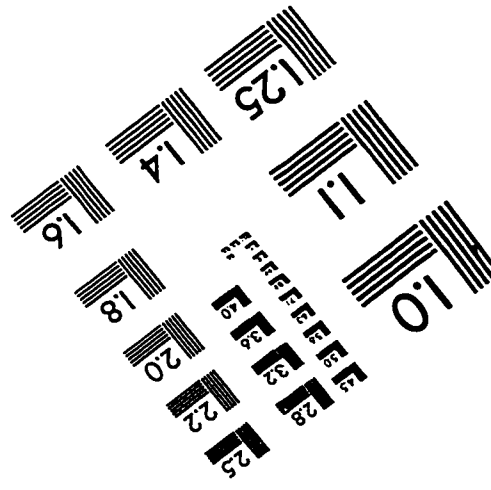
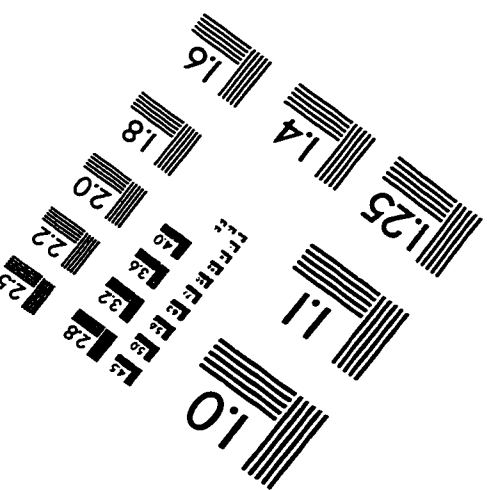
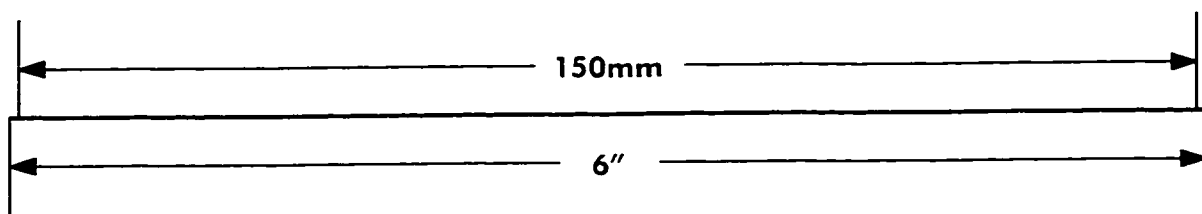
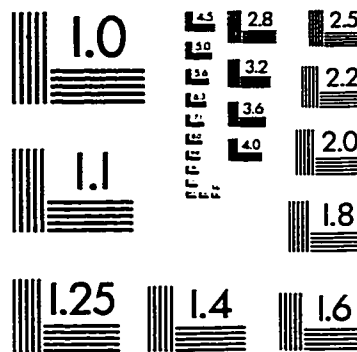
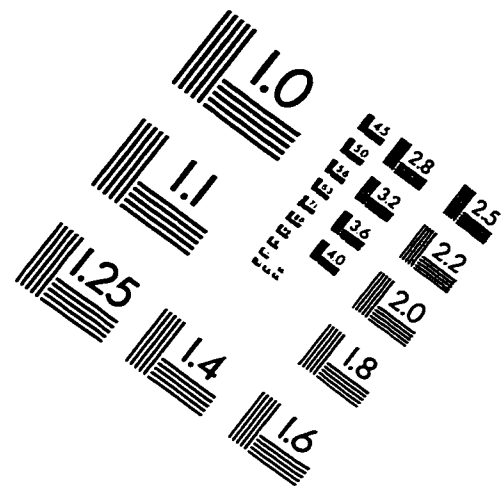
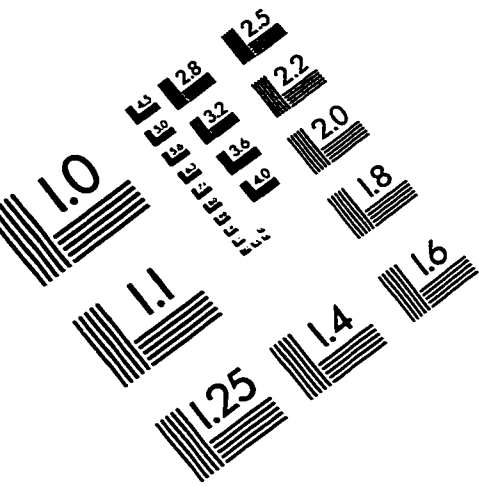
Appendix E

Particle Properties

Particle	Quark Composition	$I(J^P)$	Mass (MeV)	Mean Life 10^{-12} (sec)
π^+, π^-	$u\bar{d}, \bar{u}d$	$1(0^-)$	139.56995 ± 0.00035	
π^0	$(u\bar{u} - d\bar{d})/\sqrt{2}$	$1(0^-)$	134.9764 ± 0.0006	
η	See Appendix D	$0(0^-)$	547.30 ± 0.12	
ρ^+, ρ^-	$u\bar{d}, \bar{u}d$	$1(1^-)$	770.0 ± 0.8	
ρ^0	$(u\bar{u} - d\bar{d})/\sqrt{2}$	$1(1^-)$	770.0 ± 0.8	
ω^0	$(u\bar{u} + d\bar{d})/\sqrt{2}$	$1(1^-)$	781.94 ± 0.12	
η'	See Appendix D	$0(0^-)$	957.78 ± 0.14	
ϕ	$s\bar{s}$	$0(1^-)$	1019.413 ± 0.008	
a_1^+, a_1^-	$u\bar{d}$	$1(1^+)$	1230 ± 40	
K^{*-}, K^{*-}	$u\bar{s}, \bar{u}s$	$\frac{1}{2}(0^-)$	493.677 ± 0.016	
K^{*0}, \bar{K}^{*0}	$d\bar{s}, \bar{d}s$	$\frac{1}{2}(0^-)$	497.672 ± 0.031	
K^{*-+}, K^{*-+}	$u\bar{s}, \bar{u}s$	$\frac{1}{2}(1^-)$	891.66 ± 0.26	
K^{*-0}, \bar{K}^{*-0}	$d\bar{s}, \bar{d}s$	$\frac{1}{2}(1^-)$	896.10 ± 0.28	

Particle	Quark Composition	$I(J^P)$	Mass (MeV)	Mean Life 10^{-12} (sec)
D^+, D^-	$c\bar{d}, \bar{c}d$	$\frac{1}{2}(0^-)$	1869.3 ± 0.5	
D^0, \bar{D}^0	$c\bar{u}, \bar{c}u$	$\frac{1}{2}(0^-)$	1864.6 ± 0.5	
D^{*+}, D^{*-}	$c\bar{d}, \bar{c}d$	$\frac{1}{2}(1^-)$	2010.1 ± 0.5	
D^{*0}, \bar{D}^{*0}	$c\bar{u}, \bar{c}u$	$\frac{1}{2}(1^-)$	2006.7 ± 0.5	
B^+, B^-	$u\bar{b}, \bar{u}b$	$\frac{1}{2}(0^-)$	5278.9 ± 1.8	1.65 ± 0.04
B^0, \bar{B}^0	$d\bar{b}, \bar{d}b$	$\frac{1}{2}(0^-)$	5279.2 ± 1.8	1.56 ± 0.04
B_s^0, \bar{B}_s^0	$s\bar{b}, \bar{s}b$	$0(0^-)$	5369.3 ± 2.0	1.54 ± 0.07
J/ψ	$c\bar{c}$	$0(1^-)$	3096.88 ± 0.04	

IMAGE EVALUATION TEST TARGET (QA-3)



APPLIED IMAGE, Inc
1653 East Main Street
Rochester, NY 14609 USA
Phone: 716/482-0300
Fax: 716/288-5989

© 1993, Applied Image, Inc., All Rights Reserved